POWDER PREPARATION, MECHANICAL PROPERTIES AND AGING BEHAVIOUR OF ZrO_2-Gd_2O_3 TETRAGONAL POLYCRYSTALS

A Thesis Submitted
in Partial Fulfilment of the Requirements
for the Degree of
DOCTOR OF PHILOSOPHY

by
SANTANU BHATTACHARYYA

to the
MATERIALS SCIENCE PROGRAMME
INDIAN INSTITUTE OF TECHNOLOGY KANPUR
OCTOBER, 1995

Dedicated to
My Father
and to the Loving Memory of
My Mother

9/10/95

CERTIFICATE

This is certified that the work contained in the thesis entitled "Powder Preparation, Mechanical Properties and Aging Behaviour of ZrO_2- Gd_2O_3 Tetragonal Polycrystals" by Santanu Bhattacharyya has been carried out under my supervision and that this work has not been submitted elsewhere for a degree.

9 October, 1995.

(D. C. Agrawal)
Professor
Materials Science Programme
Indian Institute of Technology
Kanpur

ACKNOWLEDGEMENTS

I would like to thank my supervisor Prof. D. C. Agrawal for introducing me to this field of Zirconia Ceramics. I thank him for his patience, constant encouragement and excellent guidance. During this long period of stay he has taught me many things and I am grateful to him for his generosity. I wish that he will keep in touch with me in future and will continue to give his valuable advice.

I was fortunate to get the association of Dr. T. D. Singh and Dr. P. V. Krishnan. I am grateful to them for the kindness they have shown upon me.

I sincerely thank Dr. Y. N. Mohapatra for his useful suggestions and help whenever I had asked for it.

I thank all the staff of the Central Workshop, Precision Workshop and Glass Blowing Workshop for their help and support during the entire course of work.

It was a nice and memorable association with all the staff of MSP and ACMS. I wish to give them my heartfelt thanks for their constant help.

In spite of their very busy schedule, Paritosh, Atanu, Subhasish, Pravat, Ajai, Joydip and others helped me a lot in the final stage of thesis preparation. I thank them again and again.

During this long stay at I.I.T. Kanpur many people helped in different ways and it is not possible to acknowledge each of them in this small space. I thank all of them for their help and

kindness.

I thank all my labmates for their help and cooperation.

I would like to specially thank Mr. B.K. Jain for tracings, Mr. S.S. Rana for typing and Mr. N.K. Metia for print out.

The silent support from my family members was always a constant source of inspiration for me during my stay.

Santanu Bhattacharyya

CONTENTS

LIST OF TABLES

LIST OF FIGURES

FIGURE PAGE

FIGURE PAGE

SYNOPSIS

Tetragonal Zirconia Polycrystals (TZP) are ceramics in which the tetragonal (t) phase of ZrO_2 has been stabilized at room temperature by addition of some specific oxides. Transformation of the t phase to a monoclinic (m) structure under the stress field of a propagating crack is mainly responsible for high toughness (K_{IC}) and strength (σ_f) of these ceramics.

Y_2O_3 and CeO_2 are the most commonly studied and used additives for TZP. Quite high values of K_{IC} and σ_f have been reported in Y-TZP and Ce-TZP. Many other oxides, particularly the rare earth oxides such as Er_2O_3, Yb_2O_3, Gd_2O_3 are also known to stabilize the t phase. However, preparation and properties of TZP obtained using these stabilizers has not been studied particularly with respect to powder preparation, mechanical properties, aging etc. In view of the limitation of the currently available TZP's (i.e. low temperature aging, sinterability) it is of interest to develop processes to prepare active powders of TZP stabilized with other oxides which yield sintered bodies with good density, mechanical properties and less susceptibility to aging.

In the present work the author has chosen one such additive, namely Gd_2O_3 with a view to (i) prepare powders of Gd_2O_3 stabilized TZP which sinter to high density (ii) study the mechanical properties of sintered samples of Gd-TZP (iii) study their low

temperature aging behaviour and (iv) to determine the suitability of Gd-TZP powders as a reinforcement for Al_2O_3.

The work has been described in 5 chapters. Chapter 1 is a general introduction to zirconia and zirconia ceramics. It also gives background of the proposed research and statement of the problem.

Chapter 2 is divided into three parts. Part A deals with the preparation of ZrO_2- Gd_2O_3 powders. The conventional mixed oxide route is often not very successful in preparing homogeneous, active powders. A brief review of the other methods of powder preparation has been first given. The powders have been prepared by three different methods, namely the mixed oxide (MO), hybrid sol-gel (HSG) and coprecipitation (CP). Powders having 2, 3, 5 and 8 mol % Gd_2O_3 were prepared.

Thermal analysis of the powders was carried out to arrive at a suitable calcination temperature. In the HSG powder the amorphous - crystalline transformation is found to be spread over a wide temperature range (470 - 550°C) while it is quite sharp (470°C) for the CP powder. The amounts of t phase were determined after calcination and sintering.

After calcination only the m phase was obtained in the MO powders. In HSG powder the (t + c) phase increased from 22 % to 62 % as the Gd_2O_3 content increased from 2 to 8 % . In the CP power 100 % t phase was obtained in all the cases. After sintering, the maximum (t + c) phase obtained in the MO and HSG powders was 44 %

and 87 % respectively while in the CP powder this amount was 96 % for 2 mol% Gd_2O_3 and 100 % for higher Gd_2O_3 contents. Only the powder from CP method was selected for further investigation.

A major problem encountered was the low sintered density. The density of sintered MO samples was lowest in most cases and was nearly independent of Gd_2O_3 content for the other two powders. The sintered density peaked at 3 mol% Gd_2O_3. The drop in sintered density at higher Gd_2O_3 contents is believed to be due to increasing amounts of cubic phase grains which have relatively large size. The highest density was obtained for 3 mol% Gd_2O_3 CP powder. However, the highest density was low (88%).

In Part B of Chapter 2, variation in calcination and sintering conditions of the CP powders were attempted in order to improve the sintered density. Higher calcination temperature produced highly agglomerated powder having low specific surface area and led to deterioration in density as well as to lesser amount of retained t phase. Increasing the sintering temperature led to grain growth and to a low density and low amounts of t phase.

Transmission electron microscopy, compaction behaviour and specific surface area measurements indicated that the as prepared powders may be agglomerated. Such agglomeration is known to occur in powders during drying from an aqueous slurry. To reduce such agglomeration, an additional step of washing with propanol was incorporated in the preparation of CP powders. This part of the work is described in Part C of Chapter 2. Infrared study, specific

surface area and compaction behaviour of the powders was studied. Washing the powder with propanol replaces the surface hydroxy group with propanol and propoxy group. The specific surface area increased from 90 m^2/gm to 150 m^2/gm on propanol washing of the CP powders. The agglomerate strength, as measured by the break in the pressure density plot is 36 MPa for water washed powder. For the propanol washed powders this break is not very sharp and occurs at 20 MPa. These results show that agglomeration of the powder is reduced to a significant degree by propanol washing and that the agglomerates produced are softer. This is also supported by the TEM evidence. Finally significantly higher sintered densities were obtained for all compositions using propanol washed powders. A density as high as 99 % could be obtained for 3 mol% Gd_2O_3 powder by sintering at 1400°C.

Chapter 3 deals with transformability, microstructure and mechanical properties of ZrO_2-Gd_2O_3 alloys. A review of the various toughening mechanisms believed to be operative in ZrO_2 ceramics is first given. This is followed by a summary of the existing data on the mechanical properties of other TZP's. The experimental work is then described. Powders containing 1.75, 2, 2.5, 3, 4, 5 and 8 mol% Gd_2O_3 were prepared by CP route, calcined and sintered as before. Density, phases lattice parameter and transformability of the t phase, fracture toughness, and strength were determined. Microstructures of the polished surfaces were examined.

Maximum density (99 %) was obtained for 3 mol% Gd_2O_3 sample. Density of four compositions, viz. 2, 2.5, 3 and 4 mol% Gd_2O_3 were all ≥ 90 % . A decrease in density occurs at >4 mol% Gd_2O_3 due to grain growth in the cubic phase.

Only t phase was obtained in the 2.5, 3 and 4 % samples. In 1.75 and 2 mol% samples, 12 vol % and 6 vol% m phase was respectively present. The 5 and 8 mol% samples had 9 and 80 % cubic phase respectively. The c/a ratio of the t-phase decreases with increasing Gd_2O_3 and extrapolates to 1 (cubic phase) at 9.6 mol % Gd_2O_3. The phases obtained are in metastable equilibrium as long times (~ 200 hours at 1400°C) are reportedly required for attaining equilibrium phases.

The extent of t ⟶ m transformation was measured on liquid N_2 quenched, fractured, hand ground and machine ground samples. Except for LN_2 quenched samples, all other samples had maximum transformability in 2 mol% Gd_2O_3 composition. In LN_2 quenched samples the t ⟶ m transformation takes place due to undercooling hence it depends on M_s temperature of the samples. Accordingly 1.75 mol % Gd_2O_3 sample has the highest M_s temperature and shows highest transformability (~ 75%). All other treatments showed a lower transformability because of the presence of m phase which inhibits autocatalytic t ⟶ m transformation. Liquid nitrogen quenching was quite effective at low Gd_2O_3 contents while fracturing and hand grinding was effective at higher Gd_2O_3 contents also. Due to

significant rise in temperature during machine grinding, the observed m phase on the machine ground surface is low.

The fracture toughness, K_{IC} was measured by single edge notch beam (SENB) method as well as by indentation method. The maximum K_{IC} obtained by indentation method is 12 MPa$\sqrt{m}$ for 2 mol% Gd_2O_3 and is $\geq$ 10 MPa$\sqrt{m}$ for 1.75 to 4 mol % Gd_2O_3. The SENB method gives the same trend but higher values of toughness as expected. A fracture strength of 750 - 800 MPa is obtained for 2 mol% samples. In the range 2 to 3 mol% Gd_2O_3, the strength values are in the range 700 to 750 MPa.

To quantify the contribution of transformation toughnening, the fraction of t phase transformed on fracture surface and transformation zone depth was measured. It was found that most of the enhancement in toughness could be accounted for by transformation toughening. A correlation between the relative critical flaw size and the density was observed, indicating that failure occurred form the flaws generated during processing.

Chapter 4 describes the low temperature aging behaviour of ZrO_2-Gd_2O_3 ceramics. Available data on the effect of low temperature aging on the mechanical properties is first reviewed. Ideas proposed to explain the mechanism of aging are described briefly. Some of the methods available to inhibit the low temperature aging are also described. This is followed by a description of the present experiments.

2, 2.5 and 3 mol% Gd_2O_3 samples were aged between 180- 200°C at 0.01 MPa water vapour pressure for times varying from 5 to 50 hours. 2Gd-TZP samples were also aged at different water vapour pressure (0.1 MPa to 2.5 MPa). Lattice parameter of the t phase was measured during the initial stages of aging in air and in 0.1 MPa water vapour.

Increasing the Gd_2O_3 decreases the extent of t $\longrightarrow$ m transformation. Activation energy of t $\longrightarrow$ m transformation were determined to be 85, 89 and 116 kJ /mol for 2, 2.5 and 3 mol% samples respectively. However, this variation in activation energy needs to be confirmed. The values are higher than reported for Y-TZP (73 - 94 kJ/ mol). Samples of Y-TZP prepared in the laboratory and aged under similar condition cracked extensively or disintegrated. Thus the Gd-TZP may have better aging resistance. This can be rationalized to certain extent by the lower ionic radius of Gd^{3+} (0.97 A°) vs. 1.06 A° for Y^{3+}.

An increase in the cell volume of the t phase was observed during the early stages of aging. This increase was more for water vapour aged samples than for air aged samples. It tends to support the hypothesis that the aging mechanism involves entry of OH^- group into the ZrO_2 lattice. It also indicates that the early stage of aging depends on the H_2O vapour pressure.

In the 5th Chapter, the results of Al_2O_3- ZrO_2 composites prepared using Gd-TZP are described. Composites having 5, 10, 15 and 20 vol % Gd-TZP (2 % and 3 mol% Gd_2O_3) were prepared by the

hybrid sol-gel route. Densities obtained were rather low (≤ 90%), perhaps due to the short sintering term (1.5 hours) employed. A peak in K_{IC} was observed in 10 vol% ZrO_2 samples. K_{IC} is higher for 2 mol% Gd_2O_3 than for 3 mol% Gd_2O_3. The total amount of t phase transformed on the fracture surface is also maximum at 10 vol % ZrO_2. At higher ZrO_2 contents, agglomeration of ZrO_2 occurs and the total amount of t -ZrO_2 available for transformation decreases.

A sharp drop in strength occurs at ~ 10 to 15 vol% ZrO_2. This is believed to be due to the presence of microcracks which form due to the t $\longrightarrow$ m transformation during cooling after sintering.

CHAPTER 1

INTRODUCTION

1.1 *GENERAL*

ZrO_2 occurs as naturally occurring mineral baddeleyite which contains about 80% ZrO_2. The other main source is zircon sand ($ZrSiO_4$) which occurs as secondary deposits in India, Australia and United States [1,2]. Due to its high refractive index, transparent zirconia crystals are used as gems. In the periodic table Zr is placed between Ti and Hf and hence many of the ZrO_2 contain TiO_2 and HfO_2 as impurities.

Pure ZrO_2 exists at room temperature in monoclinic phase. This transforms to tetragonal at ~ 1100°C which further transforms to a cubic flourite structure at about 2370°C. Properties such as high melting point, inertness to chemicals, high hardness, etc. make ZrO_2 an attractive material for many applications. However, the tetragonal to monoclinic transformation during cooling after sintering is accompanied by a volume increase of 4-6% and a shear strain of 1-2%. This deleterious volume expansion renders the product useless. This problem can be overcome by alloying ZrO_2 with oxides such as CaO, MgO, Y_2O_3 and CeO_2 which fully or partially stabilize the cubic or the tetragonal phase of ZrO_2 at room temperature. The resulting ceramics are called fully stabilized zirconia (FSZ), partially stabilized zirconia (PSZ) or tetragonal zirconia polycrystals (TZP) depending on the microstructure and have found wide ranging applications. Presence

of tetragonal zirconia leads to enhanced mechanical properties due to stress induced t $\longrightarrow$ m transformation. This aspect has been extensively investigated during the last several years due to its scientific and technological importance.

As mentioned above, the t $\longrightarrow$ m transformation is accompanied by 4-6% volume expansion and 1-2% shear strain. This causes cracking of the sintered body of ZrO_2 upon cooling from the sintering temperature. Therefore, there has been great interest in developing methods to retain the high temperature phase of ZrO_2 at room temperature. Although the stable phase at room temperature is monoclinic, it is found that pure ZrO_2 can exist in tetragonal or cubic structure when the critical size of crystallites is very small ($\leq$ 30 nm) [3]. Such small crystallites are usually obtained when ZrO_2 is prepared by chemical methods like precipitation or by prolonged ball milling of m-ZrO_2 [4,5,6]. Proposed mechanisms for the metastability of the t phase in small crystallites are discussed later. However, sintering of a powder containing such crystallites would be accompanied by grain growth and it loses the ability to retain the t phase in the bulk upon cooling to room temperature.

For the bulk applications the t or c phases are stabilized by the addition of certain metal oxides known as "stabilizers". These can be classified into two categories - one having low solid solubility and the other having high solid solubility in ZrO_2. The features of these cases are shown in Fig. 1.1. [7]. In the first case, for a particular composition A, the additive, due to its low solid solubility separates out under equilibrium conditions, below the eutectoid temperature. However, if the

cooling is done at a sufficiently rapid rate from the solution treatment temperature in the cubic phase field region (T_1 in Fig. 1.1), a metastable structure consisting of cubic grains with fine (in the nm range) tetragonal precipitates inside them is retained at room temperature. The structure is subsequently aged in the (cubic + tetragonal) phase region (T_2 in Fig. 1.1) in order to coarsen the t particles so that they can undergo stress-induced t $\rightarrow$ m in transformation and produce toughening. As the solid solution heat treatment is carried out at high temperatures, the cubic grains have large size (10 to 100 μm). Examples of additives belonging to this category are MgO and CaO and the zirconia ceramic containing fine t particles in the matrix of large cubic grains is called **Partially Stabilized Zirconia (PSZ)**. It should be pointed out that PSZ can also be produced using additives of the second group (e.g. Y_2O_3) described below by employing suitable heat treatment.

These PSZ materials usually have a poor density with a large grain size and exaggerated grain growth. This is reflected in their moderate strength value (700-800 MPa). However, the strength of these PSZ materials can be remarkably improved by reducing the grain size to ~ 1 micron size by using powders prepared by special processing techniques. These techniques include evaporative decomposition of salt solution [8], water or air atomization of liquid precursors [9], or from fused materials [10]. Such powders sinter to a high density at low temperature without appreciable grain growth. Sintering is followed by annealing to optimize the tetragonal precipitate size. These optimized PSZ materials have high strength (> 1000 MPa) at room

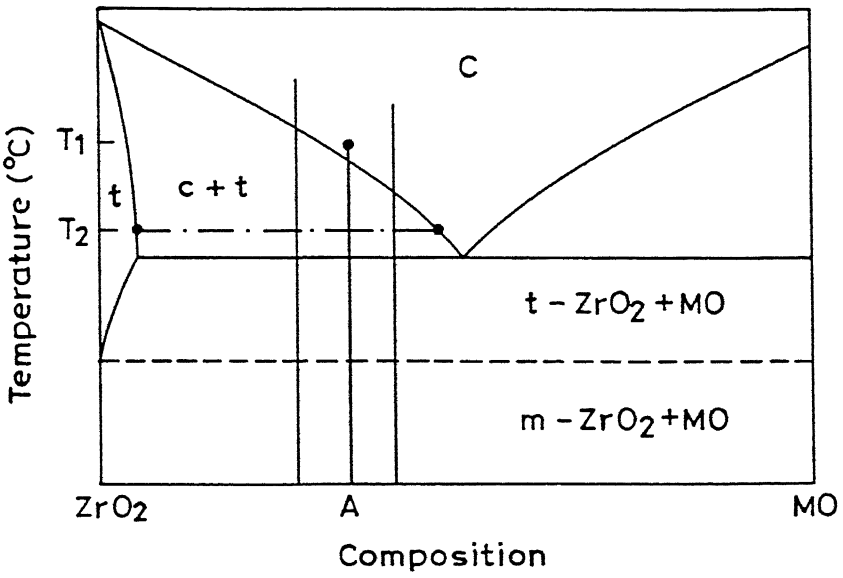

Fig. 1.1 ZrO_2-MO phase diagram for solutes having low solubility [7].

temperature as well as improved high temperature property [1].

Y_2O_3 typifies the additives of the second group (Fig. 1.2). In this case, a cubic phase with large amount of dissolved additive, is thermodynamically stable at room temperature. However, if the solution treatment (or sintering) is done in the tetragonal phase field region, or as is more usual, near the boundary of the tetragonal and cubic phase fields, (Fig. 1.2), followed by controlled cooling, a metastable structure consisting of grains of tetragonal zirconia with grain size ≤ 1 μm, is retained at room temperature. The resulting material is termed **Tetragonal Zirconia Polycrystals (TZP).** Y_2O_3 and CeO_2 are the most well known stabilizers belonging to this category. The constraint imposed by adjacent grains on one another and the extremely slow cation mobility [12] helps in the retention of the tetragonal phase in these materials. These materials are generally prepared by wet chemical routes as well as by solid state routes and sintered between 1300°C and 1450°C. The critical grain size for spontaneous t⟶m transformation during cooling ranges between 0.2-2 μm depending on solute type, solute content, sintering temperature etc. On account of high density, extremely fine grain size and high transformability of t phase, these materials exhibit high strength and toughness and are ranked among the toughest and strongest in the ZrO_2 ceramics group.

Tetragonal zirconia particles can also be used as reinforcement to enhance the toughness and strength of materials like alumina, SiC mullite etc. In zirconia toughened alumina (ZTA) strength and toughness as high as 900 MPa and 10 MPa$\sqrt{m}$ respectively can be achieved as compared to 300 MPa and 3-4 MPa$\sqrt{m}$ for pure

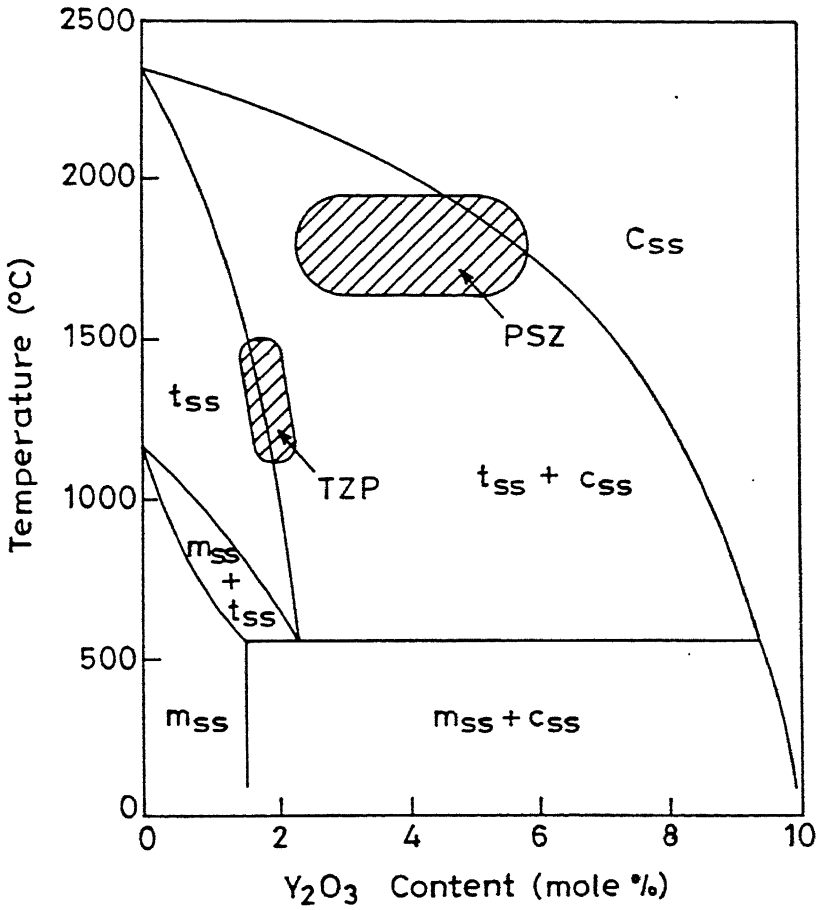

Fig. 1.2 ZrO_2-Y_2O_3 phase diagram in the ZrO_2 rich region showing high solute solubility [7].

alumina. The crucial requirement in these zirconia toughened materials is that the particles of t-ZrO_2 should not agglomerate during processing and thereby exceed the critical size for the room temperature stability of the t phase [3].

Although the ZrO_2 ceramics have already found some applications as structural ceramics, it has been found that they suffer drastic loss of properties when subjected to low temperature (200 - 500°C) annealing in air or in a humid atmosphere. Strength and toughness drop by more than 50% on aging for 100 hours at low temperature [13], and in extreme cases the samples break into small pieces [14].

In the remaining of this chapter we describe briefly certain basic features of zirconia ceramics. These are crystal structure, phase transformation and stabilization of the high temperature phases. Following this the background of the proposed study is provided and statement of the problem for present research is presented.

1.2 *CRYSTALLOGRAPHY OF ZIRCONIA*

Pure ZrO_2 occurs in three different crystallographic modifications, viz. monoclinic, tetragonal and cubic, which are discussed below.

1.2.1 Monoclinic Zirconia

In pure ZrO_2, this phase is the stable room temperature phase. In contrast to idealized cubic flourite structure, where Zr atoms are in eight fold coordination, the Zr atoms in monoclinic ZrO_2 have a coordination number 7. This results from a strong directionally oriented covalent bonding between Zr and O atoms. The two types of O atoms which are linked to Zr atom are

in two different planes (O_I and O_{II}) (Fig. 1.3). Tetrahedrally coordinated oxygen atoms are called O_I atoms and triangularly coordinated oxygen atoms are called O_{II} atoms. The Zr-O_I distance is 0.204 nm and Zr-O_{II} distance is 0.226 nm. This difference in Zr-O distances gives different structure for O_I and O_{II} atomic planes. While O_I atomic planes are planar, O_{II} planes are buckled. The two different types of oxygen atoms exert different force on Zr atoms making the Zr atoms inclined to the tetrahedrally coordinated oxygen atoms [3, 15].

1.2.2 Tetragonal Zirconia

Tetragonal zirconia can be obtained with a slight distortion of the cubic flourite structure. The monoclinic to tetragonal structure is accompanied by a change in coordination number from 7 to 8 (Fig. 1.4). Each cell has two molecules with two sets of Zr-O distances (0.2455 nm and 0.2065 nm) [16, 17]. This configuration gives rise to a strong bct reflection whose intensity decreases on doping or on raising the temperature.

1.2.3 Cubic Zirconia

Ideally in a structure analogous to CaF_2 structure (Fig. 1.5) the Zr atoms should be in eight fold coordination with oxygen atoms. However, due to strong directional covalent bonding of Zr and O atoms, cubic ZrO_2 has a coordination less than eight. In the cubic structure, oxygen vacancies are present in sufficient number [18, 19] such that Zr coordination changes from eight to between eight and seven.

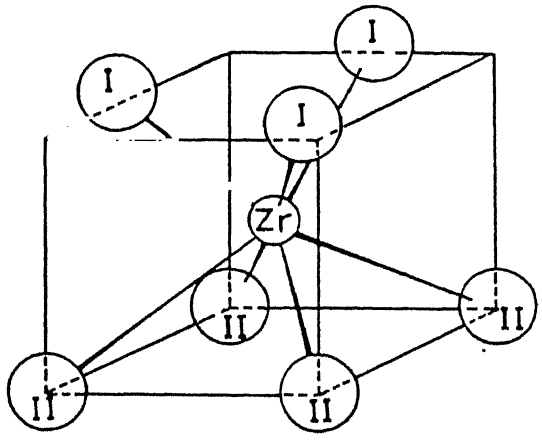

Fig. 1.3 Monoclinic ZrO_2 showing sevenfold coordination of Zr atoms with O atoms [17].

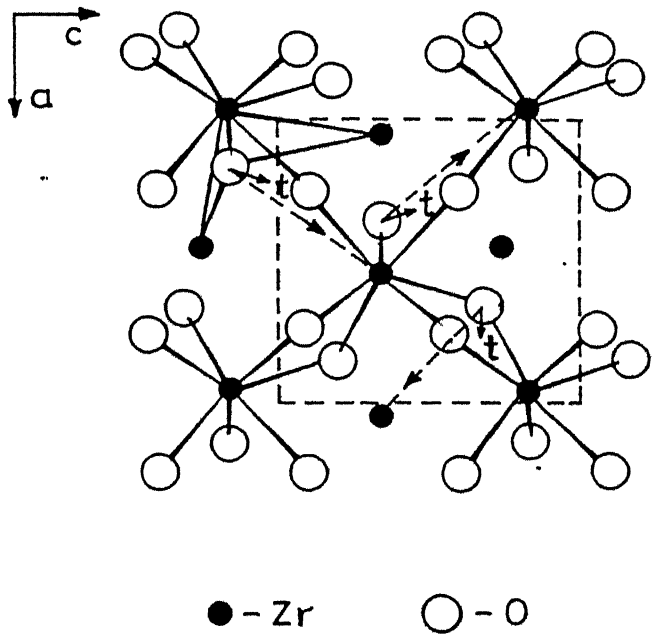

Fig. 1.4 The projection of ZrO_2 layers on (100) m plans schematically showing the monoclinic to tetragonal transition due to movement of oxygen atoms. The possible atomic movement is shown by arrows and t represents O ion position in tetragonal unit cell [17].

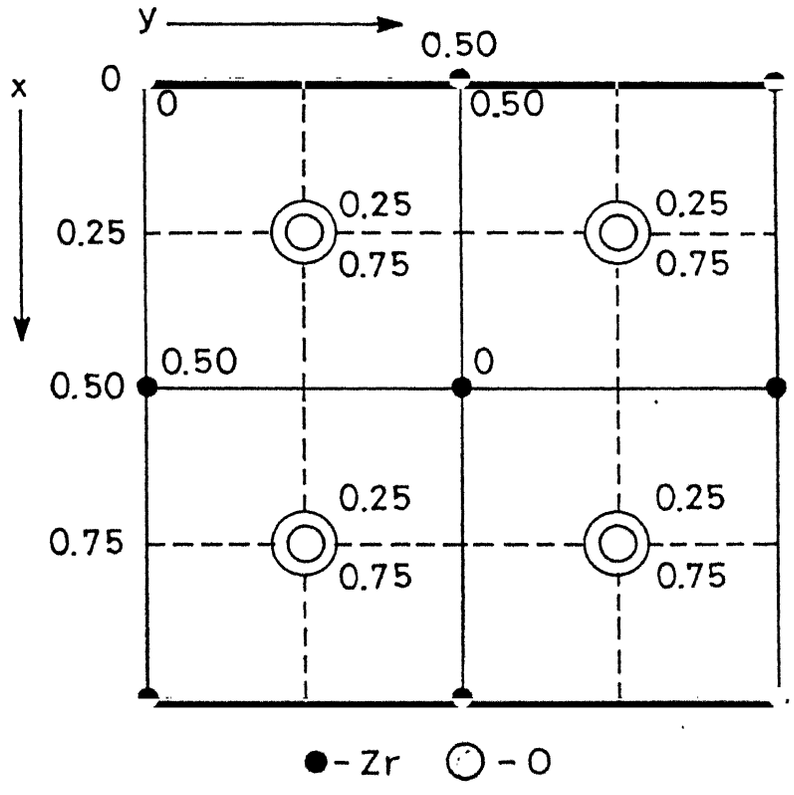

Fig. 1.5 Projection of cubic zirconia in the X-Y plane showing idealized cubic flourite structure [23].

1.3 *STABILIZATION OF THE HIGH TEMPERATURE PHASES*

As already mentioned, the high temperature phases (t and c) can be stabilized at room temperature by the addition of suitable stabilizing oxides. Crystal chemistry of such stabilization has been of much interest. Additionally it has been found that the t phase can exist at room temperature without the help of any stabilizer if the size of the particle is very small. There have been many attempts to explain this size effect and predict the critical size for stability. In the following we first discuss briefly the various ideas proposed to explain the size effect. This is followed by a discussion of the crystal chemical considerations in the stabilization of ZrO_2 by stabilizers.

1.3.1 Stabilization when the Particle Size is Small

Metastable tetragonal zirconia can be retained in pure ZrO_2 provided the particle size is kept below a certain critical size [3]. According to one view, the stability results due to lower surface free energy of tetragonal phase in comparison to monoclinic phase. The same idea has also been invoked by Mitsuhashi et. al. [20] to account for the existence of cubic barium titanate at room temperature. At a particular temperature (T), the critical crystallite size for retention of tetragonal zirconia is given by [3].

$$r_c = \frac{-3(\sigma'-\sigma)}{q\ (1 - \frac{T}{T_b})} \qquad (1.1)$$

where σ and σ' are the surface free energy of the crystallites before and after phase transformation, q is the latent heat of transformation per unit volume of an infinite crystal and T_b is the transformation temperature of an infinite crystal.

However, this model was criticized by Mitsuhashi et. al. [20] on the basis of the following:

(a) It is possible to retain tetragonal phase in crystallites larger than 10 nm size, the critical size given by the above model.

(b) The polydomain tetragonal crystallites transform to monoclinic phase only on severe grinding.

(c) The hydrothermally annealed tetragonal microcrystals transform to monoclinic very easily.

Accordingly, Garvie [21] has modified the original equation to include the effect of both the hydrostatic and nonhydrostatic stress as well as coherency strain factor on the critical crystallite size needed for retention of tetragonal pha The simultaneous effect of both stress and strain factors introduce extra degree of freedom which increases the critical c ..te size. Thus, the modified critical crystallite size is g..... by

$$r_c = \frac{-3\ \Delta\sigma^*}{(\Delta\psi + \Delta\epsilon)} \qquad (1.2)$$

where $\Delta\sigma^*$ = change in surface free energy of the precipitates

$\Delta\psi = [q(1-T/T_b)]$ = change in mechanical energy per unit volume of a particle.

$\Delta\epsilon$ = change in strain energy per unit volume of a particle.

In the light of above discussion, Garvie explained the discrepancies observed by Mitsuhashi et al [20] in the following manner:

(a) The critical crystallite size for retention of tetragonal zirconia will increase if factors like coherency strain and presence of both hydrostatic and nonhydrostatic stresses are

taken into account.

(b) During grinding, high internal stresses are generated in the crystallite which shift the critical crystallite size towards higher value. Thus, it necessitated the application of further severe grinding for transformation.

(c) To account for easy transformation in hydrothermally annealed crystals Garvie and Burke [22] introduced the concept of soft phonon mode of transformation. According to this model, transformation takes place due to excitation of soft phonon modes in the crystallites. On annealing, the crystallites were energized, thus they could be easily excited by light grinding.

A value of $2r_c$ = 31 nm [21] is obtained using

$$\Delta\sigma^* = 0.91\ J/m^2,\ T = 293\ K,\ T_b = 1448\ K,$$

$$q = -2.82 \times 10^3\ J/m^3 \text{ and } \Delta\epsilon = 0.46\ J/m^3.$$

1.3.2 Stabilization by Additives

As discussed above, pure ZrO_2 can exist in the tetragonal modification only when the particle size is $\leq 300\ A^0$. For bulk applications, the t or c phases are stabilized by the addition of certain oxides called "stabilizers".

Many ideas have been proposed to explain the stabilization of high temperature phases in ZrO_2 by various additives. These discuss the effects of various factors like solid solution, relative ionic size, valency and electronegativity of the host and solute atoms. Although the exact stabilization mechanism is not very clear, all the theories agree that oxygen vacancies play a vital role in stabilization.

On account of strong orbitally oriented covalent bonding between Zr and O atoms, the coordination number of both monoclinic and cubic ZrO_2 are seven. According to the crystal chemistry model [23] the vacancies introduced due to doping are preferably located next to Zr as the dopant itself tends to be 8 coordinated with oxygen. This reduces the coordination number of Zr to below 8, the value for the perfect cubic fluorite structure. The tendency for the stabilization of the cubic structure increases as the coordination number for Zr tends towards 7. It is postulated that when approximately 50% of the Zr^{4+} ions become seven coordinated, a stable cubic phase is obtained. This corresponds to 5-6% vacancies on O^{2-} sublattice and the coordination number of Zr is above 7.5.

As pointed out by Peng Li et al [24], the crystal chemistry model does not explain the following observations: (i) while the oversized dopants are 8 coordinated, this is not true for the undersized dopants, (such as Ga^{3+}, Fe^{3+} and Al^{3+}) which nevertheless do lead to stabilization. (ii) stabilization effect of tetravalent cations (Ce^{4+}, Th^{4+}, Ge^{4+}, Te^{4+}) which do not introduce oxygen vacancies can not be explained (iii) the stabilization of the tetragonal phase with very small doping, and hence containing low concentration of oxygen vacancies can not be explained.

Peng Li et al [24] used x-ray absorption to study the effects of dopants on zirconia stabilization. They concluded that the oversized trivalent dopants are 8 coordinated in zirconia and the vacancies are therefore preferably associated with the Zr. The undersized trivalent dopants, on the other hand, tend to be 6

coordinated and compete for oxygen vacancies with Zr so that larger amount of dopant is required for stabilization as is found to be experimentally the case.

Li et al [25] have also carried out similar studies with tetravalent dopants, Ce^{4+} and Ge^{4+}. They found that in ZrO_2 the CeO_8 cube is compressed as compared to that in CeO_2 while the GeO_8 tetrahedron is dilated as compared to that in GeO_2. However, the Ce-O bond length, though shorter than in CeO_2, is still larger than the Zr-O distance. Thus an effective dilation is experienced which decreases tetragonality and stabilizes the tetragonal phase. Undersized Ge enhances the tetragonality of the solid solution, the tetragonal structure is stabilized because of the local Ge-Zr ordering which relieves the internal strain energy of the Zr cation sublattice.

1.4 *MARTENSITIC PHASE TRANSFORMATIONS IN ZIRCONIA*

The tetragonal to monoclinic transformation which occurs in pure ZrO_2 upon cooling from a high temperature (~ 1200°C) is a martensitic transformation. While the cubic to tetragonal transformation occurs by precipitation upon slow cooling from the cubic phase field, it is found that a metastable tetragonal phase called the t′ phase can form martensitically compared to the regular t phase. The t′ phase has a smaller tetragonality, higher stabilizer content, higher resistance to stress induced t $\longrightarrow$ m transformation and has many anti-phase domain boundaries [26]. The t′ phase has been observed in a number of zirconia-rare earth oxide systems.

In view of its importance in transformation toughening, the stress induced t $\longrightarrow$ m transformation has been well studied.

Although there are several proposed models for the nucleation of t $\longrightarrow$ m transformation, the mechanism has not yet been fully understood. But there is a general consensus that all the proposed models must explain the formation of a stable monoclinic nucleus for its further growth. Two of these models - one based on classical nucleation theory and the other on nonclassical nucleation theory are described briefly.

Chen and Chiao's [27] proposed model depends on the nucleation of stable monoclinic phase by a classical nucleation mechanism. The most energetically favoured nucleation sites in this case are either preexisting intrinsic defects or stress induced extrinsic defects. The particular type of nucleation site which will dominate the nucleation process is governed by the probabilistic theory of finding a suitable defect having a shear strain of the same order as that of martensitic transformation. However, the major drawback of this model is that no evidence for such a potent nucleation site exists.

Lack of experimental evidence for the classical theory of possible nucleation site led Heuer and Rühle [28] to propose the nonclassical mechanism. Basically their model is an improvement over the soft phonon mode model originally proposed by Clapp. In the nonclassical model the transformation from parent to product phase (here t $\longrightarrow$ m) is initiated by lattice strains arising out of localized lattice vibrations (or phonons). The primary requirement of this model is the presence of a diffuse interface and of strain generation sufficient for excitation of defects. The most favourable defects are free surfaces, interfaces, strain sites from coherency sites, thermal expansion anisotropy stress,

dislocations etc. Since all the fabricated material produced either by conventional or by nonconventional routes contain these above defects to a greater or lesser extent, this model appears to provide a plausible answer for nucleation mechanism.

1.5 *FACTORS AFFECTING t ⟶ m TRANSFORMATION*

As described earlier, the high temperature t phase can be retained at room temperature by the addition of suitable stabilizers to zirconia. The interest in stabilized ZrO_2 had stemmed from the need to avoid the damaging t ⟶ m transformation in the bulk ceramics during cooling. However, PSZ ceramics much improved mechanical properties and soon it became clear that this improvement was primarily due to the stress induced t ⟶ m transformation. The focus of research then shifted to the study of factors which controlled the retention and transformation of t – ZrO_2. These factors are concentrations of the stabilizer, size of the t particle, state of constraint on the t particle and the residual stresses.

1.5.1 Transformation of Unconstrained Zirconia

The driving force for transformation is the free energy difference between the initial and the final states. The activation energy for crossing this transformation barrier can be applied either in the form of stress or temperature. The driving force and activation energy for such a transformation are also dependent on the starting particle size. Fig. 1.6 describes the change in these quantities for three different initial particle sizes. When the particle is very small (S) the net driving force for transformation is zero. In other words, these small particles have very large activation energy barrier and hence they do not

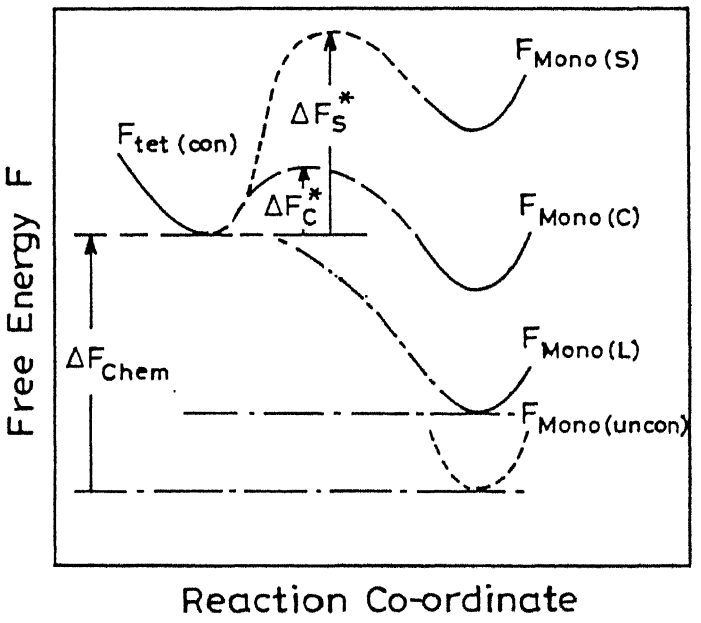

Fig. 1.6 The change in free energy for tetragonal to monoclinic phase change involving different initial particle sizes (L = large particle, S = small particle and C = critical particle size). ΔF_{chem}, ΔF_C^* and ΔF_S^* represent chemical free energy change activation energy barrier for a critical sized particle and that for a small particle respectively [7].

undergo any transformation. As the particle size is increased, the energy barrier decreases and finally for large (L) particles, there is virtually no barrier, i.e. the driving force is very large and they require no (or very little) stress or temperature assistance for complete transformation. However, a critical sized particle (c) lies in between these two extremes where a small but finite amount of energy is needed to overcome the barrier.

1.5.2 Transformation of constrained Zirconia

We have been considering so far the transformation of "unconstrained" or free tetragonal ZrO_2 particles. However, if the tetragonal zirconia is in a confined or "constrained" state which is a more practical case, the transformation kinetics will be different. Constrained tetragonal zirconia particles may be of several forms:

(a) Precipitates in partially stabilized zirconia (PSZ), e.g. Mg-PSZ and Ca-PSZ,

(b) inter and intragranular particles in zirconia toughened ceramics (ZTC), e.g., Zirconia Toughened Alumina (ZTA), and

(c) small grains, as in tetragonal zirconia polycrystals, e.g., Y- and Ce - TZP.

In any of the above cases, an additional term due to strain energy is to be considered in the free energy change accompanying the transformation.

1.5.3 Free Energy Considerations in the Transformation

Let us consider a stress free spherical zirconia particle constrained in a matrix. The free energy change for such a system undergoing t $\longrightarrow$ m transformation is given by [12]

$$\Delta G_{t \longrightarrow m} = - \Delta G^{C} + \Delta U_{se} + \Delta U_{s} \qquad (1.3)$$

where ΔG^{C} is chemical free energy change, ΔU_{se} is the net strain energy change corresponding to transformed particle and surrounding matrix and ΔU_{s} is the surface free energy change. Since for transformation $\Delta G_{t \longrightarrow m} \leq 0$, hence

$$|\Delta G^{c}| \geq U^{m}_{se} + \Delta U_{s} \qquad (1.4)$$

Since U^{m}_{se} is always positive, $|\Delta G^{c}|$ will be different for constrained and unconstrained cases. For ZrO_2 in particular, application of a constraint decreases the $|\Delta G^{c}|$ and hence the transformation temperature.

For monoclinic phase, the strain energy expression is given by

$$U^{m}_{se} = \frac{1}{2} \bar{\sigma}^{I}_{ij} \bar{\epsilon}^{t}_{ij} \qquad (1.5)$$

where $\bar{\sigma}^{I}$ is the uniform stress state within the transformed inclusion and $\bar{\epsilon}^{t}_{ij}$ is the stress free transformation strain. For an isotropic volume change, ΔV , $\bar{\sigma}^{I}_{ij}$ and $\bar{\epsilon}^{t}_{ij}$ are given by

$$\bar{\sigma}^{I}_{ij} = K \left(\frac{\Delta V}{V} \right) \qquad (1.6)$$

and

$$\bar{\epsilon}^{t}_{ij} = \frac{1}{3} \frac{\Delta V}{V} \qquad (1.7)$$

where

$$K = \frac{2E_1E_2}{(1+\nu_1)E_2 + (1-2\nu_2)E_1} \qquad (1.8)$$

From the above equations, it is seen that strain energy is directly proportional to elastic modulus of the matrix. As strain energy increases, $|\Delta G^{c}|$ decreases, thereby lowering the transformation temperature. In other words, additives which decreases $|\Delta G^{c}|$ will also decrease transformation temperature.

Hence, additions of solutes (like Y_2O_3, CeO_2) to ZrO_2 lowers the $t \longrightarrow m$ transformation.

In the above a "stress free" inclusion was considered. However, in practice residual stresses act on the dispersed phase on account of thermal expansion mismatch with the surrounding matrix. These residual stresses also influence the strain energy and thereby $|\Delta G^c|$. Depending on the relative sign of residual stress tensor and transformation stress tensor (i.e. whether they have the same or opposite sign), $|\Delta G^c|$ will either increase or decrease. For the case, where residual stress field and transformational stress field have the same sign (i.e. tensile-tensile or compressive-compressive), strain energy is increased. However if they are of opposite signs, strain energy is reduced [12].

1.5.4 Effect of Change in Surface Free Energy

The role of surface energy in stabilizing unconstrained particles in t phase has already been discussed. It also plays a vital role in determining the critical crystallite size for retaining tetragonal phase in a constrained particle. For a spherical inclusion the change in surface free energy can be expressed as [12].

$$\Delta U_s = \frac{A_m \gamma_m - A_t \gamma_t}{V} = \frac{6(\gamma_m - g_s \gamma_t)}{D} \qquad (1.9)$$

where A_m and A_t are the interfacial surface areas, γ_m and γ_t are specific surface energies, V is the transformed volume ($V = \pi D^3/6$) D = inclusion diameter and $g_s = A_t/A_m$. The subscript m and t refer to the transformed phase (i.e. monoclinic) and untransformed phase (i.e. tetragonal). Thus surface energy introduces a size effect

in the overall chemical free energy due to transformation ($|\Delta G^c|$) and its effect on the critical crystallite size for tetragonal phase retention can be written as

$$D \geq D_c = \frac{6(\gamma_m - g_s \gamma_t)}{[|\Delta G^c| - \Delta U_{se}]} \qquad (1.10)$$

where D_c is the critical crystallite size above which ($\Delta G_{t \longrightarrow m} \leq 0$).

During the t $\longrightarrow$ m transformation or during fabrication, quite often microcracking and/or twining takes place. Both these release some of the constraint present on a tetragonal crystal. Thus, it results in a loss of strain energy and consequently the critical size for spontaneous t $\longrightarrow$ m transformation changes. Accordingly there may be three different systems:

(a) Systems with microcracking only

The presence of microcracks will decrease the strain energy as well as increase surface energy due to cracked surface. If f_c is the volume fraction of microcracks present, γ_c is the fracture energy per unit area, A_C is the area of crack surfaces around V is the volume of the particle then

$$\Delta G_{t \longrightarrow m} = - \Delta G^c + \Delta U_{se} f_c + \frac{A_c \gamma_c}{U} + \Delta U_s \qquad (1.11)$$

Accordingly the critical inclusion diameter is given by

$$D \geq D_c^c = \frac{6\,[\gamma_c\, g_c + \gamma_m - g_s \gamma_t]}{|\Delta G^c| - \Delta U_{se}\, f_c} \qquad (1.12)$$

where $V \simeq \pi D^3/6$ and $A_c = \pi^2 D\ g_c$.

(b) System with twinning only

Similarly when a twin boundary is present in the material it will alter the strain energy due to relief of some of the internal strain through twinning. Accordingly, when both microcracking and

twinning are present the chemical free-energy of the system is given by

$$\Delta G_{t\longrightarrow m} = -\Delta G^{c} + \Delta\, U_{se}.f_{T} + \frac{6\gamma_{T}\, g_{T}}{D} + \Delta U_{s} \qquad (1.13)$$

and critical crystallite size is given by

$$D \geq D_{c}^{T} = \frac{6\,[\gamma_{T}g_{T} + \gamma_{m} - g_{c}\gamma_{t}]}{|\Delta G^{c}| - \Delta U_{se}\, f_{T}} \qquad (1.14)$$

In the above equation, f_{T} and g_{T} are dimensionless quantities ($f_{T} < 1$ and $g_{T} > 0$), $\frac{6\gamma_{T}\, g_{T}}{D}$ is twin energy per unit volume of transformed material. A_{T} is total twin area boundaries ($A_{T} = \pi\, D^{2}g_{T}$) and γ_{T} is the twin boundary energy.

(c) System with microcracking, twinning and transformation toughening

In the third and final situation, there can be microcracking, twinning as well as transformation toughening. For this case, the critical particle size is given by,

$$D \geq D_{c}^{c,T} = \frac{6\,(\gamma_{c}g_{c} + \gamma_{t}\, g_{t} + \gamma_{m} - g_{s}\gamma_{t})}{|\Delta G^{c}| - \Delta U_{se}\, f_{c}.f_{T}} \qquad (1.15)$$

However, like twinning where the size effect will be observed only for $|\Delta G^{c}| > U_{se}\, f_{T}$, the condition for this case is $|\Delta G^{c}| > U_{se}\, f_{T}$.

1.6 *Background of the Proposed Research and Statement of the Problem*

1.6.1 Introduction

Amongst the various ZrO_{2} ceramics, the tetragonal zirconia polycrystals (TZP) are of special interest because of their high strength and fracture toughness. The dominant contribution to the enhanced toughness is believed to be from the stress induced t$\longrightarrow$ m transformation occurring in the stress field of an advancing crack

[29]. But the t phase in pure ZrO_2 is not stable at room temperature except when the particle size is extremely small (~ 30 nm) [3]. It can be stabilized in particles of larger sizes by alloying with additives such as Y_2O_3, CeO_2 etc. [30,31]. The Y_2O_3 stabilized tetragonal zirconia polycrystal (Y-TZP) has been extensively studied in literature. However, inspite of having higher toughness and strength, the use of Y-TZP is limited owing to property degradation during its use at low temperature (200°C - 500°C) or in humid atmosphere [32,33]. On the other hand Ce-TZP has poor sinterability, so either high sintering temperature or hot pressing is needed [34]. However, properties degrades due to Ce^{4+}/Ce^{3+} reduction during such processing especially during hot pressing.

1.6.2 Gd_2O_3 As a Stabilizer for ZrO_2

Because of the above considerations it is of interest to study the preparation and properties of ZrO_2 stabilized by other oxides. The stabilization of tetragonal phase by rare earth oxides (other than CeO_2) such as Er_2O_3 and Gd_2O_3 is well known [35, 36]. However, except for CeO_2, other additives have not received much attention probably due to highly stable tetragonal phase which does not undergo stress induced t⟶ m transformation easily. Due to these problems along with high cost of Er_2O_3, the use of Er-TZP is limited. The ZrO_2 - Gd_2O_3 system has been studied by a few investigators mainly with a view to use it as a solid electrolyte i.e. the compositions were so chosen that ZrO_2 existed in the cubic phase [37 - 39]. van Dijk. et.al. [37] prepared fine grained ZrO_2 - Gd_2O_3 ceramics having composition $GdO_{.495}$ $ZrO_{.505}$ $O_{1.753}$ from alkoxide powders by hydrolysis of metal alkoxide mixture. The

metal alkoxides used were Zr-t-amyl oxide $Zr(O_5H_{11})_4$ and Gd -isopropoxide $Gd(OC_3H_7)_3$. A diluted metal alkoxide - benzene solution were added dropwise to a large excess of water while vigourously stirring. This was followed by washing of the precipitate with water and isopropanol. After calcination (650°C) and compaction, the pellets were isostatically pressed at 400 MPa and sintered in oxygen atmosphere at 1400°C - 1430°C for 5 hours. Complex admittance measurements were performed on these samples. The activation energy for grain boundary conductivity ΔH_{gb} was (18 ± 2) kJ/ mol. Grain boundary conductivity and the pre-exponential factors were an order of magnitude smaller for alkoxide processed powders in comparison to single crystals.

Moztarzadeh [38] prepared ZrO_2 - Gd_2O_3 polycrystalline ceramics by mixing high purity Gd_2O_3 by isostatic pressing. Presintered samples (800°C for 20 hours) were machined prior to sintering (1750°C for 24 hours or at 1900°C for 16 hours). Electrical conductivity was determined at different temperatures (upto 1200°C) using conventional four-probe technique. The conductivity decreased with an increase in the dopant concentration. The phenomenon was explained by formation of certain type of associates in the crystal structure in the form of complexes due to the interaction of Vö and cationic defects. In a similar way, Kang et.al [39] studied the electrical conductivity ZrO_2 - Gd_2O_3 single crystals containing 10, 12.5 and 15 mol% Gd_2O_3. The material was single phase cubic as determined by x-ray diffraction, Raman spectroscopy and Neutron diffraction. The latter test also determined the chemical homogeneity of the samples. Electrical conductivity was measured by two terminal a.c.

technique at frequency range of 5Hz to 13 MHz. The conductivity was found to be higher than that reported in the literature. This difference was due to the absence of grain boundaries in the present case as compared to other studies. The activation energy increased linearly with Gd_2O_3 content due to the formation of dopant - vacancy associates due to electrostatic interaction and strain field accommodation. Michel et.al [36] prepared single crystals of metastable tetragonal zirconia (MTZ) from high purity ZrO_2 and gadolinium sesquioxide powders. The crystals were grown by directional solidification after r.f. induction melting by a skull melting technique. Tetragonal zirconia was obtained with 3 mol% Gd_2O_3 on rapid cooling ($\geq 400^{\circ}h^{-1}$) from the melt. The crystals obtained were polydomain. They were broken by applying mechanical stress or shocks and toughness was determined by indentation technique. It was found that for a given crystallographic orientation both cubic and tetragonal zirconia possessed roughly the same hardness.The crystal fracture was found to occur by cleavage on different planes for cubic and tetragonal zirconia. Since these materials did not show any stress induced t $\longrightarrow$ m transformation the enhancement in fracture toughness (with respect to that of fully stabilized cubic zirconia) was not due to transformation toughening. Detailed fractographic analysis revealed that the domain microstructures of samples (which was induced by c $\longrightarrow$ t phase transition during the cooling process) gave rise to crack deflections on a submicrometer scale. This crack deflection was thought to be responsible for the enhanced toughness of this material. Besides this, crack pinning due to internal stresses resulting from the tetragonal lattice distortion

also contributed to toughening.

As mentioned earlier, Y_2O_3- stabilized ZrO_2 polycrystals (Y - TZP) as well CeO_2 - stabilized ZrO_2polycrystals (Ce - TZP) undergo degradation upon aging at low temperatures (200°C - 500°C) in humid atmosphere. The study of such aging is therefore important in any new stabilized ZrO_2 alloy. The kinetics of such aging is believed to be dependent on the strain in the zirconia lattice [40]. As the ionic radii of Gd^{3+} (0.97Å) is much closer to Zr^{4+}(0.87A°), than that of Y^{3+}(1.06A°), it is conceivable that stabilization by Gd_2O_3 may lead to lower strain in the lattice and thereby lower aging rates.

The as sintered TZP is usually a metastable material. Thus Lange et.al [41] showed that a sintered Y-TZP when further held at 1400°C for 100 hours, undergoes "phase partitioning" and changes into a Y_2O_3 lean tetragonal phase (having high transformability) and a Y_2O_3 rich cubic phase. The toughness of the heat treated material increased from 3 to >10 MPa$\sqrt{m}$. Similar phase partitioning has also been found in Gd_2O_3 - TZP by Leung et.al [42]. Thus the possibility exists for tailoring the microstructure and composition of tetragonal grains (and thereby the mechanical properties) of these TZP's by suitable post sintering heat treatment.

1.6.3 Statement of the problem

Guided by above considerations, a study of the preparation and characterization of ZrO_2 - Gd_2O_3 ceramics has been undertaken in this work. The aims of this study are as follows:

1. *Preparation of ZrO_2- Gd_2O_3 powders stabilized into tetragonal phase*

As discussed above, preparation of Gd_2O_3 stabilized tetragonal zirconia powders has not been reported so far. Apart from the requirement of existing in the tetragonal phase, the powders should sinter to a high density at a reasonable temperature while retaining the t phase after sintering.

2. *Study of the transformability of the t phase in ZrO_2 - Gd_2O_3 ceramics:*

For fracture toughness enhancement, it is essential that the t⟶ m transformation occur readily in the stress field of a propagating crack. The ease of such transformation is expected to depend on the Gd_2O_3 content. Transformation can also be induced by other means such as cooling to very low temperature, grinding etc.

3. *Study of the mechanical properties (strength, toughness and hardness) of the sintered ZrO_2 - Gd_2O_3 ceramics:*

Mechanical properties are of primary interest in tetragonal zirconia polycrystals. These need to be correlated with factors such as microstructure and the transformability of the t phase.

4. *Study of the low temperature aging kinetics*

A limitation of the various TZP's is their degradation in properties upon low temperature (200 - 500°C) aging. A new TZP having a slower aging kinetics will be of technological interest. Moreover, study of aging behaviour in the new system should be helpful to elucidate further the mechanisms involved in such aging.

5. *Processing, Microstructure and Mechanical Properties of Al_2O_3 -ZrO_2 Composites using Gd_2O_3 - Stabilized Tetragonal Zirconia*

One very important applications of tetragonal powders is in toughened composites such as ZrO_2 toughened alumina (ZTA). Powders of Ce - TZP and Y - TZP are at present used for this purpose. It would be interesting to study the toughening action of Gd-TZP when incorporated in Al_2O_3 matrix. For ensuring uniform dispersion, these composites will be processed via hybrid sol-gel route. The focus of the study will be dispersion behaviour and the effect of ZrO_2 volume fraction on microstructure, grain size of ZrO_2, transformability and mechanical properties of ZTA. Also, Gd- TZP having different Gd_2O_3 content will be introduced to observe the effect of Gd_2O_3 content on the transformation behaviour and mechanical properties of Al_2O_3 - ZrO_2 composites.

REFERENCES

1. E. Ryskkewitch, Chapter II.5 in Oxide Ceramics, Ist edition, Academic Press, New York, 1960.

2. E.C. Subbarao, "Zirconia - an Overview," in Advances in Ceramics, Vol. 3 pp 1. Edited by A.H. Heuer and L.W. Hobbs, American Ceramic Society, Columbus, Ohio, 1981.

3. R.C. Garvie, "Occurrence of Metastable Tetragonal Zirconia as a Crystallite size Effect", J. Phys. Chem. 69 [4] 1238 - 43 (1965).

4. K.S. Mazdiyasni, C.T. Lynch and J.S. Smith II, "Cubic Phase Stabilization of Translucent Yttria - Zirconia at Very Low Temperatures", J. Am. Ceram. Soc. 50 [10] 532 - 37 (1967).

5. J. Livage, K. Doi and C. Maziers, "Nature and Thermal Evolution of Amorphous Hydrated Zirconium Oxide", J. Am Ceram. Soc. 51 [6] 349 - 53 (1968).

6. J.E. Bailey, D. Lewis, Z.M.Librant and L.J. Porter, "Phase Transformations in Milled Zirconia", Trans. J. Brit. Ceram. Soc. 71 (1) 25 - 30 (1972).

7. D.J. Green, R.H. J. Hannink and M.V. Swain in Transformation Toughening of Ceramics, Ch. II, CRC Press Inc. (1989).

8. S.C. Zhang, G.L. Messing and M. Borden, "Synthesis of Solid Spherical Zirconia Particles by Spray Pyrolysis," J. Am. Ceram.Soc. 73 [1] 61 - 67 (1990).

9. B. Fegley Jr., P. White and H. K. Bowen, "Processing and Characterization of ZrO_2 and Y-doped ZrO_2 Powders," Am. Ceram. Soc. Bull. 64 [8] 1115 - 20 (1985).

10. K.M. Jasim, R.D. Rawlings and D.R.F.West, "Thermal Barrier Coatings Produced by Laser Cladding," J. Mater. Sci. 25, 4943 - 48 (1990).

11. N. Claussen, "Microstructural Design of Zirconia - Toughened Ceramics (ZTC)", pp 325 - 351 in Advances in Ceramics, Vol.12. Edited by N. Claussen, M. Ruhle and A.H. Heuer, American Ceramic Society, Columbus, OH, 1984.

12. F.F. Lange, "Transformation Toughening, Part 1, Size Effects associated with the Thermodynamics of Constrained Transformation", J. Mater. Sci. 17 [1] 225 - 34 (1982).

13. H - Y Lu and S - Y Chen, "Low - Temperature Aging of t - ZrO_2 Polycrystals with 3mol% Y_2O_3", J. Am. Ceram. Soc. 70 [8] 537 41 (1987).

14. J. J. Swab, "Low -Temperature Degradation of Y - TZP Materials", J. Mater. Sci. 26, 6706 - 14 (1991).

15. D. K. Smith and H. W. Newkirk, "The Crystal Structure of Baddeleyite and its relation to the Polymorphism of ZrO_2," Acta. Crystallogr. 18 [5] 983 - 91 (1965).

16. G. Teufer, "The Crystal Structure of Tetragonal ZrO_2 15 [11] 1187 (1962).

17. E.C.Subbarao, H.S. Maiti and K. K. Srivastava, "Martensitic Transformations in ZrO_2",Phys. Stat. Solidi A, 21 [1] 19 - 40 (1974).

18. R. Ruh and J. Garrett, "Nonstoichiometry of ZrO_2 and Its Relation to Tetragonal - Cubic Inversion in ZrO_2," J. Am. Ceram. Soc. 50 [5] 257 - 61 (1967).

19. P. Ramaswamy and D.C.Agrawal, "Effect of Sintering Zirconia with Calcia in very low partial pressure of Oxygen," J. Mater. Sci. 22, 1243-48 (1987).

20. T. Mitsuhashi, M. Ichihara and U. Tatsuke, "Characterization and Stabilization of Metastable Tetragonal ZrO_2", J. Am. Ceram. Soc. 57 [2] 97 - 101 (1974).

21. R.C. Garvie, "Stabilization of the Tetragonal Structure in Zirconia Microcrystals", J. Phys. Chem. 82 [2] 218 - 24 (1978).

22. S. Burke and R.C. Garvie, "Soft Phonon Modes and the Monoclinic - Tetragonal Phase Transformation in Zirconia and Hafnia", J. Mater. Sci. Letters. 12 [7] 1487 - 90 (1977).

23. S. M. Ho, "On the Structural Chemistry of Zirconium Oxide", Mater.Sci. Engg. 54 [1] 23 - 29 (1982).

24. P. Li and I. W-Chen, "Effect of Dopants on Zirconia Stabilization - An X-ray Absorption study: I, Trivalent Dopants", J. Am. Ceram 77 [1] 118 - 28 (1994).

25. P. Li, I. W-Chen and J.E. Penner - Hahn, "Effect of Dopants on Zirconia Stabilization - An X-ray Absorption Study: II, Tetravalent Dopants," J. Am. Ceram. Soc. 77 [5] 1281 - 88 (1994).

26. T.-S. Sheu, T.-Y Tien and I.-W Chen, ''Cubic -to- Tetragonal (t') Transformation in Zirconia containing Systems," J. Am. Ceram. Soc. 75 [5] 1108-16 (1992).

27. I. W-Chen and Y-H Chiao, "Theory and Experiment of Nucleation of ZrO_2 containing Ceramics and Ferrous Alloys," Acta. Metall. 33 [10] 1827 - 45 (1983).

28. A.H Heuer and M. Rühle, "On the Nucleation of the Martensitic Transformation in Zirconia (ZrO_2)," Acta. Metall, 33 [10] 2101 - 12 (1985).

29. R.M. McMeeking and A.G.Evans, "Mechanics of Transformation Toughening," J. Am. Ceram. Soc. 65 [5] 242 - 46 (1982).

30. T.K. Gupta, J.H. Bechtold, R.C.Kuczincki, L.H. Caddof and B. R.Rossing, "Stabilization of Tetragonal Phase in Zirconia," J. Mater. Sci. 12, 2421 -2426 (1977).

31. K. Tsukuma and M. Shimada, "Strength, Fracture Toughness and Vickers Hardness of Ce-Stabilized Tetragonal Zirconia Polycrystals (Ce-TZP)," J. Mater. Sci. 20 [4] 1178 - 84 (1985).

32. M. Watanabe, S. Iio and I. Fukura, "Aging Behaviour of Y-TZP," in Advances in Ceramics, Vol 12, pp 391-98. Edited by N. Claussen, M Rühle and A.H. Heuer. The American Ceramic Society, Columbus, OH, 1984.

33. T. Sato and M. Shimada, "Transformation of Yttria - Doped Tetragonal Zirconia Polycrystals by Annealing in Water," J. Am. Ceram. Soc. 68 [6] 356 - 59 (1985).

34. M. Hirano and H. Inada, "Strength and Phase - Stability of Yttria - Ceria - Doped Tetragonal Zirconia/Alumina Composites Sintered and Hot Isostatically Pressed in Argon - Oxygen Gas Atmosphere," J. Am. Ceram. Soc. 74 [11] 606 - 11 (1991).

35. P. Duran, P. Recio, J.R. Jurado, C. Pascual and C.Moüre, "Preparation, Sintering and Properties of Translucent Er_2O_3 - Doped Tetragonal Zirconia," J. Am. Ceram. Soc. 72 [11] 2088 - 93 (1989).

36. D. Michel, L. Mazerolles and M. Perez. Y. Jorba, "Fracture of Metastable Tetragonal Zirconia Crystals," J. Mater Sci. 18 2618 - 28 (1983).

37. T. van Dijk and A.J. Burggraff, "Electrical Conductivity of Flourite and Pyrochlore Ln(x) Zr(1-x)O (2-x/2) (Ln = Nd, Gd) Solid Solutions," Phys. Status, Solidi. A, 63, 229 (1981).

38. F. Moztarzadeh, " Conductivity Measurements of Gd_2O_3 - Stabilized ZrO_2 upto 2300K," pp 901-905 in Advances in Ceramics. Vol. 24B, Science and Technology Zirconia III. Edited by S. Somiya, N. Yamamoto and H. Yanagida, American Ceramic Society, Westerville, OH, 1988.

39. T.K. Kang, T. Nagasaki, N. Igawa, K.I - Hiun and H. Ohno, "Electrical Properties of Cubic Stabilized Single ZrO_2 - Gd_2O_3 Crystals," J. Am. Ceram. Soc. 75 [8] 2297 - 99 (1993).

40. M. Yoshimura, "Phase Stability of Zirconia," Am. Ceram. Soc. Bull. 67 [12] 1950 - 55 (1988).

41. F.F. Lange, D.B. Marshall and J. R. Porter, "Controlling, Microstructures Through Phase Partitioning from Metastable Precursors: The ZrO_2 - Y_2O_3 System," pp 519-32 in Ultrastructure Processing of Ceramics, Glasses and Composites. Edited by J.P. Mackenzie and D.R. Ulrich, Wiley, New York, 1988.

42. D.K. Leung, C.J. Chan, M. Rühle and F.F. Lange, "Metastable Crystallization, Phase Partitioning and Grain - Growth of ZrO_2 - Gd_2O_3 Materials Processed from Liquid Precusors," J.Am. Ceram. Soc., 74 [11] 2786 - 92 (1991).

CHAPTER 2

PREPARATION AND CHARACTERIZATION OF TETRAGONAL ZrO_2- Gd_2O_3 POWDERS

PART A

POWDER PREPARATION

2.1 *INTRODUCTION*

Ceramic processing by conventional solid state route involves mixing of two or more constituents by grinding, ball milling etc. followed by calcination to form the compound or solid solutions. The calcined product is again crushed and then sintered to give it strength and develop the desired microstructure. However, mechanical mixing of two components is hardly intimate, uniform and homogeneous and hence it results in composition fluctuation at every stage of processing which persists after sintering [1]. Often repeated calcination is required to improve the homogeneity and to attain the desired phases. The ball milling step may also lintroduce contamination due to the wear of the jar and grinding media [2]. During sintering, large diffusion paths between components (or species) induces pore migration and coalescence, which retards complete densification due to longer migration path for vacancies. Abnormal grain growth and entrapment of porosity usually occurs leading to a bimodal grain size distribution consisting of large isolated grains in a matrix of small grains and porosity [3,4]. This route is also unsuitable for introducing a dopant uniformly in a sintered body.

In the present work, we have used two routes, termed as hybrid sol-gel route and coprecipitation route to prepare powders of ZrO_2 containing different amounts of Gd_2O_3. These powders are compared with the powders prepared by the conventional mixed oxide route. Based on this comparison, one of the preparation methods has been selected for preparation of powders and investigations have been carried out to achieve high sintered density. This work is discussed in this chapter in three parts. In this part (Part A), we first briefly review some of the chemical routes of powder preparation. This is followed by the description of the processing routes used here for preparation and characterization of ZrO_2-Gd_2O_3 powders, and the results obtained. In part B and C are described the studies carried out to improve the sintered density.

Preparation of Multi Component Powders by Chemical Methods:

Because of the limitations associated with the conventionally prepared powders there has been a great interest in recent years in preparation of powders having different components in intimate and uniform mixing and capable of being sintered at relatively low temperatures. Some of the preparation methods used for the processing of such powders are briefly described below:

(i) Coprecipitation Method

In the coprecipitation method of preparing multicomponent powders, suitable salts of the respective cations are brought in solution. Precipitation of the same salt or a different salt or hydroxide is effected by adding a chemical precipitant or by change of temperature and pressure. Special precautions may be necessary to ensure that the precipitate contains the cation in

the desired ratio. Such coprecipitation is easy if the cations in solution are about the same size and chemically similar. The method has been used, for example, for preparation of powders of Ni-Fe ferrite, barium titanate etc by precipitating oxalates and then heating them to obtain oxides.

Rossi and Pelletier have described a method of preparing Y_2O_3-ZrO_2 by coprecipitation [5]. The precursors were $ZrCl_4$ and $YCl_3.6H_2O$. In order to avoid uncontrolled precipitation, the ingredients were dissolved in anhydrous ethanol. Coprecipitation was achieved by the addition of NaOH. the slurry was filtered, the cake was dried, washed with distilled water to remove soluble NaCl, and finally dried at 150°C, to a constant weight.

(ii) Evaporative Decomposition of Salt Solutions

The process involves atomization of a mixed salt solution [6,7]. A mist is prepared using an ultrasonic atomi technique using two piezo-electric transducers. The mist is dried and then decomposed in a furnace. Each droplet acts as a separate container and reaction is conducted within the droplet to yield spherical particles. For ZrO_2 powder the starting material generally is $ZrOCl_2.8H_2O$ and $YCl_3.6H_3O$ dissolved in distilled water. The mist of this solution should have a very narrow size distribution. The mist is introduced into the furnace with air as carrier gas and heated below 400°C to prevent crystallization. Particles are collected with an electrofilter and calcined at 410°C for 1 hour and then at 700°C for 2 hrs. The particle size depends most strongly on the concentration of feed solution and air jet pressure. Generally, the particles obtained from this process are hollow spheres; however by proper manipulation of

solution concentration and atomization parameter it has also been possible to obtain solid spherical particles.

(iii) Hydrolysis of Mixed Alkoxide Solutions

The solutions are prepared from Zirconium isopropoxide $Zr(OC_3H_7)_4$ and Yttrium isopropoxide $Y(OC_3H_7)_3$ in a mutual solvent such as n-hexane (C_6H_{14}) or benzene (C_6H_6) [8,9]. The hydrolysis takes place on dropwise addition of water to the vigorously stirred solution. The mixed oxide precipitates from the solution as a result of the hydrolysis of alkoxides:

$$2Y(OC_3H_7)_3 + 3H_2O \longrightarrow Y_2O_3 + 6\ C_3H_7\ OH$$

$$Zr(OC_3H_7)_4 + 2H_2O \longrightarrow ZrO_2 + 4\ C_3H_7\ OH$$

The controlled hydrolysis reaction must be done in a water free atmosphere (glove box) using anhydrous alcohols and alkoxides and water. Any small amount of water in the alcohols, atmosphere or alkoxides will cause uncontrolled hydrolysis. The precipitation time depends upon reaction temperature.

(iv) Thermal Decomposition of Alkoxides

In this method the alkoxide is pyrolyzed. As an example, when Zr-tetratertiary butoxide is pyrolyzed, mechanism of reaction is one in which olefin and alcohol are split out in successive steps as shown in Fig. 2.1 [10]. The products formed are olefin, alcohol and oxide. The rate of reaction is dependent on the concentration of the starting material. The alkoxide is introduced into the primary vapourizer, which is maintained at or close to the boiling point of the material. Inert carrier gas sweeps the vapour and hot liquid into the secondary vaporizer where remaining liquid is vaporized. The carrier gas and alkoxide vapour

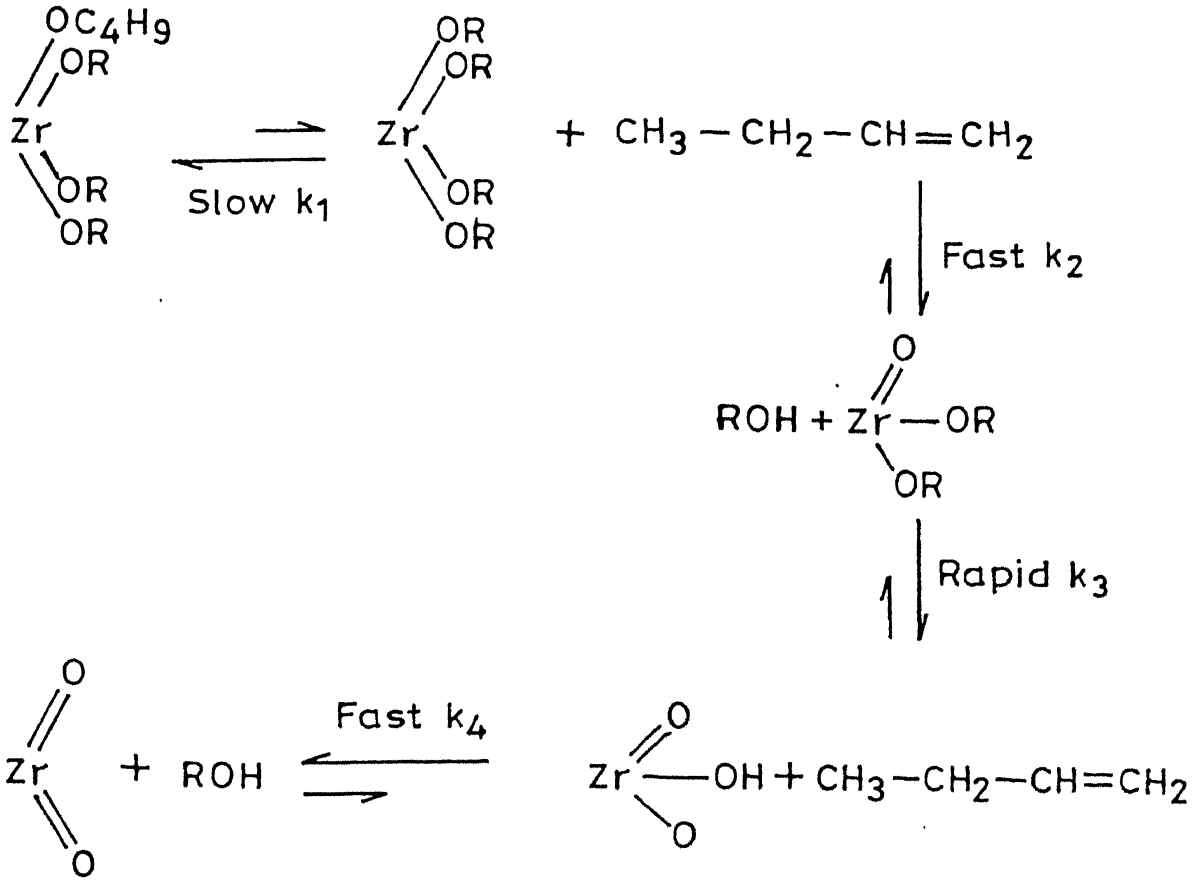

Fig. 2.1 Reaction mechanism for pyrolysis of Zr- tetratertiary butoxide to give ZrO_2 powder.

subsequently passes in the decomposition chamber where the alkoxide decomposes into olefins, alcohol and oxides. The oxide particles are collected by an electrostatic precipitator.

(v) Freeze drying of inorganic salt solutions

Rakotoson and Paulus [11] sprayed a solution of Y and Zr sulphates into liquid nitrogen to "freeze" the molecular homogeneity of the chemical species. This was followed by drying for 15 hours in vacuum (1.3-0.13 Pa). Residual water was removed at 150°C. Finally the sulphate was transformed by thermolysis into the oxide at temperatures ranging from 800°C for 1100°C. Chemically homogeneous powder was obtained after thermolysis. The grain size was controlled by changing the solution concentration and the thermolysis parameters. Prolonged thermolysis at low temperature gave the best result i.e. more complete transformation to oxide and small grain size.

(vi) Hydrothermal Preparation:

In this process, first an amorphous powder is prepared from Hf free $ZrCl_4$ solution, by precipitation with 3N NH_4OH [12,13]. The precipitate is removed and redispersed in distilled water and refiltered. After four such dispersion and filtration steps, the precipitate is dried at 120°C for 48 hours. Distilled water and solutions of 8 wt % KF; 30 wt% NaOH; 7, 15 and 30 wt% LiCl and 10 wt% KBr are used as mineralizers. The starting material and solution are poured in a Pt or Au tube and treated at 100 MPa at 200°C to 600°C for 24 hours using a test-tube-type pressure vessel of Co-Cr-W alloy. The vessel is quenched into cold water. The material is washed in distilled water, dried and characterized. Tetragonal zirconia powder is obtained under these hydrothermal

condition and is believed to be the result of topotactic crystallization on nuclei in the amorphous zirconia.

(vii) Sol-emulsion-gel method :

This method of powder preparation is a combined Sol-gel and emulsion method [14] and is cost effective because of relatively inexpensive precursors like nitrates. In this method, water droplets containing zirconium ions are suspended and stabilized in an organic nonpolar solvent by the addition of an appropriate surfactant. The emulsion droplets are gelled by NH_3 gas, and the gel droplets are then stabilized by removal of water during heterogeneous distillation. The choice of the surfactant to be used in an emulsion is determined by the compatibility of the surfactant's hydrophobic-lipophilic balance (HLB) number and the composition of the suspension. The suspension is refluxed first at 90°C and then at 140°C for 16 hrs. The powder is separated by centrifuging the mixture. The final product is dried at 120°C to 140°C for 12 to 16 hrs.

(viii) Spray- Inductively- Coupled Plasma (ICP) Process

In this process $ZrO(NO_3)_3 .2H_2O$ salt solution in distilled water is sprayed into a spray chamber with argon as carrier gas [15]. After the separation of large droplets in the spray chamber, only small droplets are introduced first into a preheated tube for quick drying and then into an argon ICP flame through a narrow tipped nozzle. The oxide powder formed is collected in a quartz tube placed beneath the flame. The argon ICP flame is generated with an oscillator of 15 kW and 6 MHz and is stabilized with argon cooling gas. For complete decomposition, the droplets should be introduced into the flame smoothly. the droplet size should be

small (0.1-1 μm) for ease of decomposition as time of residence in the flame in only a few milliseconds.

The different methods of powder preparation which have been described above yield powder with different morphology, homogeneity, agglomeration behaviour and stabilization of tetragonal phase. Out of these, the sol-gel methods are relatively simple and have the following advantages [16]:

(a) Better homogeneity (for multicomponent systems) as mixing is done in liquid state.

(b) High purity of starting raw materials leads to high purity of the end product.

(c) Lower temperatures of preparation obviates the need for high temperature furnaces and minimizes evaporation losses.

(d) Due to extremely high surface area in the liquid phase, reaction between different components take place at a much faster rate.

In the present work, therefore, we have explored three different routes for the preparation of tetragonal zirconia powder -a mixed oxide (MO) route and two modified sol-gel routes, ie., the hybrid sol-gel (HSG) and coprecipitation (CP) routes. However, as will be seen later, both MO and HSG routes could not retain 100% tetragonal phase. Moreover, in the case of MO route, calcination of powders at high temperature (>1400°C) was required to stabilize the tetragonal phase. Only the third route i.e. CP route proved to be successful in retaining 100% t phase both after calcination and sintering. However, the density of the samples prepared by this method, though highest among the three routes was still not high enough. Details of powder preparation by all the

three methods are described in this part (Part A) of this chapter. The problem of improving sintered density is dealt with in the remaining two parts.

2.2 *EXPERIMENTAL*

2.2.1 Powder Preparation

Powders of ZrO_2 - Gd_2O_3 were prepared by three different methods. Source and concentration of the raw materials (precursors) used for all the three routes are given in Table 3.1 followed by the details of the preparation procedures before the calcination step. The calcination and sintering procedure for all powders is discussed later.

Table 2.1

Source and Assay of Precursors

Sl. No.	Precursors	Source	Assay
1.	Zr-n-propoxide 70% in propanol	Alfa Chemicals, Danvers USA	99.9% for Zr-n -propoxide
2.	Gd_2O_3	Indian Rare Earth, Kerala	99%
3.	Acetic acid	S.D. Fine chemicals, Boisar, Gujrat	99.6%
4.	Propanol (Isopropyl alcohol)	- do -	99.5%
5.	Diethanolamine	Ranbaxy Lab., Bombay	98%
6.	ZrO_2 powder (Monoclinic)	Aldrich Chemicals Co. U.K.	99%
7.	Nitric acid (HNO_3)	Ranbaxy Laboratory, Bombay	69-71%

2.2.1.1 *Mixed Oxide Method*

In this method ZrO_2 and Gd_2O_3 powders were mixed in an agate mortar pestle and wet ground for about 8 hours in a polyethylene jar using propanol and alumina balls. The slurry was subsequently dried in an oven (110°C - 120°C) and the dried powder was lightly ground.

2.2.1.2 *Hybrid Sol-Gel Method*

In this method, the precursors used were zirconium-n-propoxide (Zr-n-p), Gd_2O_3, acetic acid, diethanolamine and propanol. A clear sol was prepared by mixing Zr-n-p, acetic acid, diethanolamine and propanol in the molar ratio 1:1:0.75:10 respectively. Thus for a particular batch of ZrO_2-3 mol % Gd_2O_3 the amounts were 20 gms, 3.66 gms, 4.86 gms and 73.38 gms respectively. This sol was prepared in a glove box and stirred for about 20 minutes. This was followed by the addition of Gd_2O_3 powders (0.5039 gms) after which the mixed sol was further stirred for about 30 minutes and was subsequently gelled by adding 0.25 gms triple distilled water (molar ratio Zr-n-p : H_2O = 1:0.3). The gel was dried at 120°C for 24 hours.

2.2.1.3 *Coprecipitation Method:*

In this method, the precursors were Zr-n-p, acetic acid, propanol and $Gd(NO_3)_3.6H_2O$. The first three ingredients were used in the ratio 1 : 1 : 5, e.g. 20 gms Zr-n-p, 3.66 gms acetic acid and 18.34 gms propanol.

A clear sol was first prepared by adding Zr-n-p to acetic acid in 1:1 molar ratio. This results in the formation of a clear sol via an exothermic reaction. The acetate group in acetic acid partially replaces the alkoxy groups of Zr-n-p thereby forming a

bidentate ligand. The increased gelation time results in the formation of stable substitution compound with reduced functionality [17]. However, the addition sequence is very important. It is imperative that Zr-n-p should be added to acetic acid and not the other way round else it will form particles.

The clear sol of Zr-n-p was stirred for 10 minutes. This was followed by dropwise addition of $Gd(NO_3)_3.6H_2O$ (4.76 gms $Gd(NO_3)_3.6H_2O$ dissolved in 9.20 gms propanol. The resultant clear sol was further stirred for about 20 minutes. The sol was then added in a dropwise manner to triple distilled water while stirring (H_2O : Zr-n-P :: 500 : 1). The addition of Zr-n-p to water caused partial hydrolysis of Zr-n-p. The complete precipitation of hydrous zirconia gadolinia took place upon adding solution of NH_4OH (25% strength) while stirring. The pH of the solution was always kept above 10.2 to ensure complete precipitation of both the hydroxides. The voluminous white gelatinous precipitate was stirred in its mother liquor for 4 to 5 hours, allowed to settle, and the liquor containing mainly excess ammonia was decanted off. The precipitate was washed 4 to 5 times with distilled water using about 500 ml of distilled water for each washing. It was then dried at 100°C for 24 hours.

The powder from the MO method was mixed with 3 wt% PVA solution such that it contained 3 gms PVA per 100 gms of powder batch. The powder mixture along with PVA was again made into a slurry and mixed in the agate mortar for 15-20 minutes. The slurry was then dried in an oven. The dried powder was uniaxially pressed in hardened steel die at about 200 MPa into cylindrical pellets 10 mm ϕ, 3 mm high and calcined at 1000° C for 2 hours or 8 hours.

The HSG and CP route powders were crushed to a fine powder after drying. Since these powders were partially (for HSG) or fully (for CP) amorphous, and were very intimately mixed as compared to MO method powders, these were not compacted prior to calcination. The calcination and sintering schedules of the powders prepared by the three methods are given in Table 3.2. In each case 4 different powders, containing 2, 3, 5 and 8 mol % Gd_2O_3 respectively were prepared.

Table 2.2

Calcination and Sintering Conditions.

Powder Type	Calcination Schedule T(°C)/t(h)	Sintering Schedule T(°C)/t(h)
Mixed Oxide (MO)	1000/2 1000/8	1400/2
Hybrid Sol-Gel (HSG)	700/4	1400/2
Coprecipitation (CP)	700/4	1400/2

The MO method calcined pellets were ground in an agate mortar and pestle and mixed with 3 wt% PVA solution as already mentioned. The HSG and CP powders were directly mixed with PVA solution of the same strength. The slurry was mixed for about 20 minutes in agate mortar and pestle and dried at 100°C for 4 hours. The dried cake was ground back to a fine powder and pressed into circular disks (10 mm ϕ and 3 mm high) at 200 MPa. Stearic acid solution (1 wt%) was used as die wall lubricant. The powder compact was held at the maximum pressure for 2 minutes to minimize the elastic spring back . The green pellets were dried overnight in an oven

and sintered according to the temperature time schedule given in Table 3.2. The samples were heated at the rate of 4°C/min from room temperature to 620°C, and held for 1 hour for removal of organics. Subsequently, the samples were heated at the rate of 7°C/min to the sintering temperature and held for the desired period (Table 3.2). Cooling was done at the rate of 3.5°C/min upto 1000°C, and at the rate of 4.5°C/min from 1000°C to 700°C. After that, the furnace was switched off and the samples were cooled in the furnace.

2.2.2 Characterizations

The techniques used for characterizations of the powders and the sintered samples are described below. Only some of the powders were characterized by all the techniques.

2.2.2.1 *Thermal Analysis :*

Differential Thermal Analysis (DTA) of the hybrid sol-gel prepared and coprecipitated powders were carried out primarily with the aim to determine suitable calcination temperature.

DTA was carried out on dried powders in a differential thermal analyzer (Model DTA 50, Shimadzu, Japan). The sample was kept in a Pt-crucible and the DTA plot was recorded while heating the sample upto 1000°C at a heating rate of 10°C/min.

The specific surface area was measured by single point BET method using the instrument "Quantasorb" (Quantachrome USA) Weighed amount of powder was put in a sample tube. The tube was evacuated and degassed for about 24 hours before starting the measurements. Only the desorption readings were used for surface area measurement.

The crystallite size (D) was calculated from the surface area using the relation

$$D = \frac{6}{\rho S} \qquad (2.1)$$

where S is the specific surface area and ρ is the material density.

2.2.2.2 *Compaction Response of Powders :*

The compaction behaviour of the powders was evaluated by means of the pressure density-diagrams. These were obtained by uniaxially pressing the powders in a die and recording the load and the movement of the top punch. When the green density is plotted as a function of the logarithm of the pressure, two straight line segments are usually obtained. The point of intersection of these line segments is taken to correspond to the onset of the breakage of the agglomerates. A hardened steel die (8 mm die) was used. The die was lubricated by applying a thin coating of stearic acid solution (1 wt%) in propanol. Approximately 0.25 gms of powder was filled in the die. The powder was filled slowly, then shaken gently to make the powder level uniform. The load vs. punch travel was recorded on a universal testing machine (Model 810.12, Materials Testing System, Minnesota, USA).

2.2.2.3 *Microstructure of Powders and Sintered Samples*

The powder morphologies of the dried and uncalcined powders as well as calcined powders were observed in a Transmission Electron Microscope (TEM). For this study, a very dilute suspension of the powder in propanol was made. The suspension was ultrasonicated for about 10 minutes for uniform dispersion. A

very fine drop of this suspension was placed on a carbon coated copper grid. The grid was then dried under a UV lamp. The particles were then seen in a TEM (JEOL FX 2000, Japan).

The sintered samples were seen in a reflected light optical microscope (Carl Zeiss Germany) to determine the extent of porosity. For this, the samples were polished to a mirror finish by polishing with 1 μm alumina powder, followed by 0.3 μm alumina. The polished samples were cleaned by ultrasonication for 10 minutes in triple distilled water. The samples were then washed in acetone several times and dried in an oven at 80°C and stored under vacuum until observation.

2.2.2.4 *Density of Sintered Samples :*

The sintered density of the samples was measured on the polished samples by Archimedes method using xylene as the immersion liquid. The sample was thoroughly cleaned by ultrasonication in triple distilled water followed by cleaning in acetone. The cleaned sample was dried at 110°C for 24 hours and cooled in a desiccator. The dried sample was first weighed in air (W_1). The sample was then tied with a fine copper wire and suspended freely in a beaker containing xylene. The entire assembly was then placed in a vacuum desiccator and evacuated and held at 0.1 torr for atleast an hour to ensure impregnation of xylene into the pores of the sample. The sample was then weighed while suspended in liquid (W_2), and finally the weight of the sample was taken while suspended in air (W_3). The room temperature was noted during the experiment and the density of the xylene was corrected according to the room temperature. The sintered density

was calculated from the following relation:

$$\text{Sintered density} = \frac{W_1}{W_3 - W_2} \times \rho_{xylene} \qquad (2.2)$$

2.2.2.5 *Phases and Crystallite Size by X-ray Diffraction :*

As the primary interest was in obtaining stabilized ZrO_2 the phases in the calcined and the sintered samples from powders prepared by different routes were first compared. Phases were determined by x-ray diffraction using an X-ray diffractometer (Reich Seifort Isodebyeflex, 2002, Germany) with Ni-filtered Cukα radiation and curved graphite monochromator.

The volume fraction of the monoclinic phase, ν_m was obtained using the relation [18, 19, 20].

$$X_m = \frac{I_m(11\bar{1}) + I_m(111)}{I_m(11\bar{1}) + I_m(111) + I_t(111)} \qquad (2.3)$$

and

$$\nu_m = \frac{P\ X_m}{1 + (P-1)\ X_m} \qquad (2.4)$$

Here $I_m(11\bar{1})$, $I_m(111)$ and $I_t(111)$ are the integrated peak intensity of $(11\bar{1})$ peak of monoclinic, (111) peak of monoclinic and (111) peak of tetragonal phase respectively, X_m is the ratio of the x-ray peak intensity of the monoclinic phase to the total phase (i.e. monoclinic + tetragonal + cubic), and P is given by the following relation:

$$P = \frac{R(111)_t}{R(11\bar{1})_m + R(111)_m} \qquad (2.5)$$

where R is a factor which is given by the relation:

$$R = \left(\frac{1}{V^2} \right) \left[|F^2| P \left(\frac{1 + \text{Cos}^2 2\theta}{\text{Sin}^2 \theta + \text{Cos}\ \theta} \right) \right] e^{-2m} \qquad (2.6)$$

where, V = volume of unit cell

$|F|$ = structure factor

P = multiplicity factor

$\left(\frac{1 + \text{Cos}^2 2\theta}{\text{Sin}^2 \theta + \text{Cos}\ \theta} \right)$ = Lorentz Polarization factor

ϵ^{-2m} = temperature factor (a function of θ).

The value of P is usually between 1.29 and 1.34 [18,19]. In our case, we have used P = 1.31, which is the value for Y-TZP [20].

The crystallite size was calculated by measuring the broadening of x-ray peaks due to small crystallites and using the Scherrer formula [21]

$$t = \frac{0.9\ \lambda}{B\ \text{Cos}\ \theta} \qquad (2.7)$$

where t = crystallite size (Å)

λ = wavelength of x-ray

B is the corrected line broadening given by

$$B = \sqrt{B^2_{\text{sample}} - B^2_{\text{standard}}}$$

where B_{sample} and B_{standard} are the full width at half maximum for the sample and the standard (silicon) respectively.

2.3 *RESULTS AND DISCUSSION*

2.3.1 Thermal Analysis

The DTA Plot for HSG powder is shown in Fig. 2.2 and that for CP powder in Fig. 2.3. The CP powders distinctly show only an exothermic peak at 467°C which is due to amorphous-crystalline transition. There is a broad and shallow endothermic peak between

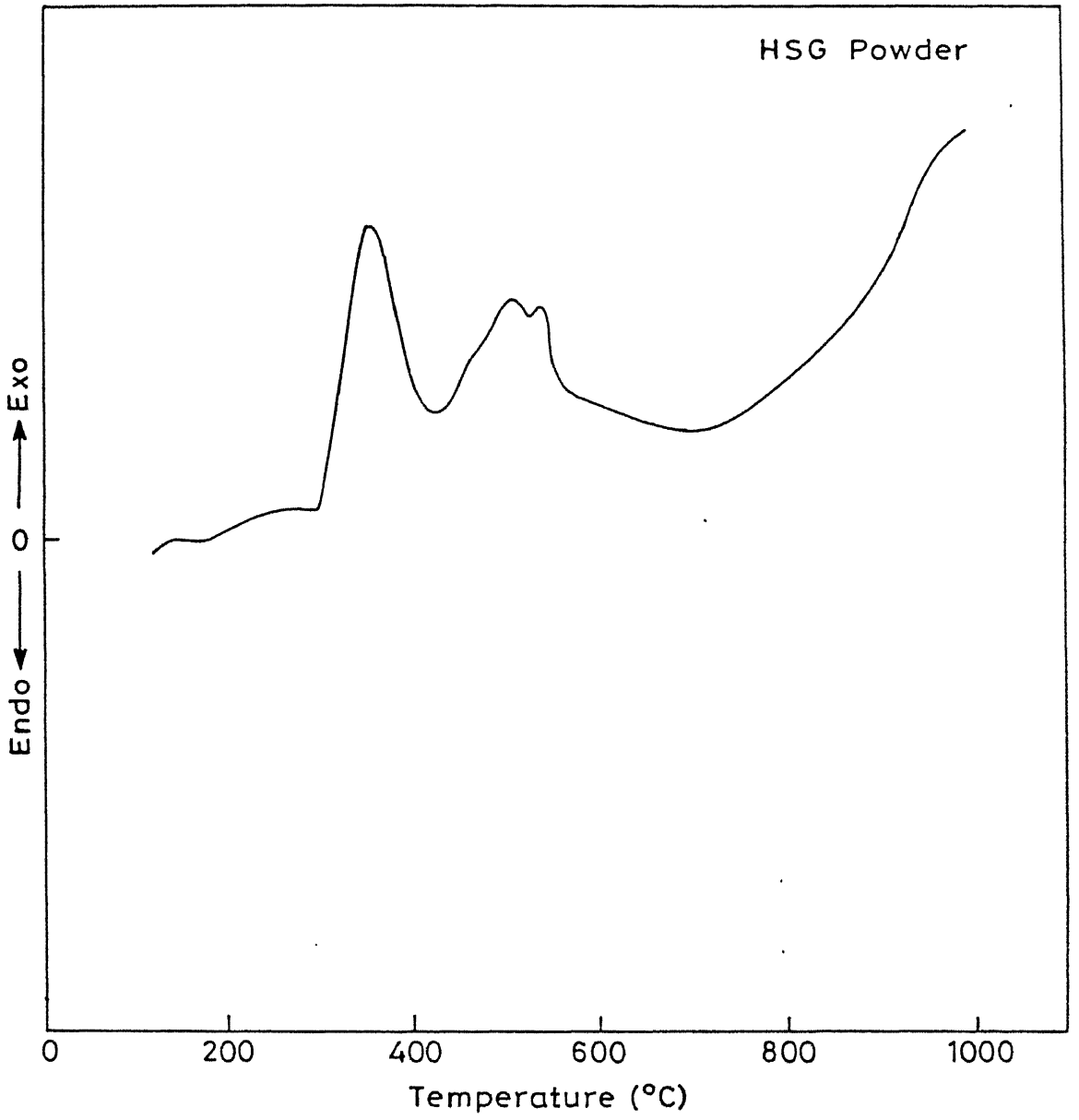

Fig. 2.2 DTA thermogram of HSG powder.

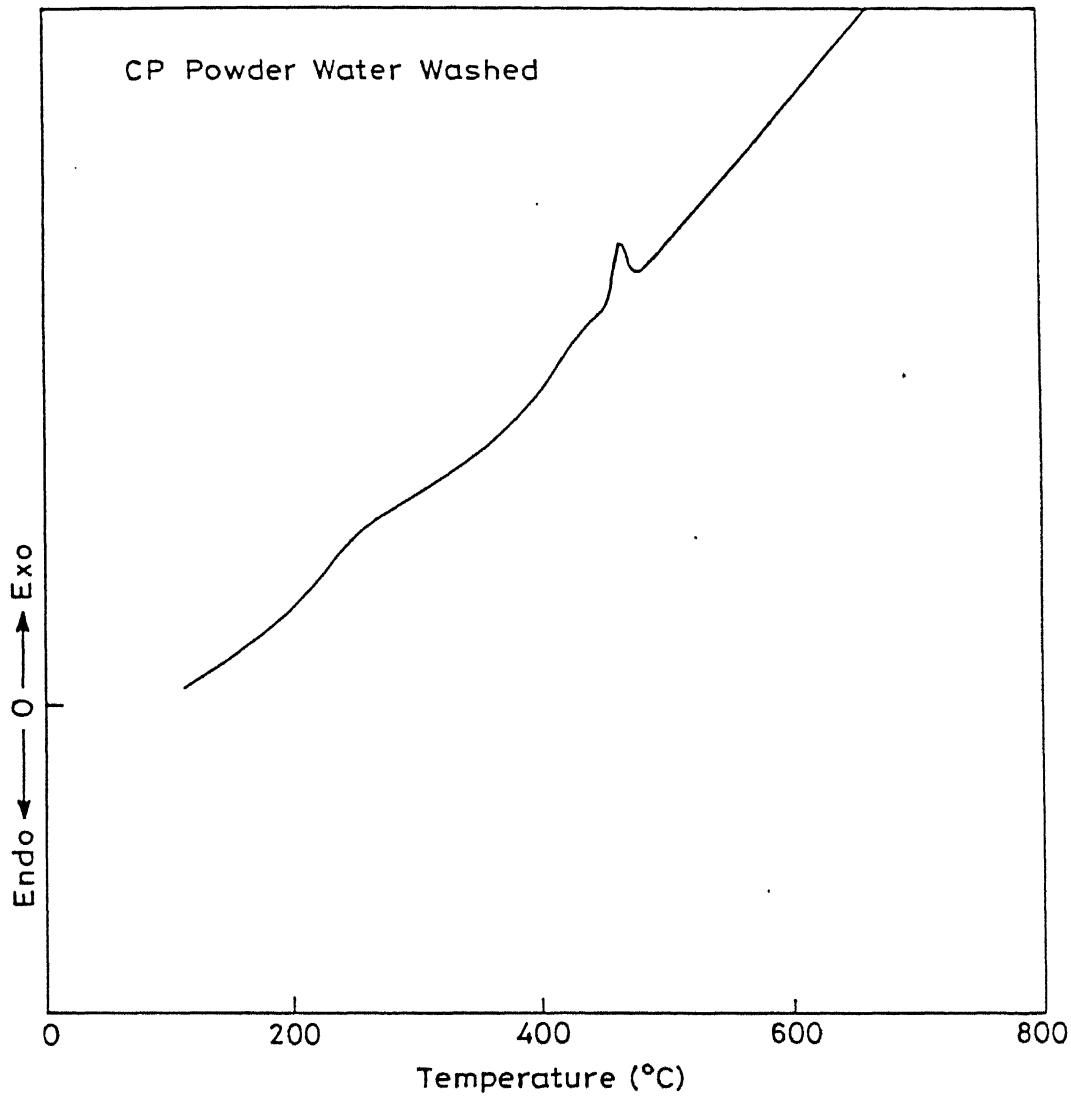

Fig. 2.3 DTA thermogram of water washed CP powder.

100 to 240°C which is due to removal of adsorbed water. There is no other noteworthy feature.

The DTA thermogram for the HSG powder is very different. The broad endothermic peak between 150° - 250°C is quite clear and is due to removal of water as in the case of the CP powder. A broad peak, which is clearly made up of at least three different peaks, is obtained between ~ 470 - 550°C. This is most probably due to the crystallization and associated reaction. In the HSG method Gd_2O_3 is added as oxide powder while ZrO_2 is obtained from the alkoxide sol. Thus the crystallization of amorphous ZrO_2 are likely to be spread over a range of temperature, resulting in multiple broad peak as observed.

An additional feature observed in the HSG powders is a broad exothermic peak at ~ 359°C. This peak is not present in the CP powders. It appears to be related to the presence of organics in the HSG powder. It is most probably due to the removal of propylene which is produced from the isopropanol used in the preparation of powders as well as removal of other organics which are residue from the alkoxide. Kaliszewski and Heuer have also observed a similar behaviour in their ethanol washed powders and have attributed it to removal of ethylene from ethanol.

In view of the results of DTA, the calcination temperature for the HSG and CP powders were fixed at 700°C. The powders calcined at 700°C for short times had a blackish colour indicating that the removal of residual carbon is not complete. After calcination for 4 hours at 700°C, the powders became fully white with no black tinge. Hence, the calcination conditions were for 4 hours at 700°C.

2.3.2 Phases

Powders prepared by MO method and calcined for 2 hours at 1000°C did not show any t phase. Only a trace amount of t phase (corresponding to amount less than 5 vol%) was observed in 5 and 8 mol% samples calcined for 8 hours. When these latter samples (i.e. calcined for 8 hours) were sintered they showed a maximum t phase of 44 vol % for 8 mol % Gd_2O_3 samples This is believed to be due to comparatively larger particle sizes ($\geq$ 1 μm) used and inhomogeneous mixing inherent to the MO method.

Fig. 2.4 shows the diffractograms of the calcined and sintered samples of ZrO_2-2 mol% Gd_2O_3 prepared by HSG method. Here it has been possible to retain some tetragonal phase even in the calcined (700°C/4 hours) samples. The volume fraction of tetragonal phase in the calcined samples increases with increasing Gd_2O_3 content, but some monoclinic phase persists even in 8 mol% samples. It has been reported that 3 mol% Gd_2O_3 is required for complete stabilization of the tetragonal phase in ZrO_2 [22]. Hence under the calcination conditions used here, the Gd_2O_3 does not go uniformly in solution in ZrO_2. Sintering at high temperature (1400°C/2 hours) is expected to promote uniform distribution of Gd_2O_3 in ZrO_2. However, even though the amount of t phase increases some of the tetragonal phase transforms to monoclinic on cooling due to large particle size thus reducing the amount of the t phase retained (Fig. 2.4b).

Of the three methods employed only the CP route leads to complete stabilization of the t phase in all the compositions studied (viz. 2 to 8 mol % Gd_2O_3). X-ray diffractograms of the calcined and sintered samples prepared from this method are shown

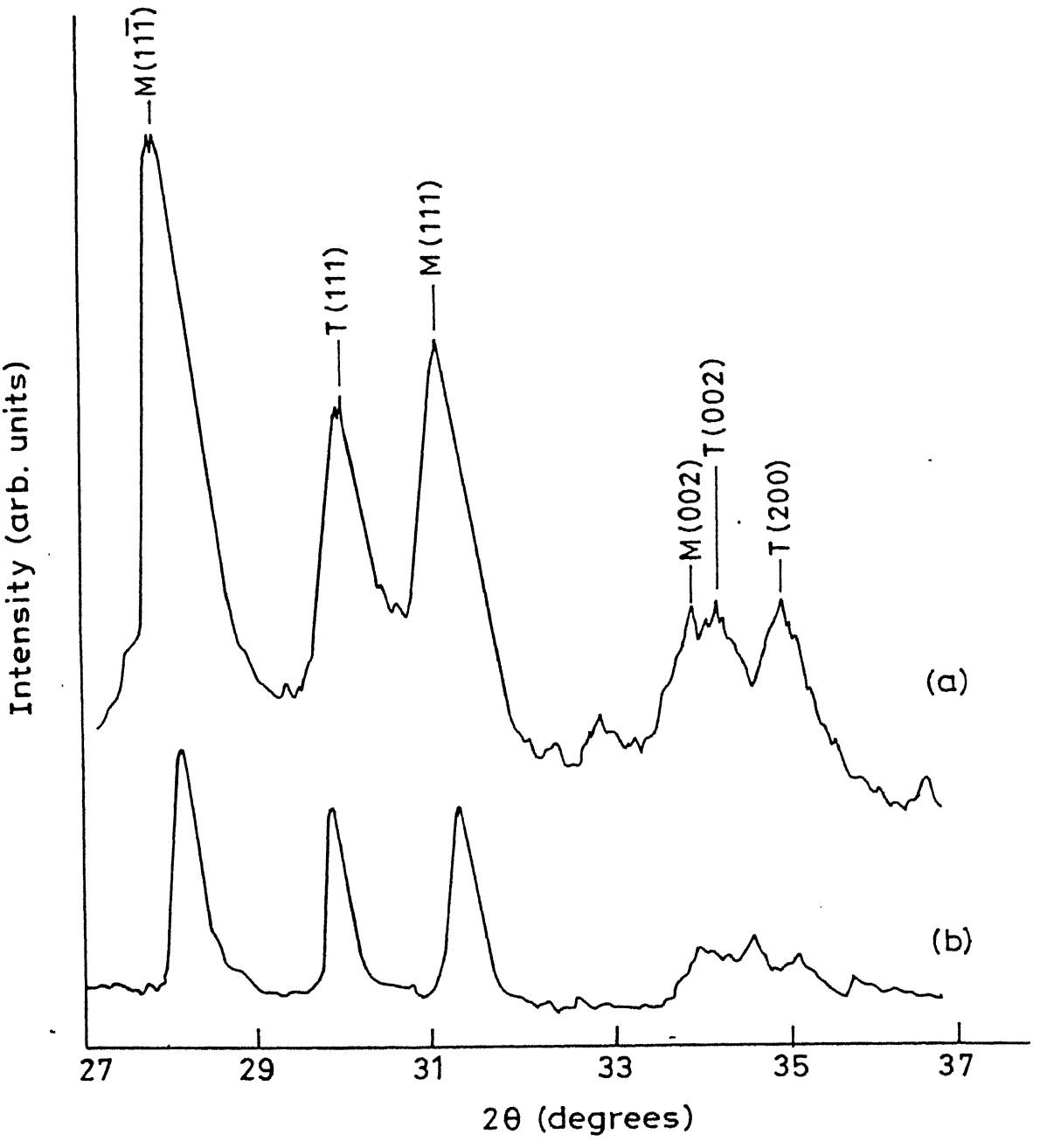

Fig. 2.4 X-ray diffractogram of ZrO_2-$2Gd_2O_3$ alloy prepared by HSG route, (a) calcined powder (700°C/4 hrs), (b) sintered sample (1400°C/2 hrs.).

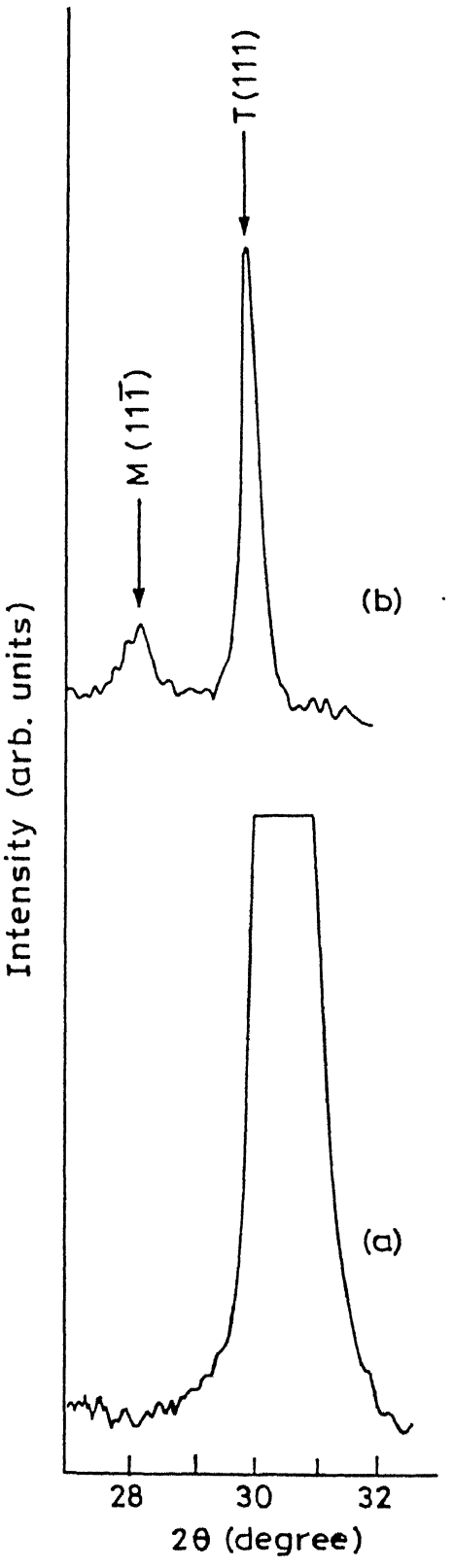

Fig. 2.5 X-ray diffractogram of ZrO_2-$2Gd_2O_3$ alloy prepared by CP route, (a) calcined powder (700°C/4 hrs), (b) sintered sample (1400°C/2 hrs.).

for ZrO_2-3 mol% sample in Fig. 2.5. All the compositions show complete stabilization of high temperature phase after

Table 2.3

Volume Fraction (t+c) Phase in the Calcined and Sintered Samples Prepared by Different Methods

Composition (Mol% Gd_2O_3)	Volume Fraction (t+c) Phase					
	Calcined powder			Sintered pellet (1400°C/2h)		
	MO (1000°C /8 hrs)	HSG (700°C /4 hrs)	CP (700°C /4hrs)	MO	HSG	CP
2	0	0.22	1	0.16	0.25	0.9
3	0	0.26	1	0.19	0.35	1
5	trace	0.52	1	0.28	0.55	1
8	trace	0.62	1	0.44	0.87	1

calcination. However, a small amount of m phase forms on sintering lower Gd_2O_3 (2 mol%) containing samples. Fig. 2.6 shows the graphical representation of (t+c) phase fraction after sintering prepared by all the three routes. The peaks are very broad due to fine crystallite size of the powder (as discussed later) and hence it is not possible to detect t and c phases separately, particularly in the low angle region ($2\theta = 27^\circ - 32^\circ$). However, it is expected that only tetragonal phase will be stabilized in samples with the lower Gd_2O_3 contents (i.e. 2 and 3 mol %), while higher (i.e. 5 and 8 mol %) Gd_2O_3 contents may lead to the stabilization of both t and c phases. In the sintered sample, 2 mol% composition shows small amount of m phase while 3 and 5 mol % sample show a definite broadening on the higher angle side of the peaks thus indicating the possibility of a second phase, which may be a cubic phase (Fig. 2.7). However, at 8 mol% sharp cubic peaks appear indicating major fraction of this sample is cubic phase.

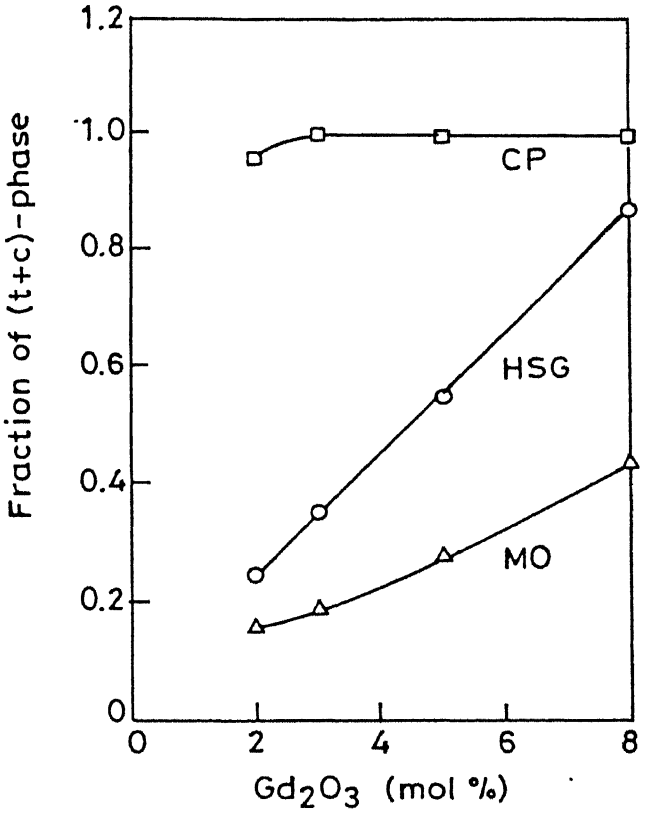

Fig. 2.6 Amount of t-phase in the sintered samples prepared by different methods.

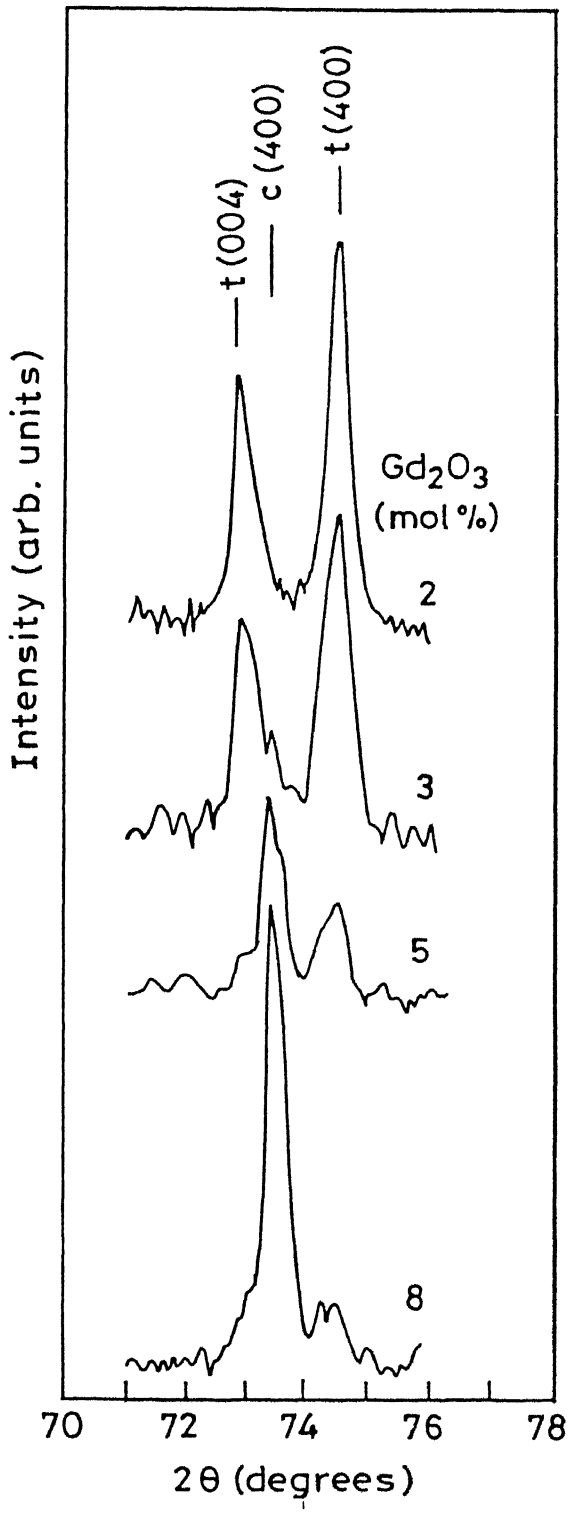

Fig. 2.7 High angle X-ray diffractogram of 2,3,5,8 mol% sample showing c phase at higher Gd_2O_3 content.

Since the tetragonal phase could be fully stabilized only by the coprecipitation method the powders prepared by this method were further characterized in detail. Results of these characterizations are presented below.

2.3.3 Density

A high sintered density is essential for any technological application of ZrO_2 ceramics such as in structures, solid electrolytes, oxygen sensors etc. However, the sintered densities from all the three methods viz. MO, HSG, and CP were poor (Fig. 2.8). For compositions studied, the maximum relative density was only about 0.88 of the theoretical (6.16 gms/cc) for ZrO_2-3 mol % composition in the powders prepared by CP method. The density decreased to lower values on either side of this composition reaching a minimum density of 77% for ZrO_2-8 mol% Gd_2O_3 samples. The samples prepared by HSG method and MO method recorded still lower values of density.

The poor density in these samples may be due to one or more of the following reasons: improper calcination, inadequate sintering temperature and/or agglomeration in the powder. The ZrO_2 ceramics are generally sintered at higher temperature but the powders prepared by coprecipitation or similar method can often be sintered well at 1400°C. However, as the results reflect this temperature may not be sufficient for complete densification. The other factors e.g. calcination and agglomeration are discussed in Parts B and C.

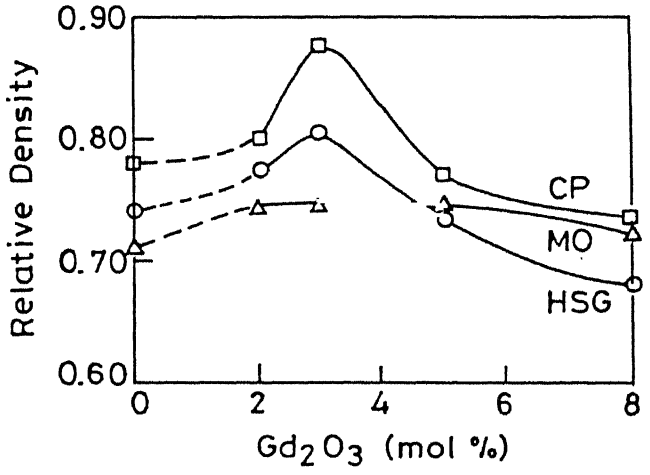

Fig. 2.8 Effect of processing route on the sintered density of ZrO_2 -$2Gd_2O_3$ samples.

2.4 *SUMMARY AND CONCLUSIONS (PART A)*

ZrO_2-Gd_2O_3 powders having different amount of Gd_2O_3 have been prepared by three different methods - mixed oxide (MO), hybrid sol-gel (HSG) and coprecipitation (CP). No t or c phase could be retained in the MO powders after calcination and only upto 44 vol % t phase was obtained in the 8 % Gd_2O_3 samples after sintering at 1400°C for 2 hours. In the HSG method it was possible to retain upto 62% tetragonal phase after calcination and upto 87% in the sintered (1400°C/2 hrs.) samples.

Among the three methods, only in the CP method it was possible to completely retain the high temperature t or c phase after calcination as well as after sintering. However, the density after sintering was poor for all the three methods with maximum density reaching only upto 88% for ZrO_2-3 mol% Gd_2O_3 samples prepared by CP method. Further efforts, as discussed in parts B and C were therefore directed towards improving the sintered density.

PART B

EFFECT OF CALCINATION AND SINTERING TEMPERATURE ON SINTERED DENSITY

2.5 *INTRODUCTION*

As found in part A, although the coprecipitated powders are able to stabilize the t phase in the sintered samples, their sintered density is low. As a first step, it was thought that it might be possible to improve the density by increasing the calcination and sintering temperatures. The possibility of incomplete removal of carbonaceous matter always exists in powders prepared from organic precursors (e.g. alkoxides). This may be overcome by increasing the calcination temperature.

Higher calcination temperature is also expected to homoge the distribution of Gd_2O_3 in ZrO_2. Secondly, ZrO_2 ceramics are usually sintered at higher temperature (1500°C to 1600°C) or not pressed/HIPed. Hence it may also be possible to improve the density by sintering at a higher temperature. Accordingly, it was decided to carry out additional experiments involving higher calcination and sintering temperatures.

As only the coprecipitated powders yielded fully stabilized ZrO_2, these additional calcination and sintering studies were carried out only on them.

2.6 *EXPERIMENTAL*

2.6.1 Variation in the calcination Conditions

A single batch of CP ZrO_2-$2Gd_2O_3$ powder was prepared using the method described earlier (section 2.2.1.3). The batch was divided into four parts for calcination at four different

temperatures, viz. 700°C, 800°C, 900°C and 1000°C. The time of calcination was 4 hours for each sample. The calcined powders were characterized with respect to their specific surface area, crystallite size and compaction behaviour. The calcined powders were uniaxially compacted at 200 MPa and sintered at 1400°C for 2 hours. The sintered pellets were characterized for sintered density, phase and microstructure.

2.6.2 Variation in the Sintering Conditions

To investigate the effect of sintering temperature on the sintered density of ZrO_2-Gd_2O_3 alloys, a similar batch of CP ZrO_2-$2Gd_2O_3$ powder was prepared. The powder was calcined at 700°C for 4 hours, compacted at 200 MPa and sintered at 1400°C/ 2 hrs., 1500°C/ 2 hrs, and 1600°C/ 1 hr. After sintering, the samples were characterized with respect to phase and density.

2.7 *RESULTS AND DISCUSSIONS*

2.7.1 Effect of Calcination Temperature

Table 2.4 lists the specific surface area of powder after calcination at different temperatures. Increasing the calcination temperature from 700°C to 1000°C decreases the specific surface area from 32 to 12 m^2/gm. At the same time, the crystallite size derived from x-ray line broadening as well as from specific surface area increases with increasing calcination temperature. The value of crystallite size as derived from x-ray line broadening are smaller and are more reliable because the BET derived size is apparently increased due to any bridging of the crystallites.

Fig. 2.9 shows the pressure vs. relative density plot on compaction of above powders. While "fill density" increases

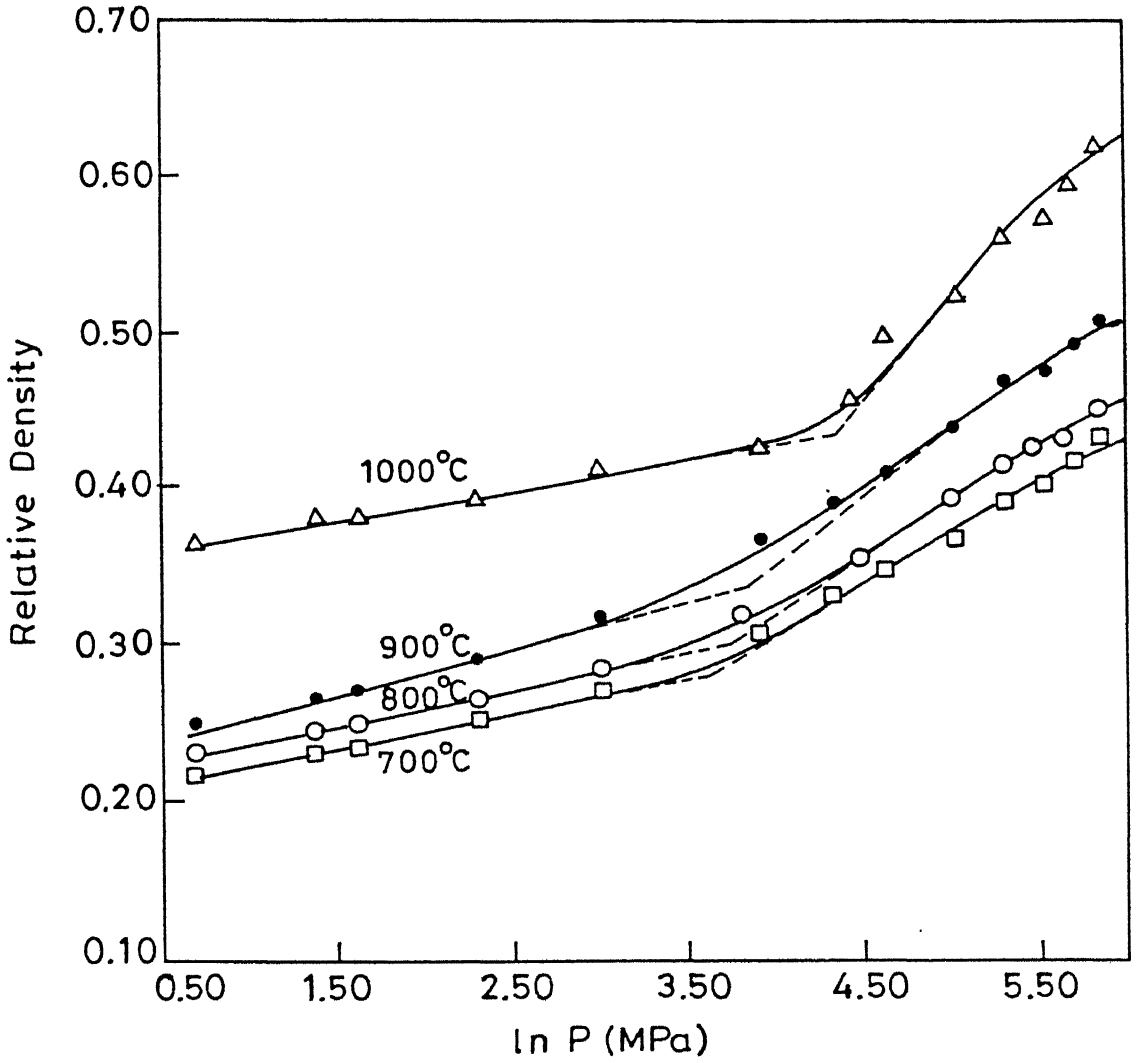

Fig. 2.9 Compaction behaviour of CP ZrO_2 -2Gd_2O_3 powders calcined at different temperatures.

significantly with increasing calcination temperature, the agglomerate strength (which is the point corresponding to inter section of the two linear parts of the curve) also increases from 36 to 75 MPa (Table 2.4).

Table 2.4

Effect of calcination temperature on specific surface area, crystallite size and agglomerate strength of ZrO_2-$2Gd_2O_3$ alloys

Calcination Temp (°C)	Sp. Surface area (m^2/gm)	Crystallite size (nm)		Agglomerate Strength (MPa)
		BET	X-ray	
700	32	30	7	36
800	22	44	9	42
900	19	51	11	48
1000	12	81	13	75

The changes in the density and in the phases of the sintered samples obtained from powders calcined at different temperatures are shown in Fig. 2.10 and Table 2.5.

Table 2.5

Effect of Calcination Temperature on Sintered Density and Phases of ZrO_2-$2Gd_2O_3$ Samples obtained from CP Powders (Sintered 1400°C/2 hours)

Calcination Temp (°C)	Relative Density	Volume Fraction Phases	
		m	(t+c)
700	0.80	0.06	0.94
800	0.64	0.32	0.68
900	0.61	0.37	0.63
1000	0.42	0.44	0.56

The steady decrease in relative density of the sintered samples calcined at progressively higher temperature is due to the particle aggregation as shown by TEM micrographs (Fig. 2.11). We

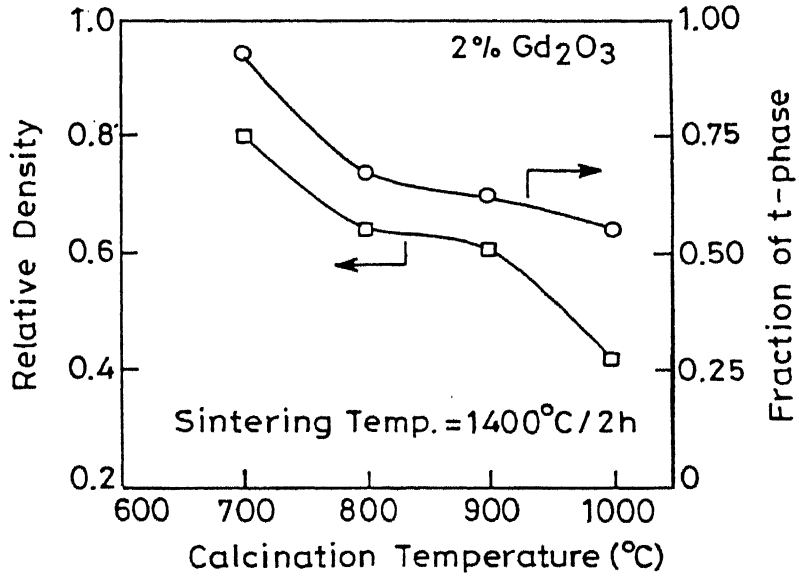

Fig. 2.10 Effect of calcination temperature on the density and amount of t-phase in the sintered ZrO_2 -$2Gd_2O_3$ alloys.

have seen that higher calcination temperature gives powder having low specific surface area and higher agglomerate strength (Table 2.4). When these aggregated powders are sintered, porosity results due to differential sintering producing low density. Also these aggregates sinter to form large particle, larger than the critical size for tetragonal phase retention. Therefore, the amount of t phase after sintering decreases. This behaviour is reflected in optical micrographs of the polished surfaces of above mentioned sample (Fig. 2.12). The black areas are the pores and the white patches are the sintered aggregates. As can be seen from the micrographs, with increasing calcination temperature these while patches increase both in number and size (Fig. a, b, c). Due to differential sintering, those aggregates sinter faster than the rest of the matrix thus producing inhomogeneous microstructure resulting in higher porosity (bigger black patches) and loss of density. Also due to larger aggregates the particle size increases beyond the critical size and this results in lower tetragonal phase on sintering.

2.7.2 Effect of Sintering Temperature

Table 2.6 and Fig. 2.13 show the density and phases (measured on the polished surface) after sintering at different temperatures.

As is seen from Fig. 2.13 and Table 2.6, sintering at higher temperature does not help in achieving higher sintered density. At the same time, it reduces the amount of retained tetragonal phase and at the highest sintering temperature used (i.e. 1600°C), a small amount of zirconate phase also forms (Fig. 2.14). Higher sintering temperature increases the grain size beyond critical

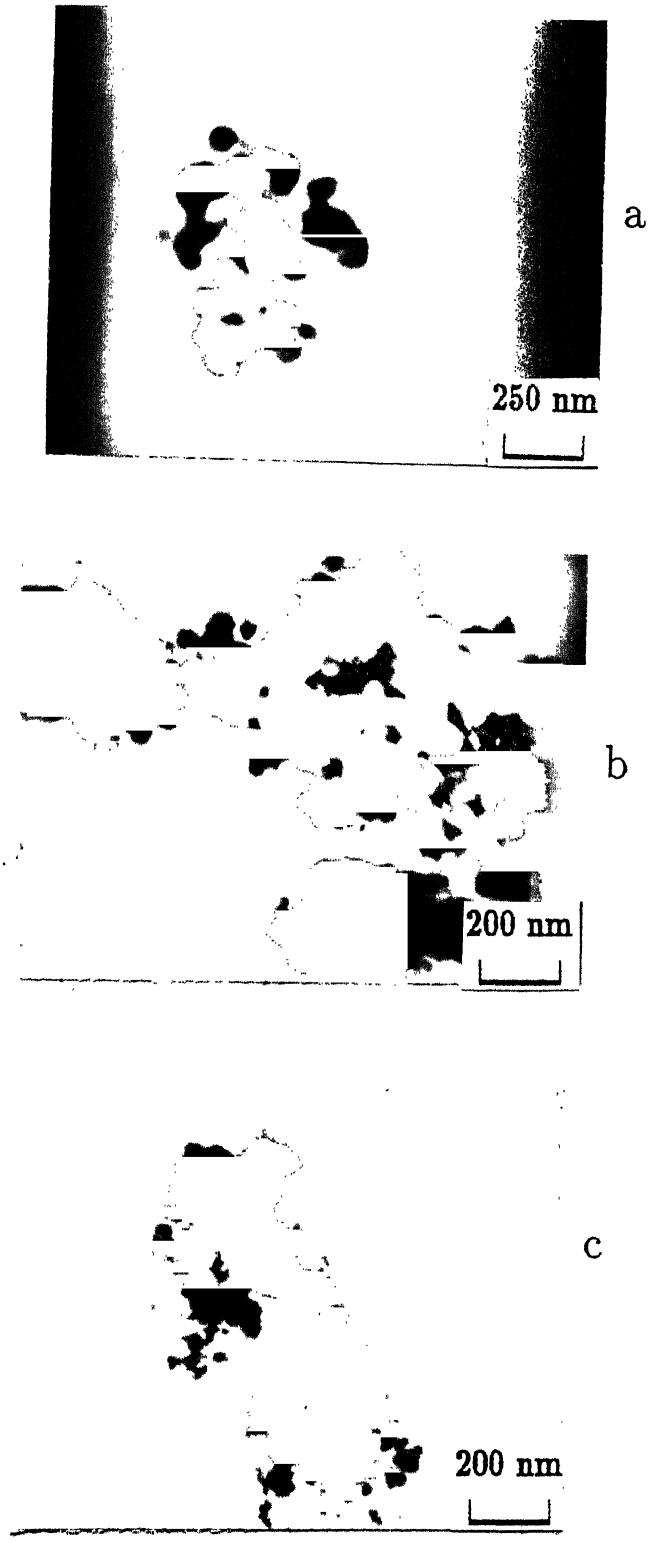

Fig. 2.11 TEM pictures of calcined powders after calcination for 4 hours at (a) 700°C, (b) 900°C and (c) 1000°C, showing increased degree of agglomeration.

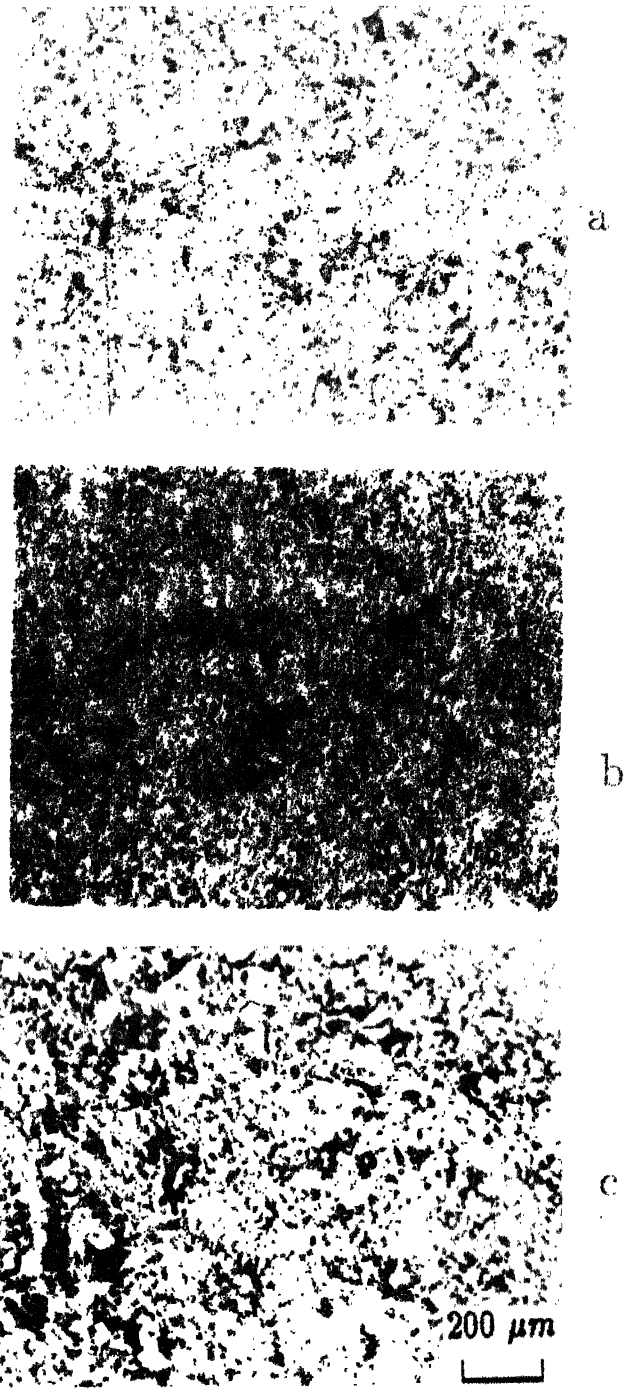

Fig. 2.12 Optical micrographs of polished surfaces of samples prepared from powders calcined at (a) 700°C, (b) 900°C, (c) 1000°C.

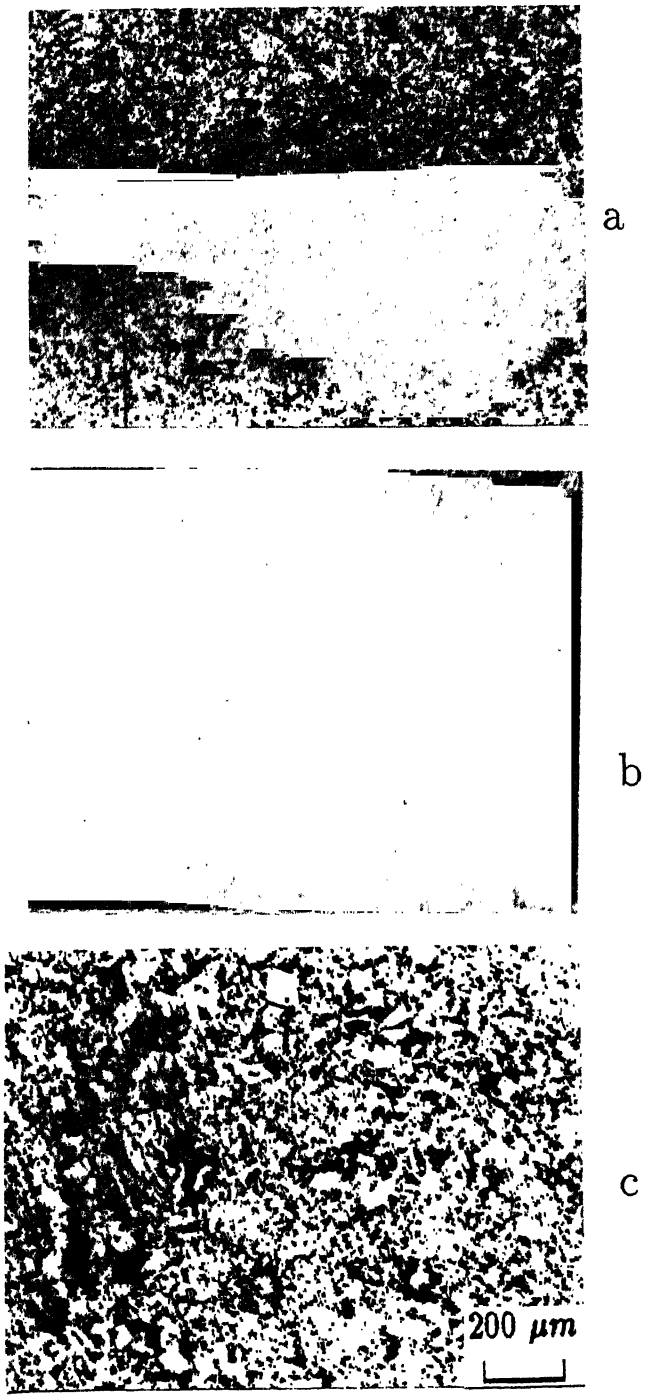

Fig. 2.12 Optical micrographs of polished surfaces of samples prepared from powders calcined at (a) 700°C, (b) 900°C, (c) 1000°C.

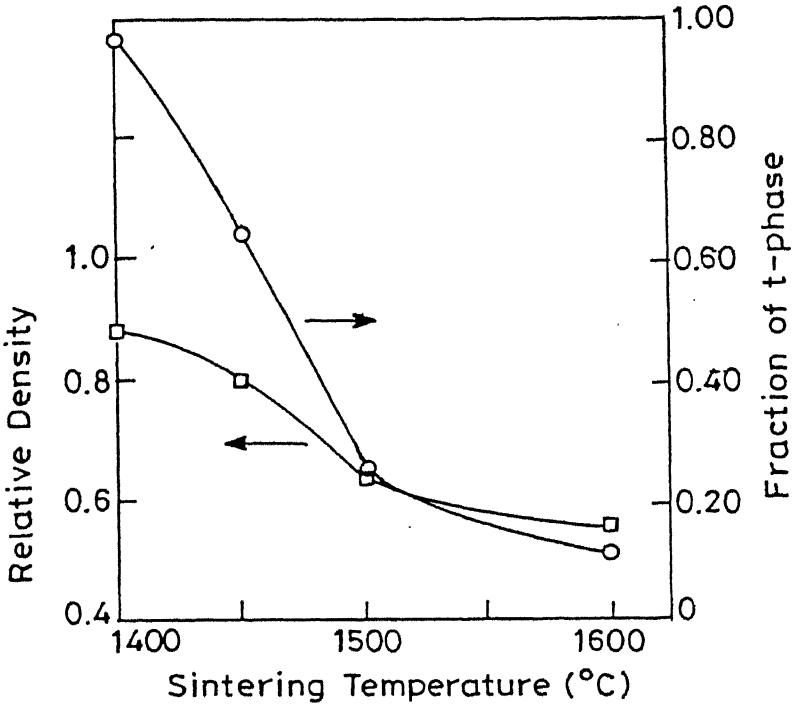

Fig. 2.13 Relative density and the amount of tetragonal phase in ZrO_2-$2Gd_2O_3$ alloys sintered at different temperatures.

Table 2.6

Effect of Sintering Temperature on Phase and Density of ZrO_2-$2Gd_2O_3$ Alloys (Calcined 700°C/4 hrs.)

Sintering Temp (°C)/ Time (hrs.)	Vol. Fract Phases		Relative Density
	m	(t+c)	
1400/2	0.04	0.96	0.88
1450/2	0.36	0.64	0.80
1500/2	0.75	0.25	0.64
1600/2	0.88	0.12	0.57

size, resulting in higher m phase in the sintered sample. The higher amounts of monoclinic phase leads to cracking of the samples as is seen in microstructure (Fig. 2.15). So neither higher sintering temperatures nor higher calcination temperatures are helpful in attaining higher sintered density in the CP samples. Higher calcination temperatures produce strong agglomerates which leads to low density as discussed earlier. Sintering at higher temperature also does not help in densification; on the other hand it reduces the amount of retained t phase due to increased grain size.

2.8 *SUMMARY AND CONCLUSIONS (PART B)*

In order to achieve high sintered density the CP powders were calcined at higher temperatures (800-1000°C). However, the treatment give highly agglomerated powders with a reduced specific surface area. The sintered samples using these powders had lower density than the powders calcined and lower t phase. Higher sintering temperature (1450-1600°C) also did not help. Rather it increased grain size thereby reducing the amount of retained t phase.

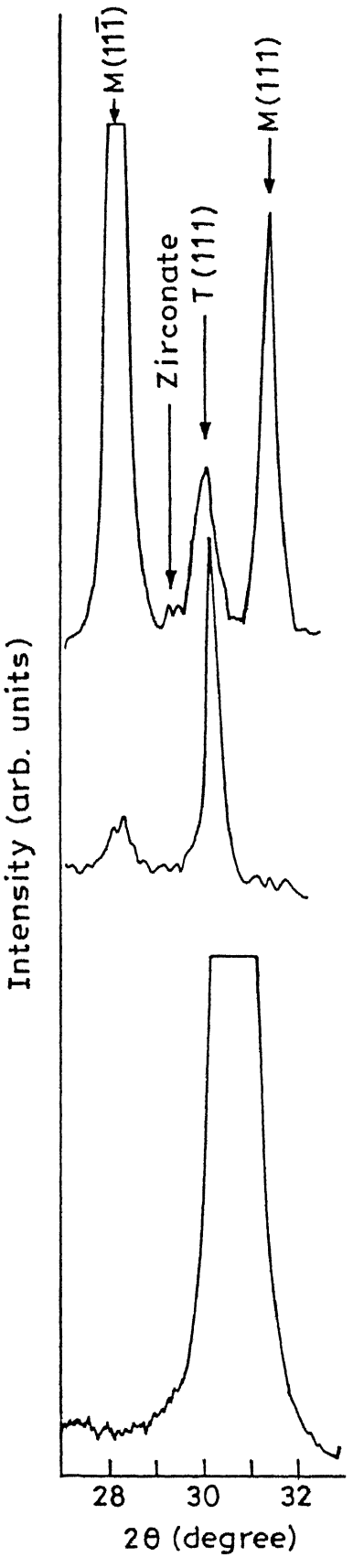

Fig. 2.14 X-ray diffractogram of ZrO_2-$2Gd_2O_3$ alloy sintered at 1600°C for 1 hour showing m and t - ZrO_2 along with zirconate phase.

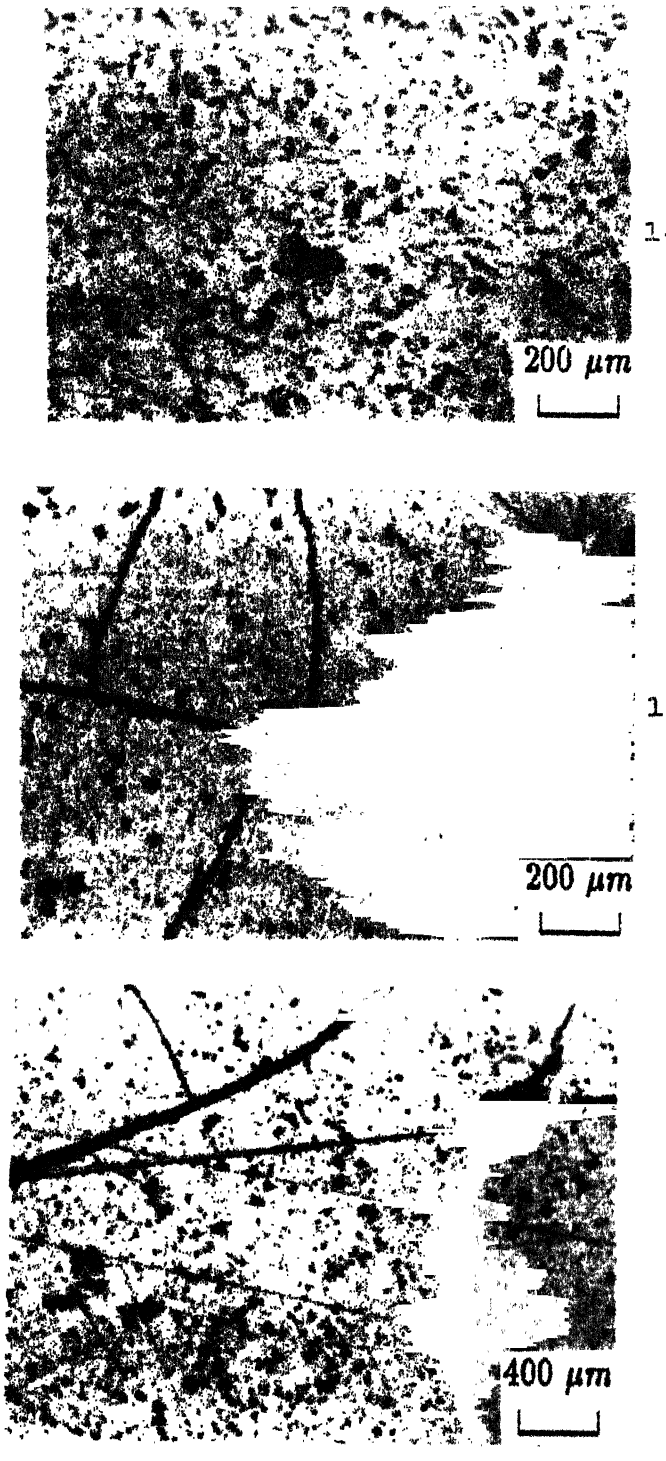

Fig. 2.15 Effect of sintering temperature on microstructure of ZrO_2-$2Gd_2O_3$ samples. Cracks appear in the samples sintered at higher temperatures due to extensive t ⟶ m transformation during cooling.

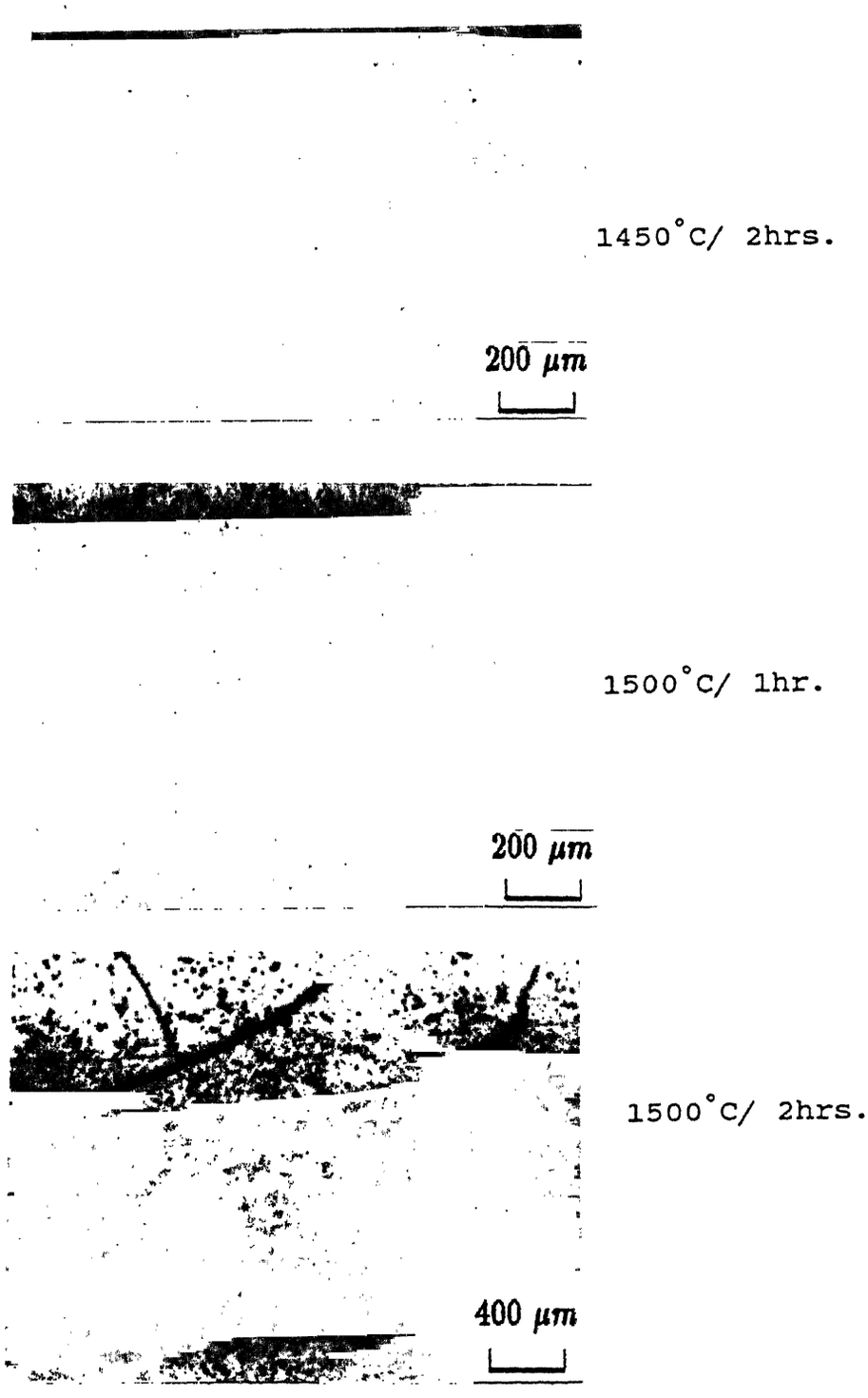

Fig. 2.15 Effect of sintering temperature on microstructure of ZrO_2-$2Gd_2O_3$ samples. Cracks appear in the samples sintered at higher temperatures due to extensive t ⟶ m transformation during cooling.

PART C

EFFECT OF PROPANOL WASHING ON SINTERED DENSITY OF ZrO_2- Gd_2O_3 ALLOYS

2.9 *INTRODUCTION*

During the drying of chemically prepared powders, very often strong bridges are formed between particles when they come in close contact due to capillary action produced during drying. Such bonding is usually due to the condensation of hydroxyl groups attached to the particles. It leads to agglomerated powders with poor sinterability. Many methods have been described in the literature for avoiding the formation of hard agglomerates during powder preparation. Some of these are the hot kerosene method [23], citrate synthesis [24], alkoxide synthesis [8] and Haberko's chloride synthesis followed by alcohol washing [23]. All of these techniques are useful in producing softly agglomerated powders. In particular alcohol has been used to control agglomeration during washing of powders [25]. Some other solvents which are also used are benzene [10], hydrogen peroxide [26] acetone-toluene- acetone [27] etc.

The change in chemical bonding between particles on alcohol washing of hydrous zirconia was studied by Jones et al [28]. Washing the hydrous zirconia gel by methanol prior to calcination results in a change in the bonding of bridging and nonbridging hydroxo-groups. Jones et al. proposed that methanol is capable of selectively extracting non-bridging hydroxo groups and free water at ambient temperature. The removal of these nonbridging hydroxo groups results in the elimination of hard agglomerates by avoiding

the condensation reaction.

$$Zr\text{-}\ OH + HO\text{-}\ Zr \longrightarrow Zr\text{-}\ O\text{-}\ Zr + H_2O$$

Similarly, Kaliszewski et. al. [29] studied the effect of ethanol washing on the inhibition of hard agglomerate formation. Consistent with the result of Jones et al [28] they also found that ethanol washing prevents hard agglomerate formation by modifying the gel structure with the replacement of excess water by ethanol [Fig. 2.16] [30]. The presence of this excess water would have otherwise led to the formation of hard agglomerates by forming hydrogen bonds with the terminal hydroxy groups. Replacement of these hydroxyl groups by ethanol groups results in the formation of surface ethoxy group which being non terminal cannot form interparticle bonding. Moreover, the presence of these surface ethoxy groups prevents close approach of particles due to steric effects. During drying, on account of close proximity of hydrogen bonded particles in water washed powders removal of terminal hydroxy groups results in actual chemical bond formation preferentially between different particles in the powder yielding hard agglomerates. On the other hand, in ethanol washed powders since the particles are well separated due to steric effect removal of these terminal ethoxy groups prevents close of approach of particles (relative to water washed powders). In this case, the ethoxy groups are preferentially removed between neighbouring groups on the same powder particle. Thus it does not result in chemical bond formation between particles as in the water washed case. The mechanism is schematically illustrated in Fig. 2.17.

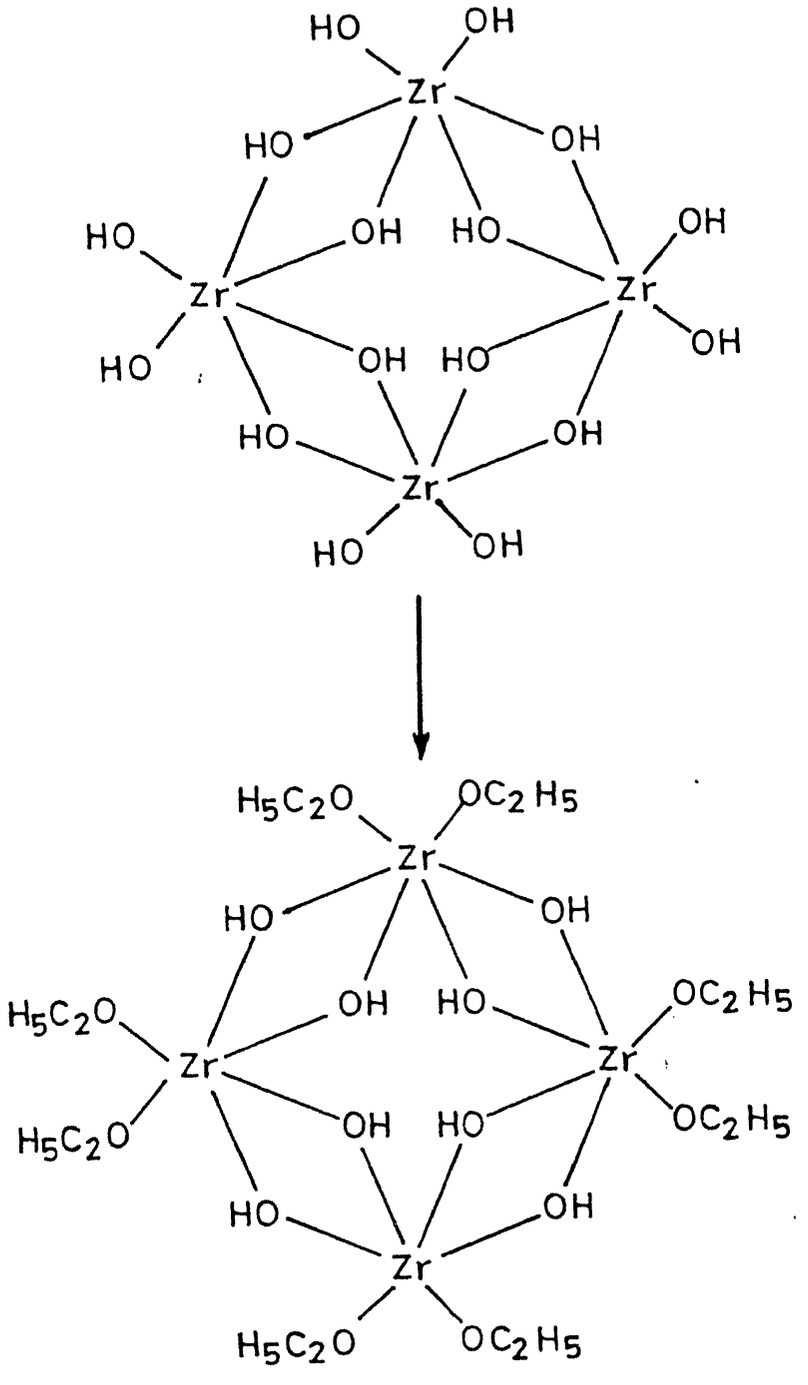

Fig. 2.16 Modification of ZrO_2 structure after washing the powder by (a) water and (b) ethanol [30].

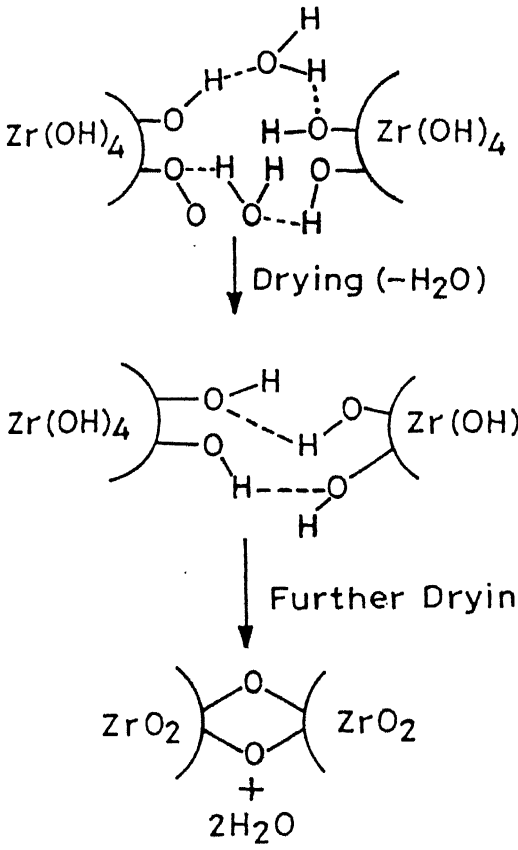

(a) Water washed ZrO_2 gel powder

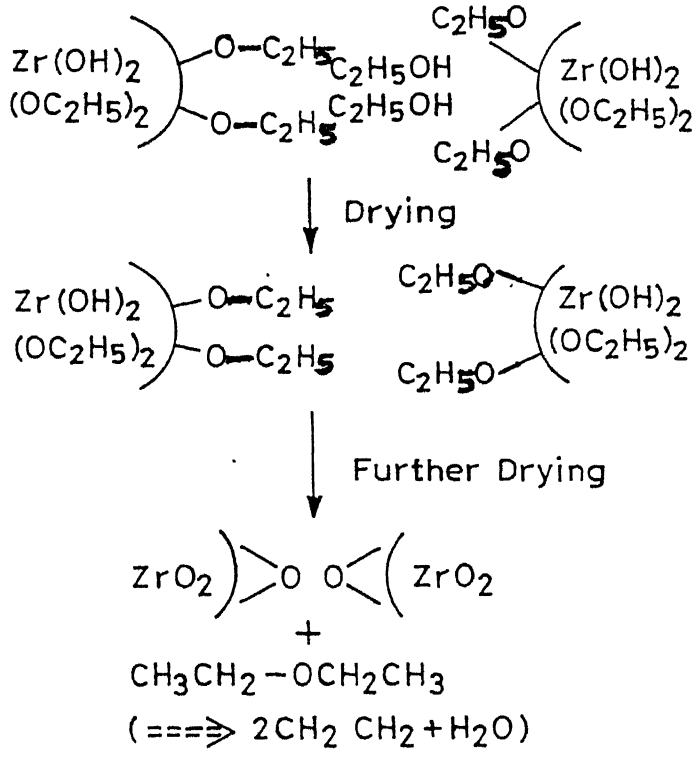

(b) Ethanol washed ZrO_2 gel powder

Fig. 2.17 Schematic illustration of the mechanism of agglomerate formation in ZrO_2 powders (a), water washed (b) ethanol washed [29].

Agglomerated powders sinter to poor density. In view of the above, in an attempt to improve the sintered density of the ZrO_2-Gd_2O_3 powders, it was decided to introduce an additional step of washing with a nonpolar liquid in the powder preparation by the CP method. The washing liquid selected is propanol due to its easy availability in our laboratory. This part of the work is described below.

2.10 *EXPERIMENTAL*

The coprecipitated ZrO_2-3 mol% Gd_2O_3 powders were prepared as described in section 2.2.1.3 except that after final washing with water, the precipitate was further washed six times with propanol using about 250 ml propanol for each washing. The precipitate was then dried at 80°C for 24 hours. The morphology of water washed and propanol washed powders before and after calcination was observed in TEM. To detect the presence of organic groups, the Fourier Transform Infrared Spectroscopy (FTIR) was carried out on dried powders. An FTIR spectroscope (Perkin Elmer, UK) was used with a dry air purge. Powder samples were purged for atleast 20 minutes prior to spectral collection.

Differential thermal analysis, specific surface area, crystallite size and compaction behaviour was studied as before. Similar characterizations were carried out for water washed powders when not already done.

The powders were calcined at 700°C for 4 hours as before. Sintering was carried out for 2 hours at five different temperatures - viz. 1000°C, 1100°C, 1200°C, 1300°C and 1400°C. The sintered density and microstructure were evaluated.

2.11 *RESULTS AND DISCUSSIONS*

2.11.1 Infrared Spectroscopy

The FTIR spectra show extensive interaction of wash solvents with the powder (Fig. 2.18). In the case of water washed powder (Fig. 2.18(a)) there is a very broad absorption band from 3800 cm^{-1} to 3000 cm^{-1} due to stretching of OH groups due to water on the particle surface. This is followed by two broad peaks at about 1580 cm^{-1} and 1350 cm^{-1} corresponding to CO_2 absorbed on the powder surface. Except for these peaks, the rest of the spectra is featureless. On the other hand, the spectra from the propanol washed powders is significantly different (Fig. 2.18(b)). This spectra also contains a very broad absorption band between 3800 cm^{-1} and 3000 cm^{-1} due to OH- stretching from water and propanol. This is followed by peak due to CO_2 stretching at 1580 and 1350 cm^{-1}. However, there are absorption bands also at 1070 cm^{-1} due to C-O stretching from chemically absorbed propanol; at 923 and 845 cm^{-1} due to CO stretching from physically absorbed propanol. Other propanol and propoxide groups could not be separated due to overlapping with water and CO_2 bands. Thus, washing the powders with propanol replaces the surface hydroxy groups with propanol and propoxy groups and based on the earlier discussion on agglomeration it can be said that the propanol washed powders are not likely to form agglomerates.

2.11.2 Differential Thermal Analysis

The DTA of the propanol washed CP powder is shown in Fig. 2.19. It differs from the DTA for water washed powders in that there are at least three extra peaks below the crystallization peak at 490°C these peaks occur at ~ 280°C, 311°C and 430°C

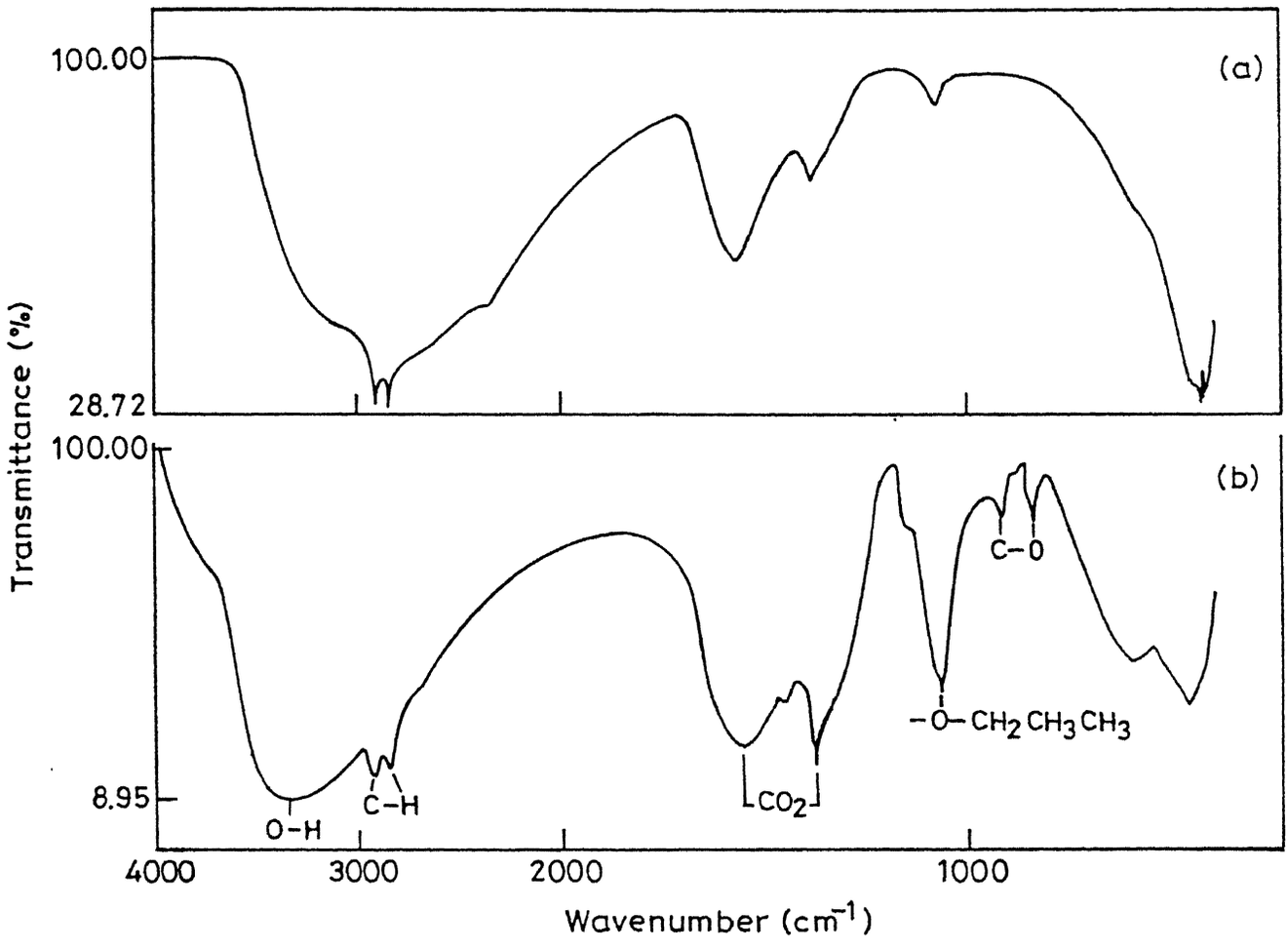

Fig. 2.18 FTIR spectra of (a) water washed, (b) propanol washed powders.

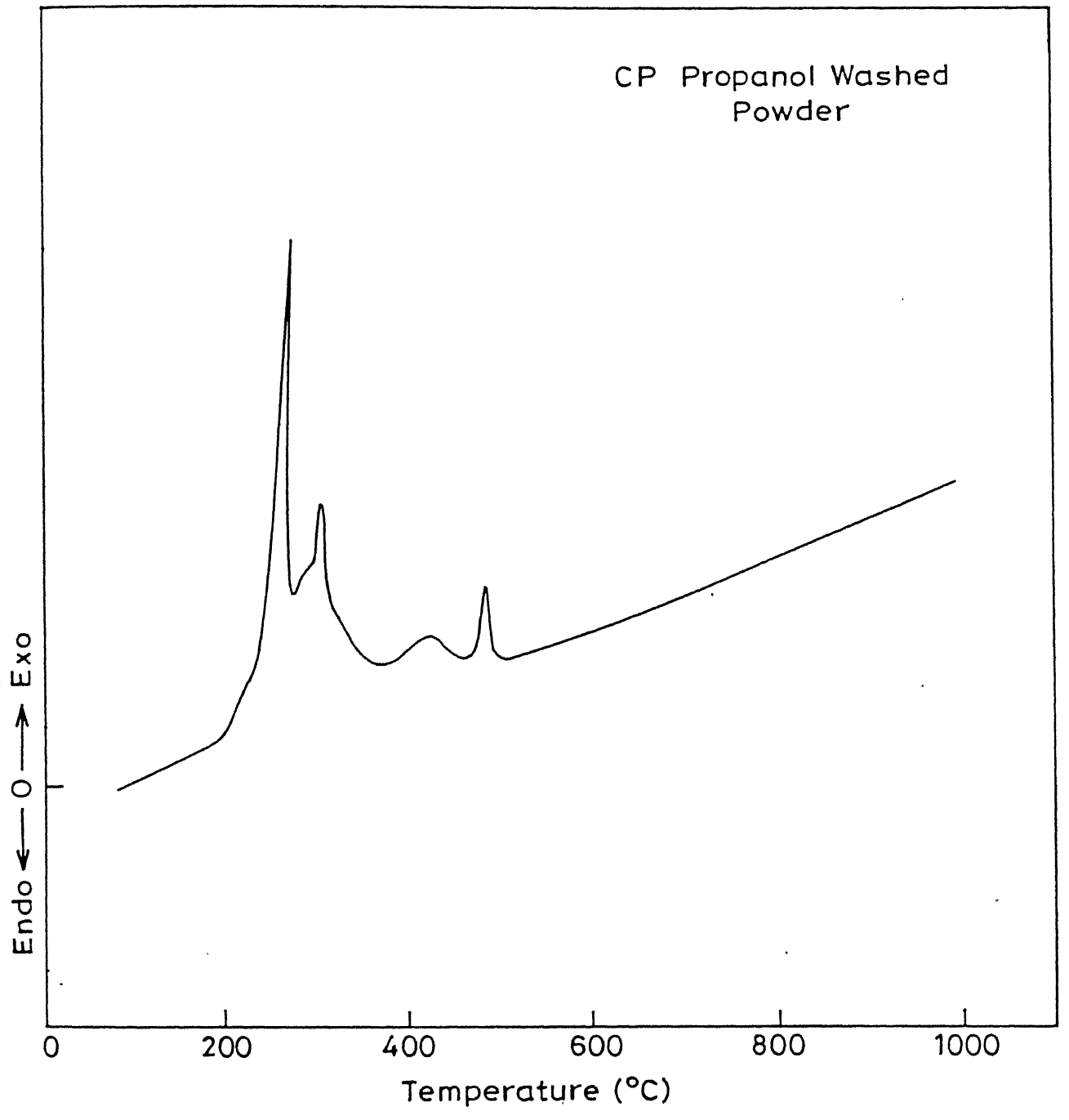

Fig. 2.19 DTA thermogram of propanol washed CP powders.

respectively. As mentioned earlier while discussing the DTA of the HSG powder, such peak are likely to result from the exothermal removal of organics. As these peaks are absent in the water washed powders, they can be attributed solely to the removal of the organic residues such as propylene gas from the propanol which was adsorbed on the ZrO_2 particles during washing of CP powders by propanol, However, the details of the underlying processes need further investigation.

2.11.3 Powder Morphology by TEM

TEM pictures (Fig. 2.20) reveal that the water washed coprecipitated uncalcined powders are agglomerated and dense while the propanol washed powders are "open" and unagglomerated, individual particles could also been in the latter case.

The powders were amorphous prior to calcination. After calcination, the selected area diffraction pattern (SADP) showed that the powders have become crystalline. Some agglomeration is present in propanol washed powders after calcination. The particle size in the water washed calcined powder is much larger than in the alcohol washed powder due to agglomeration [Fig. 2.21].

2.11.4 Specific Surface Area

The specific surface area for uncalcined, water washed powder is 90 m^2/gm, and it increased to 150 m^2/gm in propanol washed powders. The specific surface area after calcination was 32 m^2/gm and 40 m^2/gm for the above two cases respectively. The corresponding crystallite sizes, calculated from the surface area by assuming a sphere shaped crystallite are 30 nm and 24 nm respectively. These values are much higher than the value of 7 nm obtained for both the powder by x-ray line broadening.

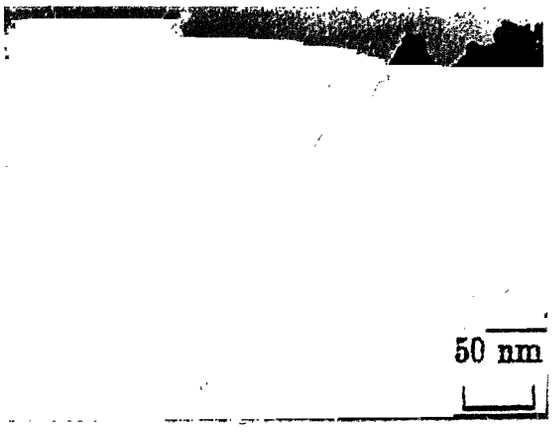

a

b

Fig. 2.20 TEM micrographs of 3 mol% Gd_2O_3 CP uncalcined powder, (a) water washed, and (b) propanol washed.

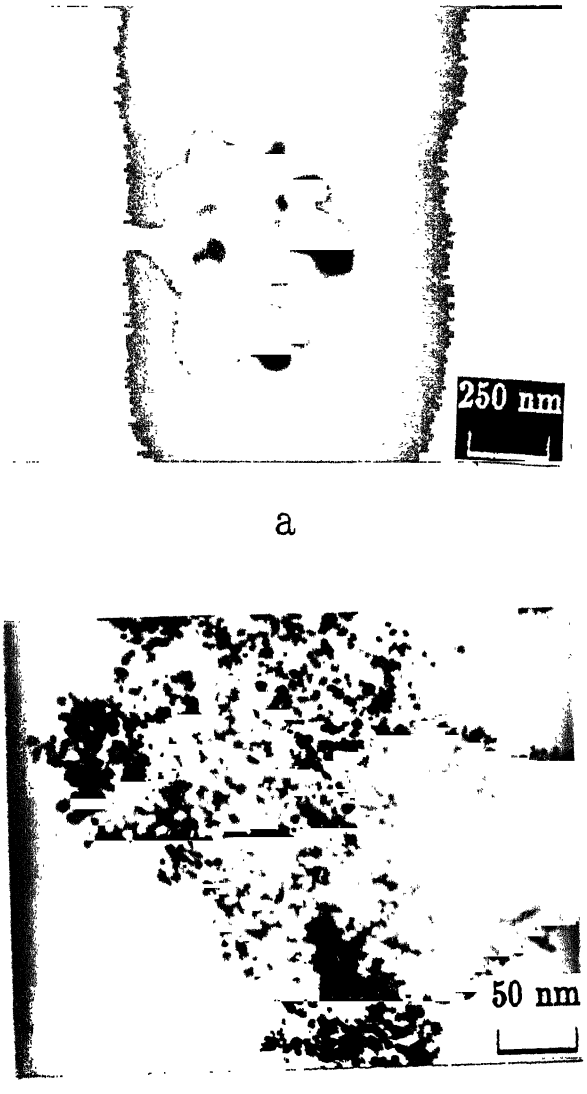

Fig. 2.21 TEM pictures of calcined ZrO_2 -$3Gd_2O_3$ powders (a) water washed (b) propanol washed.

A significantly higher surface area in propanol washed powders confirms the TEM observation that the powders are less agglomerated in this case. Most of the discrepancy in the crystallite size by the two methods is due to the presence of particle bridges which lowers the observed surface area and lead to a higher calculated value of the corresponding crystallite size in case of the BET method.

2.11.5 Compaction Response of Powders

The compaction response of the water washed and propanol washed powders is shown in Fig. 2.22. The agglomerate break point of propanol washed powder is not sharp and its value is about 20 MPa in comparison to 36 MPa for water washed powder. Thus propanol washing produces softer agglomerates which break at low pressure. Such powders should therefore produce compacts of higher sintered density.

2.11.6 Densification behaviour of water and propanol washed powders:

The sintered density vs. sintering temperature is plotted in Fig. 2.23 for both water washed and propanol washed powders. At all temperatures, the propanol washed powders have a higher sintered density than the water washed powders. The difference is about 10% at maximum sintering temperature (1400°C). The optical micrograph of the samples sintered at different temperature for both the powder types are shown Fig. 2.24. There is a distinct difference in the two cases. The water washed powders show dense areas in patches and large pores which do not get removed on increasing the sintering temperature. The dense patches are most probably agglomerated regions which sinter faster than the other

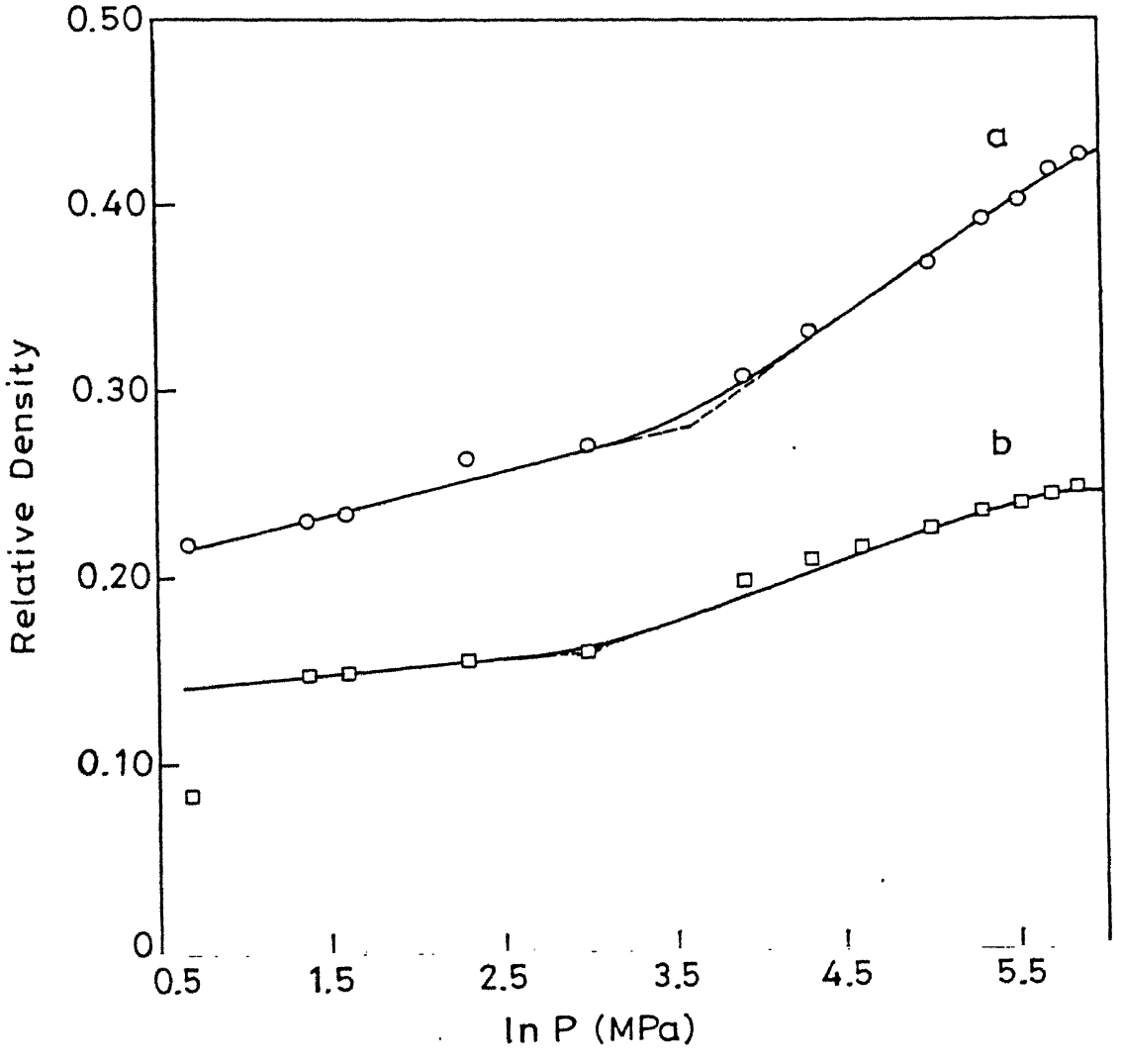

Fig. 2.22 Effect of wash liquid on the compaction behaviour of ZrO_2 -2 Gd_2O_3 calcined powders (a) water washed, (b) propanol washed.

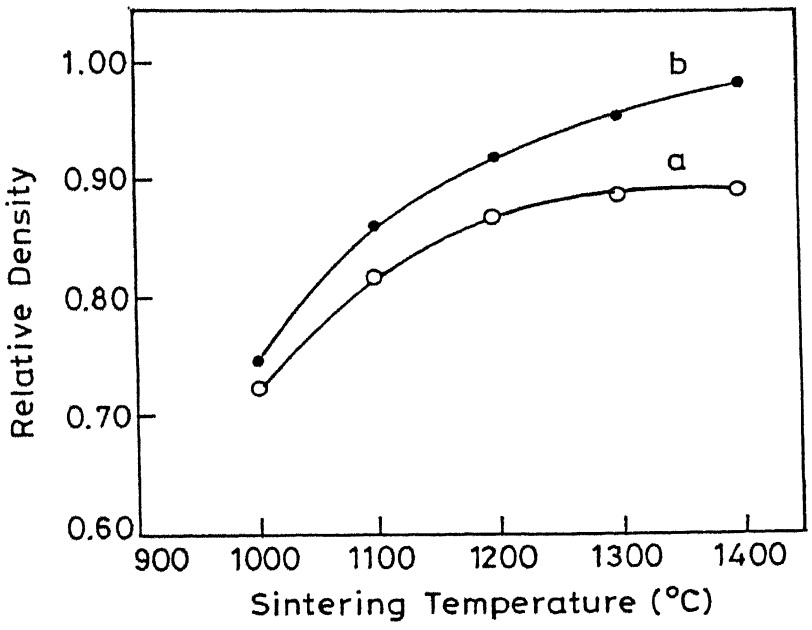

Fig. 2.23 Effect of wash liquid on the sintered density of ZrO_2 -$3Gd_2O_3$ samples sintered for 2 hours at different temperatures, (a) water washed, (b) propanol washed.

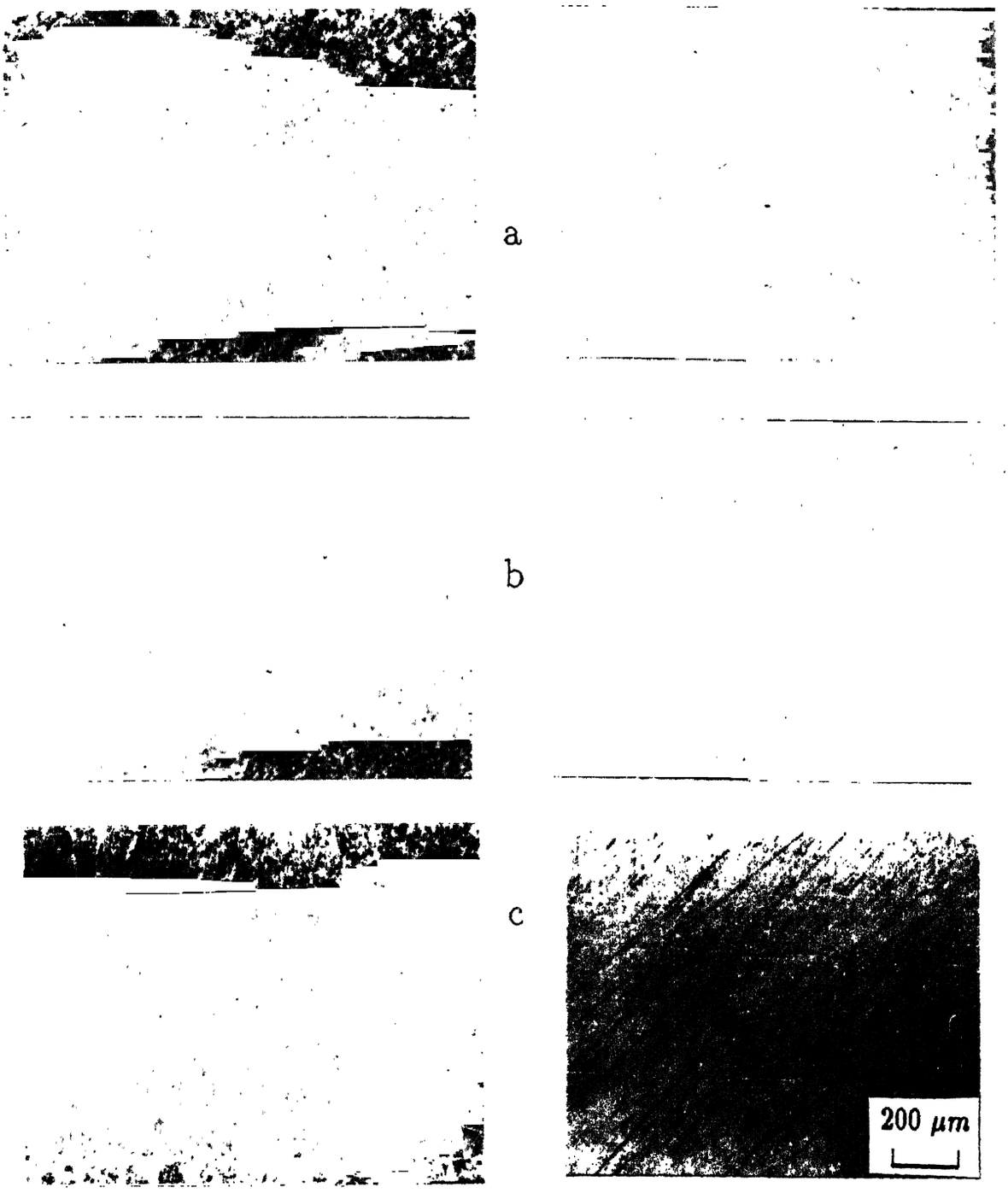

Fig. 2.24 Optical micrographs of the polished surfaces of water washed and propanol washed powders sintered for 2 hours at (a) 1100°C, (b) 1200°C and (c) 1400°C.

regions leaving behind pores. On the other hand, the propanol washed powders do not show such extensive porosity. The soft agglomerates break and pack uniformly so that the differential sintering is minimized.

2.11.7 Density vs. Gd_2O_3 content for propanol washed powders:

As the propanol washed powders led to higher density in the 3mol% Gd_2O_3 composition, the other compositions were also prepared by propanol washing and sintered. The density of ZrO_2 - Gd_2O_3 alloys as a function of Gd_2O_3 content is show in Fig. 2.25. Density for all compositions for improves significantly for propanol washed powders. The maximum density is obtained for 3 mol% Gd_2O_3 samples which is > 98% of theoretical. The other three compositions i.e. 2, 5 and 8 also show improved density with minimum density of about 85% for 8 mol% samples.

2.12 *SUMMARY AND CONCLUSIONS*

This chapter dealt with the preparation of ZrO_2 - Gd_2O_3 alloy powders. In order to judge their suitability, the powders were prepared by three different processing methods, viz. Mixed Oxide (MO), Hybrid sol-gel (HSG) and Coprecipitation (CP). The CP powders retained maximum (t+c) phase after calcination and sintering but the sintered density was found to be low. Modification in the processing parameters such as higher calcination temperature or higher sintering temperature was not effective in either retention of higher amount of tetragonal phase or in achieving a higher sintered density. A dramatic improvement in sintered density (98% of theoretical) resulted when these CP powders were washed several time by propanol prior to drying and

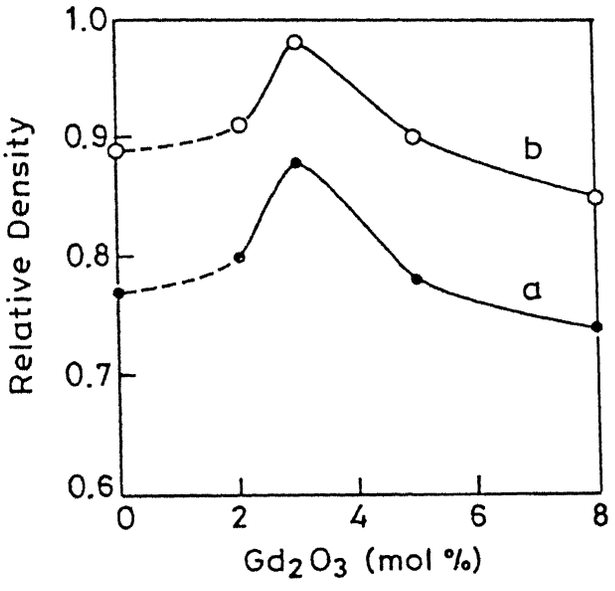

Fig. 2.25 Sintered density of ZrO_2 -Gd_2O_3 samples prepared from powders washed with (a) water and (b) propanol.

calcination, and sintered at 1400°C. The sintered pellets also retained high volume percentage of tetragonal phase.

Some of the important conclusions which emerge out of this study are as follows:

(i) Gd_2O_3 can stabilize the tetragonal phase of ZrO_2 when added in proper proportion. However the amount of retained tetragonal phase depends upon the processing route (i.e. MO HSG or CP) employed, calcination and sintering temperature etc. In the present study the maximum amount of t phase retained in the calcined powders are 25%, 62% and 100% for MO, HSG and CP powders respectively.

(ii) The amount of tetragonal phase in the calcined powders processed by MO and HSG routes increases on sintering (1400°C) to 44% and 87% respectively. Samples from CP powders also remained fully tetragonal after sintering. The increase in tetragonal phase in MO and HSG samples is due to the enhanced dissolution of Gd_2O_3 into ZrO_2 at higher temperatures.

(iii) The CP powders produce an agglomerated powder with high agglomerate strength which sinter to a low density. Maximum density is only 88% of the theoretical for ZrO_2 -3 mol% Gd_2O_3 samples. Increasing the calcination temperature in steps from 700°C to 1000°C does not improve the sintered density. Rather it increases the agglomerate strength (36 to 75 MPa) which further decreases sintered density. Similarly increasing the sintering temperature upto 1600°C also does not increase density but decreases the retained tetragonal phase from 100% at 1400°C to only 12% at 1600°C. Sintering

at 1600°C also resulted in the formation of zirconate phase.

(iv) Propanol washing of coprecipitated powders gives loosely agglomerated powders due to the replacement of surface hydroxyl groups by propoxy groups which do not produce strong chemical bonds. This is reflected in the agglomerate strength (P_j) of these two type of powders. While P_j for water washed powder is 36 MPa it decreases to 20 MPa in propanol washed powders.

(v) All compositions of propanol washed powders gave high sintered density, 85 - 98% as compared to water washed powders (74 - 88%).

REFERENCES

1. M. Paulus, "Physical and Chemical Parameters Controlling the Homogeneity of Fine Grained Powders and Sintering Materials", pp 7 - 31 in Ceramics Materials Science Research, Vol.II, Edited by H. Palmour, R.F. Davis and T.M. Hare, Plenum Press, New York 1978.

2. F.F. Lange, H. Schubert, N.Claussen and M.Ruhle," Effects of Attrition Milling and Post - Sintering Heat Treatment on Fabrication, Microstructure and Properties of Transformation Toughened ZrO_2'' , J.Mater. Sci. 21, 708 - 14, (1986).

3. T.Tien and E.C. Subbarao," Grain Growth in $Ca_{0.16}$ $Zr_{0.84}$ $O_{1.84}$", J. Am. Ceram. Soc. 46 [10] 489 - 92 (1963).

4. W. D. Kingery, "Densification during Sintering in the Presence of a Liquid Phase I. Theory, " J. Appl. Phys. 30 [3] 301 - 06 (1959).

5. G.A. Rossi and P.J. Pelletier, "Y_2O_3 - doped ZrO_2 Powders prepared in non-Aqueous Medium. Influence of the Crystallization Method on Powder Sinterability and Properties of the Y-TZP Ceramics", in Advances in Ceramics, Vol. 24A, pp 173 - 82. Edited by S. Somiya, N. Yamamoto and H. Yanagida, The American Ceramic Society, Westerville, OH, 1988.

6. B. Dubois, D.Ruffier and P. Odier, "Preparation of Fine Yttria - Stabilized Zirconia by the Spray - Pyrolysis Method," J. Am. Ceram. Soc. 72 [4] 713 - 15 (1989).

7. S.C.Zhang, G.L. Messing and M. Borden, "Synthesis of Solid, Spherical Zirconia Particles by Spray Pyrolysis," J.Am.Ceram. Soc. 73 [1] 61 - 67 (1990).

8. K.S. Mazdiyasni, C.T.Lynch and J.S.Smith II, "Cubic Phase Stabilization of Translucent Yttria - Zirconia At very Low Temperatures, " J. Am. Ceram. Soc. 50 [5] 532 - 37 (1967).

9. B. Fegley Jr., P. White and H.K. Bowen," Processing and Characterization of ZrO_2 and Y-doped ZrO_2Powder," Am. Ceram. Soc. Bull. 64[8] 1115 - 20 (1985).

10. K.S. Mazdiyasni, C.T. Lynch and J.S.Smith, "Preparation of Ultra - High - Purity Submicron Refractory Oxides," J. Am. Ceram. Soc. 48 [7] 372 - 75 (1965).

11. L. Rakotoson and M. Paulus, "Sintering of a Freeze - Dried 10 mol% Y_2O_3- Stabilized Zirconia," pp 727 - 32 in Advances in Ceramics Vol. 12. Edited by N. Claussen, M. Ruhle and A. H. Heuer. American Ceramic Society, Columbus, Ohio, 1984.

12. A.R. Burkin, H. Saricimen and B.C.H. Steele, "Preparation of Yttria- Stabilized Zirconia (YSZ) Powders by High Temperature Hydrolysis (HTH)," Trans. J. Brit.Ceram. Soc. 79 [4] 105 - 08(1980).

13. E.Tani, M.Yoshimura and S. Somiya, "Formation of Ultrafine Tetragonal ZrO_2 Powder Under Hydrothermal Conditions," J. Am. Ceram. Soc. 66 [1] 11 - 14 (1983).

14. S.D. Ramamurthy, Z.Yu and D.A. Payne, "Nanometer - Sized ZrO_2 Particles prepared by a Sol-Emulsion - Gel Method," J. Am. Ceram. Soc. 73 [9] 2760 - 63 (1990).

15. M. Kagawa, F. Honda, H. Onodera and T. Nagae "The Formation of Ultrafine Al_2O_3, ZrO_2 and $Fe_2O_3$by the Spray - ICP Technique," Mater. Res. Bull. 18 [9] 1081 - 87 (1983).

16. J. D. Mackenzie, " Applications of Sol-Gel Methods for Glass and Ceramics Processing" pp 15 - 26 in Ultrastructure Processing of Ceramics, Glasses and Composites. Edited by L.L. Hench and D.R. Ulrich. John Wiley & Sons, New York, 1984.

17. J.Livage, " Sol - Gel Chemistry of Transition Metal Oxides," pp 103-52 in Sol-Gel Science and Technology. Edited by M.A. Aegertor, N. Jafelici and D.F. Souza and E.D. Zanotto. World Scientific Publishing Co. Pte. Ltd., Suigapere, 1989.

18. H.K. Schmid, "Quantitative Analysis of Polymorphic Mixes of Zirconia by X-ray Diffraction," J.Am. Ceram. Soc. 70 [5] 367 -76 (1987).

19. H. Toraya, M. Yoshimura and S. Somiya, "Calibration Curve for Quantitative Analysis of the Monoclinic - Tetragonal ZrO_2 System by X-ray Diffraction," J. Am. Ceram. Soc. 67 [6] C-119 - C-121 (1984).

20. P.A. Evans, R.Stevens and J.G.P.Binner, "Quantitative X-ray Diffraction Analysis of Polymorphic Mixes of Pure Zirconia," Trans. J. Brit. Ceram. Soc. 83 [1] 39 - 43 (1984).

21. B.D.Cullity, Elements of X-ray Diffraction, Second Edition, pp 102, Addison - Wesley Publishing Company, Inc. MA, 1978.

22. D.Michel, L.Mazerolles and M. Perez Y. Jorba, "Fracture of Metastable Tetragonal Zirconia Crystals," J. Mater.Sci., 18 2618 - 28 (1983).

23. M.A.C.G. Van de Graff and A.J. Burggraaf, "Wet - Chemical Preparation of ZrO_2 Powders: Their Microstructure and Behaviour," pp 744-65 in Advances in Ceramics Vol.12. Edited by N. Claussen, M.Ruhle and A.H. Heuer. The American Ceramic Society, Columbus, Ohio, 1984.

24. C.Marcilly, P. Courty and B. Delmon,"Preparation of Highly Dispersed Mixed Oxides and Oxide Solid Solution by Pyrolysis of Amorphous Organic Precursors," J. Am. Ceram. Soc. 54[1] 56 - 57 (1970).

25. C.E. Scott and J.S.Reed, "Effect of Laundering and Milling on the Sintering Behaviour of Stabilized ZrO_2 Powders," Am. Ceram. Soc. Bull 58[6] 587 - 90 (1979).

26. M.Murata, K. Wakino, K. Tanaka and Y. Hamawaka, "Chemical Preparation of PLZT Powders from Aqueous Solutions," Mater. Res. Bull. 11[3] 323 - 28 (1976).

27. R. Gopalakrishnan, T.Kosmac, V. Krasevec and M. Komac, "Influence of Dewatering of Yttrium - Zirconium Hydroxide Precipitates on the sintering Behaviour of their Product," pp 281-85 in Sintering'85, Proceedings of the World Round Table Conference on Sintering 6th Herceg - Novi, 1985. Edited by G.C. Kuczynski, G. Czeslaw and M.M. Ristic.Plenum Press, New York, 1987.

28. S.L. Jones and J. Norman, "Dehydration of Hydrous Zirconia with Methanol, "J. Am. Ceram. Soc. 71[4] C-190 - C-191 (1988).

29. M.S. Kaliszewski and A.H. Heuer, "Alcohol Interaction with Zirconia Powders," J. Am. Ceram. Soc. 73 [6] 1504 - 09 (1990).

30. L.M. Zaitsev, "Zirconium Hydroxides," Russ. J. Inorg. Chem. [Engl. Transl.] 11 900 - 04 (1968).

CHAPTER 3

TRANSFORMABILITY, MICROSTRUCTURE AND MECHANICAL PROPERTIES OF ZrO_2- Gd_2O_3 ALLOYS

3.1 *INTRODUCTION*

Over about the last fifteen years, much attention has been paid to be tetragonal zirconia polycrystals, which exhibit excellent mechanical properties with high values of toughness and strength as a consequence of stress induced t $\longrightarrow$ m transformation in the stress field of an advancing crack tip. Among many tetragonal zirconia polycrystals, CeO_2 doped tetragonal zirconia polycrystals (Ce - TZP) and Y_2O_3 - doped tetragonal zirconia polycrystals (Y-TZP) have emerged as the most promising because of the wide range of mechanical properties achievable with these two materials. As recently summarized by Tsukuma and Takahata [1], bend strength as high as 2.4 GPa has been obtained for some selected compositions of Y-TZP. Similarly, fracture toughness of more than 20 MPa $\sqrt{m}$ has been obtained for Ce-TZP samples [2].

The stress induced t $\longrightarrow$ m transformation which is believed to be the dominant mechanism contributing to the high strength and toughness of ZrO_2 ceramics, is one of the so called "crack tip shielding" mechanism of toughening. In this chapter we first give a brief description of the various toughening mechanisms in ceramics. This is followed by a review of the results of the mechanical properties of various TZPs as obtained by various

investigators. Finally the present work on the transformability, microstructure and mechanical properties of ZrO_2– Gd_2O_3 alloys is described.

3.2 *TOUGHENING MECHANISMS*

The toughening mechanisms in ceramics can be broadly classified in three different categories: (i) Crack tip shielding, (ii) Crack deflection and (iii) Crack bridging. Below we describe the mechanisms briefly with reference to ZrO_2 ceramics.

3.2.1 Crack Tip Shielding

The crack tip shielding implies reduction of the stress intensity at the crack tip due to certain processes taking place within the material. Examples of these processes are t ⟶ m transformation in ZrO_2 ceramics and microcracking. While the former is limited to a few ceramics including ZrO_2 ceramics, the latter is a more general phenomenon believed to be the reasons behind enhanced toughness in many ceramics. The toughness enhancement due to t ⟶ m transformation in ZrO_2 ceramics is called "Transformation Toughening".

Consider the stress profile in front of a crack tip in the presence of an applied stress as shown in Fig. 3.1 [3]. This is shown as the curve K_A in the figure. If a stress induced phase transformation involving dilational and shear strains occur due to high stresses near the crack tip, thereby leading to a reduction in the stress intensity, then the resulting stress distribution can be shown by the cure K_L (Fig.3.1).

The condition for the advancement of the crack now is that $K_I^L > K_{IC}^0$ where K_{IC}^0 the toughness of the transformed material. However, the measured toughness K_{IC}^A is calculated on the basis of the

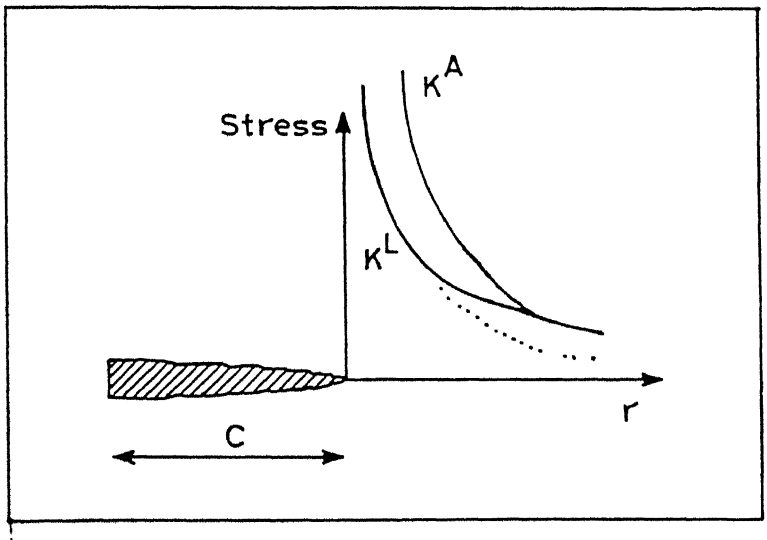

Fig. 3.1 Schematic stress profile diagram in front of a crack tip in the presence of an applied stress.

applied stress. Thus $K_{IC}^{A} - K_{C}^{L} = \Delta K_{C}$ is the observed enhancement in toughness due to the shielding of the crack tip by the stress induced transformation.

The value of K_c increases as the crack grows and reaches a constant value when the crack has advanced sufficiently and is surrounded by a zone of transformed material. In the beginning, when the crack has not advanced, a transformation zone forms in front of the crack tip. This is called the frontal zone. It has been shown, under assumption of a transformation controlled by the mean stress, that the net enhancement to toughness for a frontal zone is zero [4]. A non zero K_I^c is obtained when a steady state zone develops (Fig. 3.2).

The enhancement is toughness K_{IC} for this case has been calculated under various assumptions. The simplest case is that of purely dilatational transformation for which the following expression is obtained.

$$\Delta K_C = 0.22\ Ff\ \epsilon_{ij}^{T}\ \frac{\sqrt{h}}{(1-\nu)} \qquad (3.1)$$

Where E is the Young's modulus, f the volume fraction of the transformed phase, ϵ_{ij}^{T} are the transformation strains, h is the width of the transformation zone and ν is Poisson's ratio. Slightly different expressions are obtained under different assumptions. These are listed in Table 3.1.

In the table, supercritical transformation means that all the available $t \longrightarrow m\ ZrO_2$ within the zone undergoes complete $t \longrightarrow m$ transformation under the action of applied stress. This type of transformation is most commonly observed in PSZ materials. However, in the case of subcritical transformation, only a fraction of the t phase undergoes transformation.

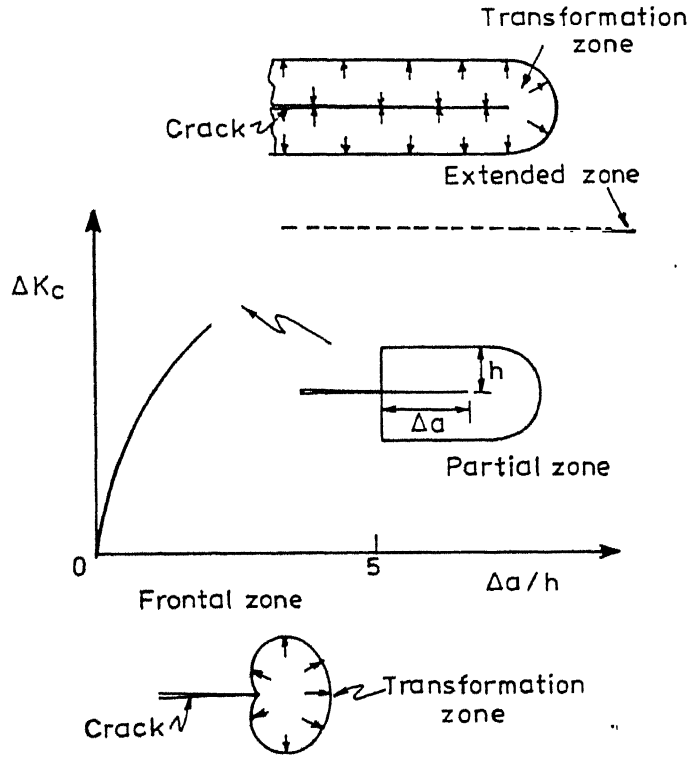

Fig. 3.2 Development of different zones of crack tip shielding during advancement of a crack.

Table 3.1

Toughness Increment due to different strain coupling and zone shape [5]

Net Strain Coupling	Zone Shape	Toughness Increment	Comment
Dilation	Hydrostatic Contour	$\frac{0.22\ E\ f\ e^T_{ij}\ \sqrt{h}}{(1-\nu)}$	Supercritical, No reversal
Dilation	Hydrostatic Contour	$\frac{0.21\ E\ f\ e^T_{ij}\ \sqrt{h}}{(1-\nu)}$	Supercritical, reversal, with maxmimum . hystersis
Dilation	Shear band Profile	$\frac{0.38\ E\ f\ e^T_{ij}\ \sqrt{h}}{(1-\nu)}$	Supercritical, No reversal
Uniaxial Dilation	Maximum Principal Stress Contour	$0.55\ E\ f\ e^T_{ij}\ \sqrt{h}$	Supercritical, No reversal
Dilational and relaxed shear strain	Relaxed shear strain	$\sim \frac{0.22\ E\ f\ e^T_{ij}\ \sqrt{h}}{(1-\nu)}$	Supercritical, No reversal

The combined action of the stresses near the crack tip and the preexisting residual stresses in the material may lead to formation of microcracks. Formation of these microcracks result in the relaxation of stresses and a volume dilation. The effect of this dilation is to shield the crack tip stresses, just like the case of the transformation toughening. Expressions have been derived in literature for simple cases in a manner analogous to that employed for transformation toughening. A comparison of these expressions shows that in the case of ZrO_2 ceramics, the transformation toughening and microcracking mechanisms should be equally effective [5].

Formation of microcracks is facilitated by the presence of

angular particles which act as stress concentrators for the nucleation of the microcracks. In multiphase composites, matrix grain boundaries can act as preferred sites for microcrack formation.

3.2.2 Crack Deflection Toughening

A propagating crack can be deflected by a fracture resistant second phase or a localized stress field [6]. The deflection may be in the form of a tilt or a twist or both. A tilt or a twist provides a reduced driving force for crack propagation. Mixed mode loading takes place for both the twisted and the tilted crack fronts. While Mode I and II are dominant in tilted crack fronts, twisted crack front have Mode I and Mode III loading. The degree of toughening is independent of size but depends on the morphology of the particles. The toughness increment also depends on whether the crack exhibits maximum twist or maximum tilt. Generally for rod shaped particles, higher the twist angle, higher is the toughness increment. But for spherical particles higher the tilt angle, higher is the toughness. However, from the particle morphology view point, rod shaped particles give maximum toughening, and spherical particles give the least, with disc shaped particles contributing in between these two extremes. Among rod shaped particles those having higher aspect ratio give higher toughening (more twist). For spherical particles tilt angle becomes more important than twist and for disc shaped particles both tilt and twist become important. With spherical particles higher toughening effect is obtained when the spheres are nearly contacting thereby achieving a twist angle of $\pi/2$. Also, the volume fraction of second phase particles should preferably be

between 10 and 20% for maximum toughening effect.

3.2.3 Crack Bridging

During crack propagation, a crack may bypass an obstacle, leaving it intact. Such obstacles may be a residually compressed region, a fibre or whisker reinforcement etc. These interactions leave the obstacle in the form of a ligament behind the crack tip. Ligaments may also form due to mechanical interlocking of the grains. In presence of these ligaments higher stress is needed for crack opening, thereby increasing the toughness. This mechanism is important in frictionally bonded fibre composites [7], large grained alumina and whisker reinforced ceramics [8]. This type of crack bridging has also been observed in PSZ materials. For the case of residual stress induced bridging, the increase in steady state toughness is given by [5].

$$K_c = 2.5\ f\ E\ \Delta\alpha\ \Delta T\ \sqrt{R} \qquad (3.2)$$

where f is the volume fraction of highly stressed grains that result in bridging ligaments, α is the thermal expansion mismatch between the matrix and the stressed region, and ΔT is the difference between the temperature at which the stresses cease to relax during cooling and the room temperature and 2R is the grain diameter.

The crack bridging gives rise to the so called 'R' curve behaviour, in which the toughness increases as the crack length increases and attains a constant value at large crack lengths. This imparts flaw tolerance to the ceramic.

3.2.4 Toughening due to Ferroelastic Domain Switching

Although transformation toughening mechanism is very

important for ZrO_2 ceramics at room temperature, this effect diminishes due to increased thermodynamic stability of the t phase with increasing temperature and should completely vanish at temperature higher than m $\longrightarrow$ t transformation (~1000°C). Despite this many investigators have reported high toughness (6 - 10 $MPa\sqrt{m}$) for TZP and PSZ at high temperature [9,10,11]. Furthermore, high toughness has been observed at room temperature in zirconia based ceramics containing tetragonal phase even though no transformation to monoclinic phase is observed. Transformation toughening cannot be responsible for toughening in these cases. This led Virkar et.al. [12] to propose domain switching as a toughening mechanism in these cases.

It has been known for quite some time that zirconia exhibits ferroelasticity. This phenomenon is quite similar to that of ferromagnetism and ferroelectricity, where a hysteresis exists between magnetization (B) and magnetic field (H) for the former and between polarization (P) and applied electric field (E) for the latter. For ZrO_2 materials (exhibiting ferroelasticity) a hysteresis loop exists between stress (σ) and strain (ε). The origin of the hysteresis is the presence of domains and their orientation above a critical value of externally applied stimulus. For ZrO_2, the stimulus is externally applied stress. Thus when tetragonal ZrO_2 is subjected to an externally applied stress (more than the critical stress), due to domain reorientation the 'c' axis shortens and 'a' axis elongates. As a result of this interchange of the tetragonal cell axes, the relative intensities of (002) and (200) type of reflections change. In the ideal case, where complete reversal of c_t to a_t axis (and vice versa) has

taken place complete reversal of peak intensities are observed. The same is also true for (131) and (113) peaks. However, the ratio of (202) to (220) (>1 in the sintered samples) increases further on domain switching. Fig.3.3 shows the schematic variation in the intensities of different peaks for a Ce - TZP sample [12] subjected to a grinding operation.

The change in intensity resulting from preferential orientation of ferroelastic domains in the above manner aligns [001] direction of a large number of crystallites orthogonally to the surface of the crystal. However, proper care should be taken before ascribing the change in peak intensity ratio to domain switching. Peak intensity ratio can also change due to twinning and/or texture. The texture in the t phase develops during t $\longrightarrow$ m transformation because most favourable orientations with respect to the stress axis transforms first. Preexisting texture in the monoclinic phase may also contribute to texture in the t phase [13,14]. In general, the characteristics of a tetragonal zirconia exhibiting domain switching are as follows:

(i) Complete absence of monoclinic phase in the mechanically treated samples (i.e. grinding or fracture etc.).

(ii) The intensity of t(111) peak should remain unchanged before and after the mechanical treatments.

(iii) It should also exhibit substantial amount of peak broadening which should persist even after annealing at high temperatures.

(iv) The tetragonal peaks should be shifted towards lower 2θ side. This shift signifies the presence of residual tensile stress on the surface.

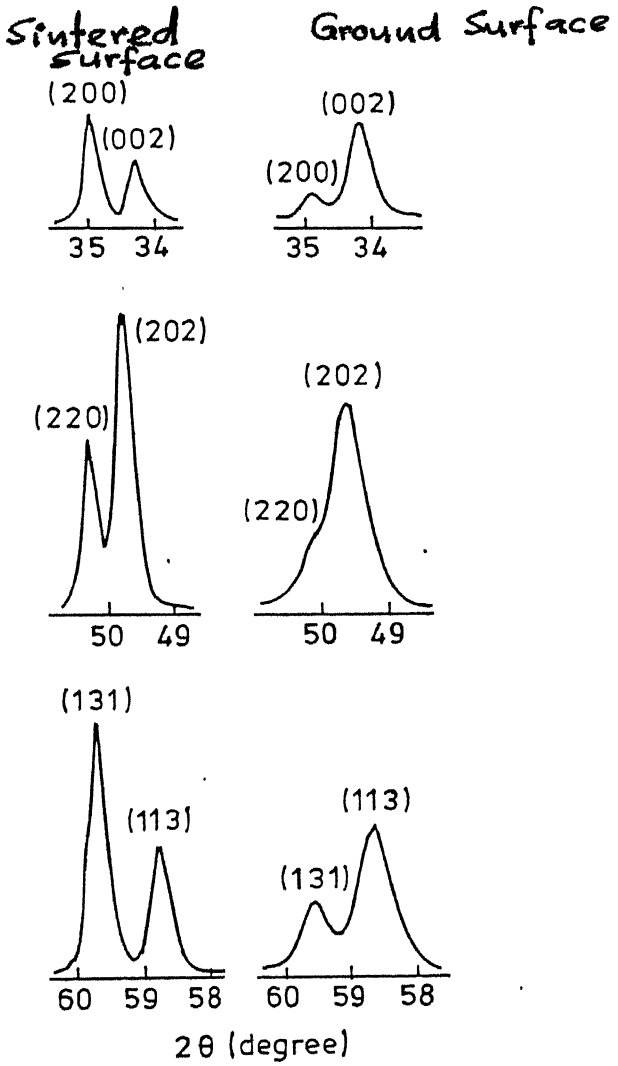

Fig. 3.3 Schematic variation in the intensities of different peaks for a Ce-TZP sample showing domain switching on ground surface.

(v) The peak intensity obtained after mechanical treatment should remain unaltered even after thermal annealing at high temperature (e.g. 1300°C).

Due to this domain rotation the crack tip stress decreases leading to a higher fracture toughness. If it is assumed that domain switching takes place at a distance 'h' from the crack tip, the resulting decrease in free energy is given by [12].

$$\Delta G_c = 2h \oint \sigma \, d\varepsilon \qquad (3.3)$$

and the toughness is given by

$$K_c = K_c^0 \left[1 + \frac{2 h E}{(1-\nu^2)(K_c^0)^2} \oint \sigma \, d\varepsilon \right]^{1/2} \qquad (3.4)$$

where K_c^0 in the toughness in absence of any domain switching, E is the Young's modulus and ν is the Poisson's ratio.

So, the above toughness expression is similar to that obtained for transformation toughening i.e. $K_c = Y \sqrt{h}$ where Y contains the toughness factor in absence of transformation toughening and 'h' is the process zone. Thus, domain switching gives a modified process zone which is different from the process zone obtained due to transformation toughening.

There are only a few reports so far in literature which show rather unambiguously the phenomenon of domain switching in ZrO_2 ceramics [12]. A controversy still exists regarding the extent of toughening it can provide [12,13,14].

3.2.5 Combined Toughening Mechanisms

Very often, more than one toughening mechanisms may operate simultaneously. In this case the two mechanisms interact and may

produce either an additive or even a synergistic effect or may lead to deterioration in the toughness. In particular, in the case of simultaneous bridging and crack tip shielding, the bridging leads to an enhancement in the tensile stresses on the crack surface and so leads to an increase in the width of the process zone. Thus the crack shielding effect is further enhanced due to a larger process zone.

In the case of simultaneous microcracking and transformation toughening, two situations may arise. When the critical stress for the microcracking is less than that of transformation toughening, only a fraction of transformation zone contributes to microcrack shielding. However, when the stress for microcracking is higher than that required for transformation, the entire transformation zone is microcracked and in this case greatest toughening for the combined mechanism is obtained.

3.3 *A SUMMARY OF DATA ON MECHANICAL PROPERTIES OF TETRAGONAL ZIRCONIA POLYCRYSTALS*

One of the major uses of stabilized tetragonal zirconia (both single and polycrystalline) is as structural material where use is being made of its high strength and toughness. The high strength arises out of high density and fine grain size whereas toughness results from stress induced tetragonal to monoclinic transformation which takes place in the vicinity of a crack tip. However, it has been recognized that strength and toughness also depend to a large extent on the microstructure. The presence of second phase, both amorphous and crystalline, affect the mechanical property. Other parameters that can affect the strength and toughness are residual porosity, grain size, grain shape,

grain size distribution, microcracks, solid solution etc. Accordingly, there have been numerous studies on the effect of microstructure on mechanical property of TZP's. Some of these studies will be discussed in this section with particular reference to Y_2O_3 - doped tetragonal zirconia polycrystals (Y - TZP) and CeO_2 - doped tetragonal zirconia polycrystals (Ce - TZP). The different parameters that will be correlated are stabilizer content, grain size, sintering conditions, addition of second phase etc.

Ingel et.al. [9] prepared single crystals of Y_2O_3 - stabilized zirconia (4 to 6 wt% Y_2O_3) by skull melting and studied their room temperature strength and toughness. High toughness (8 MPa $\sqrt{m}$) and strength (> 1000 MPa) were obtained for Y-PSZ. The FSZ crystals (20 wt% Y_2O_3), on the other hand gave low toughness (2 MPa $\sqrt{m}$) as well as low strength (200 MPa). The increase in toughness of PSZ resulted from the precipitation of tetragonal grains from the cubic matrix. The same author [10] also studied the high temperature mechanical property of Y_2O_3 - stabilized zirconia single crystals. In the high temperature range ($\geq$1500°C) Y-PSZ could retain higher toughness and strength than FSZ crystals. But the drop was much more drastic for polycrystalline TZP. It was proposed that transformation toughening was not the sole toughening mechanism in this material. Other mechanisms also taking part could probably be crack precipitate interaction resulting from lattice, elastic or thermal expansion mismatch between the cubic matrix and the tetragonal precipitates.

The mechanical property of tetragonal zirconia polycrystals (TZP) prepared by coprecipitation technique and containing 2 to 4

mol% Y_2O_3 was studied by Tsukuma et.al. [15]. The samples were prepared either by uniaxial pressing - cold isopressing - sintering routes or by uniaxial pressing - cold isopressing - hot isopressing route. While sintering was done between 1400°C-1600°C for 2 hrs., HIPing was carried at 1400°C-1600°C at 150 MPa. Micro Indentation (MI) fracture toughness was 10-12 MPa$\sqrt{m}$ and fracture strength was between 1.1 - 1.5 GPa. The result could not be explained on the basis of transformation toughening alone. It was thought that some other toughening mechanisms were also operating concurrently. As already explained, grain size influences the M_s temperature and so it will also affect the strength and toughness. This effect was studied in detail by Wang et.al. [16] while investigating the mechanical properties of certain commercial Y-TZP containing 2 - 3 mol% Y_2O_3 (Toyosoda, Japan). The grain size ranged between 0.3 - 2.1 μm. The strength measured in three point bending and K_{IC} (measured by MI technique), were similar to the values obtained by Tsukuma et.al. A linear relation was observed between grain size and $V_f\sqrt{h}$ (V_f = volume fraction of the transformed phase and h is zone width). Higher values of $V_f\sqrt{h}$ were attributed to the larger grain sizes. Extrapolation to lower grain size gave values of $V_f\sqrt{h}$ similar to that obtained by others. Thus the results appear to be attributable to transformation toughening alone. Similar explanations for toughness increment have also been put forward by Lange et.al. [17], who prepared a 3Y-TZP by a solid state reaction between Y_2O_3 and ZrO_2. The toughness from MI technique was between 6-7 MPa$\sqrt{m}$. Grain size dependence of strength and toughness has also been studied by Masaki et.al. [18] and Swain [19]. Masaki [18] prepared Y-TZP by

coprecipitation from $ZrOCl_2$ and YCl_3. The samples were either hot pressed or hot isostatically pressed. In the low toughness region, strength was controlled by toughness and grain size. Swain et.al. [19] observed that increasing the grain size increases the toughness from 6 to 14 MPa$\sqrt{m}$. This was because larger grains were more conducive for stress induced to t $\longrightarrow$ m transformation.

Ball milling of calcined powders is often carried out in order to reduce the particle size and to break down the agglomerates. However, ball milling may introduce impurities which form glassy phase during sintering. These not only changes the sintering kinetics but also makes the grains more round thus making the transformation difficult. Mecartney et.al. [20] observed a decrease in fracture toughness from 5 to 4 MPa $\sqrt{m}$ after ball milling 2.5 Y-TZP for 9 hours. However, Lange et.al. [21] did not observe any difference in the mechanical properties of samples prepared with or without attrition milling. They attributed it to the beneficial relaxation of the residual stresses due to the presence of glassy phase.

Tetragonal and cubic phases are stabilized at room temperature by adding suitable stabilizers. However, these phases are nonequilibrium metastable phases and hence have a natural tendency to attain the stable equilibrium configuration. So, when a TZP (with metastable phase) is heated for long periods, it phase partitions into equilibrium phases. Thus when 2.3 mol% Y-TZP, having fully tetragonal phase was subjected to post sintering heat treatment (1400°C - 1600°C) it partitioned into a tetragonal and a cubic phase [22-23]. The tetragonal phase thus formed had a lower

Y_2O_3 content, while cubic phase became enriched in Yttrium. The cubic phase did not form as precipitates within tetragonal grains which require relatively short range diffusion, but it developed as abnormally large grains at external or internal surfaces. Hence, it was proposed that the cubic grains at these surfaces grow under nonequilibrium condition. Lange et.al. [24] also observed that the fracture toughness of sintered (1400°C/ 1 hr) 3Y-TZP increased from 3 to 10 MPa$\sqrt{m}$ after heat treatment at 1400°C for 100 hrs. However, as the grain size remained unaffected during this heat treatment, the enhanced fracture toughness (as a result of higher transformability) was not the result of larger grain size but due to phase partitioning.

Small additions of dopants have been found to be very effective in altering the properties of TZP. These dopants include MgO, Al_2O_3, MnO etc. Each of these dopants modify the microstructure mechanical property relationship in their own characteristic way. Tu et.al. [25] prepared a 2.7 mol% Y-PSZ with and without 5 wt% Al_2O_3 addition by a sol-gel process. The addition of Al_2O_3 helped in higher tetragonal phase retention (due to high elastic modulus), higher density and higher fracture toughness. The higher toughness resulted from the higher tetragonal phase retention and higher sintered density. Drenan et.al. [26] studied the effect of adding SrO on the microstructure-mechanical properties of MgO-PSZ. SrO was added to counteract the deleterious effect of SiO_2- MgO reaction (thus forming Mg_2SiO_4 at the sintering temperature) during sintering. The presence of this secondary glassy grain boundary phase results in a loss of stabilizer and also degrades the mechanical property

particularly at elevated temperatures. The addition of SrO initiates the preferential reaction between SrO and SiO_2 to form $SrSiO_3$. This reaction helps in sintering by forming a liquid phase at the sintering temperature, prevents loss of MgO to SiO_2 and thus helps in improving the high temperature strength of these ceramics.

Kimura et.al. [27] studied the effect of MnO additions (0.3 wt%) on the mechanical properties of 1.75 Y-TZP. The addition of MnO decreased both the sintering temperature and grain size. However, inspite of small grain size, the toughness increased from 12 to 14.5 $MPa\sqrt{m}$ and strength from 800 to 1050 MPa. It was proposed that the improvement was due to a combined effect of transformation toughening and MnO additions. In a similar manner. Kim et.al. [28] studied the effect pentavalent ion addition (Ta^{5+}, Nb^{5+}) on c/a axial ratio, transformability, strength and toughness of 2 and 3 mol% Y-TZP. Both c/a and transformability increased with increasing amount of Ta_2O_5 and Nb_2O_5 reaching maximum at 1.5 mol% Ta_2O_5 addition. The fracture toughness also increased from 6-7 $MPa\sqrt{m}$ to 14 $MPa\sqrt{m}$ on adding 1.5 mol% Ta_2O_5 . It also increased the strength from 600 to 750 MPa. The enhanced toughness was attributed to the increased c/a ratio which in turn increased the transformability.

Post sintering heat treatment atmosphere was also found to play a vital role in modulating the fracture toughness of TZPs. Haberko et al [29] observed that for a composition of 13 mol % TiO_2 -3 mol % Y_2O_3 -84 mol% ZrO_2 (sintered at 1350°C for 1 hr. in air), a post sintering annealing of the polished samples at 1300°C for 1 hr. in a carbon atmosphere increased the monoclinic phase on

the surface to 26% and the toughness to 21 MPa$\sqrt{m}$. The extraordinary high toughness was due to the presence of a large amount of monoclinic phase formed on the surface which leads to surface compressive stresses.

The sintering and heat treatment of zirconia alter its properties due to a change in phases grain size etc. Cutler et.al. [30] prepared monoclinic, tetragonal and cubic zirconia by suitably altering the composition and sintering schedule for each case to enable them to undergo the desired phase transformation. For example, the tetragonal samples (with 0-6 mol% Y_2O_3) were sintered at 1500°C, annealed in the cubic phase stability field and were rapidly cooled to permit displacive c $\longrightarrow$ t' transformation. It was observed that ferroelastic monoclinic and tetragonal zirconia were more than twice as tough as paraelastic cubic zirconia. The high toughness of tetragonal and monoclinic zirconia were the result of domain structure and low microcrack density. It was suggested that microcracking and crack bridging played a dominant role in the toughness enhancement.

Besides Y_2O_3 doped tetragonal zirconia polycrystals (Y-TZP), the other stabilized zirconia that is well studied is CeO_2-doped tetragonal zirconia polycrystal (Ce-TZP). In comparison to Y_2O_3, CeO_2 has a much wider tetragonal solubility range in zirconia (2-4 mol% for Y_2O_3 as against 8-20 mol% for CeO_2), large critical grain size for retention of tetragonal phase (2 μm), and higher toughness (> 20 MPa$\sqrt{m}$). However, Ce-TZP have relatively low strength (600-800 MPa) and poor sinterability. So, the focus of different studies was to optimize the strength, toughness and density in these material and some of this work is summarized

here.

The first study on the mechanical properties of Ce-TZP was reported by Tsukuma et.al. [31]. They prepared CeO_2 doped tetragonal zirconia polycrystal (Ce-TZP) by varying the CeO_2 content from 7 to 16 mol%. The samples were sintered in air between 1400°C to 1600°C for 2 hours. Fracture toughness was measured by MI and Chevron Notched Beam (CNB) method and strength by there point bending. While MI method reported a high value of fracture toughness (18 $MPa\sqrt{m}$ for 8-10 mol% CeO_2 doped ZrO_2), CNB method reported a more modest value (10 $MPa\sqrt{m}$) for the same composition. The highest strength was 800 $MPa\sqrt{m}$ for 10-12 mol% Ce-TZP composition. Toughness increment was attributed to stress induced t $\longrightarrow$ m transformation. The difference in fracture toughness by two methods is due to different fracture behaviour in the two methods. While notched beam fracture toughness is related to crack initiation, MI technique depends on crack propagation. In the MI technique, since the transformed particles around the indent were plastically deformed, the crack had difficulty in propagation. So, the K_{IC} from MI technique was higher than CNB technique. Tsukuma [2] also studied the effect of small amount of impurities on the mechanical properties of Ce-TZP. The Ce-TZP was prepared from $ZrOCl_2$ and commercial $CeCl_3$ powders. The latter contained around 7% [(La, Nd) Cl_3]. This impurity reacted with ZrO_2 at the sintering temperature to produce [$(La, Nd)_2Zr_2O_7$] - a zirconate phase. High toughness was obtained (> 35 $MPa\sqrt{m}$) for a material having 12 mol% CeO_2 doping and a grain size of 1 μm. However, the strength was only 700 MPa for this composition, but increased to 800 MPa for other combination of dopant concentration

and grain size. It was proposed that the presence of zirconate phase gave increased stability and toughness of this material. The material also exhibited significant plasticity which also might have contributed to strength - toughness data. Rossi [32], on the other hand prepared a 12 mol% Ce-TZP + Al_2O_3 (60 to 80 vol %) composites by a rapid solidification technique. The addition of Ce-TZP increased the toughness of alumina to 7.5 MPa$\sqrt{m}$ for 60 vol% Al_2O_3 addition. However, the toughness dropped to 6.1 MPa$\sqrt{m}$ on increasing Al_2O_3 content to 80 vol%. It was reasoned that both transformation toughening and microcracking were playing a role.

As already mentioned Ce-TZP sinters poorly, thus giving low strength while Y-TZP sinters to a high density with small grain size and thus it have high fracture strength. Thus partial replacement of CeO_2 by Y_2O_3 was thought to give the right composition having both high toughness and strength. However, replacement of 12 Ce by a combination of either (11 Ce + 1 Y) or 10 Ce + 2 Y) did not give the desired result [33]. The density increased a little, but toughness decreased from 18 to 7 MPa$\sqrt{m}$ for (10 Ce + 2Y) composition. This was due to increased stability of the resultant tetragonal phase. It appears that the effectiveness of stabilizing the tetragonal phase is more for Y_2O_3 than CeO_2 because of the different stabilization mechanism for the two cases.

However, Hirano et.al. [34] did just the opposite thing to that of Duh et.al. [33] in that they replaced part Yttria by Ceria. In this case, Yttria - Ceria doped tetragonal zirconia ((Y, Ce)-TZP) -alumina composites were fabricated by hot isostatic pressing at 1400°C to 1450°C and 196 MPa in an Ar-O_2 gas

atmosphere. The composites containing 25 wt% Al_2O_3 and tetragonal zirconia with compositions 4 mol% $YO_{1.5}$ - 4 mol% CeO_2-ZrO_2 and 2.5 mol% $YO_{1.5}$ -5.5 mol% CeO_2-ZrO_2 exhibited high strength (more than 2 GPa). However, the toughness decreased from 10.6 to 6.3 MPa $\sqrt{m}$ on adding 25 wt% alumina. At the same time, the composites showed superior structural stability and low degradation under hydrothermal conditions compared to conventional 3Y-TZP. The addition of Al_2O_3 decreased the grain size, enhanced the stability of tetragonal phase along with Vickers hardness and elastic modulus.

Most of the commercial TZP powders contain a certain amount of SiO_2 as an impurity, which forms a glassy phase on sintering at high temperature. The presence of this glassy phase decreases strength and transformability and creates problem during subsequent heat treatment. It has been found that in MgO-PSZ [26], addition of SrO preferentially leaches out SiO_2 (by forming $SrSiO_3$), thus improving property. This idea was implemented in Ce-TZP and Ce-TZP/ Al_2O_3 composites where $SrZrO_3$ was added in definite proportion [35]. The fracture toughness increased from 12 MPa$\sqrt{m}$ (for Ce-TZP) to 15.1 MPa$\sqrt{m}$ (for Ce-TZP + 30 vol% Al_2O_3 + 4 wt% $SrZrO_3$). At the same time fracture strength also increased from 388 MPa to 530 MPa for the same composition. The microstructure of $SrZrO_3$ added samples contained Sr-aluminate platelets. It was proposed that multiple mechanisms were operative in this material like transformation toughening, crack deflection, crack bowing etc.

As already mentioned the additions of transition metal ions to Y-TZP have enhanced the densification kinetics and lead to

higher toughness and strength. Though exact mechanism for this enhancement was not known, the idea was extended to Ce-TZP also. There are a few instances of MnO_2 addition to Ce-TZP and/or Ce-TZP/ Al_2O_3 composites. Maschio et.al. [36] added 0.3 wt% MnO_2 to Ce-TZP which was prepared by solid state route. The Indentation Strength in Bending (ISB) fracture toughness was 14 MPa $\sqrt{m}$ for Ce-TZP + 0.3 wt% MnO_2 in comparison to 12 MPa $\sqrt{m}$ for pure Ce-TZP. The strength also increased from 380 to 450 MPa. It was proposed that addition of MnO_2 introduces other toughening mechanisms over and above that of transformation toughening. The effect of MnO_2 (0.2 wt%) addition to Ce-TZP as well as to 12 Ce-TZP + 10 wt% Al_2O_3 on its mechanical property was studied by Wang et al. [37] and Tsai et al [38]. Both the samples were prepared by identical routes i.e. solid state mixing- uniaxial pressing - isopressing and sintering. While the former author tested the toughness by single edge notched beam (SENB) method and strength by four point bending, it was short rod test in compression and four point bending strength for the latter. Wang et.al. [37] reported a toughness of 9.3 MPa$\sqrt{m}$ and strength of 557 MPa and Tsai et al [38] obtained toughness of 8.5 MPa$\sqrt{m}$ and strength of about 650 MPa. Both the authors related the enhanced toughness to the presence of insitu formed cerium aluminate phase ($CeMnAl_{11}O_{19}$) platelets. Sato et.al. [39] studied the combined effect of Al_2O_3 addition and HIPing on the mechanical properties of Ce-TZP. The samples were uniaxially pressed followed by cold isostatic pressing at 200 MPa and then this was either sintered at 1450°C - 1600°C in air or sintered in air followed by hot isopressing at 100 MPa at 1450°C. Indentation fracture toughness

of sintered Ce-TZP was 15 MPa$\sqrt{m}$ while it was 20 MPa$\sqrt{m}$ on HIPed samples. Simultaneously, the strength also increased from 450 to 550 MPa on HIPing. In the Ce-TZP/10 vol% Al_2O_3 composites the fracture toughness remains the same (15 MPa$\sqrt{m}$) both in the sintered and HIPed samples but strength increased from 500 to 700 MPa on HIPing. It appeared that Al_2O_3 addition decreased the grain size of Ce-TZP thus improving stability and density. This resulted in a decrease in fracture toughness but helped in enhancing the strength.

The sintering behaviour and microstructural characterizations have been studied in $ZrO_2.TiO_2.CeO_2$ system [40]. A fully tetragonal structure with theoretical final density has been achieved after liquid phase sintering at 1350°C to 1400°C for 2 hours. Sintering at higher temperatures resulted in a loss of stabilizer from the matrix due to the formation of zirconium titanate and a cerium titanate rich liquid. The loss of stabilizer was so much that in the temperature range 1500°C to 1600°C, extensive transformation from tetragonal to monoclinic occurred spontaneously during cooling. The tetragonal zirconia formed after sintering was very stable though it had a very high c/a ratio. The stability of the tetragonal phase is believed to be associated with extremely high c/a ratio.

As already mentioned Er_2O_3 is another rare earth oxide which has been successfully used to stabilize the t phase in ZrO_2. This was reported by Duran et.al. [41] who prepared translucent 3Er-TZP from erbium nitrate and zirconium tetrabutoxide using coprecipitation technique. These samples when sintered at 1500°C showed high density and nearly single phase tetragonal material.

However, the toughness of these materials as measured by indentation technique was not very high (~ 6 MPa$\sqrt{m}$) and hardness about 13 GPa. These materials were also isothermally aged for long periods (60 hrs.) at 1400°C to study the stability of tetragonal phase. During this process of aging the density decreased due to rapid grain growth and from development of porosity. This resulted in a decrease in hardness but the toughness did not change during this process. This indicates that the t phase stabilized in this system are very stable and do not undergo t $\longrightarrow$ m transformation easily.

In the present work we have used Gd_2O_3 to stabilize the t phase in ZrO_2. As described in Chapter 2, it has been possible to prepare powders of ZrO_2 with different amount of Gd_2O_3 and having a good sinterability by a coprecipitation route. In the following is described the preparation of sintered samples from these powders and the phases, microstructure, transformability of the t phase under different stimuli and the mechanical properties of the resulting ceramics.

3.4 *EXPERIMENTAL*

3.4.1 Sample Preparation

ZrO_2-Gd_2O_3 powders having 1.75, 2, 2.5, 3, 4, 5 and 8 mol% Gd_2O_3 were prepared by coprecipitation from Zr(IV) propoxide (Fluka Chemie AG, Switzerland) and Gd $(NO_3)_3.6H_2O$ as described in Chapter 2. The coprecipitated powders were calcined at 700°C for 4 hrs. followed by sintering at 1400°C for 2 hrs, as also described in Chapter 2. The sintered samples were subjected to following characterizations: (i) density, (ii) phase analysis and lattice parameter, (iii) transformability of the tetragonal phase

under different treatments, (iv) fracture toughness and strength and (v) microstructural characterizations. These are described below.

3.4.2 Characterizations

The density of the sintered samples was determined by Archimedes method using xylene as the immersion liquid. The phases were determined by x-ray diffraction on the polished surface of the sintered pellets as described earlier. Relative amounts of monoclinic (m) and tetragonal (t) phase were determined as given in Chapter 2. For determining the relative amounts of (t) and cubic (c) phase, the x-ray data in the 2θ range 72°-76° was used. The relative amounts of t and c phases was obtained using the relation

$$\frac{V_c}{V_t} = \frac{0.8472\ I_c(400)}{I_t(004) + I_t(400)} \qquad (3.5)$$

and

$$V_m + V_c + V_t = 1 \qquad (3.6)$$

The factor 0.8472 was calculated (Appendix I) from the structure factor of cubic and tetragonal phase of (004) and (400) reflections and using the relation given by Evans et.al. [42], Klug and Alexander [43] and Cullity [44].

Lattice parameter of the tetragonal phase was determined using a least square fitting routine on a minimum of eight peaks.

The extent of t $\longrightarrow$ m transformation was determined by x-ray diffraction after subjecting the samples to the following treatments:

(i) Quenching in Liquid Nitrogen (LN_2): The polished samples were held under liquid nitrogen for 24 hours.

(ii) Fracturing (Fr): The samples were broken in three point bend fixture.

(iii) Hand grinding (HG): The polished samples were slowly ground on 400 grit SiC slurry for about 10 minutes so as to remove about 100 μm thick layer.

(iv) Machine grinding (MG): The polished samples were glued to a stainless steel stub and pressed against a diamond wheel rotating at 2800 r.p.m. for 2-3 minutes to remove approximately a 100 μm layer.

For treatments (i), (iii) and (iv) the extent of t $\longrightarrow$ m transformation was measured on the treated surface while for treatment (ii) the fracture surface was measured.

In all the cases, the data was corrected for the amount of the monoclinic phase initially present on the polished surface.

Fracture toughness (K_{IC}) was measured by single edge notched beam (SENB) technique as well as by indentation technique.

In the SENB technique, rectangular bars with depth to breadth ratio 3 were cut from sintered circular disks by a low speed wafering saw using a 0.3 mm thick diamond blade. After cutting, the samples were polished on all sides by 12 μm alumina powder followed by 1 μm and 0.3 μm micropolish alumina powder. The sharp edges were rounded off. A single edge straight notch was made into the sample. The notch depth was 0.35-0.55 of the sample depth. The samples were subsequently broken in three point bending on a universal testing machine (Instron 1195, MA, USA).

In the indentation technique, the samples were indented by a Vickers indentor (Model HP 0250, Fritz Heckert, Leipzig, Germany) at 30 kg load and the crack length c and the length of the indent

diagonal (2a) were measured. All the measurements were done on polished surfaces. The fracture toughness was calculated using the following relations:

(a) For SENB Technique [45]

$$K_{IC} = \frac{3PLc^{1/2}}{2WD^2}\left[A_0+A_1(c/D) + A_2(c/D)^2 + A_3(c/D)^3 + A_4(c/D)^4\right] \qquad (3.7)$$

Here, P is the breaking load for the sample, l is the span length, c is the notch depth, W is the width and D is the depth of the sample. This relationship is valid for $c \simeq 0.5D$. A_0, A_1 are constants and their value is calculated from the following relations:

$$A_0 = 1.90 + 0.0075\ (L/D)$$

$$A_1 = -3.39 + 0.08\ (L/D)$$

$$A_2 = 15.4 - 0.2175\ (L/D)$$

$$A_3 = -26.24 + 0.2815\ (L/D)$$

$$A_4 = 26.38 - 0.145\ (L/D)$$

(b) For Indentation Technique [46]

$$K_{IC} = \frac{0.016\ \ (E/H)^{0.5}\ P}{c^{3/2}} \qquad (3.8)$$

where E is elastic modulus, H is the hardness and P is the load. Hardness was calculated from the slope of the plot of applied load and square of the half diagonal (a^2) at no crack condition of the indent using the relation [47]

$$H = 0.47 \times \text{slope} \qquad (3.9)$$

The fracture strength was measured in three point bending. To conserve on the sample material, small sized specimens, 12 mm x 2.4 mm x 0.8 mm were used. The samples were polished on all sides by 12 μm alumina powder. Some samples were also tested using test

bars of size 1.5 mm x 2 mm x 25 mm in a four point bending having 10 x 20 span as per ASTM specification [48].

The transformation zone depth (d) was determined using the relation [49]:

$$d = \frac{\sin \theta}{2 \mu} \left[\frac{X_{meas} - X_{bulk}}{X_{surf} - X_{meas}} \right] \qquad (3.10)$$

where X_{meas} and X_{bulk} are integrated x-ray intensity ratios of the monoclinic phase and measured on the fractured surface and from the as sintered surface respectively. X_{surf} is the integrated x-ray intensity ratio of m-ZrO_2 from the very top of the fracture surface. As the x-rays have a finite penetration depth, this quantity cannot be measured directly. Its value is taken to be Y_{bulk} , the value for the transformable phase in the bulk of the sample, i.e. it is assumed that all the transformable tetragonal phase is transformed at the top of the fracture surface. θ is taken to be 15° and μ is the linear absorption coefficient of TZP for x-rays [50].

For microstructural observations the samples were polished and thermally etched in air at 1350°C for 20 minutes. These were then examined in the scanning electron microscope (Model JSM 840A, JEOL, Japan). The average grain size ($\bar{D}$) was calculated by the line intercept method using the relation of Smith et.al. [51] and Mendelson [52],

$$\bar{D} = 1.558 \, \bar{L} \qquad (3.11)$$

where $\bar{L}$ is the average intercept length over a large number of grains as measured on the plane of the polished samples. At least 200 grains were measured for each value of average grain size. At higher concentration of Gd_2O_3 (5 and 8 mol%), some grains larger than the others were present.

For these two compositions, average grain size was separately determined for each of the two types of grains.

3.5 *RESULTS*

3.5.1 Density

The relative density of the samples, as a function of Gd_2O_3 content is shown in Fig. 3.4. The density of undoped sample (100% monoclinic) could not be measured by Archimedes method on account of severe cracking. Hence its density was measured geometrically. For other compositions, the relative density increases with increasing Gd_2O_3 content, reaches a maximum at 3 mol% Gd_2O_3 and then falls off again. However, the density in the four compositions, viz. 2, 2.5, 3 and 4 mol% Gd_2O_3 are all ≥ 90% of the theoretical. The maximum density is 99% for 3 mol % sample.

3.5.2 Phases

The relative amounts of different phases in the sintered samples vs. Gd_2O_3 content is shown in Fig. 3.5. Michel et.al. [11] found that a minimum of 3 mol % Gd_2O_3 is necessary to stabilize the tetragonal phase. However, in the present case, we found this amount to be 2.5 mol% Gd_2O_3. Even with 1.75 mol % Gd_2O_3 only ~ 12 vol % monoclinic phase is present. The monoclinic phase content drops to ~ 6 vol % at 2 mol % Gd_2O_3. While 2.5, 3 and 4 mol % compositions are single phase tetragonal material. Higher compositions, i.e. 5 and 8 mol % Gd_2O_3 samples show the presence of t and c phase. However, the amount of c phase in 5 mol % sample is only about 9 %, but it increases to about 80% for 8 mol % Gd_2O_3 samples. In comparison, Leung et.al. [53] have reported complete stabilization of cubic phase at 8 mol % Gd_2O_3 samples.

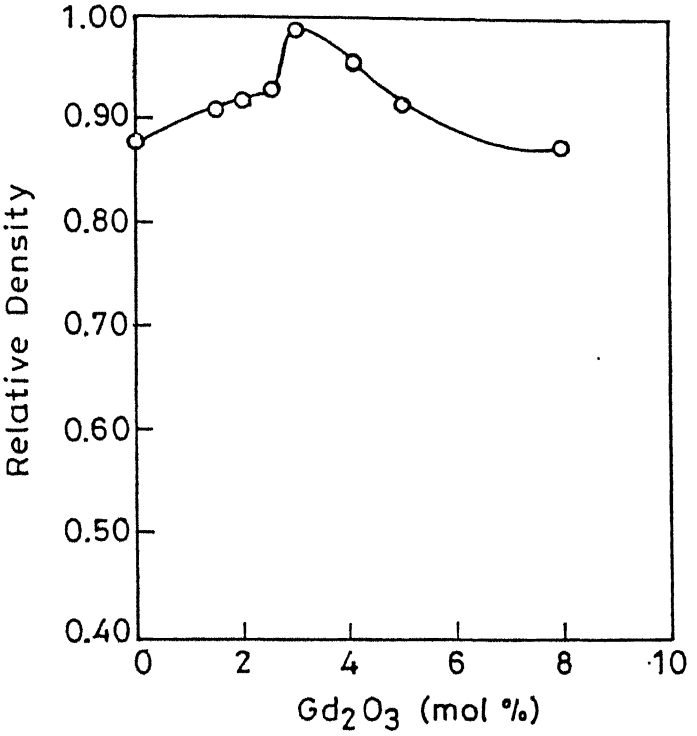

Fig. 3.4 Relative density of ZrO_2 -Gd_2O_3 samples as a function of Gd_2O_3.

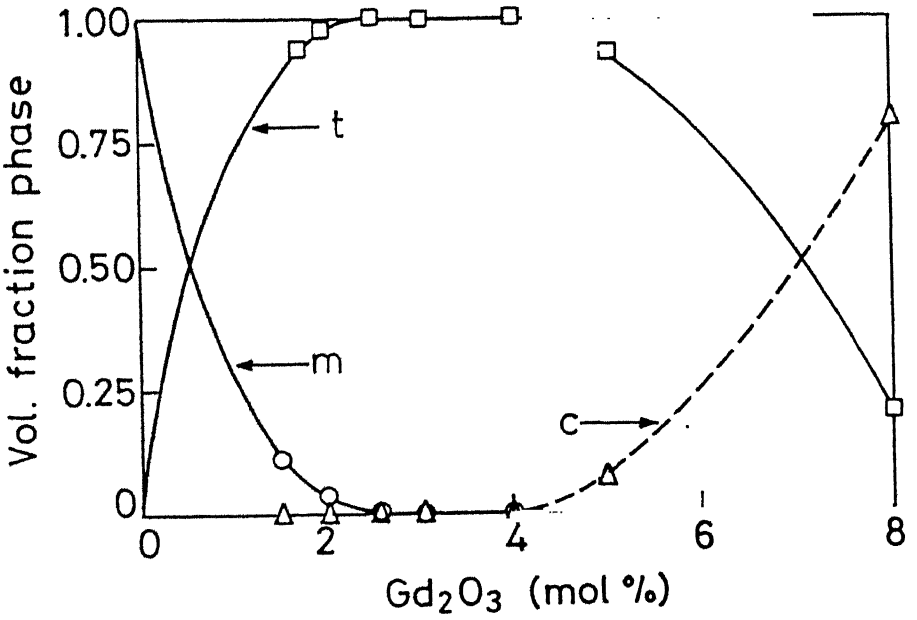

Fig. 3.5 Relative amounts of different phases in the sintered samples with increasing Gd_2O_3 content.

3.5.3 Lattice Parameter and c/a axial ratio

The change in lattice parameters and the c/a ratio of the tetragonal phase with change in Gd_2O_3 content is shown in Figs. 3.6 and 3.7 respectively. The c-axis shortens while the a-axis elongates with increasing Gd_2O_3 content. The lattice parameter for pure tetragonal phase with no dopant (0% Gd_2O_3) is taken from Tsheu et.al. [54]. A least square fit of the data indicates that c/a would become unity (i.e. a cubic phase would be obtained) at ~ 9.6 mol % Gd_2O_3 [Fig. 3.7].

3.5.4 Transformability of Tetragonal Phase under Different Treatments

The amount of tetragonal phase transformed to monoclinic phase under different treatments is shown in Fig. 3.8. For all treatments except that in LN_2 quenched samples, highest m- phase was registered in 2 mol% samples. The m- phase gradually decreased to lower value at higher Gd_2O_3 content. However, in LN_2 quenched samples, highest m- phase was obtained in 1.75 mol% samples (~ 75%) and it dropped to 70% for 2mol%. Following this, there was a sharp drop to 46% at 2.5 mol% which further dropped to 5% for 3 mol%. While very little transformation was observed in 4 mol% samples no transformation could be measured in 5 and 8 mol% samples. However, for all other treatments the transformability of 1.75 mol % samples is lower than that of 2 mol % samples giving a peak at 2 mol % samples. The transformation zone depth was determined from the fractured surface transformability data. The zone depth shows a similar trend to that of transformability data (Fig. 3.9). The maximum zone depth is 3.4 μm and minimum is 0.5

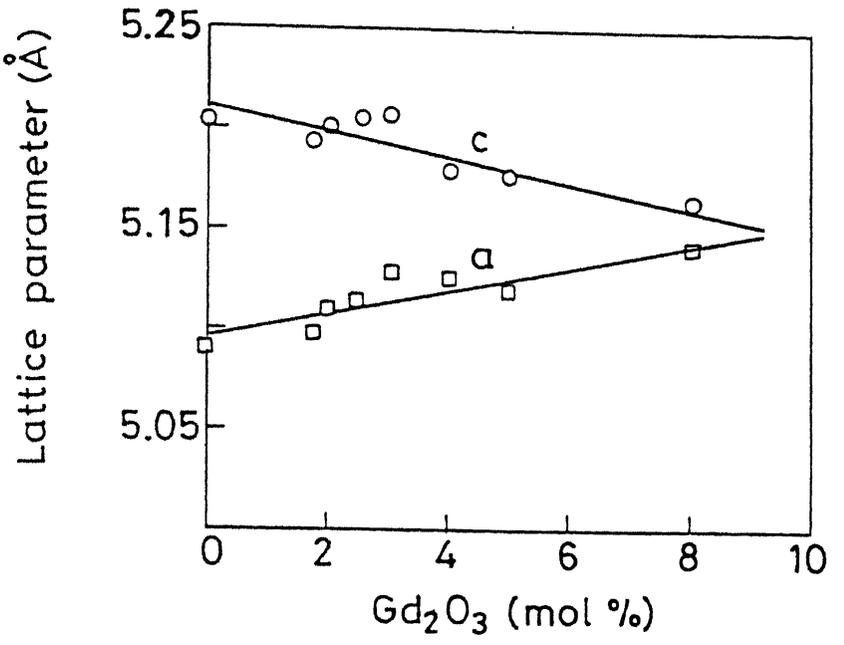

Fig. 3.6 Lattice parameters of ZrO_2-Gd_2O_3 alloys with increasing Gd_2O_3 content.

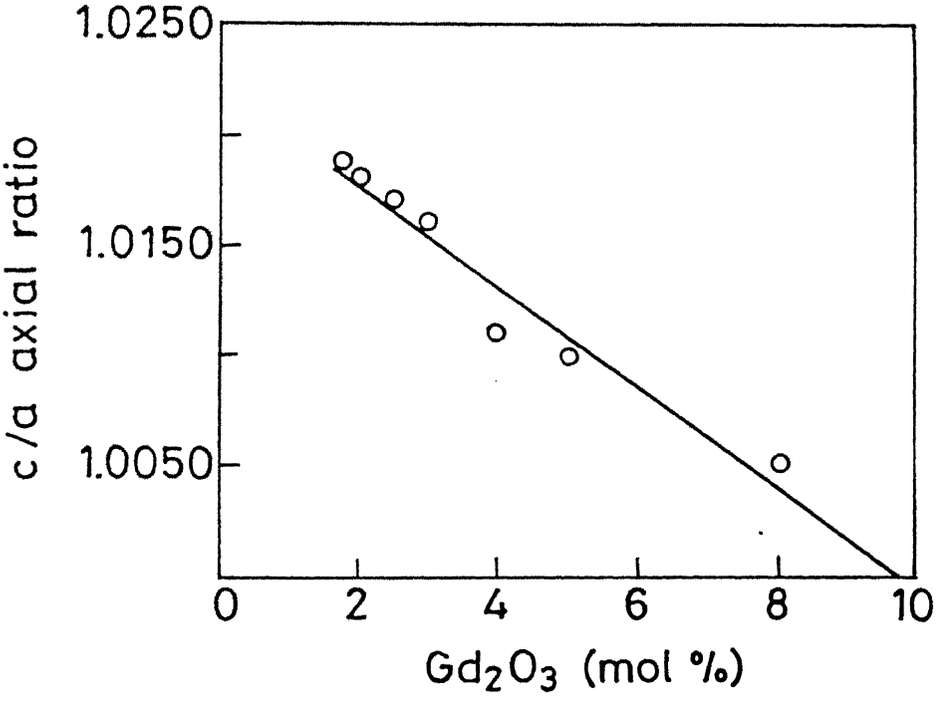

Fig. 3.7 Tetragonality (c/a axial ratio) with increasing Gd_2O_3 content.

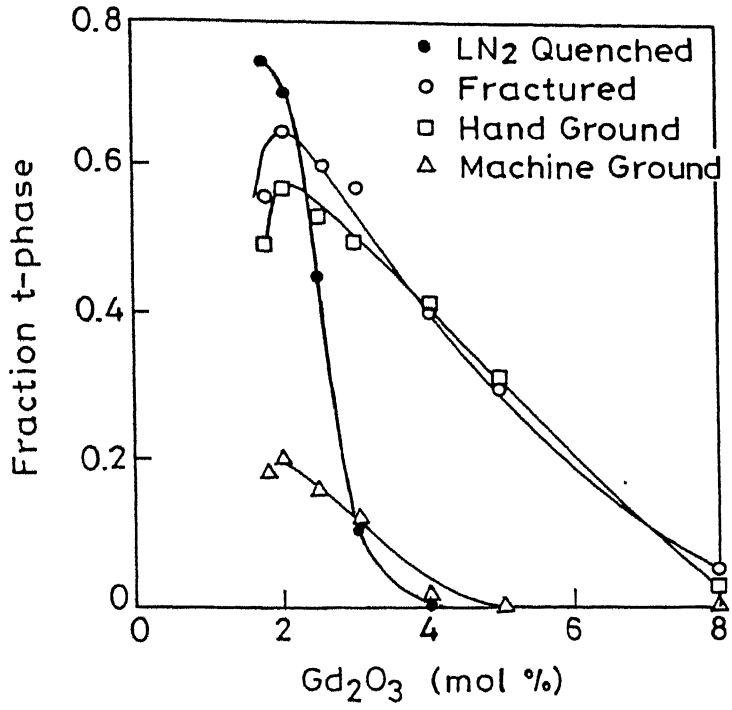

Fig. 3.8 Amount of t-phase transformed under different treatments.

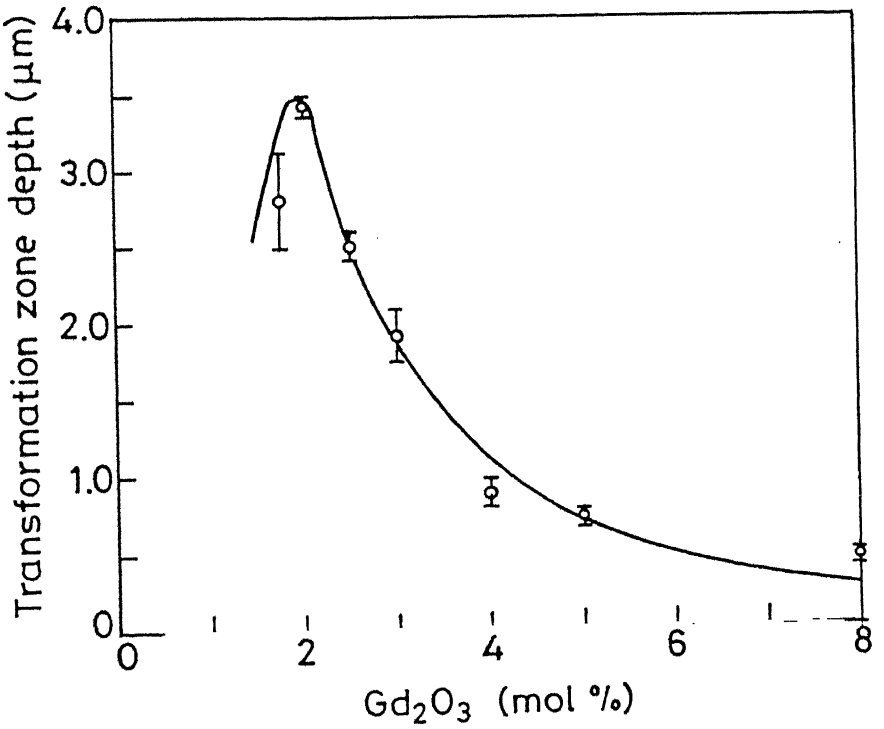

Fig. 3.9 Transformation zone depth with increasing Gd_2O_3 content.

μm. The zone depth for 1.75 mol % Gd_2O_3 is lower than that for 2 mol % samples, again giving a peak at 2 mol % Gd_2O_3.

3.5.5 Fracture Toughness, Strength and Hardness

As already discussed, the fracture toughness was measured by two different methods, viz. SENB method and indentation method. In SENB method, maximum toughness obtained is 14.7 MPa$\sqrt{m}$ for ZrO_2 - 2 mol % Gd_2O_3 samples (Fig. 3.10(a)). However, there is broad maxima in toughness for the composition range 1.75 to 4 mol % Gd_2O_3 where the toughness varies from 12 to 14.7 MPa$\sqrt{m}$. The toughness drops to less than 10 MPa$\sqrt{m}$ for 5 mol % samples and it is only about 2 MPa$\sqrt{m}$ for 8 mol % samples.

On the other hand, the maximum toughness obtained by indentation technique is about 12 MPa$\sqrt{m}$ for 2 mol % samples (Fig. 3.10(b)) and the toughness drops to lower values on either side of this composition. However, the toughness is ≥ 10 MPa$\sqrt{m}$ for 1.75 - 4 mol% Gd_2O_3. At higher concentration, (viz. 5 and 8 mol%), the toughness again drops down to lower values.

Fracture strength was also calculated by three point bending. The nature of the curve (Fig 3.11) is similar to that of toughness curve . Here also the maximum (~ 900 MPa) is obtained for 2 mol % samples and between 2-3 mol %, the strength values are in the range of 830 to 880 MPa. As the sample size used were smaller than the standard, these values are likely to overestimate the strength. To determine the extent of overestimation samples of 2 mol% Gd_2O_3 were tested using standard sized test bars as described before. The results are also shown by dotted bars in Fig. 3.8 . It is seen that the small sized samples overestimate the strength values by 10 to 15 %.

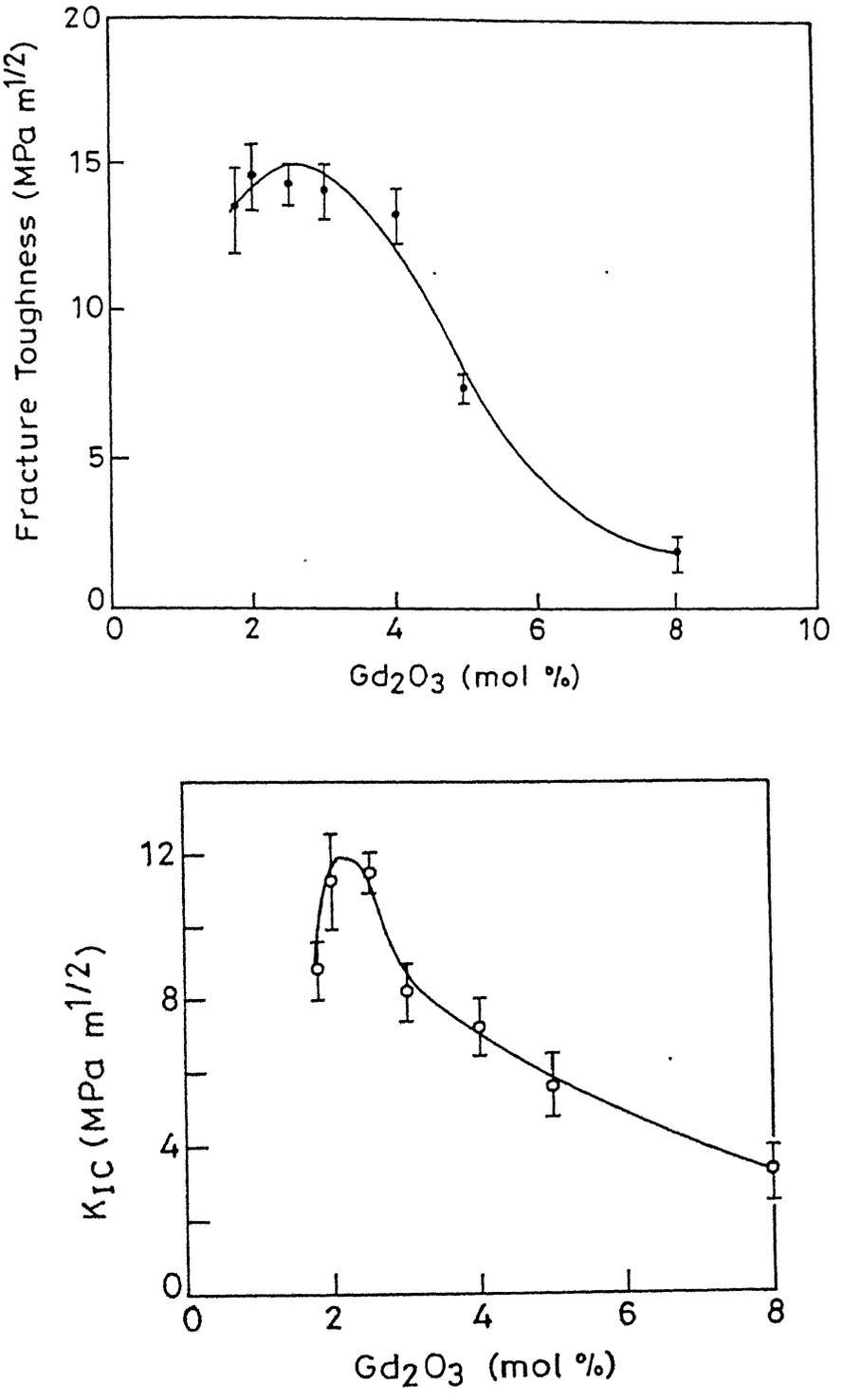

Fig. 3.10 Fracture Toughness of ZrO_2 -Gd_2O_3 alloys with increasing Gd_2O_3 content (a) SENB method, (b) Indentation method.

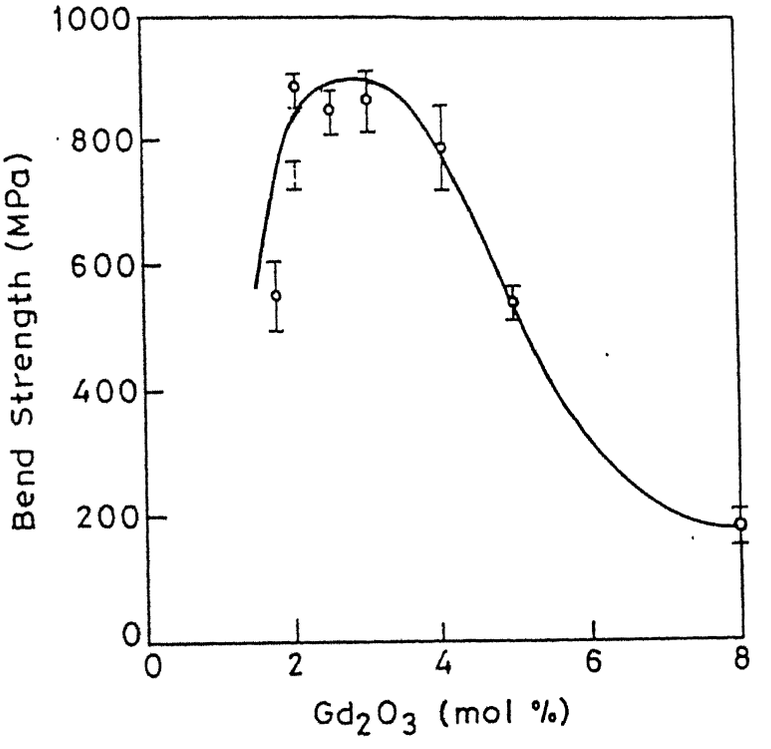

Fig. 3.11 Fracture strength of ZrO_2-Gd_2O_3 alloys with increasing Gd_2O_3 content.

The variation of Vickers hardness with Gd_2O_3 content, as determined by the slope of the P vs. a^2 plot is shown in Fig. 3.12. There is a broad maxima in hardness (~ 14.2 GPa) for 2.5 to 5 mol % samples. The hardness decreases to ~ 12.5 GPa for 2 mol % samples and it further drops to ~ 10 GPa for 1.75 mol % samples. In the higher concentration region, the hardness drops to about 8 GPa for 8 mol % samples.

3.5.6 Microstructural Characterizations

Fig. 3.13(a) to 3.13(d) show the representative microstructure of polished surface of sintered ZrO_2 - Gd_2O_3 samples. Except for 8 mol % Gd_2O_3 (Fig. 3.13 (d)) all the grains are rounded and have extremely fine grain size (0.10 - 0.15 μm). The average grain size (Table 3.1) does not change much in the range 1.75 to 4 mol % Gd_2O_3.

Table - 3.1

Grain Size and Density of ZrO_2- Gd_2O_3 Alloys

Composition (mol% Gd_2O_3)	Grain Size (μm) Average	Std. deviation	Relative Density
1.75	0.14	0.04	0.90
2	0.11	0.02	0.92
2.5	0.13	0.01	0.93
3	0.14	0.02	0.99
4	0.13	0.02	0.96
5	0.17 0.35	0.02 0.03	0.92
8	0.20 0.67	0.03 0.02	0.88

But for compositions, 1.75 - 2.5 mol % Gd_2O_3, a bimodal grain size distribution is observed. Almost uniform grain size is observed for 3 and 4 mol % samples. At higher concentration of dopant

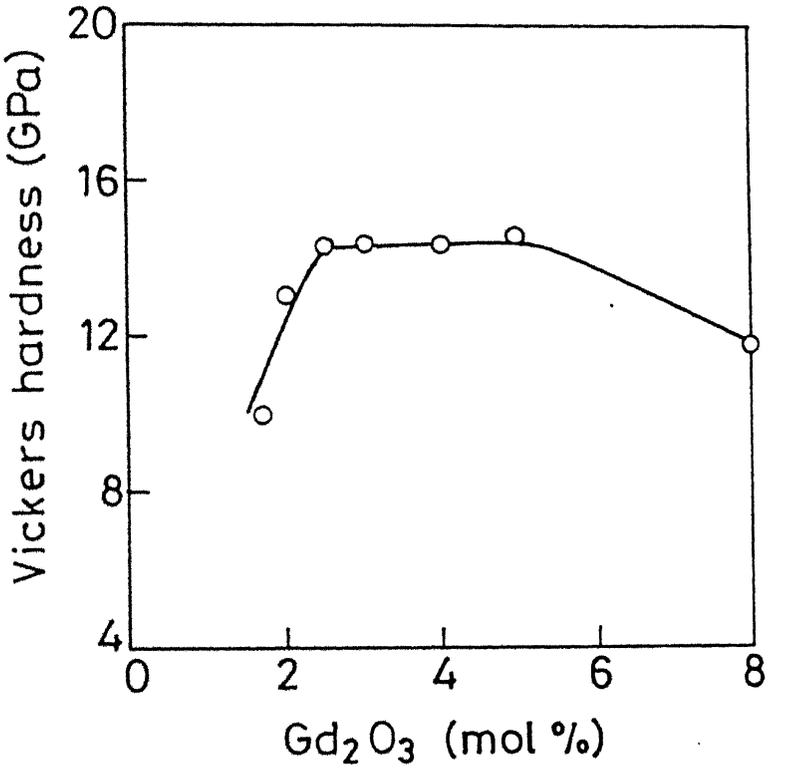

Fig. 3.12 Vickers Hardness of ZrO_2-Gd_2O_3 alloys.

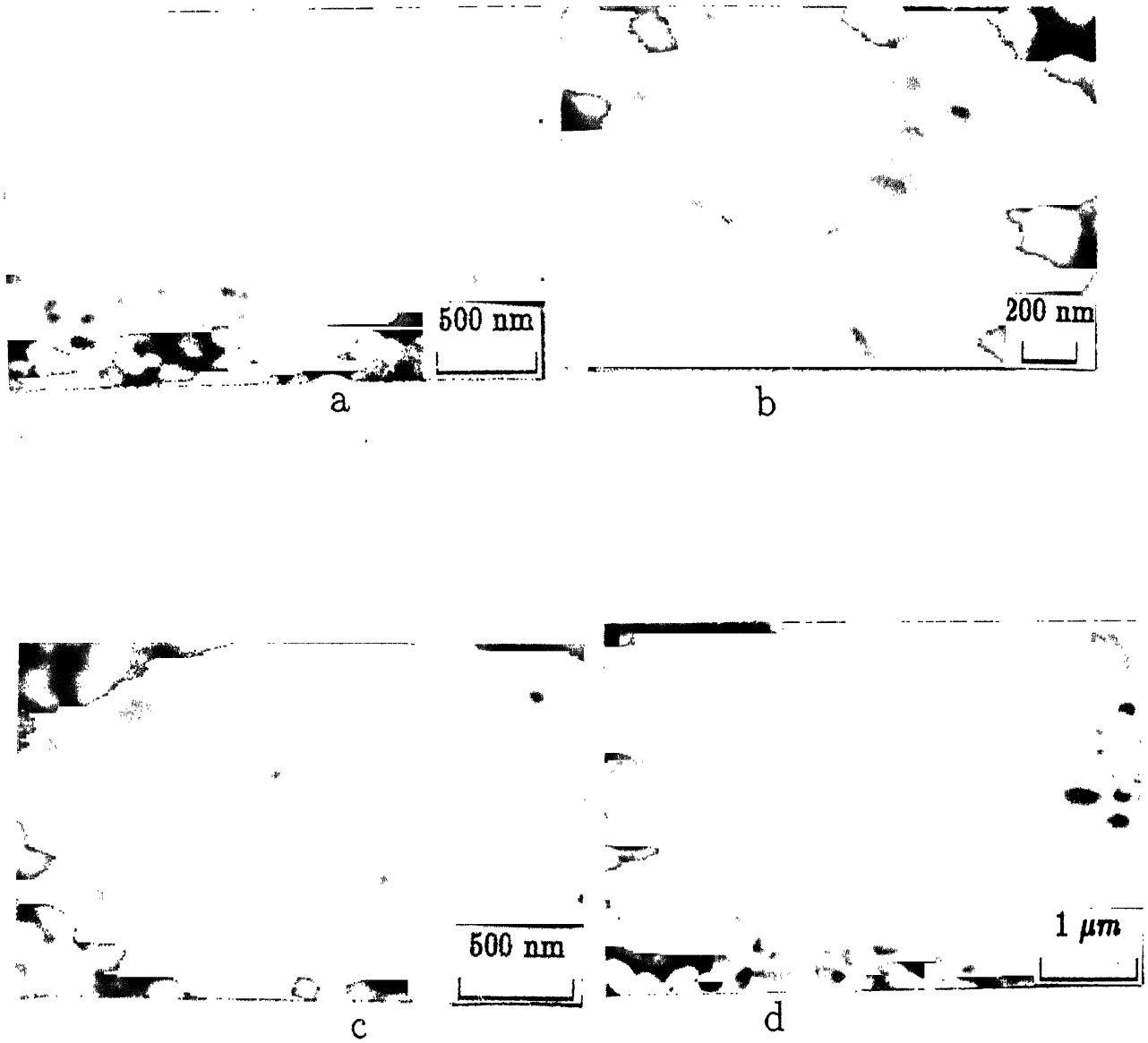

Fig. 3.13 Polished surface microstructures of ZrO_2-Gd_2O_3 alloys (a) 1.75 mol% Gd_2O_3, (b) 3 mol% Gd_2O_3, (c) 5 mol% Gd_2O_3 (d) 8 mol% Gd_2O_3.

the attainment of equilibrium in ZrO_2-Gd_2O_3 alloys is a slow process needing about 200 hours at 1400°C. Leung et.al. prepared ZrO_2-Gd_2O_3 powder from aqueous precursors using Zirconium acetate and Gadolinium nitrate. Subsequently amorphous thin film and granules were crystallized from it by heating in air at different temperature. It was found that phase partitioning of 3 mol % samples (having t phase) took place depending on heating rate. While faster heating rate slowed down or prevented phase partitioning, it took place appreciably in slowly heated samples. They also found that a metastable tetragonal phase is obtained subsequent to precursor pyrolysis when Gd_2O_3 content is ≤ 6.5 mol % which upon holding at high temperatures (1400°C), partitions into tetragonal and cubic phases. They estimated the maximum equilibrium solid solubility of Gd_2O_3 in tetragonal ZrO_2 to be 1.0 ± 0.1 mol % and 8.0±0.2 mol % for cubic ZrO_2. As compared to this, we find the maximum solid solubility of Gd_2O_3 in tetragonal phase to be as high as 4 mol % (Fig. 3.5). Similarly, when the c and a lattice parameters of the tetragonal phases are extrapolated to c/a = 1, the minimum solid solubility of Gd_2O_3 in cubic ZrO_2 is estimated to be 9.6 mol % (Fig. 3.6 and 3.7). This was verified by preparing two alloys containing 9 and 9.6 mol % Gd_2O_3. While some t phase was present in the former, (Fig. 3.14(a)) the latter showed only cubic phase (Fig. 3.14(b)). Similarly results were also obtained Li et al.[58]. Clearly, therefore, the phases in the present work are in metastable equilibrium. This is expected because the samples were held at 1400°C only for 2 hours, as compared to 200 hours required (as reported by Leung et al) to

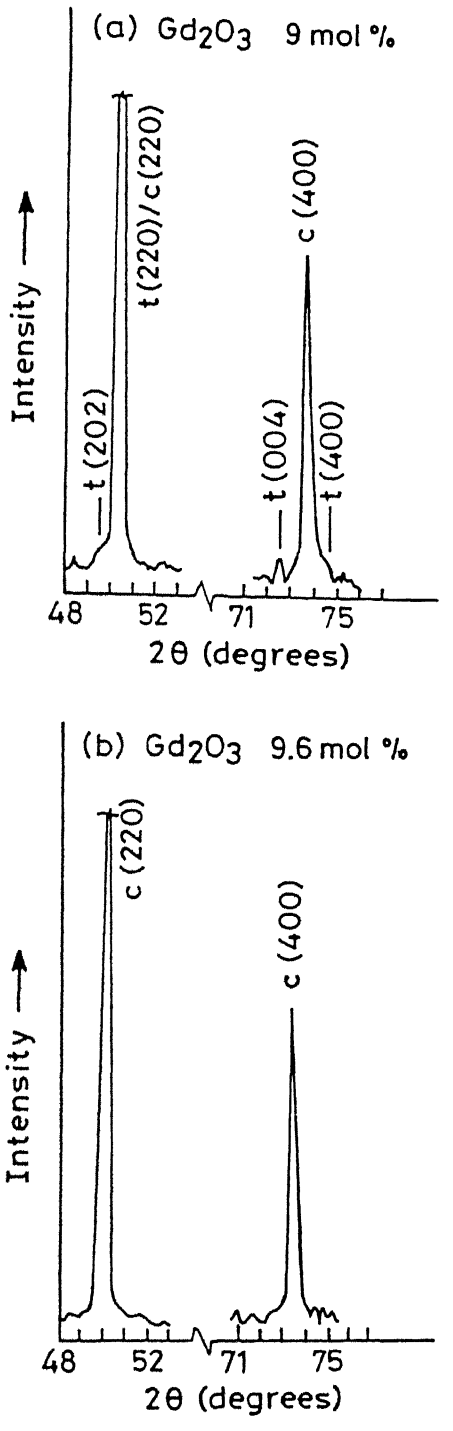

Fig. 3.14 X-ray diffraction pattern of (a) ZrO_2-9 mol% Gd_2O_3 and (b) ZrO_2-9.6 mol% Gd_2O_3. While former shows presence of t-phase, the latter shows only cubic phase.

attain equilibrium concentrations in the tetragonal and, the cubic ZrO_2 phases.

3.6.3 Microstructure and Grain Size

Fig. 3.13(a) to 3.13(d) show the microstructure of sintered ZrO_2-Gd_2O_3 samples. Except for 8 mol % Gd_2O_3 (Fig. 3.13(d)) all the grains are rounded and have extremely small grain size (0.10 - 0.15 μm). The grain size (Table 3.1) is constant over the range 1.75 to 4 mol % Gd_2O_3. At 5 mol % a few large grains (0.3 - 0.4 μm) appear and at 8 mol % majority of the grains are large (0.6 μm), though there are smaller grains (0.25 μm) lying at the junction of 3 to 4 grains. These large grains, unlike the smaller grains are faceted i.e. they are sharp corners. The existence of small grains in the single phase tetragonal region and two phase (tetragonal + cubic) regionhave been addressed by many investigators. The proposed models are solute drag model [59], space charge drag model [60] and coherency strain model [61]. In the cubic phase, the grain growth is not inhibited. This correlates well with increasing number of large grains present in the 5 and 8 mol % samples which contain 9 and 90 % cubic phase respectively. Similar results concerning grain growth and composition have also been reported [59].

3.6.4 Transformation Under Different Treatments

The t $\longrightarrow$ m transformation in TZP's can be initiated by stress and temperature. However, the susceptibility to transformation depends on the treatment. As shown in Fig. 3.8, the maximum transformation (~ 75%) is obtained in 1.75 mol % Gd_2O_3 samples quenched in LN_2. In LN_2 samples, the extent of transformation decreases very rapidly with increasing Gd_2O_3 due to decrease in

the M_s temperature with composition.

Both Fr and HG samples show comparable values of t $\longrightarrow$ m transformation because these transformation is actuated by stress. However, the actual amount of transformation that takes place during fracture or hand grinding may be more than the observed value. This is due to the possibility of reverse m $\longrightarrow$ t transformation that may take place in these cases. On the other hand, MG samples recorded very small t $\longrightarrow$ m transformation. This is due to the reason that during machine grinding a considerable amount of heat is generated [62]. Although, precise measurement of temperature was not possible, these investigators reported it to be between 700°C-2000°C. This high temperature reverts back most of m phase to t phase resulting in a decrease in the observed value.

Finally, the decrease in t $\longrightarrow$ m transformation for Gd_2O_3 < 2 mol % needs to be discussed. In general, the t $\longrightarrow$ m transformation should become thermodynamically easier as the stabilizer content decreases. However, if the transformation is nucleation controlled, as appears to be the case [63-64], then the presence of second phase separating the grains would also affect the total amount of t $\longrightarrow$ m transformation. Such a microstructure suppresses the autocatalytic nucleation events and leads to reduction in the fraction of transformed t phase. Thus the presence of about 10 vol % monoclinic phase in the 1.75 mol % Gd_2O_3 samples may be responsible for a decrease in the total t $\longrightarrow$ m transformation in this sample.

3.6.5 Contribution of Transformation Toughening to K_{IC}

To quantify the contribution of transformation toughening

($K_{IC\ TT}$), the fraction t phase transformed on the fractured surface and the transformation zone depth were determined. These are shown in Fig.3.8 and 3.9 respectively. $K_{IC\ TT}$ was calculated using the following equation:

(a) Dilatation only: [65]

$$K_{IC\ TT} = \frac{0.22\ E\ V_f\ e^T\ \sqrt{h}}{(1-\nu)} \qquad (3.12)$$

(b) Shear only: [65]

$$K_{IC\ TT} = 0.55\ E\ V_f\ e^T\ \sqrt{h} \qquad (3.13)$$

(c) Shear and Dilatation: [66]

$$K_{IC\ TT} = \frac{0.48\ E\ V_f\ e^T\sqrt{h}}{(1-\nu)} \qquad (3.14)$$

The experimental values of K_{IC} and the $K_{IC\ TT}$ calculated according to the above three equations are shown in Fig. 3.15. The largest contribution by transformation toughening is observed when shear and dilatation both are considered (Eq. 3.14 above). The values of K_{IC} calculated using eq. 3.14 is able to account for most of the toughness. The sources of the additional toughness could be (i) m $\longrightarrow$ t reversal on the fracture surface after the passage of the crack, this would lead to an underestimate of the contribution due to transformation toughening, (ii) domain switching in the tetragonal phase, (iii) other effects like crack branching, microcracking.

In order to determine whether there was any significant contribution to fracture toughness from domain switching, the ratios I(202)/I(220) and I(113)/I(131) for the t phase before and after the transformation were examined. These are shown in Fig. 3.16. The values of these ratios as found by Virkar et al [12] is

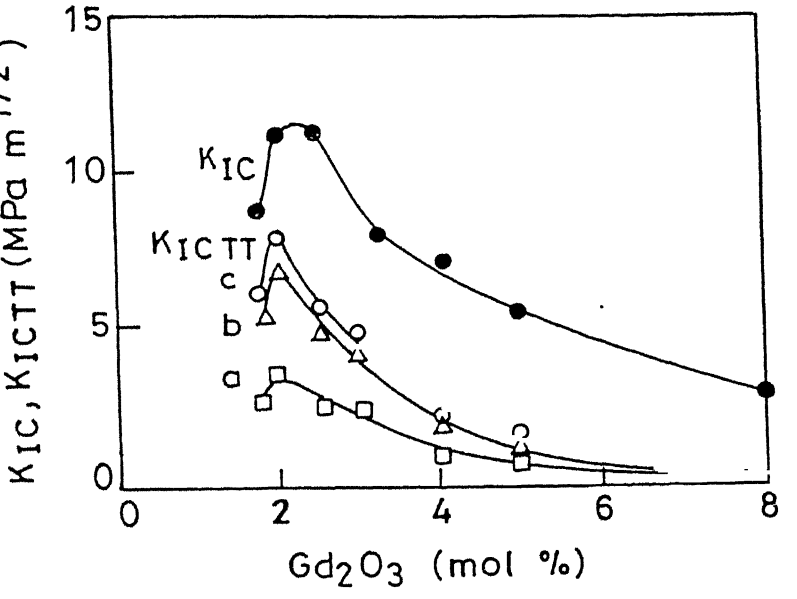

Fig. 3.15 Experimental value of K_{IC} and calculated $K_{IC\ TT}$ with increasing Gd_2O_3 content.

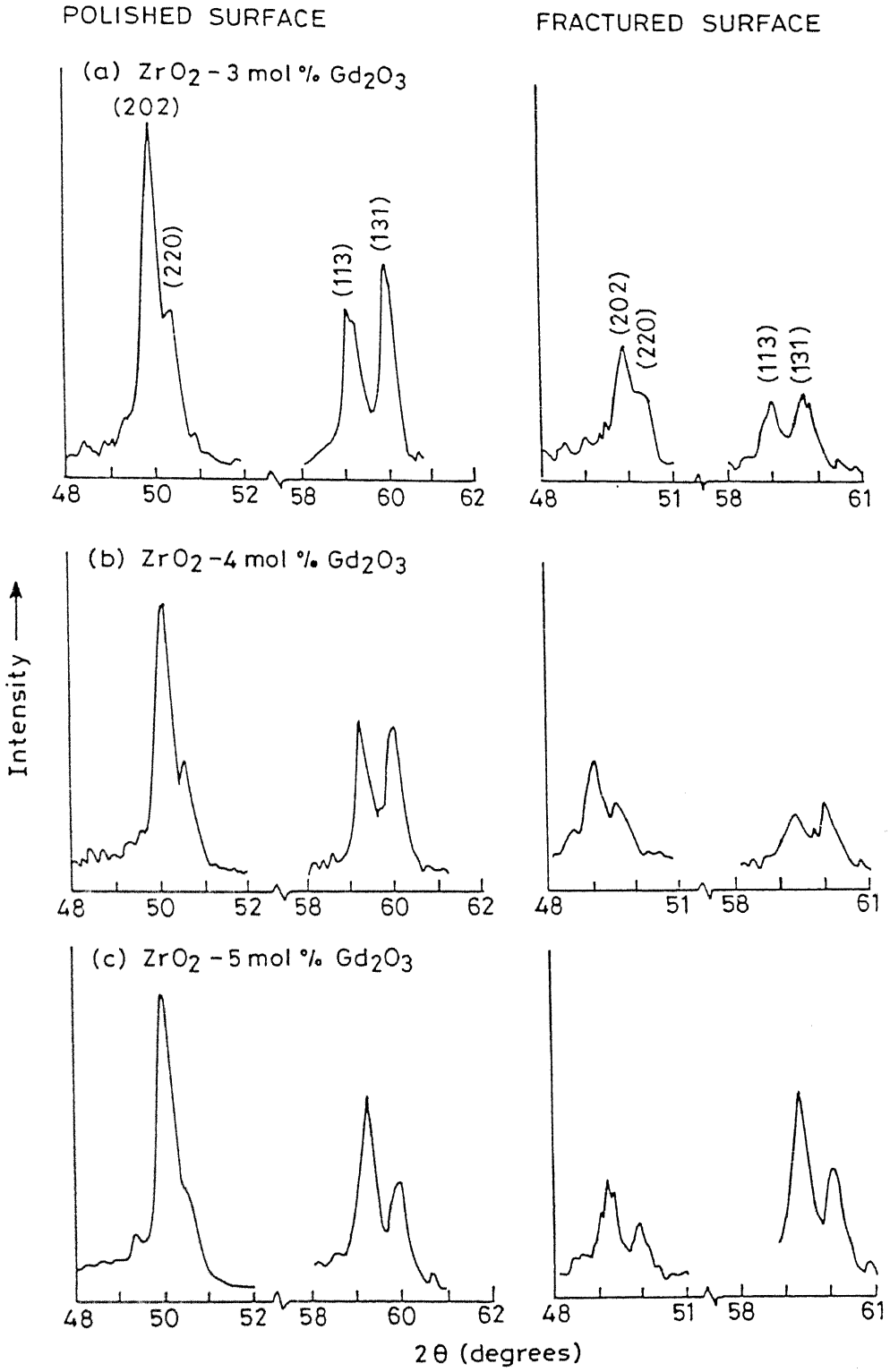

Fig. 3.16 X-peak intensity ratios for I(202)/I(220) and I(113)/I(131) for t-phase in the sintered and fractured samples.

reproduced in Table 3.2.

The change in the intensity ratios are very small as compared to those reported by Virkar et.al. [Table 3.2]. As there was significant amount of t $\longrightarrow$ m transformation the texture due to such transformation,[13,14] would also be present and would obscure the changes due to domain switching. However, the peaks in Fig. 3.13 are significantly broadened after the transformation as is characteristic of domain switching [12]. It is possible therefore that domain switching may also be contributing to K_{IC}.

3.6.6 Strength and Hardness

The strength of brittle solids is determined by the size of the most severe flaw. For a brittle solid, K_{IC} and fracture strength (σ_f) are related by

$$K_{IC} = Y\ \sigma_f (C)^{1/2} \qquad (3.15)$$

where Y is a geometrical factor which is constant for all the samples and c is the half length of critical flaw from which fracture originates. Thus, knowing K_{IC} and σ_f from the above relation relative values of c can be calculated. The normalized critical flaw size are tabulated in Table 3.4 along with relative porosity [i.e. (1-relative density)] and grain size. It is often stated that the larges[illegible] flaw size scales with grain size. However, in the present case, [illegible]here is no such correlation between the relative values of t[illegible]ritical flaw size and grain size. On the other hand, the rela[illegible] critical flaw size correlates quite well with the relative pc[illegible]y as shown in Fig. 3.17. Obviously, the fracture or failure [illegible]nates from the pores or voids present in the sintered samples.

Table 3.2

Ratio of I(202)/I(220) and I(113)/I(131) in Sintered and in the ground Surface [12]

	Theoretical	As Sintered	After Surface Grinding
I(202)/ I(220)	2.0	2.16	8.21
I(113)/ I(131)	0.5	0.53	2.79

The corresponding data for ZrO_2-Gd_2O_3 samples is shown in Table 3.3.

Table 3.3

Relative Changes in the X-ray Peak Height Ratios of I(202)/I(220) and I(113)/I(131) on Fractured Surface

Composition (mol% Gd_2O_3)	I(202)/I(220)			I(113)/I(131)		
	Polished	Fractured	% Relative change in intensity	Polished	Fractured	% Relative change in intensity
3	2.16	1.61	-25.4	0.79	0.84	+6.3
4	2.52	1.75	-30.6	1.03	0.87	-15.1
5	3.44	3.00	-12.8	1.86	1.67	-9.1

Table 3.4

Normalized Critical Flaw Size [Y^2c], Relative Porosity and Grain Size of ZrO_2-Gd_2O_3 Alloys

Composition (mol% Gd_2O_3)	Normalized Y^2c	Relative Porosity	Average Grain Size (μm)
1.75	2.47	0.10	0.14
2	1.73	0.08	0.11
2.5	1.44	0.07	0.13
3	1.00	0.01	0.14
4	1.08	0.04	0.13
5	1.67	0.08	0.17 0.35
8	2.27	0.12	0.20 0.67

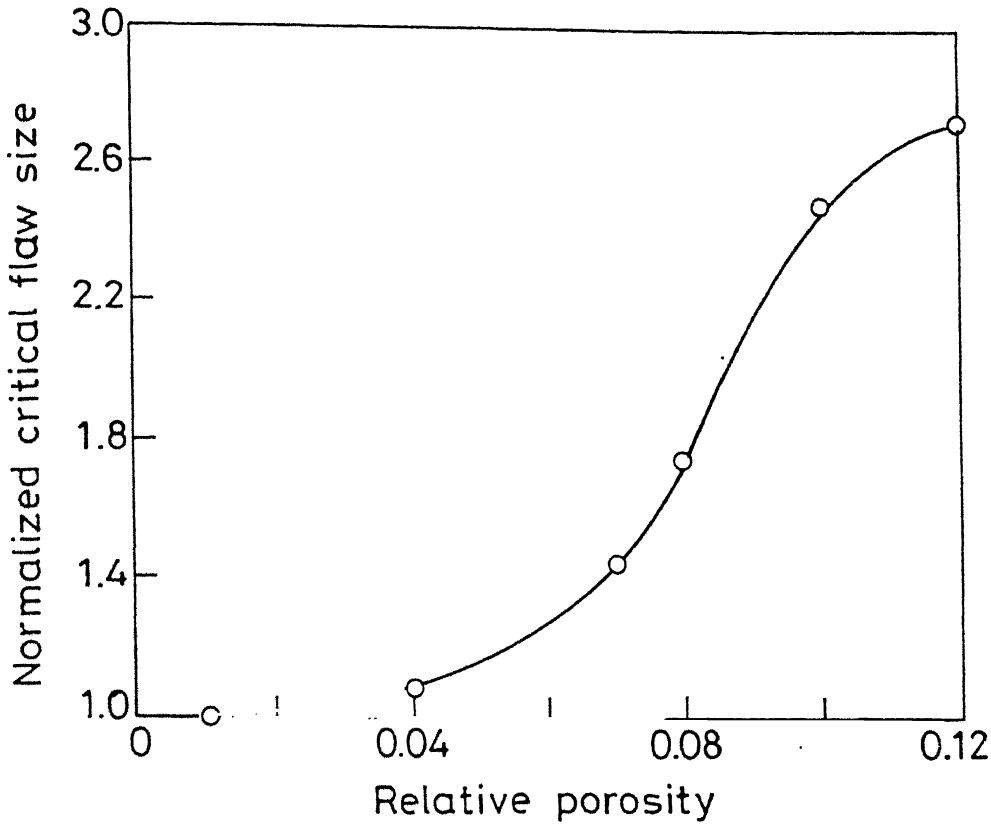

Fig. 3.17 Changes in relative critical flaw size with relative porosity.

The hardness is found to be maximum and nearly constant between 2.5 and 5 mol% Gd_2O_3 samples (Fig. 3.9). The tetragonal phase with strains due to tetragonal distortion, is expected to have a higher hardness than the cubic phase. However, while c/a ratio continuously decreases as the Gd_2O_3 content is increased, the hardness remains nearly constant in the composition range 2.5 to 5 mol %. Moreover, at 1.75 and 2 mol % Gd_2O_3, the hardness values are lower than the maximum even though the c/a is nearly the highest and the phase is nearly fully tetragonal. The presence of monoclinic phase in these two samples seems to have an effect on the hardness of these two composition. Monoclinic phase not only relieves the strain accumulated due to retention of metastable tetragonal but also introduces some cracks or pores in the material. These defects along with release of strains is expected to lower the hardness value.

3.7 *SUMMARY AND CONCLUSIONS*

As already mentioned in the Chapter 2, it has been possible to prepare dense tetragonal zirconia polycrystals in the ZrO_2, Gd_2O_3 system. So, the focus of the present chapter was to investigate the evolution of different phases of zirconia with change in Gd_2O_3 concentration, the stability of the tetragonal phase under different treatments, the effect of Gd_2O_3 content on the strength, toughness and hardness of ZrO_2-Gd_2O_3 alloys, the change in microstructural features of the above ZrO_2-Gd_2O_3 alloys and to try to find a correlation between phase, transformability, microstructure and mechanical properties. In order to study these effects seven compositions of ZrO_2 samples were prepared by co-precipitation route having Gd_2O_3 content between 1.75 and 8

mol% followed by sintered at 1400°C for 2 hours. Following are some of the important conclusions arrived at from such study:

(i) With increasing Gd_2O_3 the phases in the sintered samples changed from two phase mixture of monoclinic and tetragonal (for 1.75 and 2 mol % Gd_2O_3) to a two phase mixture of cubic and tetragonal (5 and 8 mol %) through a region of single phase tetragonal (2.5, 3 and 4 mol %).

(ii) The tetragonal phase exhibited varying degree of stability when exposed to different treatments. Only in LN_2 quenched samples maximum transformability was obtained in 1.75 mol% samples (~ 75%). All the other treatments showed maximum transformability in 2 mol% samples with highest transformability (~ 70%) in fractured sample and lowest(~ 25%) in machine ground samples.

(iii) High toughness value was registered in samples having composition between 1.75 to 4 mol % Gd_2O_3, which decreased to lower values in the 5 and 8 mol %. Although 2 mol % samples registered highest toughness its value depended on the measurement technique. Thus, it was 14.7 $MPa\sqrt{m}$ for SENB technique and 12 $MPa\sqrt{m}$ for indentation technique.

(iv) The strength values also show similar trend with change in Gd_2O_3 content. Here high strength values were recorded in 1.75 to 4 mol% samples (between 880-770 MPa) while 5 and 8 mol% registered lower values (450-200 MPa). However, highest strength was again recorded for 2 mol% samples (880 MPa). Due to small size of sample used, these values are believed to overestimate the strength. Actual strength values, measured on standard sized samples, are likely to be lower by about 15 %.

(v) The hardness of ZrO_2-Gd_2O_3 alloys remained constant from 2.5 to 5 mol % samples, before going down to lower values on either side of this range.

(vi) The grain size remained constant (0.1-0.15 μm) over the range 1.75 to 4 mol % samples. However, 5 and 8 mol % samples had some larger grains (0.3-0.6 μm) as also smaller grains (0.18 - 0.2 μm). These latter samples also registered cubic phase (9% for 5 mol % and 80% for 8 mol % Gd_2O_3).

(vii) Transformation toughening was able to account for most of the toughening in these samples. However, other mechanisms like domain switching also probably contributes to some extent.

(viii) The strength values were governed by the relative flaw size and porosity in the samples. Samples having lower strength had larger relative flaw size and a higher porosity.

REFERENCES

1. K. Tsukuma and T. Takahata, "Mechanical Property and Microstructure of TZP and TZP/Al_2O_3 Composites", pp. 123-35 in Advanced Structural Ceramics. Edited by P.F. Becher, M.V. Swain and S. Somiya, Materials Research Society, Pittsburgh, PA, 1987.

2. K. Tsukuma, "Mechanical Properties and Thermal Stability of CeO_2 Containing Tetragonal Zirconia Polycrystals", Am. Ceram. Soc. Bull 65 [10] 1386-89 (1986).

3. D. J. Green, R. H. J. Hannink and M. V. Swain, Transformation Toughening of Ceramics pp 65. CRC Press Inc., Florida, 1989.

4. A.G. Evans, "Toughening Mechanisms in Zirconia Alloys," pp 193 - 201 in Advances in Ceramics, Vol. 12, Science and Technology of Zirconia II. Edited by N. Claussen and A.H. Heuer, American Ceramic Society, Inc. Columbus, Ohio, 1984.

5. A.G. Evans and R.M. Cannon, "Toughening of Brittle Solids by Martensitic Transformations", Acta. Metall. 34 [5] 761-800 (1986).

6. K.T. Faber and A.G. Evans, "Crack Deflection Process - I. Theory", Acta. Metall. 31 [4] 565-76 (1983).

7. D.B. Marshall and A.G. Evans, "Failure Mechanism in Ceramic-Fibre/ Ceramic Matrix Composites", J. Am. Ceram. Soc. 68 [5] 225-31 (1985).

8.. P.L. Swanson, C.J. Fairbanks, B.R. Lawn, Y.-W. Mai and B.J. Hockey, "Crack-Interface Grain Bridging as a Fracture Resistance Mechanism in Ceramics", J. Am. Ceram. Soc. 70 [4] 2279-89 (1987).

9. R.P. Ingel, R.W. Rice and D. Lewis, "Room Temperature Strength and Fracture Toughness of ZrO_2- Y_2O_3 Single Crystals", J. Am. Ceram. Soc. 65 [7] C-108 (1982).

10. R.P. Ingel, D. Lewis, B.A. Bender and R.W. Rice, "Temperature Dependence of Strength and Fracture Toughness of a ZrO_2 Single Crystal", 65 [9] C-150 (1982).

11. D.Michel, L. Mazerolles and M., Perez Y. Jorba, "Fracture of Metastable Tetragonal Zirconia Crystals," J. Mater. Sci. 18 2618-28 (1983).

12. A.V. Virkar and R.L.K. Matsumoto, "Ferroelastic Domain Switching as a Toughening Mechanism in Tetragonal Zirconia", J. Am. Ceram. Soc. 69 [10] C-224 - C-226 (1986).

13. K. J. Bowman, "Texture from Domain Switching of Tetragonal Zirconia," J. Am. Ceram. Soc. 74 [10] 2690-92 (1994).

14. K.J. Bowman and I. W - Chen, " Transformation Textures in Zirconia," J. Am. Ceram. Soc. 76 [1] 113-22 (1993).

15. K. Tsukuma, Y. Kubota and T. Tsukidate, " Thermal and Mechanical Properties of Y_2O_3 Stabilized Tetragonal Zirconia Polycrystals", pp. 382-90 in Advances in Ceramics, Vol.12. Edited by N. Claussen, M. Ruhle and A.H. Heuer, American Ceramic Society, Columbus, OH 1984.

16. J. Wang, M. Rainforth and R. Stevens, "The Grain Size Dependence of the Mechanical Properties of TZP Ceramics", Trans. J. Brit. Ceram. Soc. 88 [1] 1-6 (1989).

17. F.F.Lange, "Transformation Toughening Part 3: Experimental Observations in the ZrO_2- Y_2O_3 System", J. Mat. Sci. 72 [1] 240-46 (1982).

18. T. Masaki, "Mechanical Properties of Toughened ZrO_2-Y_2O_3 Ceramics", J. Am. Ceram. Soc. 69 [8] 638- 40 (1986).

19. M.V. Swain, "Grain Size Dependence of Toughness and Transformability of 2 mol% Y-TZP Ceramics", J. Mat. Sci. Letters. 5 [11] 1159-62 (1986).

20. M.L. Mecartney, "Influence of an Amorphous Second Phase on the Properties of Yttria-Stabilized Tetragonal Zirconia Polycrystals", J. Am. Ceram. Soc. 70 [1] 54-58 (1987).

21. F.F. Lange, H. Schubert, N. Claussen and M. Ruhle, "Effects of Attrition Milling and Post-Sintering Heat Treatment on Fabrication, Microstructure and Properties of Transformation Toughened ZrO_2", J. Mat. Sci. 21 668-76 (1984).

22. C. Pascual and P. Duran, "Subsolidus Phase Equilibria and Ordering in the System ZrO_2- Y_2O_3," J. Am. Ceram. Soc. 66 [1] 23-27 (1983).

23. R. Ruh, K.S. Mazdiyasni, P.G. Valentine and H.O. Bielstein, "Phase Relations in the System ZrO_2-Y_2O_3 at Low Y_2O_3 Contents", J. Am. Ceram. Soc. 67 [9] C-190 - C-192 (1984).

24. F.F. Lange, D.B. Marshall and J.R. Porter, Controlling Microstructures Through Phase Partitioning From Metastable Precursors: The ZrO_2-Y_2O_3 System", pp. 519-32 in Ultrastructure Processing of Advanced Ceramics. Edited by J.D. Mackenzie and D.R. Ulrich, John Wiley & Sons, New York, 1988.

25. G. F. Tu, Z. T. -Sui, Q. Huang and C.Z. Wang, "Sol-gel Processed Y-PSZ Ceramics with 5 wt % Al_2O_3," J. Am. Ceram. Soc. 75 [4] 1032-34 (1992).

26. J. Drenan and R. H. J. Hannink, "Effect of SrO Additions on the Grain Boundary Microstructure and Mechanical Properties of Magnesia-Partially Stabilized Zirconia", J. Am. Ceram. Soc. 69 [7] 541-46 (1986).

27. N. Kimura, S. Abe, J. Morishita and H. Okamura, "Low Temperature Sintering of Y-TZP and Y-TZP-Al_2O_3 Composites with Transition Metal Oxide Additions," pp. 1142-48 in Sintering '87, Vol. 2. Edited by S. Somiya, M. Shimada, M. Yoshimura and R. Watanabe, Elsevier Applied Sciences, London, 1988.

28. D.J. Kim, "Effect of Ta_2O_5, Nb_2O_5 and HfO_2 Alloying on the Transformability of Y_2O_3- Stabilized Tetragonal Zirconia", J. Am. Ceram. Soc. 73 [1] 115-20 (1990).

29. K. Haberko, W. Pyda, J. Piekarczyk and M. M. Bucko, "Effect of Carbon-Reduction on the Properties of 13 mol % TiO_2- 3 mol% Y_2O_3- 84 mol% ZrO_2," J. Am. Ceram. Soc. 75 [5] 1272-75 (1990).

30. R. A. Cutler, J. R. Reynolds and A. Jones, "Sintering and Characterization of Polycrystalline Monoclinic, Tetragonal and Cubic Zirconia", J. Am. Ceram. Soc. 75 [8] 2173-83 (1990).

31. K. Tsukuma and M. Shimada, "Strength, Fracture Toughness and Vickers Hardness of CeO_2 -Stabilized Tetragonal Zirconia Polycrystals", J. Mat. Sci. 20 [4] 1178-84 (1985).

32. G. A. Rossi, "CeO_2 -ZrO_2 Toughened Alumina Ceramics of High Strength and Toughness", pp. 271-81 in Zirconia '88: Advances in Zirconia Science and Technology. Edited by S. Meriani and C. Palmonari, Elsevier Applied Sciences, London, 1989.

33. J. G. Duh, H. T. Dai and B -S Chiou,"Sintering, Microstructure, Hardness and Fracture toughness of Y_2O_3 -CeO_2 -ZrO_2", J. Am. Ceram. Soc. 71 [10] 813-19 (1988).

34. M. Hirano and H. Inada, "Strength and Phase Stability of Yttria -Ceria -Doped Tetragonal Zirconia/ Alumina Composites Sintered and Hot Isostatically Pressed in Argon- Oxygen gas Atmosphere", J. Am. Ceram. Soc. 74 [3] 606-11 (1991).

35. R. A. Cutler, R. J. Mayhew, K. N. Prettyman and A. V. Virkar, "High -Toughness Ce-TZP/Al_2O_3 Ceramics with Improved Hardness and Strength, " J. Am. Ceram. Soc. 74 [1] 179-86 (1991).

36. S. Maschio, O. Sbaizero, S. Meriani and E. Bischoff, "Sintering Aids for Ceria -Zirconia Alloys," J. Mater. Sci. 27 2734-38 (1992).

37. J. S. Wang, J. F. Tsai, D. K. Shetty and A. V. Virkar, "Effect of MnO on the Microstructures, Phase Stability and Mechanical Properties of Ceria -Partially Stabilized Zirconia (Ce-TZP) and Ce-TZP-Al_2O_3 Composites," J. Mater. Res. 5 [9], 1948-1957 (1990).

38. J. F. Tsai, U. Chou, N. Ramachandran and D. K. Shetty, "Transformation Plasticity and Toughening in CeO_2 -Partially -Stabilized Zirconia-Alumina (Ce-TZP/Al_2O_3) Composites Doped with MnO", J. Am. Ceram. Soc. 75 [5] 1229-38 (1992).

39. T. Sato, T. Endo and M. Shimada, "Post Sintering Hot Isostatic Pressing of Ceria -Doped Tetragonal Zirconia /Alumina Composites in an Argon -Oxygen Gas Atmosphere", J. Am. Ceram. Soc. 72 [5] 761-64 (1989).

40. V.C. Pandolfelli, M. Rainforth and R. Stevens, "Sintering and Microstructural Studies in the System ZrO_2. TiO_2. CeO_2", J. Mater. Sci. 25 2233-44 (1990).

41. P. Duran, P. Recio, J. R. Jurado, C. Pascual and C. Moure, "Preparation, Sintering, and Preparation of Translucent Er_2O_3 - Doped Tetragonal Zirconia. " J. Am. Ceram. Soc. 72 [11] 2088 -93 (1989).

42. P. A. Evans, R. Stevens and J. G. P. Binner, "Quantitative X-ray Diffraction Analysis of Polymorphic Mixes of Pure Zirconia", Trans. J. Brit. Ceram. Soc. 83 [1] 39 -43 (1983).

43. H.P. Klug and L.E. Alexander, "X-ray Diffraction Procedures for Polycrystalline and Amorphous Materials", pp. 880- 92, 2nd edition. John Wiley, New York, 1974.

44. B. D. Cullity, "Elements of X-ray Diffraction", pp. 520-28, Addison-Wesley Publishing Co. Inc., Massachusetts, 1977.

45. D. R. Larson, J. A. Coppola, D. P. H. Hasselman and R. C. Bradt, "Fracture Toughness and Spalling Behaviour of High-Al_2O_3 Refractories", J. Am. Ceram.Soc. 57 [10] 417-21 (1974).

46. G. R. Anstis, P. Chantikul, B. R. Lawn, and D. B. Marshall, "A Critical Evaluation of Indentation Techniques for Measuring Fracture Toughness: I, Direct Crack Measurements," J. Am. Ceram. Soc. 64 [9] 533-38 (1981).

47. A. G. Evans and E. A. Charles, "Fracture Toughness Determination by Indentation", J. Am. Ceram. Soc. 59 [7-8] 371-72 (1976).

48. G. D. Quinn and R. Morell, "Design Data for Engineering Ceramics: A Review of the Flexure Test," J. Am. Ceram. Soc. 74 [9] 2037-66 (1991).

49. Y. Mori, Y. Kitano, A. Ishitani and Masaki, "Determination of Transformation Zone Size in Toughened Zirconia Ceramics", J. Am. Ceram. Soc. 71 [7] C-322 - C-324 (1988).

50. T. Kosmac, R. Wagner and N. Claussen, " X-Ray Determination of Transformation Zone Depths in Ceramics Containing Tetragonal Zirconia," J. Am. Ceram. Soc. 64 [4] C-72 - C-73 (1981).

51. C.S. Smith and L. Guttman, "Measurement of Internal Boundaries in Three Dimensional Structures by Random Sectioning", Trans. AIME, 197 [1] 81-87 (1953).

52. M.I. Mendelson, "Average Grain Size in Polycrystalline Ceramics", J. Am. Ceram. Soc. 52 [8] 443-46 (1969).

53. D.K. Leung, C.J. Chan, M. Ruhle and F.F. Lange, "Metastable Crystallization, Phase Partitioning and Grain -Growth of ZrO_2-Gd_2O_3 Materials Processed from Liquid Precursors", J. Am. Ceram. Soc. 74 [11] 2786-92 (1991).

54. T. -S. Sheu, T. -Y Tien and I. -W Chen, "Cubic-to- Tetragonal (t′) Transformation in Zirconia - Containing Systems," J. Am. Ceram. Soc 75 [5] 1108-16 (1992).

55. M. Perez, Y. Jorba, "Diagrammes D'equilibre Des Systemes Zircone-Oxydes de Terres Rares", Ann. Chim. (Paris) 7 509 (1962).

56. J. Lefevre, "Les Solutions Solides Primaries Zircone-Oxydes de Terres Rares," Ann. Chim. (Paris), 8 [1-2] 128 (1963).

57. A. Rouanet and M. Foex, "System ZrO_2-Gd_2O_3 at High Temperature", in Phase Diagram for Ceramists, 1975 Supplement. Edited by E.M. Levin and H.F. McMurdie. The American Ceramic Society Inc. Fig. 4417.

58. P. Li, I. W -Chen and J. E. Penner- Hahn, "Effect of Dopants on Zirconia Stabilization - An X-ray Absorption Study: I, Trivalent Dopant," J. Am. Ceram. Soc. 77 [1] 118-28 (1994).

59. J. W. Cahn, "The Impurity Drag Effect in Grain Boundary Motion," Acta Metall. 10 [9] 789-98 (1962).

60. F.F. Lange, "Correlation Between Grain Size Control and Composition in the System ZrO_2-Y_2O_3", J. Am. Ceram. Soc. 69 [3] 240-42 (1986).

61. S - L. Hwang and I.- W. Chen, "Grain Size Control of Tetragonal Zirconia Polycrystals Using the Space Charge Concept," J. Am. Ceram. Soc. 73 3269-77 (1990).

62. M. V. Swain and R. H. J. Hannink, "Metastability of the Martensitic Transformation in a 12 mol% Ceria - Zirconia Alloy: II, Grinding Studies," J. Am. Ceram. Soc. 72 [8] 1358-64 (199).

63. I.W.- Chen and Y- H Chiao, "Martensitic Transformation in ZrO_2 and HfO_2. An Assessment of Small Particle Experiments with Metal and Ceramic Matrices", pp. 33-45 in Advances in Ceramics, Vol. 12, Science and Technology of Zirconia II. Edited by N. Claussen, M. Ruhle and A.H. Heuer. The American Ceramic Society, Columbus, OH, 1984.

64. I-W Chen and Y-H Chiao, "Theory and Experiments of Martensitic Nucleation in ZrO_2 containing Ceramics and Ferrous Alloys", Acta. Metall. 33, [10] 1827-45 (1985).

65. R.M. McMeeking and A.G. Evans, "Mechanics of Transformation Toughening in Brittle Materials", J. Am. Ceram. Soc. 65 [5] 242-46 (1982).

66. P. E. Reyes Morel and I.-W. Chen, "Transformation Plasticity of CeO_2-Stabilized Tetragonal Zirconia Polycrystals I: Stress Assistance and Autocatalysis", J. Am. Ceram. Soc. 71 [5] 343-53 (1988).

67. G.Teufer, "Crystal Structure of Tetragonal Zirconia," Acta. Crystallogr. 15 [11] 1187 (1962).

APPENDIX

The ratio of volume fraction cubic (V_c) to volume fraction tetragonal (V_t) phase is calculated from the following formula:

$$\frac{V_c}{V_t} = \frac{[R(hkl)_t + R(h'k'l')_t]\ [I_c(hkl)]}{R_c(hkl)\ [I(hkl)_t + I(h'k'l')_t]} \qquad (3.16)$$

where (hkl) represents the miller indices of the plane,

$$R\ (hkl) = \frac{1}{V^2}\ p\ LP\ |F|^2 \qquad (3.17)$$

where V = volume of unit cell

p = multiplicity factor

LP = Lorentz Polarization factor

F = Structure Factor

In order to clearly resolve t and c peaks, high angle peaks (2θ = 72° - 76°) was used for this calculation. In that region there are two t peaks [t(004) at $2\theta = 72.67^\circ$ and t(400) at $2\theta = 74.2^\circ$] and one c peak [c(400) at $2\theta = 73.5^\circ$].

For the present system the numerical values of different factors are calculated as follows:

(i) Structure Factor (F):

The structure factor is given by the following relation:

$$|F|^2 = [\ \sum_j f_j \cos 2\pi\ (hu_j + kv_j + lw_j\ )]^2 + [\ \sum_j f_j \sin 2\pi\ (hu_j + kv_j + lw_j\ )]^2 \qquad (3.18)$$

where (hkl) and (uvw) represents the position of two nearest atoms in the unit cell. For cubic ZrO_2, having cubic flourite structure, the Zr atoms are at (000) and oxygen atoms are at (1/4 1/4 1/4).

Hence

$$|F|^2 = [f_{zr} \cos 2\pi O + f_o \cos 2\pi (h/4 + k/4 + l/4)]^2 + [f_{zr} \sin 2\pi O + f_o \sin 2\pi (h/4 + k/4 + l/4)]^2 \quad (3.19)$$

or, $$|F|^2 = f_{zr} + f_o \cos \frac{\pi}{2} (h+k+l)^2]^2 + f_{zr}.O + f_o \sin \frac{\pi}{2} (h+k+l)^2]^2 \quad (3.20)$$

or, $$|F|^2 = [f_{zr} + f_o]^2 + [0 + 0] \quad (3.21)$$

or, $$|F|^2 = [f_{zr} + f_o]^2 \quad (3.22)$$

Now, $f_{zr}^{4+} = 23.39$ and $f_o^{2-} = 2.7$ [43]

$\therefore \quad |F|^2 = 680.68$

For tetragonal ZrO_2, the structure factor values are taken from Teufer [66]. Its value is 19.3 for (004) reflection and 15.8 for (400) reflection.

(ii) Volume of unit Cell (V):

Volume of unit cell (V) is calculated from experimentally obtained lattice parameters. Its value is 135 $(A^\circ)^3$ for cubic zirconia and 136 $(A^\circ)^3$ for tetragonal zirconia.

(iii) Multiplicity Factor (p):

The value of multiplicity factor (p) is 2 for $(004)_t$ reflections and 4 for $(400)_t$ reflections. For cubic zirconia with $(400)_c$ reflections its value is 6 [43, 44].

(iv) Lorentz Polarization Factor (LP):

Lorentz Polarization factor (LP) is calculated from the following relation:

$$LP = \frac{1 + \cos^2 2\theta}{\sin^2\theta \cos \theta} \quad (3.22)$$

where 2θ is the Bragg diffraction angle. So, putting the values of θ for $(004)_t$, $(400)_t$ and $(400)_c$ reflection we get

LP = 3.848 for $(004)_t$

LP = 3.696 for $(400)_t$

and LP = 3.7680 for $(400)_c$

So putting all the values in the expression for R(hkl) we obtain them as

$R(400)_c = 0.8443$

$R(004)_t = 0.1572$

$R(400)_t = 0.2005$

This gives the final form of eqn. (1) as

$$\frac{V_c}{V_t} = \frac{0.8472\ [I_c\ (400)]}{[I_t(004) + I_t(400)]} \qquad (3.23)$$

CHAPTER - 4

LOW TEMPERATURE AGING BEHAVIOUR Gd - TZP CERAMICS

4.1 *INTRODUCTION*

Kobayashi et.al [1] first observed that when Y-TZP is aged (or annealed) at low temperature (200°- 300°C) it undergoes a severe degradation in properties. Since then many investigators have observed this behaviour and their main findings are summarized below:

(i) The degradation occurs both in mechanical and electrical properties of ceramics and is due to the formation of monoclinic phase at the surface [1,2].

(ii) This spontaneous t ⟶ m transformation at the surface occurs over a wide range of temperature (100°- 400°C) in air, humid atmosphere, water and also in presence of certain organic solvents [3,4,5,6]. The transformation peaks at around 250°- 400°C; lower temperature slows down the transformation rate and higher temperature (≥ 400°C) makes t phase thermodynamically more stable.

(iii) The transformation progresses from surface to interior of the material and is accelerated by the presence of water or water vapour [5,6].

(iv) The transformation rate is dependent on the grain size and dopant concentration.

4.1.1 Effect of Aging on Mechanical Properties:

Although there exists a large number of studies that deal with the kinetics of the aging behaviour, only a limited amount of work has been done on mechanical property degradation during aging.

Watanabe et.al [7] studied the effect of aging in air between 100°C and 800°C on density, phase and strength of certain Y-TZPs containing 2 to 5 mol% Y_2O_3. The samples were prepared by conventional MO route using Y_2O_3 and the m- ZrO_2 powder. Sintering was done at 1400°C to 1600°C. Subsequently the samples were aged for 100 and 1000 hours at different temperatures between 100°and 800°C. The unaged samples had a three point bend strength of 700 MPa. The strength decreased with aging and reached a minimum (50 MPa) after 100 hours aging between 200°C - 300°C. Aging at temperatures higher than this made little effect on strength. Similar trend was observed for density. This decrease in strength between 200°- 300°C indicates that t ⟶ m transformation rate is maximum at this temperature. At lower aging temperature, the transformation rate is slower while at higher temperature t phase becomes thermodynamically stable.

Tsukuma et.al [8] studied the effect of thermal aging (200°C - 300°C) on bend strength and phases of Y-TZP samples containing 2 - 6 mol% Y_2O_3. The samples were prepared by coprecipitation technique, compacted and sintered between 1400°C and 1600°C for 2 hours followed by hot isostatic pressing at the same temperature at 150 MPa. The aging was faster for large grain size materials.The aging behaviour was also dependent on dopant concentration. Samples containing ≥ 2.3 mol% Y_2O_3 showed no significant aging. The bend strength decreased rapidly on aging

between 200°- 300°C. For example, they found that aging at 230°C for 1200 hours decreased the strength from 850 MPa to less than 100 MPa. However, it should be noted that strength degradation was also dependent on grain size. While for materials having grain ≥ 1 μm, the strength decreased in the above mentioned manner, it remained virtually same in samples having grain size between 0.2 - 0.4 μm.

Masaki et.al [9] also observed a similar decrease in bend strength on aging at 200°C for 200 hours. However, the strength degradation was observed only for lower Y_2O_3 content samples (i.e. 2 - 3 mol% Y_2O_3) where the strength drops to about 50 MPa from an initial value of more 1000 MPa.

Swab [10] tested seven different commercial Y-TZP materials to determine the degree of susceptibility to hydrothermal aging at low temperature. The flexure specimens were exposed to 800 Pa of water vapour pressure for 50 hours between 200°C and 400°C. They found that only one composition had its property unaffected by the hydrothermal treatment. Three composition failed catastrophically and broke into fragments or small pieces. The rest three underwent significant strength degradation with a minimum decrease of atleast about 50%. This drastic decrease in strength and other physical properties was attributed to the presence of water vapour which is known to accelerate the rate of aging.

Sato et.al. [11] reported the degradation in strength of Y-TZP samples aged at 50 to 500°C and in presence of 3.35 KPa water vapour pressure. The decrease in strength was inversely proportional to the grain size. In samples having 0.86 μm grain size the strength dropped from >1000 MPa to about 200 MPa after 50

hours aging at 200°C. However for TZP with 0.53 μm grain size, the drop was only upto 800 MPa at 300°C.

4.1.2 Mechanism of Aging:

Although there is an agreement regarding the basic features of low temperature aging, there is no unanimity regarding the details of the mechanism. Different investigators working in this area have proposed a number of theories some of which are discussed below:

Lange et.al. first proposed that aging takes place due to the reaction of glassy SiO_2 with water [12]. This glassy phase results on sintering a material containing SiO_2, a common impurity found in most of the commercial TZP. The reaction scheme is similar to that of stress corrosion cracking.

However, after carrying out a detailed study of aging, they themselves rejected this theory. They studied the aging behaviour of a few commercial TZP, some of which were intentionally mixed with different quantities of SiO_2. No difference was found in the aging behaviour between SiO_2 containing samples and the non silica samples. Detailed TEM study of samples showed the presence of fine crystallites adjacent to monoclinic grains in the aged samples. These crystallites were identified as $Y(OH)_3$. Based on this, they proposed that aging takes place due to the reaction of Y_2O_3 with water. This reaction forms $Y(OH)_3$, producing Y_2O_3 deficient t - ZrO_2. A nucleus of m- ZrO_2 forms which on growing to a critical size initiates further t $\longrightarrow$ m transformation and microcracking in the material.

But Schubert et.al [13] criticized this theory of Y^{3+} depletion as the diffusivity of cations in ZrO_2 is very low. They

agreed on the formation of $Y(OH)_3$ but suggested this to be due to diffusion of OH^- having higher mobility. However, the rate of reaction will be still controlled by the slowest moving species (which is Y^{3+} in this case). On the basis of this, Yoshimura [17] suggested that $Y(OH)_3$ formation can not be responsible for observed degradation rate as this will need exceedingly long period of time (over years) for a small degradation to take place.

Hernandez et.al [14] found evidence of YO(OH) species on the aged surface using X-ray Photoelectron Spectroscopy (XPS). They proposed that the degradation mechanism consists of the following steps, (i) formation of YO(OH) by attack of OH^- ions at the more active points (Y_2O_3) on the surface, (ii) formation of pure tetragonal embryos which are coherent with the matrix and (ii) transformation of these embryos to m phase when these grow to a critical size. This is accompanied by macrocracking and possibly spalling, thus exposing fresh surface for attack. Thus the problem of cation diffusion is circumvented by formation of microcracks and spalling.

Yoshimura [15] on the other hand, suggested (Fig.4.1) that during aging at first OH^- groups are chemisorbed on the surface. This leads to the formation of Zr - OH and/or Y-OH at the surface which creates stressed sites. Further absorption and migration of OH^- creates more stressed sites at the surface and in the lattice. Ultimately this leads to the formation of nucleating defects resulting in t$\longrightarrow$m transformation accompanied by micro and macrocrackings. The absorption of OH^- expands the lattice which reverts back to its original size when heated at high temperature in air or vacuum.

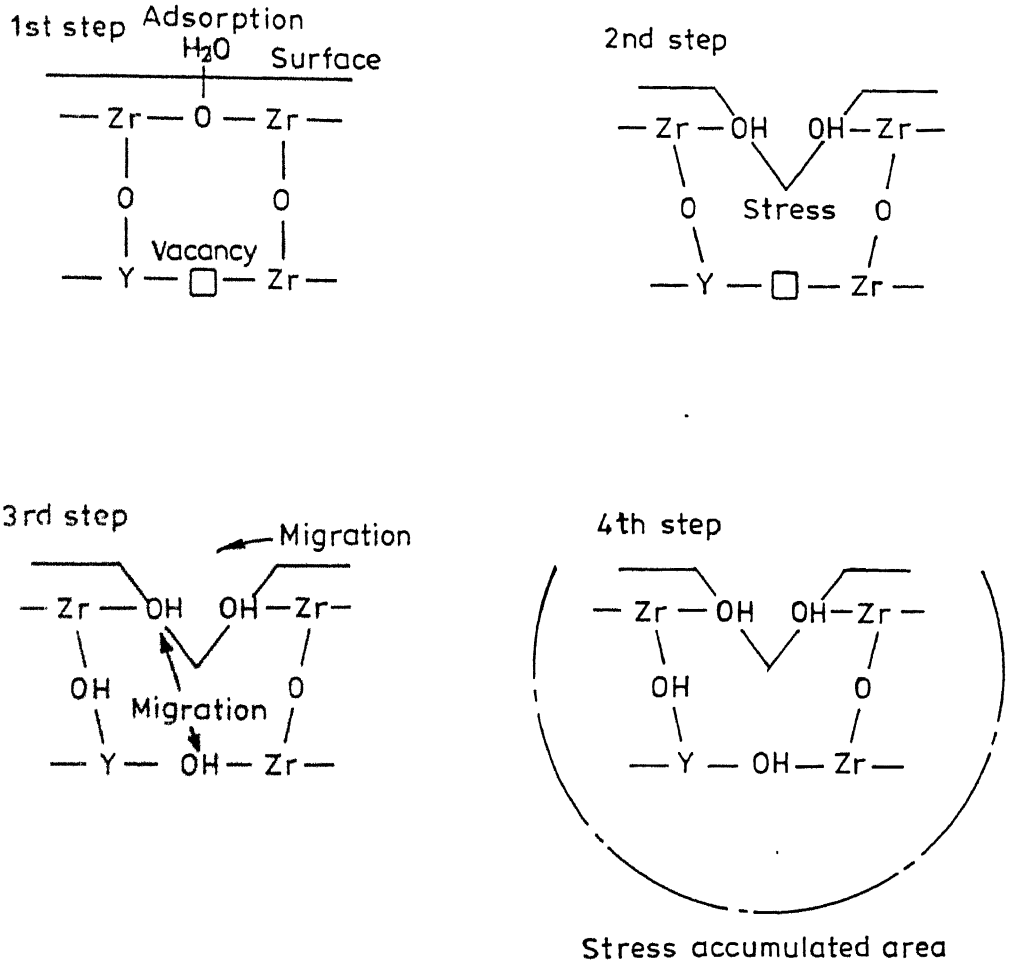

Fig. 4.1 Schematic view of degradation process during low temperature aging in presence of water.

Sato et.al [6] have also proposed a chemical reaction between Zr-O-Zr and H_2O but in their view this caused the corrosive growth of the preexisting flaws and led to further degradation. According to them, any liquid containing a lone pair of electron orbital opposite a proton donor site will initiate and propagate such crack. Thus not only water but organic liquids like alcohol and acetone will induce aging. Later on the same authors extended their idea to water vapour and showed that transformation rate increases with increase in partial pressure of water vapour [19].

Schmauder et.al. [16] calculated the residual stress in different grains and suggested that the presence of residual stress a part in enhancing aging behavior. In a polycrystalline material grains having high amount of residual stress will undergo aging first.

Schubert et.al. [17] also investigated the role of internal stress within t grains on the aging behaviour. They carried out annealing experiments on TEM foils before and after aging. It was observed that the internal stresses decreased with increasing stabilizer content. They found that growth of transformed layer was rapid for a material having grains with composition less than the critical composition. These type of materials easily initiated microcracks in the surrounding matrix. However, once the grain composition exceeds the critical composition, the growth of transformed layer is prevented. Thus homogeneous distribution of Y_2O_3 within the grains is also equally important in checking the t$\longrightarrow$ m transformation during aging.

4.1.3 Inhibition of Low Temperature Aging:

All the factors which inhibit the t ⟶ m transformation will also inhibit the low temperature aging.

4.1.3.1 *Effect of grain size and dopants:*

As already mentioned [Chapter 1] the free energy change for t ⟶ m transformation, $\Delta G_{t\longrightarrow m}$ is given by

$$\Delta G_{t\longrightarrow m} = \Delta G_e + \Delta G_{se} + \Delta G_s \qquad (5.1)$$

where ΔG_c is the change in chemical free energy

$= (\Delta G_c^m - \Delta G_c^t)$

ΔG_{se} is the strain energy.

and ΔG_s is the surface free energy.

Thus t ⟶ m transformation can be prevented by increasing $\Delta G_{t\longrightarrow m}$. The ΔG_c^t can be lowered by alloying with oxides like CeO_2, Y_2O_3. ΔG_{se} can be increased by dispersion of oxides such as Al_2O_3 having high modulus. Incorporating these oxides (which are generally nonreactive with ZrO_2) increases the strain energy component due to an effectively higher modulus. ΔG_s can be increased by decreasing the grain size of ZrO_2 in sintered bodies. This necessitates the use of fine powders and lower sintering temperature.

Lange et.al [12] studied the influence of grain size and composition on the aging behaviour of Y-TZP ceramics and found that by decreasing the grain size and increasing the Y_2O_3 content the aging behaviour in these materials could be controlled. Similar studies of Y-TZP aging have also been carried out by Watanabe et.al [7]. They observed that a critical grain size exists for t ⟶ m transformation, the value of which increases

with the increase in dopant concentration. For Y-TZP they found this critical size to increase from 0.2 to 0.6 μm as the Y_2O_3 content was increased from 2 to 5 mol%. When 3Y-TZP was aged in hydrothermal condition (water vapour pressure 0.1 MPa) the critical grain size below which no aging took place decreased from 0.52 μm to 0.37 μm with an increase in the aging temperature from 100°C to 500°C.

There have been many reports regarding addition of different oxides to suppress the aging behaviour. Thus Sato et.al [5] added CeO_2 (0 - 20 wt%) or Al_2O_3 (0 - 40 wt%) to ZrO_2 2Y, ZrO_2 3Y and ZrO_2 4Y TZP materials.The samples were sintered at 1400°to 1600°C for 1 hour. The aging experiments were carried out in hot water at different temperature conditions. It was found that both CeO_2 and Al_2O_3 decreased the aging rate, but among the two CeO_2 was more effective. When ZrO_2 3Y was alloyed with ≥ 10 wt% CeO_2 and ZrO_2 2Y was alloyed with ≥ 15 wt% CeO_2, t ⟶ m transformation on aging could be totally suppressed.

However, Hirano et.al [20] reported that CeO_2 alloying in Y-TZP could slow down the degradation of Y-TZP during air aging only. When aged in the presence of water vapour these materials easily transformed to monoclinic phase. Al_2O_3 could be effectively used to retard aging only below 100°C. Besides Al_2O_3, similar beneficial results were also obtained by dispersing mullite, spinel etc.

4.1.3.2 *Modification of Surface Structures:*

The possibility of decreasing the grain size using fine particles and using high stabilizer content to make t phase stable against aging leaves the material with reduced toughness as under

these conditions the t phase does not undergo stress induced t ⟶ m transformation. The other alternative is to modify the surface conditions such that t⟶ m transformation does not take place easily. This idea is based on the fact that all aging transformation initiates from the surface.

Iio et.al [19] found that the thickness of the transformed layer in a Y-TZP sample aged at 300°C in air increased from about 10 μm to ~65 μm on increasing the aging time from 24 hours to 215 hours. They showed that the t⟶m transformation is completely restrained in a sample coated by Al_2O_3 using CVD.

Schubert et.al [20] suggested that by forming a surface layer of finite thickness comprising of cubic ZrO_2, the degradation can be controlled. Alternatively Whalen et.al [21] observed that grinding the ZrO_2 surface followed by annealing at a suitable temperature results in the recrystallization of fine grains of tetragonal zirconia at the surface. This layer of fine grained tetragonal zirconia at the surface slows down the aging process.

4.1.4 The Present Study :

As mentioned earlier (Cf. statement of problem) the ionic radius of Gd^{3+} suggests that its aging kinetics may be slower. Hence we have carried out aging experiments on Gd - TZP samples prepared by us. Also, as no experiments have so far been carried out on the effect of water vapour pressure on the aging behaviour, we carried out aging experiments at different water vapour pressures. Efforts were also made to compare our results with Y-TZP by carrying out similar experiments on Y-TZP samples prepared in the laboratory. Finally to determine the changes taking place in the t phase in the early stages of aging, the

changes in the cell volume of the t phase were determined by x-ray diffraction. The details are given below.

4.2 *EXPERIMENTAL:*

The aging experiments were carried out on three different compositions (2, 2.5 and 3 mol% Gd_2O_3) of Gd-TZP. The samples were prepared from the powders made by coprecipitation techniques as described in Chapter 2. After calcination (700°C/4 hours) and compaction these samples were sintered at 1400°C for 2 hours. The sintered samples were polished and cut to a size of 5mm x 5mm x 2mm for aging experiments.

An x-ray scan was carried out on the polished surface to determine the amount of m phase prior to aging. The aging experiments, were done in sealed quartz tubes at different water vapour pressures obtained by placing a measured quantity of water in the tube. Aging study was done at three different temperature. To determine the peak transformation temperature for Gd-TZP, 2 mol% Gd-TZP samples were aged for 50 hours at 2.5 MPa water vapour pressure and at different temperatures ranging from 80°C to 300°C. After the completion of aging, the samples were quenched in air. The amount of monoclinic phase was determined by x-ray diffraction. The data was corrected for initial amount of the monoclinic phase.

The aging kinetics was next studied at three different temperatures chosen in the light of above experiment. These were 180°C, 200°C and 220°C. The samples were aged at 0.01 MPa water vapour pressure for times varying from 5 to 50 hours. This vapour pressure was chosen so as to be able to compare our results with data in the literature on other TZP materials [4]. Moreover, to

study the effect of water vapour pressure on aging kinetics, 2Gd-TZP samples were also aged at 0.1 MPa and 2.5 MPa.

Some of the 2.5 Gd-TZP samples were also aged both in water vapour hydrothermally at 0.1 MPa water vapour pressure and in air for shorter duration (< 10 hours). This study was carried out to explore the changes in t phase during the early stage of aging. This change was monitored by measuring the changes in the tetragonal cell volume.

4.3 *RESULTS:*

4.3.1 Determination of Peak Transformation Temperature:

Figure 4.2 shows the amount of monoclinic phase formed on hydrothermally aging of 2 mol% Gd-TZP samples at a water vapour pressure of 2.5 MPa for 50 hours at different temperatures. The t⟶m transformation increases at first with increase in the aging temperature and peaks at 200°C. Above this temperature the transformation again decreases with further increase in temperature. The transformability is only slightly less at 180°C and 220°C. So, these three temperatures (180, 200 and 220°C) were selected as the temperatures for studying aging kinetics.

4.3.2 t ⟶ m Transformation of 2, 2.5 and 3 Gd-TZP:

Figure 4.3 to 4.5 show the amount of m-phase found on aging 2,2.5 and 3 mol% Gd-TZP samples at 0.01 MPa water vapour pressure for different times. Despite the scatter it is clear that the amount of m phase decreases with increasing Gd_2O_3 content. While about 80% m-phase forms after 50 hours in a 2 and 2.5 mol% samples, this amount is less than 60% for 3 mol% samples. Moreover, the transformation increases with increase in the aging temperature from 180°C to 220°C.

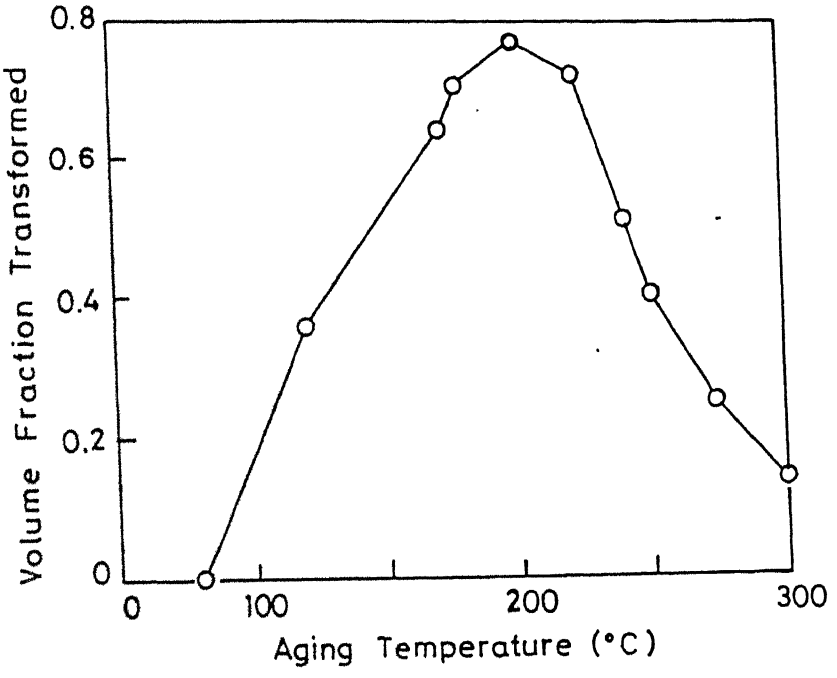

Fig. 4.2 Effect of temperature on aging of a ZrO_2-2 mol% Gd_2O_3 sample of 2.5 MPa steam pressure.

4.3.3 Effect of water vapour pressure on aging of 2 mol% Gd-TZP:

Figure 4.6 to 4.8 show the amount of monoclinic formed at different temperatures as a function of water vapour pressure. Within the experimental scatter, the results indicate no effect of water vapour pressure on the aging kinetics.

4.3.4 Aging of 3Y-TZP at 0.01 MPa and 0.1 MPa water vapour pressure:

In an attempt to compare the aging behaviour of Gd-TZP with Y-TZP an effort was made to study the aging kinetics of 3Y-TZP samples. The 3Y-TZP samples were prepared in the laboratory from TOSOH 3% Y_2O_3 - ZrO_2 powders (Toyosoda Co., Japan), pressed into bars and sintered at 1500°C for 1 hour. These samples were also hydrothermally aged at 0.01 and 0.1 MPa water vapour pressure in sealed quartz tubes. The aging temperature was 180°C, 200°C and 220°C. However, it was found that these Y-TZP samples underwent severe cracking, fragmentation and in cases, disintegrated into powders. Thus no further study was carried out on these samples.

4.3.5 Effect of Aging on tetragonal cell volume:

Figure 4.9 shows the effect of aging on the tetragonal cell volume during the initial stage of aging of 2.5 Gd-TZP at 200°C and 0.1 MPa water vapour pressure and in air. As shown the cell volume increases with an increase in aging time at first slowly upto 5 hours and then more rapidly from 5 to 10 hours. However, the cell volume increase is more in hydrothermal condition (water vapour pressure 0.1 MPa) than in air aged samples.

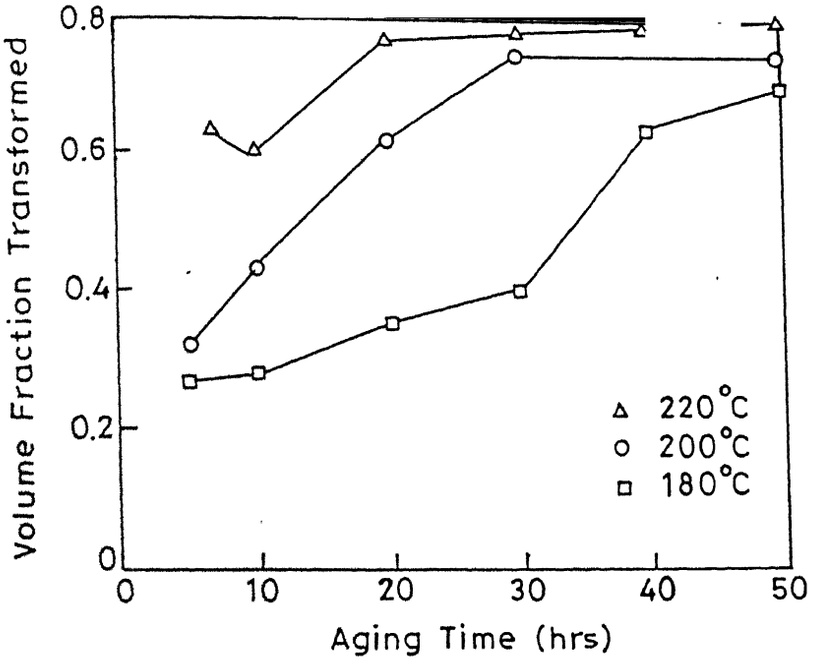

Fig. 4.3 Amount of t-phase transformed during aging of 2Gd TZP at 0.01 MPa water vapour pressure at different temperatures.

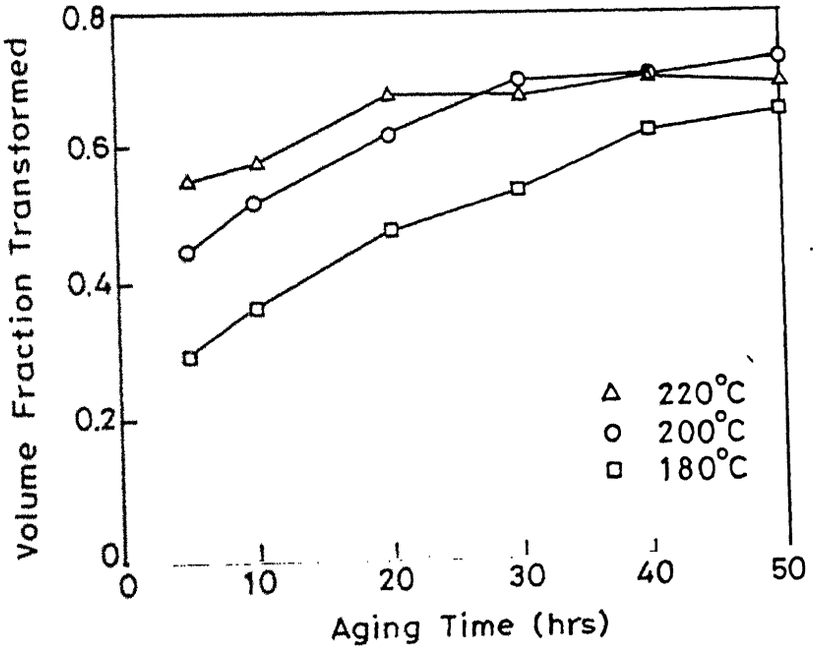

Fig. 4.4 Amount of t-phase transformed during aging of 2.5 Gd TZP at 0.01 MPa water vapour pressure at different temperatures.

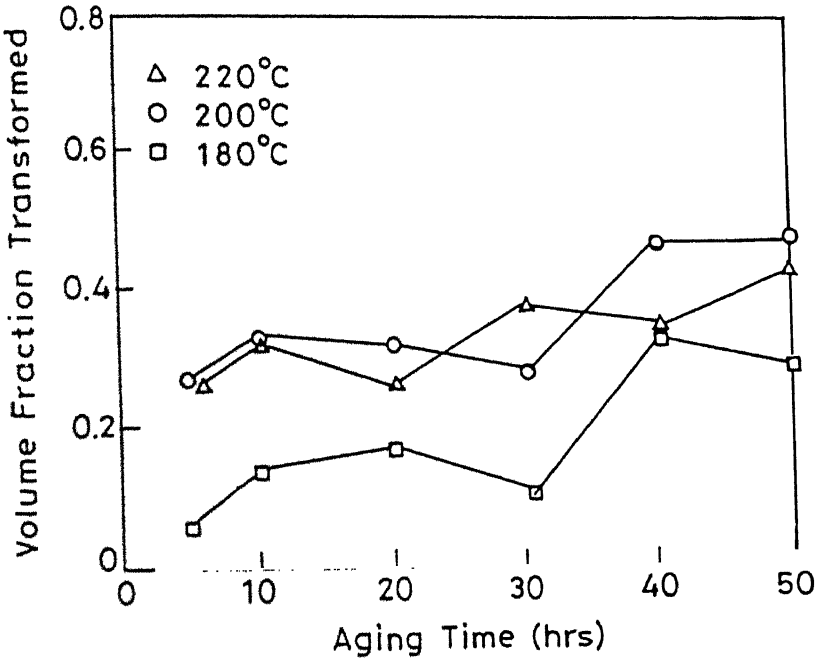

Fig. 4.5 Amount of t-phase transformed during aging of 3Gd TZP at 0.01 MPa water vapour pressure at different temperatures.

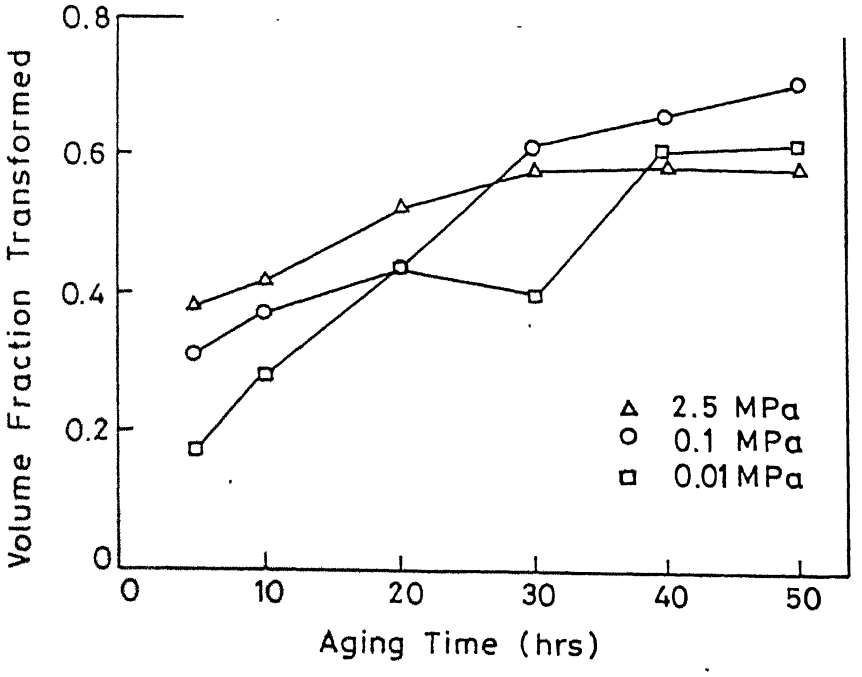

Fig. 4.6 Amount of t-phase transformed during aging of 2Gd TZP at 220°C at different water vapour pressure.

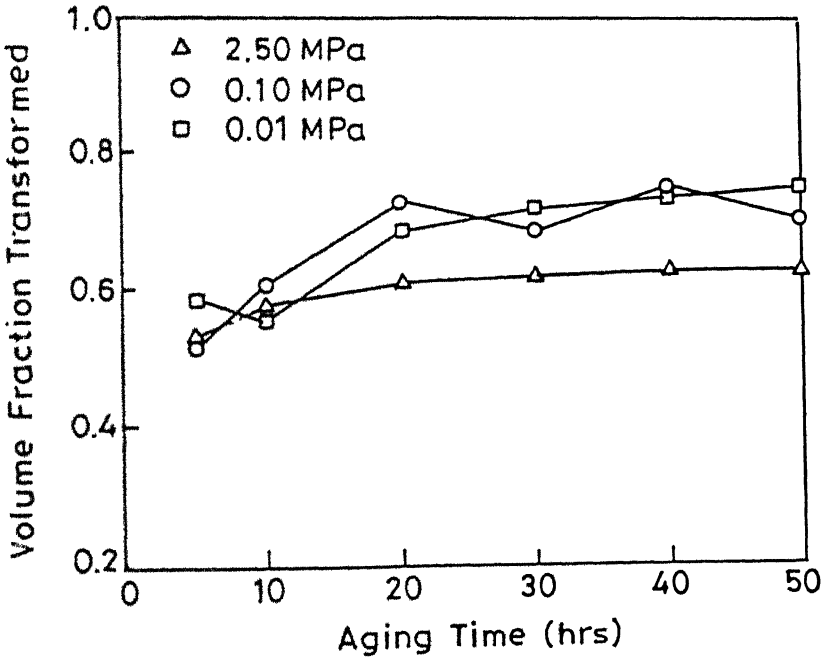

Fig. 4.7 Amount of t-phase transformed during aging of Gd TZP at 200°C at different water vapour pressure.

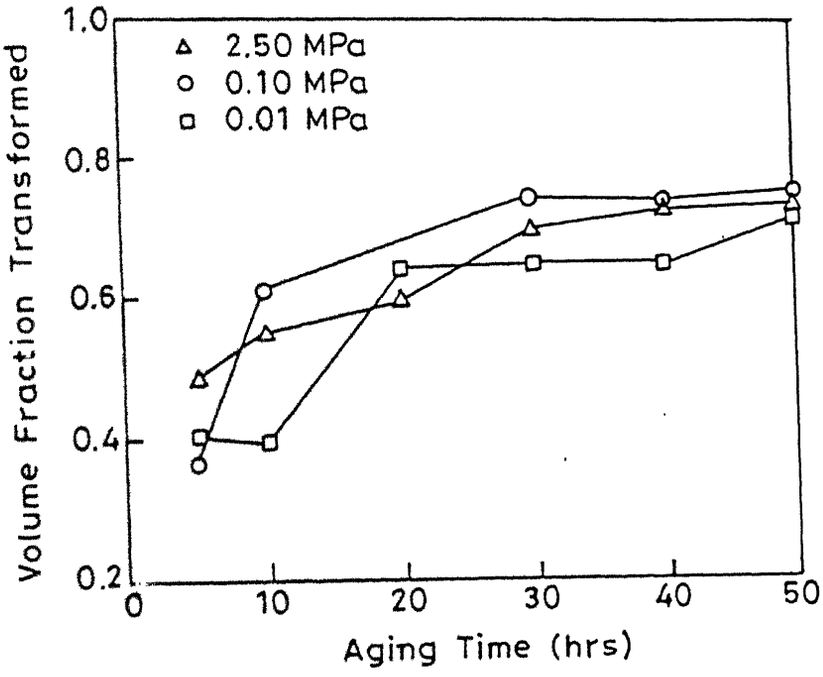

Fig. 4.8 Amount of t-phase transformed during aging of 2Gd TZP at 180°C at different water vapour pressure.

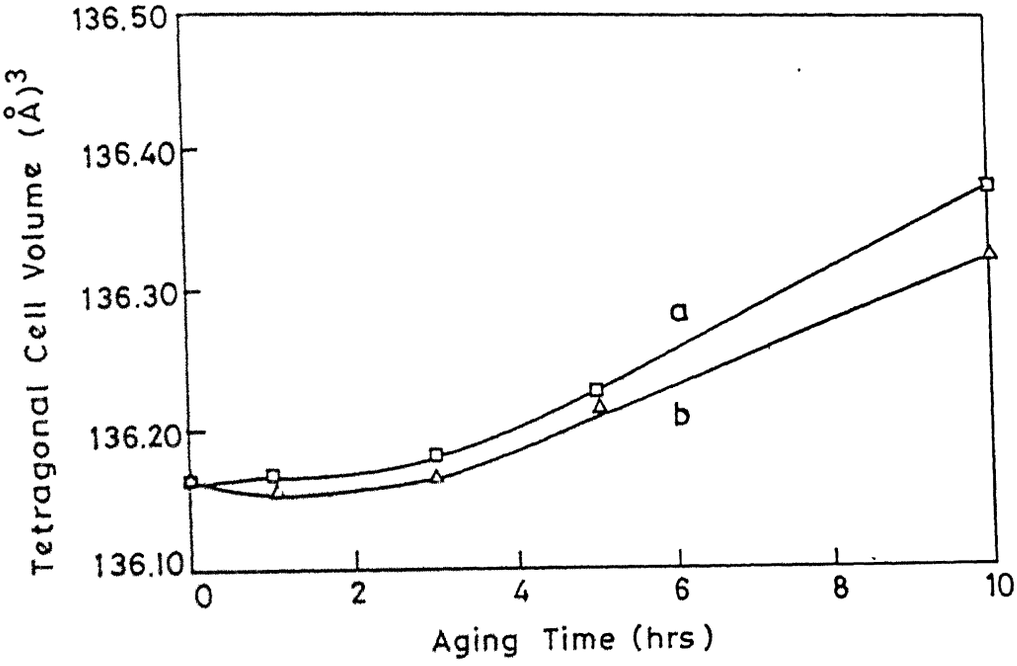

Fig. 4.9 Changes in the tetragonal cell volume during initial aging period of 2.5 Gd TZP at 200°C, (a) aged at 0.1 MPa water vapour pressure, (b) aged in air.

4.4 *DISCUSSION:*

4.4.1 Effect of Gd_2O_3 concentration on transformation:

Inspite of the scatter in the experimental data, the results indicate that increasing Gd_2O_3 concentration decreases the amount of t⟶m transformation. This is consistent with the results reported for other TZP's. With increase in stabilizer concentration, t phase stability increases and so t⟶m transformation decreases.

4.4.2 Activation energy for t⟶m transformation during aging :

The activation energy for 2 mol% Gd-TZP samples was calculated by combining the data for all vapour pressures. For 2.5 and 3 mol% Gd-TZP samples, the activation energy was calculated using the data of 0.01 MPa, the only pressure at which these two samples were aged.

Sato et.al.[5] have calculated the activation energy assuming a first order kinetics using the rate equation

$$\ln (1 - \alpha) = kt^n \qquad (4.1)$$

However, when we plotted our experimental data to the above equation, it gave poor fit. Moreover, the curve had a negative curvature. For this types of curves Burke [22] has suggested that a better fit is obtained using Austin Rickett equation [28] which is given as follows:

$$\frac{\alpha}{(1- \alpha)} = kt^n \qquad (4.2)$$

Figure 4.10 shows an example of fitting data to this equation. Figure 4.11 show a plot of rate constant vs 1/T for determination of activation energy. The activation energies calculated using this equation are 85, 89 and 116 kJ/mole for 2,

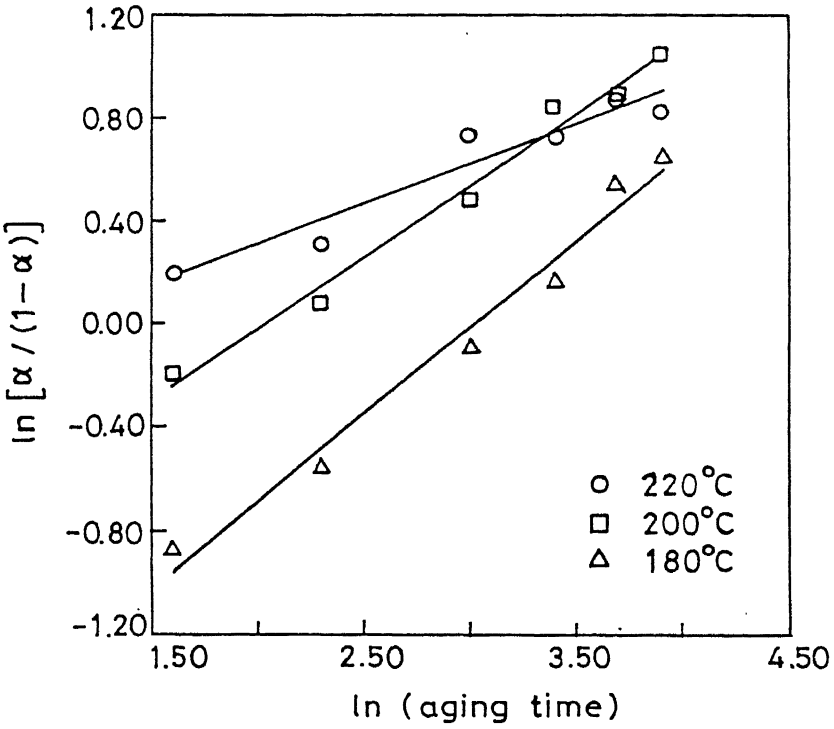

Fig. 4.10 Plot of ln [α/(1-α)] vs. ln [aging time] for ZrO_2-2 mol% Gd_2O_3 aged at three different temperatures.

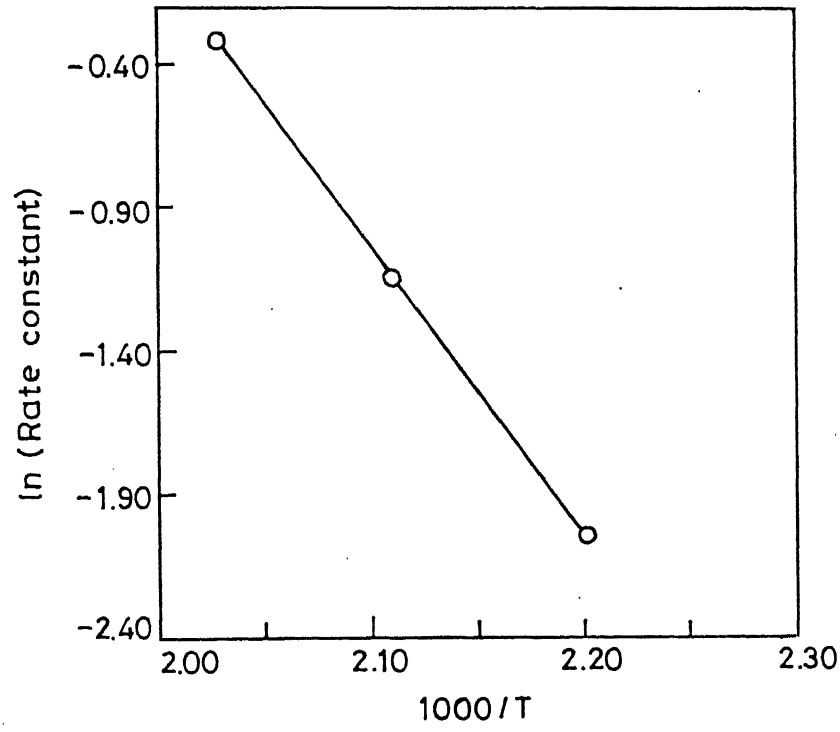

Fig. 4.11 Plot of ln [rate constant] vs. 1/T for ZrO_2-2 mol% Gd_2O_3.

2.5 and 3 mol% Gd-TZP respectively. Thus there appears to be definite trend in the activation energy with stabilizer content. No such trend has so far been reported. It is possible that the apparent trend is within the scatter of the data and will disappear on more careful measurements. This needs to be further explored. The activation energy values are comparable or higher than that reported for Y-TZP [5]. Sato et.al. reported a value to 73 to 94 kJ/mol for 2 to 4Y-TZP's aged in air or water or in presence of water vapour. The results thus indicate that Gd-TZP may have a better aging resistance than Y-TZP. This is supported by our results on the Y-TZP samples. Thus the 3Y-TZP samples aged at shorter times were severely cracked although not fragmented. Samples aged for 20 hours or more turned into powder. This kind of behaviour was also observed by Swab et.al [10] when aging some commercial Y-TZP's at about 800 Pa ($8x10^{-4}$MPa) of water vapour pressure. However, no such drastic degradation in the physical properties was observed in Gd-TZP samples.

4.4.4 Change in Cell Volume on Aging:

Yoshimura [23] suggested that during aging the OH^- are chemisorbed on the surface from which they enter the lattice. This results in an increase in the cell parameter. They measured the cell parameter of monoclinic phase before and after aging and found that the cell volume increases on aging. In the present study however, we have measured the changes in the tetragonal cell volume during the early stages of aging. Similar to the findings of Yoshimura we also find an increase in the tetragonal cell volume. This higher cell volume supports the hypothesis that OH^- groups enter the lattice. The air aged samples show relatively

smaller volume dilation as compared to samples aged in water vapour. Thus the vapour pressure of water appears to have some effect on the kinetics of aging in the early stages.

4.5 *SUMMARY AND CONCLUSIONS:*

The aging experiments were carried out to determine the susceptibility of tetragonal Gd-TZP towards t⟶m transformation during low temperature aging. Hydrothermal aging behaviour of three tetragonal Gd-TZP compositions which had high strength as well toughness was studied. Additional aging studies were carried out on 2Gd-TZP samples to study the influence of water vapour pressure on aging characteristics. Results were also compared with the response to aging of a 3Y-TZP sample prepared in the laboratory. Finally changes in the cell volume at t phase in the early stage of aging in water vapour as well as in air were measured. The summary of the results of these studies are briefly described below:

(i) Like other TZP materials, Gd-TZP also undergoes aging when aged in presence of water vapour or in air.

(ii) The activation energy for aging of Gd-TZP is higher than that for Y-TZP as reported in the literature. Moreover, a 3Y-TZP sample prepared from a fine commercial powder undergoes severe cracking and disintegration on aging while no such changes occur in the Gd-TZP material. The Gd-TZP thus may be superior to Y-TZP in aging resistance.

(iii) Due to scatter in the data, the dependence of aging kinetics on water vapour pressure, if any, could not be observed. However, in the early stages of aging, the increase in the tetragonal cell volume was found to be significantly larger

in water vapour aged samples than in air aged samples indicating that the water vapour pressure has an effect on aging kinetics, at least in the early stages.

(iv) Increase in the t - cell volume on aging supports the hypothesis that an early step in aging is the entry of OH^- groups in the ZrO_2 lattice.

REFERENCES

1. K. Kobayashi, H. Kuwajima and T. Masaki, "Phase change and Mechanical properties of ZrO_2 - Y_2O_3 Solid Electrolytes After Aging," Solid State Ionics, 3/4, 484 - 95 (1981).

2. M. Kuwabara, M. Ashizuka, Y. Kubota and T. Tsukidate "Degradation of the Electrical Properties of Y_2O_3 - partially Stabilized Zirconia Ceramics, owing to Microcracking during Annealing," J. Mater. Sci. Lett. 5, 7 - 9 (1986).

3. M.Matsui, T. Soma and I. Oda, "Effect of Microstructure on the strength of Y-TZP Components." pp 371 - 78 in Advances in Ceramics, vol 12. Science and Technology of Zirconia II. Edited by N. Claussen, M. Ruhle and A.H. Heuer. American Ceramic Society, Columbus, OH, 1984.

4. T. Sato, S. Ohtaki, T. Endo and M. Shimada, "Transformation of Yttria - Doped Tetragonal ZrO_2 Polycrystals by Annealing under Controlled Humidity Conditions," J. Am. Ceram. Soc. 68 [12] C-320 - C-322 (1985).

5. T. Sato and M. Shimada, ''Control of the Tetragonal- to -Monoclinic Phase Transformation of Yttria -Partially -Stabilized Zirconia in hot water," J. Mater. Sci. 20, 3988-92 (1985).

6. T. Sato and M. Shimada, "Transformation of Yttria - Doped Tetragonal ZrO_2 Polycrystals by Annealing in Water", J. Am. Ceram. Soc. 68 [6] 356 - 59 (1985).

7. M. Watanabe, S. Iio and I. Fukuura, ''Aging Behaviour of Y-TZP", pp 391 - 98 in Advances in Ceramics, Vol. 12, Science and Technology of Zirconia II. Edited by N. Claussen, M. Ruhle and A.H. Heuer, American Ceramic Society, Columbus, OH, 1984.

8. K. Tsukuma, Y. Kubota and T. Tsukidate, "Thermal and Mechanical Properties of Y_2O_3 Stabilized Tetragonal Zirconia Polycrystals," pp 382-90 idem.

9. T. Masaki in Int. J. High Technology Ceramics, 2, 85-98(1986) as quoted by M. Hirano in "Inhibition of Low Temperature Degradation of Tetragonal Zirconia Ceramics - A Review," Trans. J. Brit. Ceram. Soc. 91 [5] 139-47 (1992).

10. J. J. Swab, "Low Temperature Degradation of Y-TZP Materials,"J. Mater. Sci. 26, 6706-14 (1991).

11. T. Sato, S. Ohtaki, T. Endo and M. Shimada, "Improvement to the Thermal Stability of Yttria-Doped Tetragonal Zirconia Polycrystals by Alloying with Various Oxides," pp 29-38 in Advances in Ceramics, volume 24A, Science and Technology of Zirconia III. Edited by S. Somiya, N. Yamamoto and H. Yanagida, Westerville, Ohio, 1988.

12. F.F. Lange, G. L. Dunlop and B.I.Davis, "Degradation During Aging of Transformation - Toughened ZrO_2-Y_2O_3 Materials at 250°C," J. Am. Ceram. Soc. 69 [3] 237-40 (1986).

13. H. Schubert in Zirconia Ceramics, Vol.7, Edited by S. Somiya and M. Yoshimura, Uchida Rokakuho, Tokyo, 1986, pp 65-81 as quoted by M. Hirano "Inhibition of Low Temperature Degradation of Tetragonal Zirconia Ceramics - A Review, " Trans. J. Brit. Ceram. Soc. 91 [5] 139-47 (1992).

14. M.T. Hernandez, J. R.Jurado, P. Duran and J.L.G. Fierro, "Subeutectoid Degradation of Yttria-Stabilized Tetragonal Zirconia Polycrystal and Ceria-Doped Yttria-Stabilized Tetragonal Zirconia Polycrystal Ceramics," J. Am. Ceram. Soc. 74[6] 1254-58 (1991).

15. M.Yoshimura, T.Noma, K.Kawabata and S. Somiya, "Role of H_2O on the Degradation Process of Y-TZP," J. Mater. Sci. Lett. 6 463-467 (1987)

16. S. Schmauder and H. Schubert, "Significance of Internal Stresses for the Martensitic Transformation in Yttria-Stabilized Tetragonal Zirconia Polycrystals During Degradation," J. Am. Ceram. Soc. 69 [7] 534-40 (1986).

17. H. Schubert and G. Petzow, "Microstructural Investigations on the Stability of Yttria-Stabilized Tetragonal Zirconia," pp 21-28 in Advances in Ceramics Vol.24A, Science and Technology of Zirconia III. Edited by S.Somiya, N. Yamamoto and H. Yanagida, American Ceramic Society, Westerville, Ohio, 1988.

18. M. Hirano and H. Inada, "Hydrothermal Stability of Yttria - and Ceria - Doped Tetragonal Zirconia -Alumina Composites," J. Mater. Sci. 26, 5047-52 (1991).

19. S. Iio, M.Watanabe, K. Kuroda, H. Saka and T. Imura, "Tetragonal - To - Monoclinic Transformation in Y-TZP During Low - Temperature Aging and Its Restraint by Coating," pp 49-54 in Advances in Ceramics Vol. 24A, Science and Technology of Zirconia, Edited by S. Somiya, N. Yamamoto and H. Yanagida. American Ceramic Society, Westerville, OH, 1988.

20. H.Schubert, N.Claussen, and M. Ruhle, ''Surface Stabilization of Y-TZP, "Proc. Br. Ceram. Soc. 34, 157-60 (1984) as quoted by P.J. Whalen, F.Reidinger and R.F. Antrim in "Prevention of Low Temperature Surface Transformation by Surface Recrystallization in Yttria - Doped Tetragonal Zirconia, J.Am. Ceram. Soc. 72 [2] 319-321 (1989).

21. D.P.J. Whalen, I. Reidinger and R.F.Antrim, "Prevention of Low-Temperature Surface Transformation by Surface Recrystallization in Yttria - Doped Tetragonal Zirconia," J. Am. Ceram. Soc. 72 [2] 319-321 (1989).

22. J. Burke, Kinetics of Phase Transformations in Metals, Pergamon Press, Oxford, England, 1965.

23. J.B. Austin and R.L. Rickett, "Kinetics of the Decomposition of Austenite at Constant Temperature," Trans. AIME, 135, 396 - 415 (1939).

CHAPTER 5

PROCESSING AND MECHANICAL PROPERTIES OF Al_2O_3-Gd_2O_3-ZrO_2 COMPOSITES

5.1 INTRODUCTION

Alumina (Al_2O_3) is an important and versatile ceramic which has manifold uses owing to its high hardness, wear resistance, modulus, inertness, refractoriness, and adequate strength. However, due to low fracture toughness, the use of Al_2O_3 as a structural ceramic is limited. Alumina can be considerably toughened by dispersing ZrO_2 in its matrix which increases its toughness at least by a factor of two and it may be as high as 12 $MPa\sqrt{m}$ with a concurrent increase in strength from about 300 MPa to more than 700 MPa. Depending on the crystal structure of ZrO_2 particles, the dominant toughening mechanism is different in ZrO_2toughened alumina (ZTA). When ZrO_2 is in monoclinic phase substantial amount of toughening results from microcrack toughening [1]. Here high toughness is achieved with little change in strength. However, when the dispersed ZrO_2 is in tetragonal phase, toughness increment results mainly from transformation toughening. In these materials there is a direct correlation between strength and toughness provided the ZrO_2 is mostly in t phase [2,3]. Y_2O_3 and CeO_2 stabilized zirconia polycrystals are therefore commonly used. By optimizing the dopant concentration and volume fraction of ZrO_2 dispersed in Al_2O_3 matrix it has been possible to prepare ZTA having high toughness and improved strength [4-10].

The retention of ZrO_2 in t phase during cooling from the sintering temperature is aided by the constraint provided by the surrounding high modulus Al_2O_3 matrix. Thus higher particle size can be retained in the t phase. A key requirement in the processing of these composites is to achieve an uniform distribution of ZrO_2 particles in the Al_2O_3 matrix. Agglomeration of ZrO_2 would result in ZrO_2 particles of size larger than the critical size for t phase retention.

Al_2O_3 - ZrO_2 composites prepared from conventional processing result in agglomeration of ZrO_2 and can retain only about 40% t - ZrO_2 after sintering. Some of the processing approaches that have been tried to achieve microstructural homogeneity are reactive sintering [11], chemical synthesis [12], evaporative decomposition of slurry [13], colloidal processing [14], spray-ion coupled plasma [15] etc.

Chemical synthesis of Al_2O_3 - Y_2O_3 doped-ZrO_2 composites [12] prepared by hydrazine process produces uniform dispersion of fine Al_2O_3 and ZrO_2 particles in the calcined powder as well as in hot isostatically pressed composites. Evaporative decomposition of solutions [13] uses liquid precursors of Al_2O_3 and ZrO_2 and by simultaneous decomposition of salt solution achieves uniform dispersion of fine ZrO_2 particles in Al_2O_3 matrix. Initial fine size of ZrO_2 particles ensures retention of t - phase after sintering also.

Similarly spray - ICP process [15] also uses aqueous precursors of ZrO_2 and Al_2O_3 and after spraying, a mixture of t-ZrO_2 and γ - Al_2O_3 is obtained. Bleir et.al. [14] used colloidal processing route to ensure uniform dispersion of ZrO_2 in

Al_2O_3. By controlling the pH the surface charges on both Al_2O_3 and ZrO_2 particles could be changed such that Al_2O_3- Al_2O_3 and ZrO_2- ZrO_2 repulsion and Al_2O_3- ZrO_2 attraction increases. This ensures uniform dispersion of ZrO_2 in Al_2O_3. A toughness increment by 7-8 MPa$\sqrt{m}$ over that of Al_2O_3 (3-4 MPa$\sqrt{m}$) was reported.

In the present study Gd_2O_3 doped tetragonal zirconia polycrystals have been dispersed in Al_2O_3 matrix. As already mentioned in Chapter 3, these Gd-TZP's have both high toughness and strength (≥ 12 MPa$\sqrt{m}$ and ~ 800 MPa respectively). As described below, the Al_2O_3-Gd TZP composites have been prepared by a hybrid sol-gel route. The effect of the amount of t-ZrO_2 and its volume fraction on the microstructure and the mechanical properties have been studied.

5.2 *EXPERIMENTAL*

5.2.1 Processing of Al_2O_3 -ZrO_2 Composites

A modified hybrid sol-gel route [16] employing α-Al_2O_3 powder and a zirconia sol has been used to prepare the Al_2O_3-Gd-ZrO_2 composites. 2 mol% Gd-TZP and 3 mol% Gd-TZP (here after called 2 Gd-TZP and 3 Gd TZP respectively) were dispersed in Al_2O_3 matrix. Four different amounts of ZrO_2 (5, 10, 15 and 20 vol%) were used.

First a clear zirconia sol is prepared using acetic acid, Zr(iv) propoxide and propanol as described in Chapter 2. To this sol, required amount of Gd-$(NO_3)_3$ $6H_2O$ dissolved in propanol is added to give 2 or 3 mol% Gd_2O_3. To the stable clear sol of ZrO_2-Gd_2O_3, fine alumina powder of 0.3 μm nominal size (AKP-50, Sumitomo, Japan) is added while stirring. The mixed sol is then stirred at high speed for about 20 minutes followed by

ultrasonication for another 20 minutes. The mixed sol is subsequently gelled by adding triple distilled water in the ratio Zr(iv) propoxide : water = 3 :1. The gel is dried in oven at 100-120°C, followed by calcination at 700°C for 4 hours in air.

The calcined powder is mixed with 3 wt% PVA solution in an agate mortar for 20 minutes. The resultant paste is dried at 100-120°C for 2 to 3 hours followed by regrinding and sieving of the powders. The powder is uniaxially pressed at 200 MPa into a disk of 15 min ϕ x 3 mm high. The disks are then sintered in air at 1550°C for 1.5 hours following the same heating and cooling cycles as described in Chapter 2.

5.2.2 Characterizations

Sintered and polished samples are characterized for density and phases. Sintered density is measured by Archimedes principle using xylene as the immersion liquid. The phases were studied by x-ray diffraction. The samples were scanned in the 2θ range 27°-32° for identifying $(111)_t$, $(11\bar{1})_m$ and $(111)_m$ peaks. Tetragonal to monoclinic transformation was measured on the fractured surface after mechanical testing. Strength and toughness was measured on rectangular bars were cut from these disks. The cut slices were polished on all the six sides first with 600 grit followed by 800 grit silicon carbide powders. Final polishing was done using 3 μm diamond paste. Fracture toughness and strength was measured in three point bending as described in chapter 3. Grain size, shape and grain size distribution was observed in SEM on polished and etched samples. For this, the samples were polished successively on 600 and 800 grit silicon carbide powder and finally with 3 μm and 1 μm diamond lapping paste. After

thoroughly cleaning by ultrasonication using acetone as solvent, the samples were thermally etched at 1350°C for 25 minutes.

5.3 *RESULTS*

Fig. 5.1 shows the change in relative density of Al_2O_3- ZrO_2 composites with increasing volume percent of zirconia. The theoretical density was calculated by assuming density of Al_2O_3 and 2 GdTZP to be 3.98 gms/cc and 6.15 gms/cc respectively. In Al_2O_3-2Gd-TZP, composites the maximum relative density is only 0.9 for Al_2O_3 - 10 vol% ZrO_2. The density decreases to 0.84 for 20 vol% ZrO_2.

In Al_2O_3 -3Gd-TZP composites the density is still lower. The maximum density in this case is only 0.87 at 10 vol% ZrO_2. At higher vol% of ZrO_2 (15 and 20 vol%) the density decreases and reaches a minimum (relative density = 0.8) at 20 vol % ZrO_2.

Fig. 5.2 shows the amount of monoclinic phase in the polished surface of sintered samples. At 5 vol % ZrO_2, the amount of monoclinic phase is 17% for 2 Gd-TZP and 7.5% for 3 Gd-TZP. It decreases on further addition of ZrO_2 reaching a minimum of 10 vol% for Al_2O_3-2 Gd-TZP and 5% for Al_2O_3- 3 Gd-TZP. On further increase in ZrO_2 content the monoclinic content increases rapidly reaching a maximum value of 34% for composites with 2 Gd-TZP and 27% in composites with 3 Gd-TZP.

On the other hand, the fraction of t phase transformed to m phase on the fractured surface decreases steadily with higher volume % of ZrO_2 (Fig. 5.3). The maximum transformability (24%) is recorded for Al_2O_3- ZrO_2 (2 Gd-TZP) at 5 vol% ZrO_2 while it is 20% for composites with 3 Gd-TZP at the same vol % of ZrO_2. Finally, the minimum transformability is registered for 20 vol %

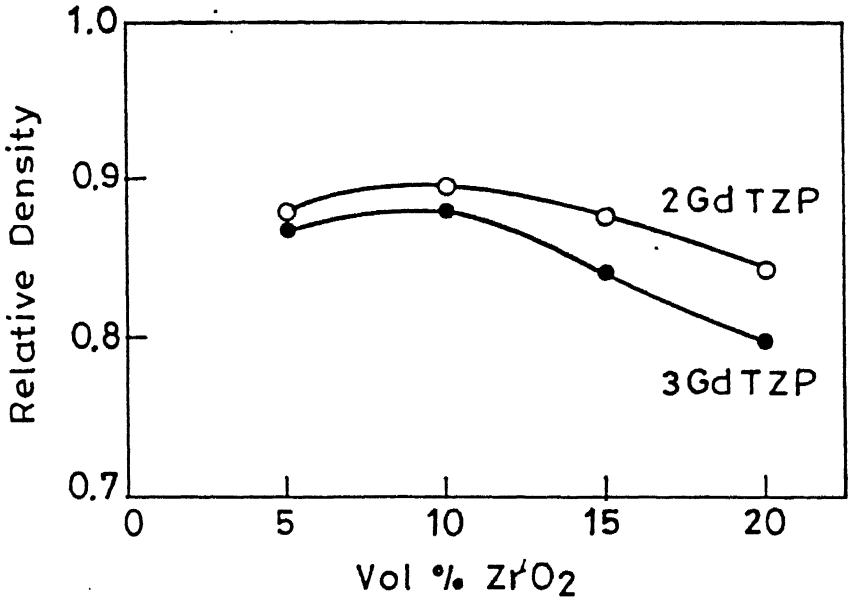

Fig. 5.1 Relative density of Al_2O_3-ZrO_2 composites vs. vol% ZrO_2.

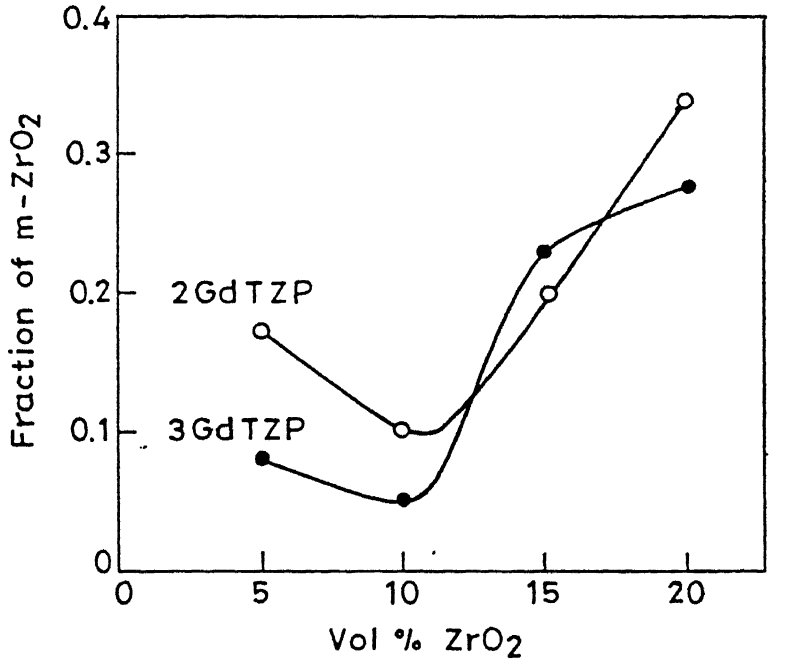

Fig. 5.2 Amount of $m\text{-}ZrO_2$ on polished surface of sintered $Al_2O_3\text{-}ZrO_2$ composites.

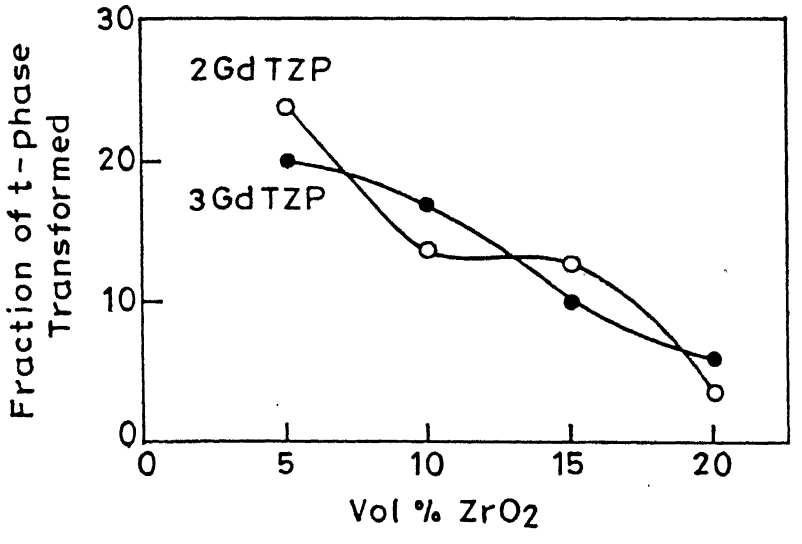

Fig. 5.3 Amount of m-phase on fractured surface of sintered $Al_2O_3\text{-}ZrO_2$ composites.

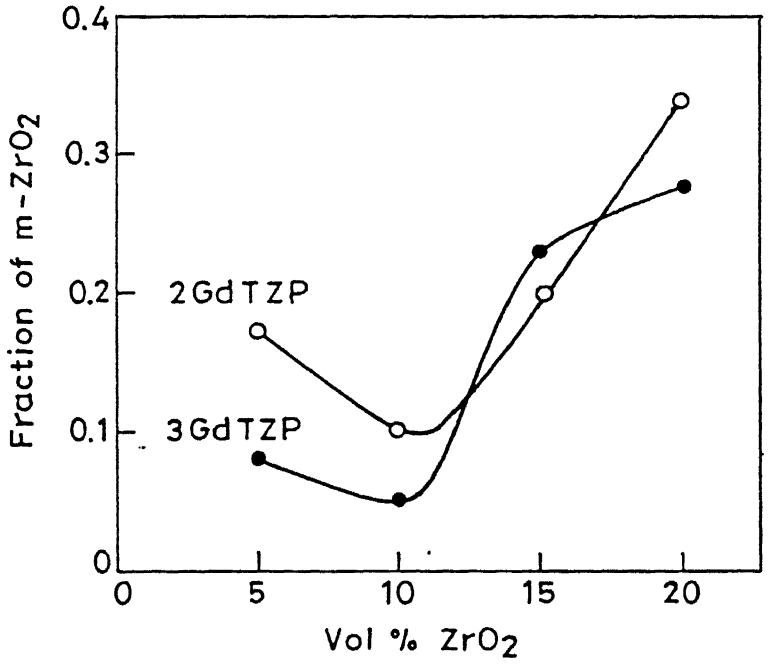

Fig. 5.2 Amount of m-ZrO_2 on polished surface of sintered Al_2O_3-ZrO_2 composites.

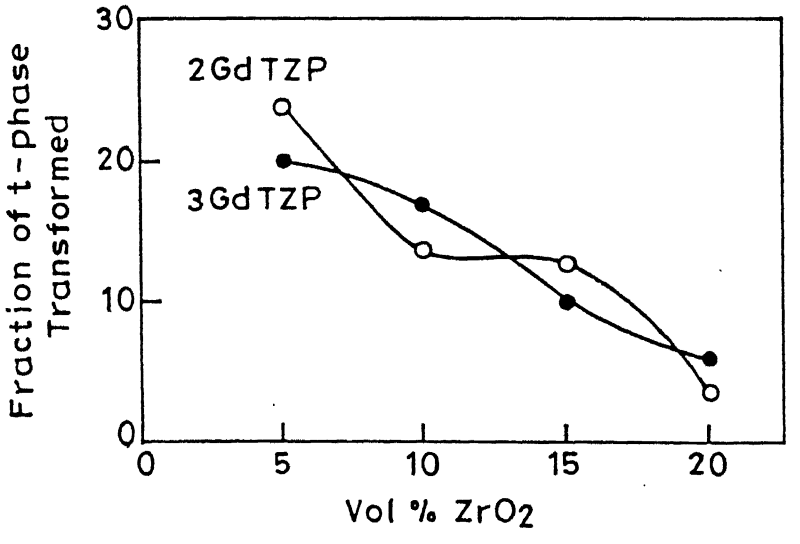

Fig. 5.3 Amount of m-phase on fractured surface of sintered Al_2O_3-ZrO_2 composites.

composites both for 2 Gd-TZP and 3 Gd-TZP.

Fig. 5.4 and 5.5 show the fracture toughness and strength for these composites respectively. Both toughness and strength register higher values for ZTA with 2 mol% Gd-TZP composites as compared to that with 3 mol% Gd TZP. The fracture toughness of composites with 2 mol% Gd-TZP increases from 3.6 MPa$\sqrt{m}$ for Al_2O_3 to a maximum value of 6.5 MPa $\sqrt{m}$ at 10 vol% ZrO_2 before falling off again at 15 and 20 vol% ZrO_2. However, the decrease is quite small at 5 and 15 vol% ZrO_2 giving a somewhat broad peak at 10 vol% ZrO_2. On the other hand, in ZTA with 3 Gd-TZP although the trend of toughness is similar to that with 2 Gd-TZP, the toughness values are lower for all ZrO_2 content. Maximum toughness in this case is 5.75 MPa$\sqrt{m}$ also at 10 vol% ZrO_2. However, in this case, the decrease in toughness at 5 and 15 vol% ZrO_2 is more sharp than for 2 Gd-TZP.

The strength data is shown in Fig. 5.5. The strength remains nearly constant for small amounts of ZrO_2 but then drops sharply at higher Gd_2O_3 content. The drop occurs earlier (10-15 vol% ZrO_2) for Al_2O_3-3 Gd-TZP and later (15-20 vol% ZrO_2) for Al_2O_3-2 Gd-TZP. The strength values are slightly higher for 2 Gd-TZP except at 20 vol% ZrO_2 where they are same.

Fig. 5.6 and 5.7 show the microstructures of the polished surfaces of Al_2O_3- ZrO_2 composites. At 5 vol% ZrO_2, fine ZrO_2 particles (~ 0.2 μm) are seen to be nearly uniformly dispersed in the Al_2O_3 matrix (Fig. 5.6(a), 5.7(a)). As the vol% of ZrO_2 increases, the ZrO_2 particle size also increases. At 20 vol% ZrO_2, large ZrO_2 particles exceeding 1 μm in size are seen (Fig. 5.6d, 5.7c). The porosity decreases with increasing ZrO_2 content.

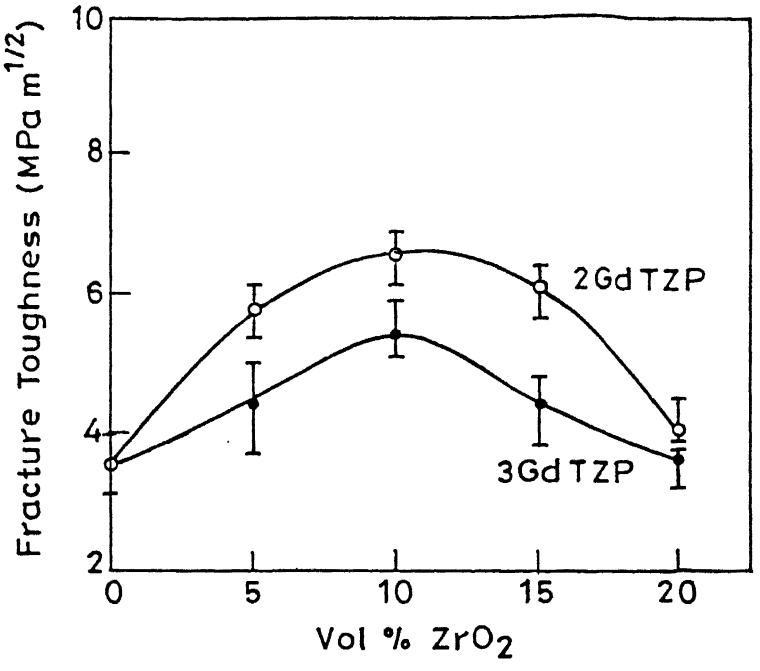

Fig. 5.4 Fracture toughness of Al_2O_3-ZrO_2 composites vs. ZrO_2 content.

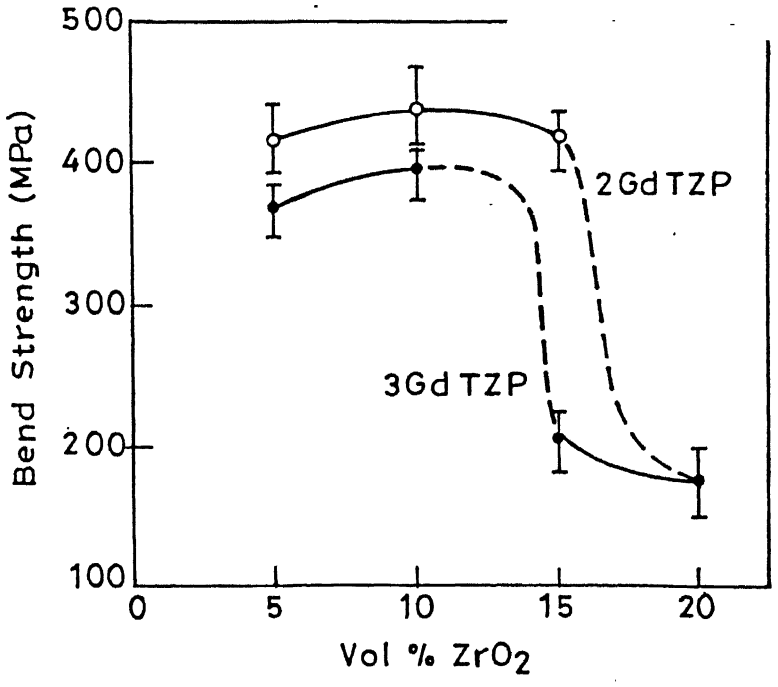

Fig. 5.5 Bend strength of Al_2O_3-ZrO_2 composites vs. ZrO_2 content.

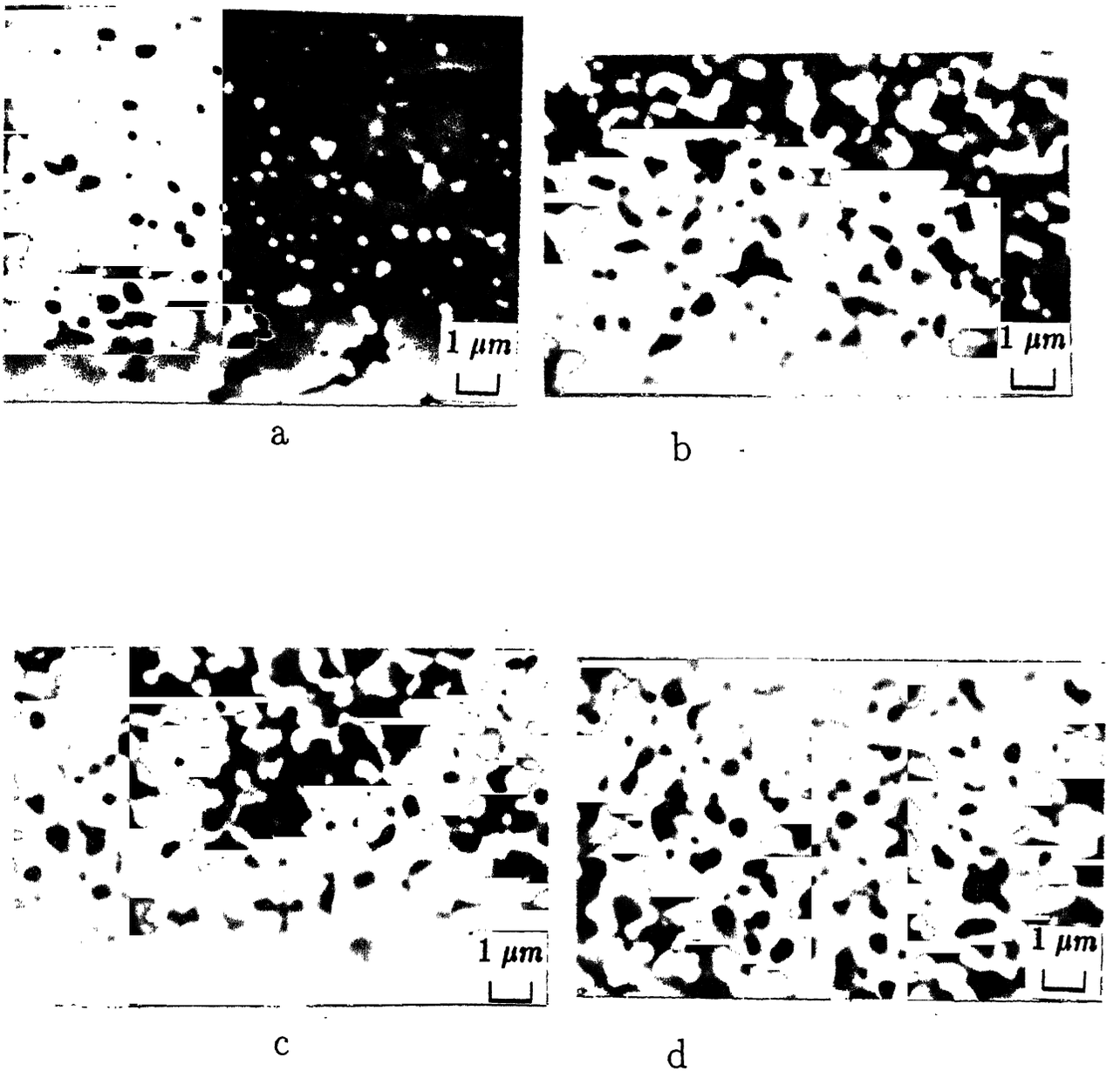

Fig. 5.6 Polished surface microstructure of Al_2O_3-ZrO_2 (2Gd TZP) composites at different vol% ZrO_2 (a) 5, (b) 10, (c) 15 and (d) 20.

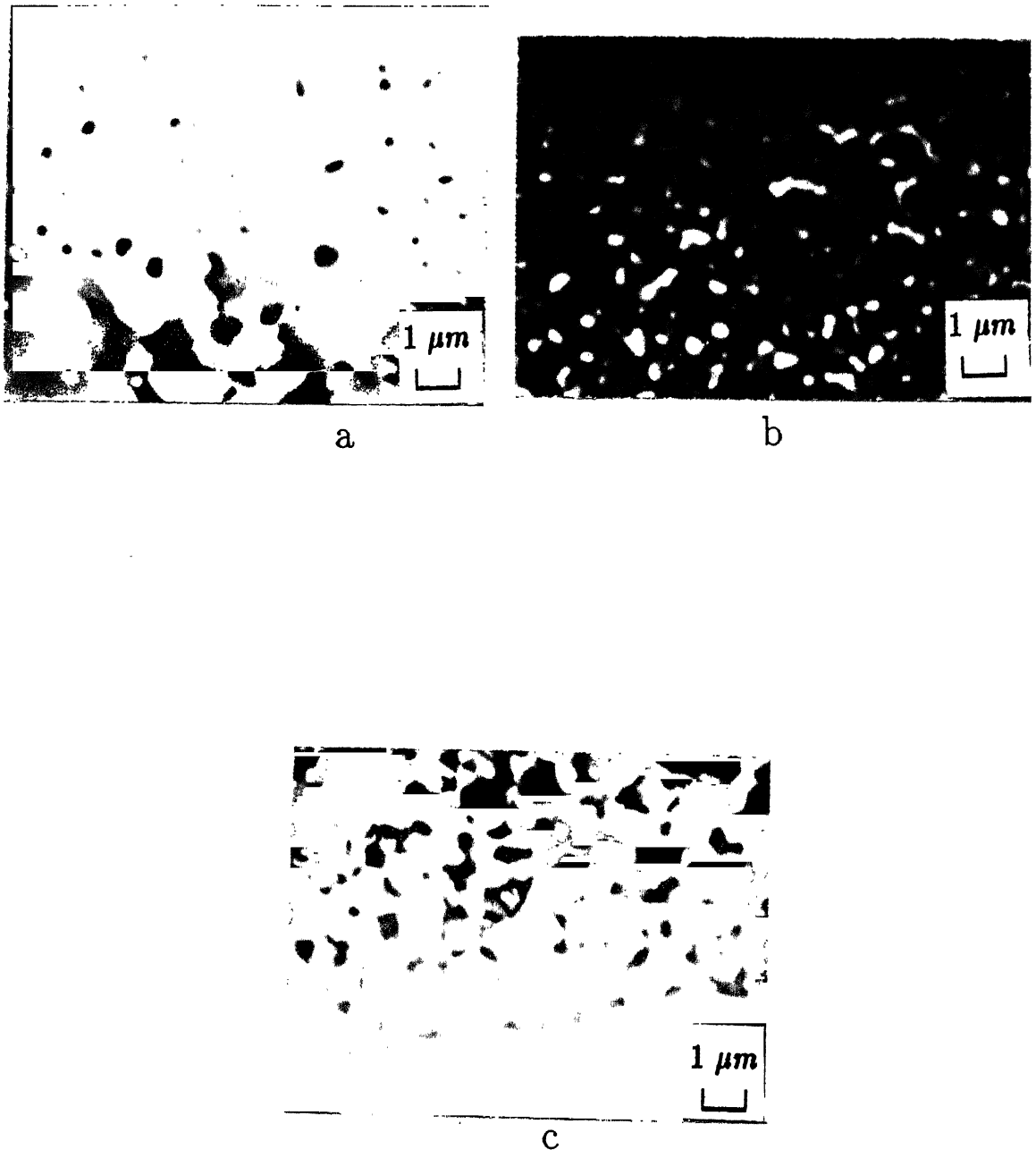

Fig. 5.7 Polished surface Microstructure of Al_2O_3-ZrO_2 (3Gd TZP) composites at different vol% ZrO_2 (a) 5, (b) 10, (c) 20.

5.4 *DISCUSSION*:

5.4.1 Density

Significant amount of porosity is present in the Al_2O_3 - 5 vol% ZrO_2 composites (Fig.5.6 (a) and 5.7 (a)). This shows that the sintering conditions used (1550°C/1.5 hours) in this study are not adequate for the Al_2O_3 and Al_2O_3- ZrO_2 composites. The porosity decreases very significantly as the amount of ZrO_2 increases. This is in agreement with the known effect of ZrO_2 in inhibiting grain growth and promoting sintering in Al_2O_3. Even though the porosity as observed in the micrographs, decreases with addition of ZrO_2; the measured density decreases at higher ZrO_2 contents, probably due to microcracking which accompanies the t $\longrightarrow$ m transformation.

5.4.2 Amount of m phase in sintered samples

The amount of the m-ZrO_2 present in the as sintered samples is low at 5 vol% ZrO_2. It further decreases to a minimum for 10 vol% ZrO_2 and then increases steeply upon further increase in ZrO_2 content (Fig.5.2). The m- content is in general larger for 2% Gd_2O_3. The observations are the result of interactions of the following factors:

(i) Gd_2O_3 Content: Higher stabilizer content (3%) makes the t -phase more stable so that less m is observed in the sintered samples.

(ii) ZrO_2 Particle Size: Particles of t - ZrO_2 exceeding the critical size transform to m -ZrO_2 on cooling. At higher ZrO_2 contents, more agglomeration of ZrO_2 particles occurs which sinter to larger sized ZrO_2 particles and thus transform to m phase on cooling from the sintering

temperature.

(iii) Constraint of the Matrix: This factor appears to be responsible for the higher amount of m -phase in 5% ZrO_2 sample as compared to the 10% sample. At 5%, the samples has large porosity and its effective modulus is low so that less constraint is provided to the t $\longrightarrow$ m transformation.

5.4.3 Fracture Toughness and Strength

Fig. 5.8 shows the total amount of t -phase that has transformed at the fractured surface. This is obtained by taking into account the amount of the initial m -phase (Fig.5.2) and the fraction transformed (Fig.5.3). It is seen that, within experimental error, the total amount of transformed t-phase peaks at 10-15 vol% ZrO_2, which is nearly the volume fraction at which the peak in toughness is obtained. Thus the major contribution to enhancement in toughness is by the stress induced t $\longrightarrow$ m transformation of ZrO_2. The enhancement in toughness is appreciable but relatively small and probably can be further improved by improving the processing.

The strength of the composites remains nearly constant with initial addition of ZrO_2 but then drops steeply when the ZrO_2 content exceeds 10-15 vol% (Fig.5.5). This steep drop in strength is almost certainly due to the flaws generated during cooling of these samples. The pores in the 5 vol% ZrO_2 samples are thus not as effective in degrading the strength as the sharp flaws that are produced due to t $\longrightarrow$ m transformation. The enhancement in strength is again rather low and can be further improved by optimizing the processing.

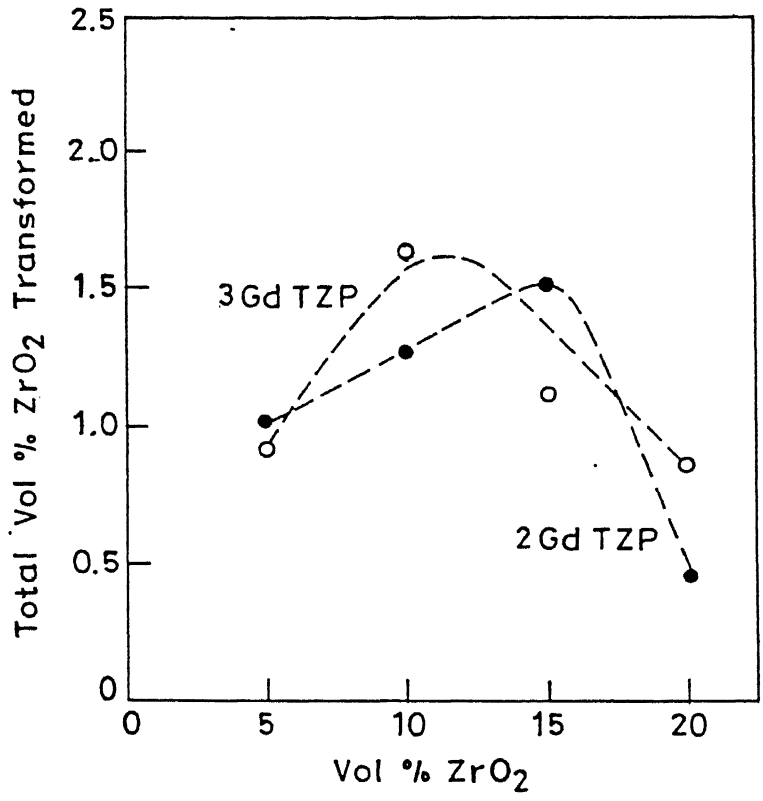

Fig. 5.8 Total vol% ZrO_2 Transformed vs. vol% ZrO_2 in the composites.

5.5 *SUMMARY*

Al_2O_3 - Gd - TZP composites sinter to a relatively low density at 1550°C/1.5 hours. The amount of porosity in the sintered samples decreases substantially on incorporation of ZrO_2. However, the density decreases again at high contents of ZrO_2 possibly due to the cracks which may be forming during t ⟶ m transformation on cooling. The extent of such t ⟶ m transformation decreases initially as the ZrO_2 content is increased to 10 vol% due to decrease in porosity and a consequent increase in the constraint by the matrix. On further increase in the amount of ZrO_2, the amount of m -phase increases due to agglomeration of ZrO_2. The total amount of t - ZrO_2 which transforms during fracture is maximum at about 10 vol% ZrO_2 and a maximum in K_{IC} is also observed at this point. The maximum K_{IC} achieved is 6.5 MPa$\sqrt{m}$. The strength changes a little up to about ~ 10 to 15 vol% ZrO_2 but then drops sharply, most probably due to the presence of flaws which are produced due to the t ⟶ m transformation during preparation of the samples. Best properties are obtained with 10 vol% ZrO_2 (2% Gd_2O_3) composites.

REFERENCES

1. N. Claussen, "Fracture Toughness of Al_2O_3 with an Unstabilized ZrO_2 Dispersed Phase," J. Am. Ceram. Soc. 59 [1-2] 49-51 (1976).

2. P.F. Becher, "Transient Thermal Stress Behaviour in ZrO_2 - Toughened Al_2O_3", J. Am. Ceram. Soc. 64 [1] 37-39 (1981).

3. F.F.Lange, "Transformation Toughening, Part 4, Fabrication, Fracture Toughness, and Strength of Al_2O_3 - ZrO_2 Composites", J. Mater. Sci. 17 [1] 247-54 (1982).

4. D.W. Shin, K. K. Orr and H. Schubert, "Microstructure - Mechanical Property Relationship in Hot - Isostatically Pressed Alumina and Zirconia - Toughened Alumina", J. Am. Ceram. Soc. 73 [5] 1181-88 (1990).

5. L.J. Yuan and T. - S. Yen, " Major Influences on the Particle size - Transformation Temperature Relation in Al_2O_3 - ZrO_2 Composites", J. Am. Ceram. Soc. 75 [9] 2576-90 (1990).

6. Y Matsumoto, K. Hirota, O. Yamaguchi, S. Inamura, H. Miyamoto, N. Shiokawa and K. Tsuji, "Mechanical Properties of Hot- Isostatically Pressed Zirconia - Toughened Alumina Ceramics Prepared from Coprecipitated Powders", J. Am. Ceram. Soc. 76 [10] 2677-80 (1993).

7. K. Tsukuma, K. Ueda and M. Shimada, "Strength and Fracture Toughness of Isostatically Hot - Pressed Composites of Al_2O_3 and Y_2O_3 - Partially Stabilized ZrO_2", J. Am. Ceram. Soc. 68 [1] C-4 - C-5 (1985).

8. S.Hori, M. Yoshimura and S. Somiya, " Strength -Toughness Relations in Sintered and Isostatically Hot- Pressed ZrO_2-Toughened Al_2O_3", J. Am. Ceram. Soc. 69 [3] 169 - 72 (1986).

9. A. Bleier, and C.G. Westmoreland, "Effect of pH and Particle Size on the Processing of and the Development of Microstructure in Alumina - Zirconia Composites", J. Am. Ceram. Soc. 74 [12] 3100-11 (1991).

10. T. Kimura, Y. Kaneko and T. Yamaguchi, "Consolidation of Alumina - Zirconia Mixtures by a Colloidal Process", J. Am. Ceram. Soc. 74 [3] 625-32 (1991).

11. N. Claussen and M. Ruhle, "Design of Transformation - Toughened Ceramics, " pp. 137-63 in Advances in Ceramics, Vol.3, Science and Technology of Zirconia. Edited by A.H. Heuer and L.W. Hobbs. American Ceramic Society, Columbus, OH, 1981.

12. S. Kimoto, K. Hirota, O. Yamaguchi, H. Kume, S. Inamura and H. Miyamoto, "Formation and Sintering of Yttria-Doped Tetragonal Zirconia with 50 mol% Alumina Prepared by the Hydrazine Method", J. Am. Ceram. Soc. 77 [6] 1694-96 (1994).

13. D.W. Sproson and G.L. Messing, "Preparation of Alumina - Zirconia Powders by Evaporative Decomposition of Solutions, J. Am. Ceram. Soc. 67 [5] C-92 (1984).

14. A. Bleier, P.F.Becher, K.B. Alaxander and C.G. Westmoreland, "Effect of Aqueous Processing Conditions on the Microstructure and Transformation Behaviour in Al_2O_3 - ZrO_2 (CeO_2) Composites", J. Am. Ceram. Soc. 75 [10] 2649-59 (1992).

15. M. Kagawa, M. Kikuchi, Y. Syono and T.Nagae, "Stability of Ultrafine Tetragonal ZrO_2 Coprecipitated with Al_2O_3 by the Spray - ICP Technique", J. Am. Ceram. Soc. 66 [11] 751-54 (1983).

16. A. Saha, D.C. Agarwal and A. Sharma, "Microstructure and Mechanical Properties of Hybrid Sol-Gel Processed Al_2O_3 - ZrO_2 Composites", pp 497-507 Ceramic Transactions, Vol.38. Edited by N.P. Bansal. American Ceramic Society, Westerville, OH, 1994.

CHAPTER - 6

SUMMARY AND SUGGESTIONS FOR FURTHER WORK

6.1 *SUMMARY:*

This study was devoted to the processing of Gd-TZP powders and the characterizations of sintered TZP ceramics prepared from these powders. The first part deals with processing of Gd-TZP powders and optimization of t phase and density. The powders were processed by three different methods, viz. a mixed oxide (MO) method and two modified sol-gel methods i.e. hybrid sol-gel method (HSG) and coprecipitation (CP) method. It was found that only CP method could retain 100% t phase in all the calcined powders and in most of the sintered samples. On the other hand HSG method could stabilize a maximum of 62% t phase after calcination which increased to 87% in sintered samples. However, only trace t phase could be retained in the calcined MO samples which increased to a maximum of 44% after sintering. This result differs markedly from that of other TZP's, i.e. Y-TZP and Ce-TZP where t phase can be retained in the calcined sample prepared by MO method. It appears that the slower diffusion coefficient of Gd^{3+} may be responsible for the difficulty in the formation of the of t phase.

However, like other two methods (i.e. MO and HSG), the CP method also gave poor sintered density (<90%) despite having high amount of t phase. In order to overcome this problem different calcination and sintering conditions were tried to maximize both the t phase and the sintered density. However, this approach did

not succeed. TEM pictures, specific surface area and compaction behaviour of these powders indicated that these powders were agglomerated as a result of interaction with H_2O. Following this, an additional step of propanol washing was introduced in powder processing to replace this water by propanol. This resulted in softly agglomerated powders and resulted in a remarkable improvement in sintered density (~ 99%). Thus by washing the CP powders by propanol, it was possible to prepare high density Gd-TZP ceramics by pressureless sintering at low temperature (1400°C).

In the second part of the study these sintered Gd-TZP ceramics were characterized with respect to phases, microstructure, fracture toughness, strength, hardness and low temperature aging behaviour. Depending on the amount of Gd_2O_3 content, these ceramics had a two phase mixture of (m + t) at low Gd_2O_3 content (1.75 and 2 mol%) or (t + c) at higher Gd_2O_3 content (5 and 8 mol%). Between these two extreme situations, the samples had only t phase at 2.5, 3 and 4 mol% Gd_2O_3. All the samples from 1.75 to 4 mol% had very small and equiaxed grains (0.10 - 0.15 μm). At 5 mol% few large grains (0.35 μm) of cubic phase appeared and at 8 mol% majority of the grains were large cubic grains (0.6-0.7 μm) with a few small grains (0.2 μm) of t phase lying in between.

High toughness was observed as measured by indentation technique in the composition range 1.75 - 4 mol% Gd_2O_3 (≥ 10 MPa$\sqrt{m}$). The highest toughness was observed from 2 mol% samples (12 MPa$\sqrt{m}$). When measured by SENB method, although a similar trend was observed the values were higher with maximum toughness

at 14.7 MPa$\sqrt{m}$ also for 2 mol% samples. The above samples also registered high strength (750 - 800 MPa) as measured by three point bending. Even considering the factor of overestimation (which was found to ≤ 15%) due to the small sample sizes used in these measurements, the values are quite good when compared with pressureless sintered Ce-TZP (700 - 900 MPa) or Y-TZP (1.1 - 1.2 GPa). In this material, the strength appears to be controlled by internal flaws and pores present during processing.

Like Y-TZP, in Gd-TZP also the composition has a strong influence on its M_s temperature. An indirect evidence of this fact was obtained from the transformability of t phase in liquid nitrogen quenched samples. The amount of m phase dropped sharply from 75% at 1.75 mol% to about 5% at 3 mol%. Transformability measured by other methods like hand grinding, fracture and machine grinding show a different trend wherein a peak transformability is obtained at 2 mol%. For these conditions, the transformability drops to a lower value at 1.75 mol% possibly due to the suppression of autocatalytic transformation (owing to the presence of about 10 vol% m phase in this sample). The transformation zone depth also show a similar trend and maximum zone depth (~ 3.5μm) was obtained for 2 mol% samples.

The zone depth was utilized to explain the toughening effect using different existing models. It was found that most of toughening in this material could be accounted for by transformation toughening.

In contrast to Y-TZP and Ce-TZP where the strength and toughness do not peak at the same composition, both strength and toughness in this material were maximum at the same composition (2

mol%). This is a new and interesting result and needs more detailed study.

When these Gd-TZPs were incorporated in Al_2O_3, significant increase in toughness and strength was observed despite the processing of the composites being unoptimized, i.e. composites had low density. The toughness correlates well with the total volume percent of transformed t phase. Thus the major toughening in the composites is also from transformation toughening. The strength remains almost constant at low volume percent of ZrO_2 followed by a sharp drop at ≥ 10 vol% ZrO_2 addition. This sharp drop indicates the presence of microcracks formed due to t⟶ m transformation during cooling.

Low temperature aging of 2, 2.5 and 3 mol% Gd-TZP gave activation energy values between 85 and 116 kJ/mol. There appears to be a composition dependence of activation energy on the Gd_2O_3 content. An increase in the tetragonal cell volume was observed during the early stages of aging. The result confirms the hypothesis of Yoshimura that OH^- ions enter the lattice during aging. The cell volume dilation was more in presence of water vapour than in air. Thus water vapour pressure appear to play a role in the early stages of aging kinetics.

6.2 *SUGGESTIONS FOR FURTHER WORK:*

This study reports for the first time the processing of Gd-TZP powders which could be sintered to a high density by pressureless sintering and the properties of the sintered bodies obtained from these powders.

Below are given some suggestions which can be pursued in any further work in this area:

(1) The powders produced are very fine and are difficult to press to high green density. Spray drying of the powders should be helpful in improving the green density. It may also be possible to eliminate the propanol washing step by using the spray dried powders.

(2) Inspite of having very small grain size, these TZP's show high stress induced t $\longrightarrow$ m transformability. Thus there exists a possibility of increasing the grain size within the critical limit by manipulating the sintering conditions. This will give larger grains with enhanced transformability and thus the toughness can be enhanced.

(3) As already mentioned, the strength is limited by flaws present in the material. Therefore a possibility exists for increasing the strength by hot pressing or hot isostatic pressing.

(4) These TZP ceramics have metastable t phase which can undergo phase partitioning when subjected to high temperature heat treatments for long hours. Similar studies on other TZP have reported an enhancement in toughness as a result of such treatment. Thus it will be of interest to study the effect of heat treatment on phase, microstructure and mechanical properties of these TZP ceramics.

(5) Due to extremely fine grain size, these material are likely to exhibit superplastic behaviour. It will be interesting to study this phenomenon.

(6) Finally a preliminary trial on an unoptimized Al_2O_3 - Gd - TZP composites show that this TZP have the potential to increase the strength and toughness of other matrices. More

carefully planned experiments with proper choice of calcination and sintering conditions should give a composites with much improved properties.

ERRATA

In the final paragraph of the report the examiner has said that point nos. (h), (o), (s), (t) and (x) need to be definitely addressed while response to the other points has been left to the discretion of the candidate.We first provide our response to the points (h), (o), (s), (t) and (x).

(h) In all cases, the value of the theoretical density used was calculated from lattice parameters determined by x-ray diffraction as suggested by the examiner. This was not explicitly mentioned in the thesis. The following phrase will be added to the caption of Fig. 2.8 at page 61.

"The theoretical densities for each composition were calculated using the lattice parameters and the amounts of the various phases as determined by x-ray diffraction (Appendix-II)".

The value of the theoretical density given on page 60 in section 2.3.3 contains typographical error. It should be 6.10 and will be corrected.

The appendix (Appendix- II) given at the end of response will be included in the thesis.

(o) This point is already answered in point 'h'. To make it more clear the following will be added to the caption of Fig. 3.4 on page 127:

"The theoretical densities used were calculated from the lattice parameters (Appendix- II).

(s) The value of E and e^T are for the tetragonal phase because that is the phase undergoing transformation. We have used the following values:

$$E = 220 \text{ GPa}, \quad e^T = 0.046$$

There may be a small variation in the values of E and e^T with the amount of Gd_2O_3, however, the errors caused by neglecting this variation are expected to be small and have been neglected. To take care of the above the following will be added after the first sentence of paragraph 2 in page 142:

"To calculate K_{ICTT} we have used values of E (22Ø GPa) and e^T (Ø.Ø46) from reference 65 and 66 for ZrO_2 -2.3mol% Y_2O_3 as no values for E and e^T for ZrO_2-Gd_2O_3 system are available in the literature and the behaviour of ZrO_2-Gd_2O_3 system is more like that of ZrO_2-Y_2O_3 than ZrO_2-CeO_2, the other well studied system''.

The examiner has also raised a point regarding the transformation zone size. The transformation zone size for ZrO_2-Y_2O_3 is about 1-5 μm (ref. 49, 5Ø) which is comparable to the one obtained by us for ZrO_2-Gd_2O_3. The fracture toughness for ZrO_2-Gd_2O_3 is also in the same range as that for ZrO_2-Y_2O_3. The following will be inserted at the end of the first paragraph on page 131:

"In comparison the reported values for the zone depth are 1-5 μm for ZrO_2-Y_2O_3 (reference 49, 5Ø) However, for Ce-TZP no definite value for zone size has been reported because of the difficulty in measuring it due to the presence of plastic zone in this material."

(t) We agree with the points made by the examiner that in general the pores in sintered bodies approach a spherical pore and have zero stress intensity factor. As we have not characterized the pore size distribution and the pore shapes have not been analyzed we agree that without further study it may be best to avoid emphasizing the correlation between porosity and strength. We have looked again at our data and find that in general there is a decrease in the strength as the largest grain size in the sample increases. In section 3.6.6 (Strength and Hardness), Fig. 3.17 will be replaced by the histogram of grain size distribution and the matter after the eighth line to the end of the paragraph will be replaced by the following:

"The normalized critical flaw sizes are tabulated in Table 3.4. The histograms of the grain sizes are given in Fig. 3.17. It can be seen that in general there is a decrease in strength as the size of the largest grain present in the sample increases. This agrees with the observation that in most materials the size of the strength determining flaws scales with the grain size. Very often pore induces a microcrack and then the (pore + microcrack) acts as the critical flaw. The size of the critical flaw is thus expected to be larger in samples with large grains leading to a decrease in strength.

(x) The reviewer has pointed out that while the micrographs show that the porosity decreases with increasing ZrO_2 content, the relative density as shown in Fig. 5.1 decreases. This appears to be due to Fig. 5.1 showing the relative

density and not the actual density. To take care of this point the following changes will be made.

(i) The first line of the first paragraph of section 5.3 will be replaced by the following:

"Fig. 5.1 shows the actual density and the relative density of Al_2O_3-ZrO_2 composites with increasing volume percent of ZrO_2."

(ii) The Fig. 5.1 is now modified to include the actual density and is appended to this response.

(iii) The following will be added to the third sentence of the section 5.4.1:

"the porosity decreases very significantly (as is evident from the micrographs viz., Fig. 5.6 and 5.7) and the increase in actual density with increasing ZrO_2 content (Fig. 5.1)."

(iv) The last sentence of 5.4.1 will be deleted.

The answer to the other points are now given in sequential order:

Technical contents of the thesis:

(a) References are given in the first paragraph - ref. 1 and 2.

(b) Yes.

(c) The reference for Klapp's paper is given below and will be included in the thesis:

P. C. Klapp, "A Localized Soft Mode Theory for Martensitic Transformations", Phys. Status Solidi B, **57**, 561 (1973).

(d) This section deals with the transformation of constrained zirconia. This was wrongly titled. The titles of subsections 1.5.1 and 1.5.2 will be modified as follows:

1.5.1 Transformation of Constrained Zirconia - Effect of Particle Size

1.5.2 Systems with Constrained Zirconia

Moreover, in section 1.5.2 first two sentences will be deleted and the section will begin with the sentence, "The constrained tetragonal zirconia may be of several forms:".

(e) The particle sizes of ZrO_2 and Gd_2O_3 are not available.

(f) Eq. 2.1 is simply derived by assuming a spherical geometry of the particle.

(g) The reference for Kaliszewski and Heuer is 29 and is given later. THe last sentence of third paragraph on page 53 will be modified as follows:

"Kaliszewski and Heuer have also observed a similar behaviour in their ethanol washed powder, as described later in Part C of this chapter, and have

attributed it to the removal of ethylene from ethanol".

(i) Propanol washing did not change the amount of (t+c) phase.

(j) (t+c) phase can be used only for 5 and 8 mol% samples which form cubic phase also. To avoid cluttering we have used only t. The meaning is clear from the context.

(k) The reference for eq. 3.1 is provided in Table 3.1, page 102.

(l) The reference is already provided in 12th line of page 104.

(m) The caption of left column of Fig. 3.3 is "Sintered Surface" and for the right column is "Ground Surface", and will be included.

(n) The value of K_{IC} is correct.

(p) The description for zone size measurement is given in page 125 second paragraph.

(q) Agreed - the reference [59] should be [60]. Other references are correct. The above correction will be included.

(r) No literature is available on effect of Gd_2O_3 content on M_s.

(u) Reference for paragraphs 2 and 3 of section 4.1.2 on page 163 is same [12].

(v) Agreed - the references will be provided for the following figures.

Fig. no.	Reference
2.1	10
3.1	3
3.2	4
3.3	12
4.1	15

(w) In almost all ZrO_2 containing ceramics it has been observed that the as sintered surface contains a reasonable amount of m-phase. This is because of the fact that unlike ZrO_2 grains at the interior, the ZrO_2 grains at the surface can transform to m-phase due to lack of constraint. So, the usual procedure is to remove this surface layer of m-phase by polishing and the measurement is done on polished surface. THe polishing stresses are kept low to avoid t→ m transformation.

(y) This is already taken care of while answering point (x).

(z) The last sentence of the first paragraph on page 206 will be replaced by:

"In the materials the critical flaw determining the strength appears to scale with the size of the largest grain."

Corrections in punctuations, grammar, spelling, typing or language:

(a) No change- complex admittance is correct.

(b) No change- the sentence is reasonably clear.

(d) No change. It is felt that there is no need for a separate section.

(g) The extra "for" in the middle of the sentence will be removed.

(j) No change - as the sentence is reasonably clear.

(l) "inversely" will be changed to "directly".

(m) The last word is "ionic" and it will be made legible.

(c), (e), (g), (i), (k) - agreed, the suggested changes will be made and will be included in the thesis.

APPENDIX - II

1. Lattice Parameters of ZrO_2-Gd_2O_3 ceramics:

The lattice parameters of ZrO_2 - Gd_2O_3 ceramics were determined using a least square fitting routine on a minimum of eight peaks as described in Page 122 and Fig. 3.6 (Page 129). The individual values of 'a' and 'c' axis are given in the following Table.

Table - II.1 Lattice Parameters of ZrO_2 - Gd_2O_3 Ceramics

	Gd_2O_3 (mol%)						
	1.75	2	2.5	3	4	5	8
c (Å)	5.22	5.2Ø	5.21	5.2Ø	5.18	5.18	5.17
a (Å)	5.1Ø	5.11	5.11	5.12	5.13	5.12	5.14

2. Determination of Atomic Mass of ZrO_2 - Gd_2O_3 Ceramics:

The atomic mass was calculated from stoichiometric cell formula of ZrO_2-Gd_2O_3 ceramics using the fact that both Zr and Gd are in eightfold coordination with O atom. Therefore in an unit cell there will be 4 atoms each of Zr and Gd and 8 atoms of O. Table II.2 show the composition, cell formula and mass of unit cell for all the ZrO_2 - Gd_2O_3 compositions.

Table II.3 show the theoretical density for all the composition of ZrO_2-Gd_2O_3 based on the above calculation.

Table - II.2 Unit Cell Mass of ZrO_2 - Gd_2O_3 Ceramics

Composition (mol% Gd_2O_3)	Atomic Formula	Atomic Mass (x 10^{-23} gm) of unit cell	Cell Volume $(Å)^3$
1.75	$Zr_{.9825}Gd_{.0175}O_{1.991}$	82.46	135.30
2	$Zr_{.980}Gd_{.02}O_{1.99}$	82.56	136.15
2.5	$Zr_{.975}Gd_{.025}O_{1.987}$	82.74	136.27
3	$Zr_{.970}Gd_{.03}O_{1.985}$	82.94	136.30
4	$Zr_{.960}Gd_{.04}O_{1.98}$	83.33	136.32
5	$Zr_{.950}Gd_{.05}O_{1.975}$	83.71	135.92
8	$Zr_{.920}Gd_{.08}O_{1.96}$	84.86	136.64

Table - II.3 Theoretical Density for ZrO_2 - Gd_2O_3 Ceramics

Composition (mol% Gd_2O_3)	Preparation Method	Vol Fraction Phase m	(t+c)	Theoretical Density (gm/cm^3)
1.75	CP	0.12	0.88	6.04
2	MO	0.84	0.16	5.89
	HSG	0.75	0.25	5.90
	CP	0.04	0.96	6.06
2.5	CP	0.0	1.0	6.07
3	MO	0.81	0.19	5.90
	HSG	0.65	0.35	5.94
	CP	0.0	1.0	6.10
4	CP	0.0	1.0	6.12
5	MO	0.72	0.28	5.94
	HSG	0.45	0.55	6.02
	CP	0.0	1.0	6.16
8	MO	0.56	0.44	6.01
	HSG	0.13	0.87	6.16
	CP	0.0	1.0	6.21

3. Theoretical Density Calculations for Al_2O_3 - ZrO_2 Composites:

The theoretical density for the Al_2O_3 - ZrO_2 composites were calculated from the rule of mixture, i.e.,

Density = (Vol. fraction Al_2O_3 x Density) + (Vol. fraction ZrO_2 x Density)

The theoretical density of Al_2O_3 is 3.98 gm/cm^3 and the theoretical density of ZrO_2 is calculated from the amount of m and t phase present in ZrO_2. These are listed in Table II.4

Table II.4 Theoretical Density for Al_2O_3 - ZrO_2 Composites

(a) Al_2O_3 - 2Gd TZP Composites:

Vol frct. ZrO_2	Vol frct phase in ZrO_2		Theoretical Density Al_2O_3	ZrO_2	Density of Al_2O_3 - ZrO_2
	m	t			
Ø.Ø5	Ø.18	Ø.82	3.98	6.Ø2	4.Ø8
Ø.1Ø	Ø.1Ø	Ø.9Ø	3.98	6.Ø4	4.18
Ø.15	Ø.2Ø	Ø.8Ø	3.98	6.Ø2	4.28
Ø.2Ø	Ø.34	Ø.56	3.98	5.99	4.38

(b) Al_2O_3 - 3Gd TZP Composites:

Vol frct. ZrO_2	Vol frct phase in ZrO_2		Theoretical Density Al_2O_3	ZrO_2	Density of Al_2O_3 - ZrO_2
	m	t			
Ø.Ø5	Ø.Ø9	Ø.91	3.98	6.Ø5	4.Ø8
Ø.1Ø	Ø.Ø5	Ø.95	3.98	6.Ø7	4.19
Ø.15	Ø.24	Ø.76	3.98	6.Ø4	4.29
Ø.2Ø	Ø.27	Ø.73	3.98	6.Ø3	4.39

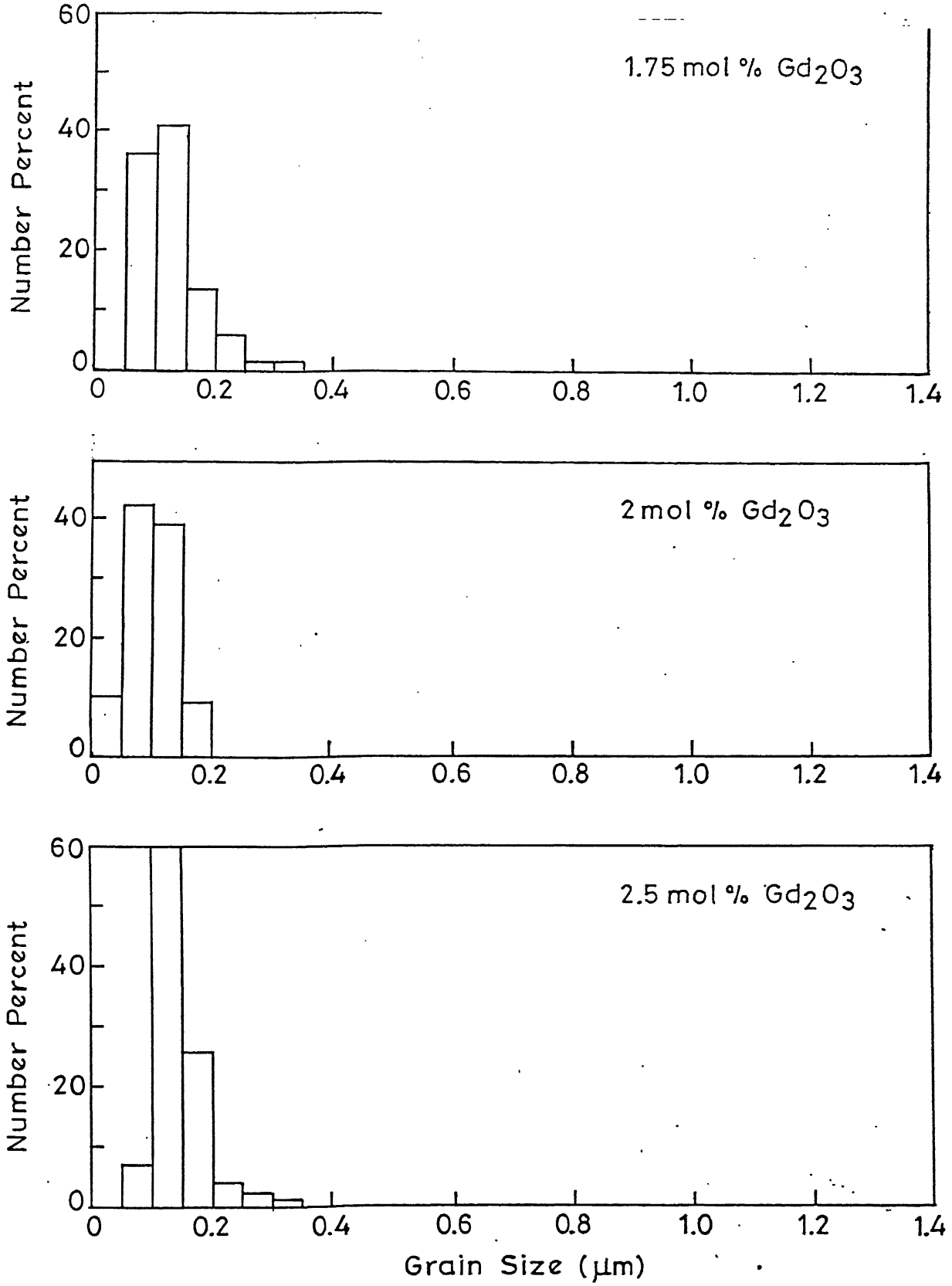

Fig. 3.17 Histogram of the Grain Sizes of $ZrO_2 - Gd_2O_3$ ceramics

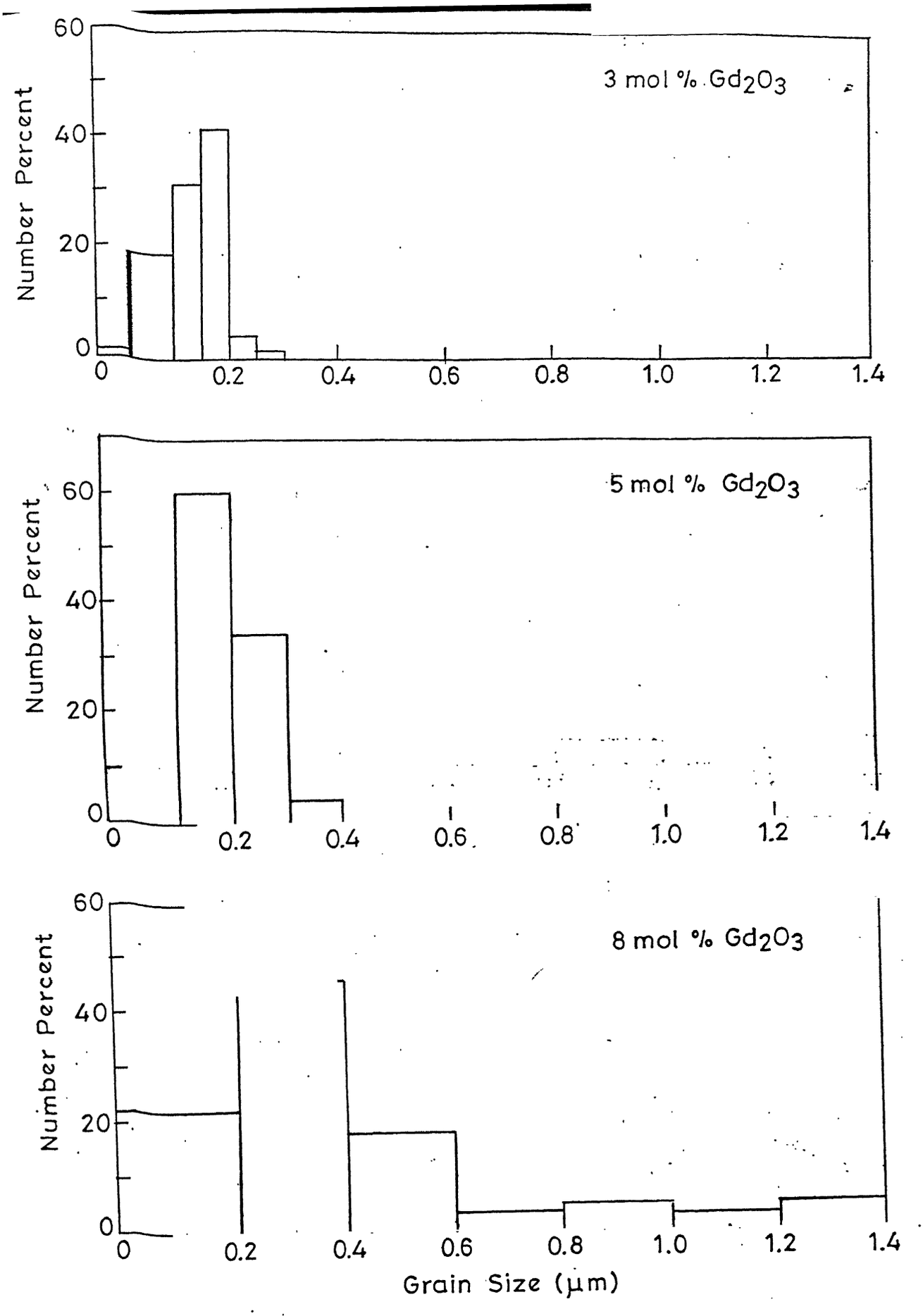

Fig. 3.17 (contd.) Histogram of the Grain Sizes of $ZrO_2 - Gd_2O_3$ ceramics

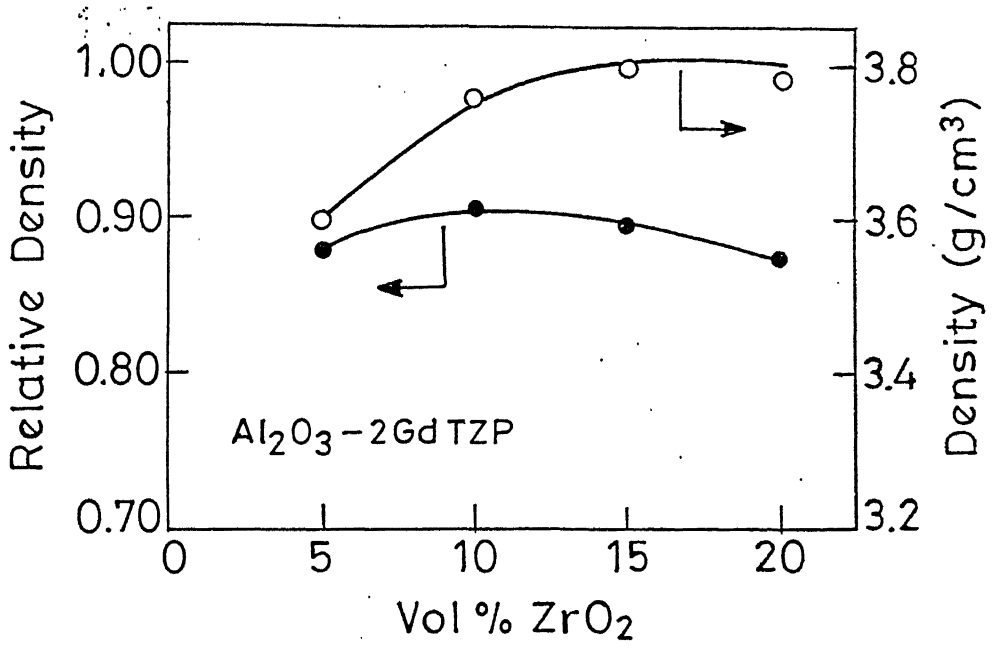

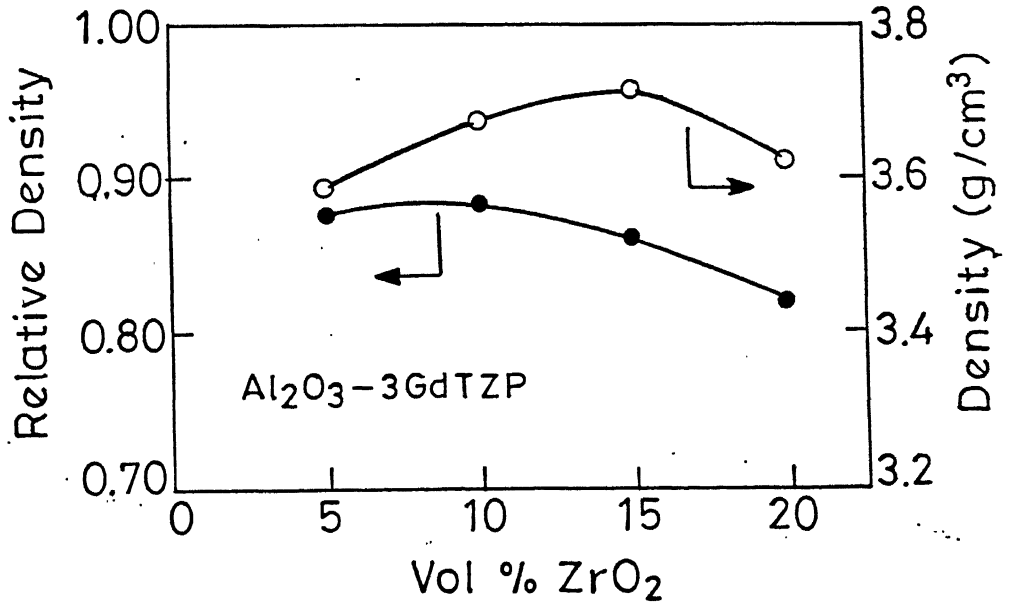

Fig. 5.1 Density of Al_2O_3 - ZrO_2 composites vs. Vol% ZrO_2, (a) Al_2O_3- 2GdTZP and (b) Al_2O_3- 3GdTZP.